UNCLASSIFIED

AD NUMBER

AD823809

NEW LIMITATION CHANGE

TO

Approved for public release, distribution unlimited

FROM

Distribution: No Foreign.

AUTHORITY

AFRPL ltr dtd 27 Oct 1971

THIS PAGE IS UNCLASSIFIED

AFRPL-TR-67-261

AD823809

STUDY AND EVALUATION OF SEGMENTED SPHERE PRESSURE VESSELS PHASE I TECHNICAL REPORT

J. W. FARRELL
MISSILES AND SPACE DIVISION · TEXAS
LTV AEROSPACE CORPORATION

TECHNICAL REPORT AFRPL-TR-67-261
November 1967

This document is subject to special export controls and each transmittal to foreign governments or foreign nationals may be made only with prior approval of AFRPL(RPPR/STINFO).

AIR FORCE ROCKET PROPULSION LABORATORY
RESEARCH AND TECHNOLOGY DIVISION
AIR FORCE SYSTEMS COMMAND
EDWARDS AIR FORCE BASE, CALIFORNIA

NOTICES

When U.S. Government drawings, specifications, or other data are used for any purpose other than a definitely related Government procurement operation, the Government thereby incurs no responsibility nor any obligation whatsoever, and the fact that the Government may have formulated, furnished, or in any way supplied the said drawings, specifications, or other data, is not to be regarded by implication or otherwise, or in any manner licensing the holder or any other person or corporation, or conveying any right or permission to manufacture use, or sell any patented invention that may in any way be related thereto.

STUDY AND EVALUATION
OF
SEGMENTED SPHERE PRESSURE VESSELS
PHASE I TECHNICAL REPORT

J. W. FARRELL

This document is subject to special export controls and each transmittal to foreign governments or foreign nationals may be made only with prior approval of AFRPL(RPPR/STINFO).

FOREWORD

The Segmented Sphere Pressure Vessel Study is a design feasibility evaluation conducted by the Missiles and Space Division - Texas (MSD-T), LTV Aerospace Corporation under USAF Contract No. FO 4611-67-C-0040. This work was performed for the Air Force Rocket Propulsion Laboratory, Edward Air Force Base, California under the direction of Mr. Charles H. Richard, AFRPL Project Engineer.

This report documents analyses, design procedures, and study results obtained through completion of the Phase I - Analysis and Design portion of the study program. Continuation effort under this program will include Phase II - Pressure Vessel Fabrication and Phase III - Verification Testing and Performance Evaluation.

Grateful acknowledgment is given for the many important contributions to this study by the following MSD-T personnel: P. M. Kenner and L. S. Howell for programming and evaluating the digital computer solutions; C. E. Rorick for material process and welding consultation; H. T. Armstrong for explosive forming assistance; C. M. Bailey, A. K. Kerekes, and J. D. Vaught for planning and expediting Manufacturing operations; and T. D. Holley for reduction and preparation of Engineering data.

This report has been reviewed and is approved.

Charles H. Richard
AFRPL Project Engineer

ABSTRACT

Two methods of structurally analyzing segmented sphere pressure vessels were developed. The method referred to as "AMC," defines design features to provide a membrane stress state in any segmented sphere system. The second method adapts a digital computer routine "PETS" to solutions of the general stress-strain equations. The results of the more rigorous but cumbersome computer solutions served to validate the AMC method as a simple and accurate design procedure. Process development studies and fabrication trials succeeded in demonstrating good producibility for longitudinally symmetric and toroidal systems. However, manufacture of systems employing segments of mixed diameter was complicated by inability to utilize the standard shell module scheme used in the constant diameter systems. Pressure tests on full scale vessels indicate actual stress-strain conditions are in conformance with membrane theory. A design criteria was developed by parametric exercises with mathematical models. This criteria shows effects and interactions of the many design variables. Dimensioning formulas are explained and demonstrated by example problems.

PRECEDING PAGE BLANK--NOT FILMED

TABLE OF CONTENTS

SEGMENTED SPHERE PRESSURE VESSEL STUDY
PHASE I REPORT

Section 1

Introduction

Section II

Design Selection

Section V

Fabrication

Section VI

Pressure Tests

Section VII

Segmented Sphere Pressure Vessel Design Criteria

LIST OF FIGURES

LIST OF TABLES

LIST OF SYMBOLS

TERM	MEANING
P	internal pressure (psi)
P'	1.0 ksi internal pressure
F	allowable stress (psi)
E	Young's modulus of elasticity (psi)
u	Poisson's ratio
σ	stress (psi)
ϵ	material strain
ρ	density LB/cu.in.
n	design factor
f	band pressure (psi)
N	shell stress (psi)
V	volume (cu. in.)
W	weight (lbs.)
A	rea (sq. in.)
Y	cylindrical radius to sphere and nodal section tangency point (in.)
R	sphere radius (in.)
r	node radius (in.)
$\bar{R}$	mean radius of band inner surface
s	band width
y	cylindrical radius to lowest point of node
t	thickness (in.)
AMC	Achievement of Membrane Conditions
DPO	Design Parameter Optimisation
PETS	Computer Routine for Shells of Revolution

TERM	MEANING
A_s	Meridian Amplification Factor
A_σ	Circumferential Amplification Factor
	Ideal membrane stress (psi)
η (eta)	efficiency index
ψ (psi)	efficiency parameter
ϕ (phi)	node angle (degrees)
λ (lambda)	circumferential angle formed by revolving the radius, "R"
β (beta)	included angle R to any point on sphere, and the axis of symmetry
α (alpha)	special value for β to theoritical point of intersection of spheres (degrees)

SUBSCRIPTS

U	ultimate
Y	yield
B	burst condition
P	proof condition
O	zero pressure
s	meridian directions
σ	circumferential directions
z	radial direction
f	induced by band pressure
f'	induced by 1.0 psi band pressure

SUPERSCRIPT

S	shell
b	band
Sb	shell beneath band
A	point on node with least cylindrical radius to axis of symmetry

SECTION I

INTRODUCTION

1. BACKGROUND

The segmented sphere pressure vessel concept, treated in this study, was conceived in mathematical models (Reference 1). Engineering principles basic to the concept had been validated by laboratory tests conducted on small scale vessels (Reference 2). Weight saving potentialities were shown as derivable from three unique features. These are: spheric geometry for all structural modules, composite material construction utilizing high strength filament wound bands, and optimized band preloads. In addition, shape versatility features a wide choice of segment sizes integrated in shapes for best use of available installation space. In addition to intrinsic attributes of the segmented sphere vessel, significant weight and reliability advantages are to be expected by elimination of inter-connections joining an equivalent cluster of separate vessels.

2. OBJECTIVES

This study is a feasibility evaluation of segmented sphere pressure vessel designs at the technical level of applied research. Objectives are to demonstrate methods of designing full scale high performance hardware and achievement of good producibility features, structural integrity and performance advantages for Aerospace Systems. Towards this end, requirements were foreseen for development of advanced SSPV analyses techniques during this study as well as innovation in manufacturing methods and processes. Engineering models were planned as the proving ground for theory and processes. Complimentary to the evaluation results of the engineering models a Design Criteria was planned as a major product of the Phase I effort. Its purpose is to provide design aides in the form of analyses procedures and data graphs.

3. STUDY APPROACH

A program plan was prepared in Phase I which broke each major work category into detail task descriptions, presented schedules and assigned departmental responsibilities. Major work categories were:

- o Evaluation of materials,
- o Development of analytical methods,
- o Development tests,
- o Design of engineering models,
- o Development of manufacturing processes and tools,
- o Fabrication of engineering models,
- o Assessment of manufacturing problems,
- o Test and evaluation of engineering models,
- o Detail design vessels for fabrication in Phase II,
- o Design Criteria,
- o Phase II Manufacturing Plan,
- o Phase III Test Plan.

The Phase I study approach was planned around mathematical models and engineering test hardware. Engineering models were to be fabricated of the same basic modules which would ultimately make up large systems in Phase II. Evaluations would test newly derived design methodology and checkout fabrication methods.

SECTION II

DESIGN SELECTION

1. MATERIAL CONSIDERATIONS

Maximal performance hardware was not required of this program. Rather, the selected materials and designs should permit meaningful assessment of design theory and SSPV producibility. It was important to select material which would entail minimum risk to completion of design evaluations. However, the added information to be gained by demonstrating minimal weight designs was appreciated and held as a consideration in the formative design stage.

The means of selecting suitable shell and band materials is clear when based solely on material factors, such as: availability, mathematical model ratings, cost, etc. However, suitability is a more comprehensive term. Whether a material was or was not suitable was dependent upon design details of the shell which in turn was subject to formability and producibility tradeoffs.

It was essential that analyses be made with shell material stress allowables and maximum elongations based on 1:1 biaxial tensile load conditions. Applied values are given in Table I.

S-901 glass was the only filament material considered for hardware. This selection was based on preliminary mathematical model data and availability considerations. However, all feasible filament materials, given in Table II, were included in the Design Criteria studies.

2. DESIGN CONSIDERATIONS

a. Engineering Model Criteria

Make or buy decision on components for engineering models was planned for the Phase I preliminary design studies.

Spherical component sizes of 12 inch diameter and 17-18 inch diameter were selected because these dimensions bracketed sizes frequently listed by pressure vessel vendors.

A design operating pressure of 1500 psi was selected in conjunction with a design burst factor of 2.25. These values evolved from the corresponding design burst pressure of 3375 psi which required wall thicknesses based on strength to be in agreement with standard thicknesses of sheet for several candidate shell materials.

In the design of conventional pressure vessels, the Design Proof Factor seldom governs in sizing the structure because yield stress of today's high strength metals is very near their ultimate stress. However,

in SSPV design the ratio of design proof factor to design burst factor does enter into the analyses. It occurs in the optimization of filament band dimensions and preload. Since pressure vessel proof factor criteria varies between agencies and vehicles this SSPV criteria is purposely unspecific on that requirement. Instead, a range of 0.5 to 0.666 is applied as the ratio of design proof to design burst loads.

An additional SSPV criterion, in favor of minimal weight band, permits strains at proof pressure in the shell material underlying the band to differ from other locations and to approach yield.

Design burst pressure is usually the critical load condition and at this pressure it is desirable to design for identical shell stress at all locations. Membrane condition at burst is applied as a third criterion to assure minimum stress amplification from secondary bending at the critical loading.

b. Efficiency of Composite Structure

The mathematical model, described in detail in Section VII, paragraph 2.0, was applied in a preliminary evaluation of candidate materials. Design parameters were based on the previously described engineering models. Figure 1 provides comparison of pressure vessel efficiency indices for several shell materials reinforced by either S-901 fiber glass or boron filaments. In all such data, the term "welded" makes distinction between a continuous shell and shell components welded circumferentially at the location of the filament band. Reductions in maximum shell plastic strain due to welding requires an increase in ring stiffness for strain compatibility of the composite structure. Figure 1 shows that titanium shell designs, with boron or S-901 filament reinforcement are significantly degraded by a weld joint underlying the band. 4340 steel heat treated to 230 ksi is slightly less efficient than annealed 6AL4V titanium in combination with either band material.

c. Ductility Requirements of Shell Material

Table III summarizes published fracture toughness data on candidate shell materials. The index (K_{c1}/F_u^6) indicates maximum percentage of ultimate tensile strength for design of pressure shells having a reasonable tolerance to crack like flaws. Annealed 6AL4V titanium, 2014-T6 aluminum and 301 stainless steel appears to offer low risk of premature structural failure for pressure shells working near material ultimate tensile stress conditions.

d. Material Availability

A preliminary survey on availability of sheet stock in the thickness range of .050 to .100 inches indicated all materials except maraging steel could be delivered within 2 to 3 weeks from date of order. Maraging steel sheet required mill order with a 9 to 12 week delivery time.

TABLE I MATRIX OF MATERIAL AND GEOMETRY PARAMETE

39.45 PERCENT EPOXY BY VOLUME

TYPE FILAMENT	SSPV BAND PROPERTIES		
	ULT PSI TENSION	YOUNG'S MODULUS PSI X 10^{-6}	DENSITY LB/IN^3
S 901 GLASS (1)	205	9.00	0693
BORON	175.65	42.66	068
THORNEL 25	79.045	17.90	050
S 901	205	9.00	0693
THORNEL 50	146.38	35.58	050
970-S 36 AEROJET GENERAL	251.77	10.76	.071
STEEL	263.48	17.75	188
SILICON CARBIDE	130.00	44.4	.085
BERYLLIUM	63.25	25.44	.058

SHELL ALLOY	CONDITION	ULTIMATE STRESS TENSILE PSI		TENSILE MODULUS PSI X 10^{-6}	P R
		YIELD			
4340 STEEL		230	270	30.0	
MARAGING STEEL	900°F AGED	300	305	30.0	
6AL-4V TITANIUM	ANNEALED	152	168	17.0	
301 STAINLESS	FULL HARD	210	240	30.0	
17-7 ST	PH	225	230	30.0	
6AL-4V TITANIUM	ANNEALED	152	168	17.0	
6AL-4V TITANIUM	ANNEALED AS WELDED	118	145	17.0	
2014 ALUMINUM	T-6	62	66	10.5	
	T-6 WELDED	40	48	10.5	
MARAGING STEEL	800°F AGED	282	287	30.0	
$5Cr_4Mo_1V$ (H-11) STEEL		232	240	30.0	
	WELDED	240	304		

NOTES:

(1) BASED ON TEST DATA PRESENTED IN TABLE V.

LE I MATRIX OF MATERIAL AND GEOMETRY PARAMETERS

L OY	CONDITION	1:1 BIAXIAL STRESS TENSILE KSI YIELD	1:1 BIAXIAL STRESS TENSILE KSI ULT	PROPERTIES TENSILE MODULUS PSI X 10^{-6}	PROPERTIES POISSON'S RATIO	PROPERTIES ELONG. IN/IN	ρ LBS/IN^3
EL		230	255	30.0	0.3	.030	.28
AGING EL	900°F AGED	300	305	30.0	0.3	.012	.28
-4V NIUM	ANNEALED	152	168	17.0	0.3	.035	.16
NLESS	FULL HARD	216	240	30.0	0.3	.060	.28
ST	PH	22[illegible]	230	30.0	0.3	.018	.28
-4V NIUM	ANNEALED	152	168	17.0	0.3	.035	.16
-4V NIUM	ANNEALED AS WELDED	118	145	17.0	0.3	.020	.16
	T-6	62	66	10.5	0.3	.025	.10
INUM	T-6 WELDED	40	48	10.5		.010	.10
AGING L	800°F AGED	282	287	30.0	0.3	.020	.28
V)		232	240	30.0	0.3	.025	.28
L	WELDED	240	304				

OPERATING PRESSURE PSI	n_p/n_B	SEGMENT ANGLE α DEGREES
1500	.666	10
		20
		30
		45
		55
		65
		75
		85
	.500	65
2375	.666	45
		55
		65
		75
		85
	.500	65
3250	.666	45
		55
		65
		75
		85
	.500	65
4125	.666	45
		55
		65
		75
		85
	.500	65
5000	.666	45
		55
		65
		75
		85
	.500	65

1500	.666	65
	.500	
2375	.666	65
	.500	
3250	.666	65
	.500	
4125	.666	65
	.500	
5000	.666	65
	.500	

2

TABLE II PROPERTIES OF UNIDIRECTIONAL FILAMENT WOUND COMPOSITES

Filament	Source	Filament Strength (psi)	Composite Density (lb/cu in)	Composite Tensile Strength (psi)	Composite Modulus of Elasticity (psi x 10^{-6})	Status of Development
E-Glass		270,000	0.076	182,000	7.03	Commercial production; state-of-the-art material.
S-Glass	U. S. Air Force/ Owens-Corning	350,000	0.073	234,000	8.30	Commercial production state-of-the-art material.
4-Hl Glass	U. S. Air Force/ Aerojet-General	380,000	0.076	256,000	9.35	Experimental.
Hi-Stren	Aerojet-General	390.000	0.075	262,000	9.07	Pilot plant production for specialized use.
970-S 36 Glass	U. S. Air Force/ Aerojet-General	430,000	0.075	289,000	10.01	Experimental.
Steel		450,000	0.199	292,000	18.83	Commercial production state-of-the-art material.
Beryllium	Brush Beryllium/ Beryllium Co. of America	150,000	0.058	97,500	29.25	Pilot plant.
Boron	U. S. Air Force/ Texaco Experiment	300,000	0.071	195,000	39.00	Production for laboratory research and specialized use for prototype production.
Graphite:	U. S. Air Force/ Union Carbide					
Thornel 25		135,000	0.051	88,000	16.25	Pilot plant production for specialized use in laboratory production.
Thornel 50		250,000	0.051	164,000	32.50	
Carbon	U. S. Air Force/ U. S. Navy/ Union Carbide	128,000	0.051	83,000	3.9	Pilot plant production
Silicon Carbide	U. S. Air Force/ General Technologies	200,000	0.090	130,000	45.5	Pilot plant production.

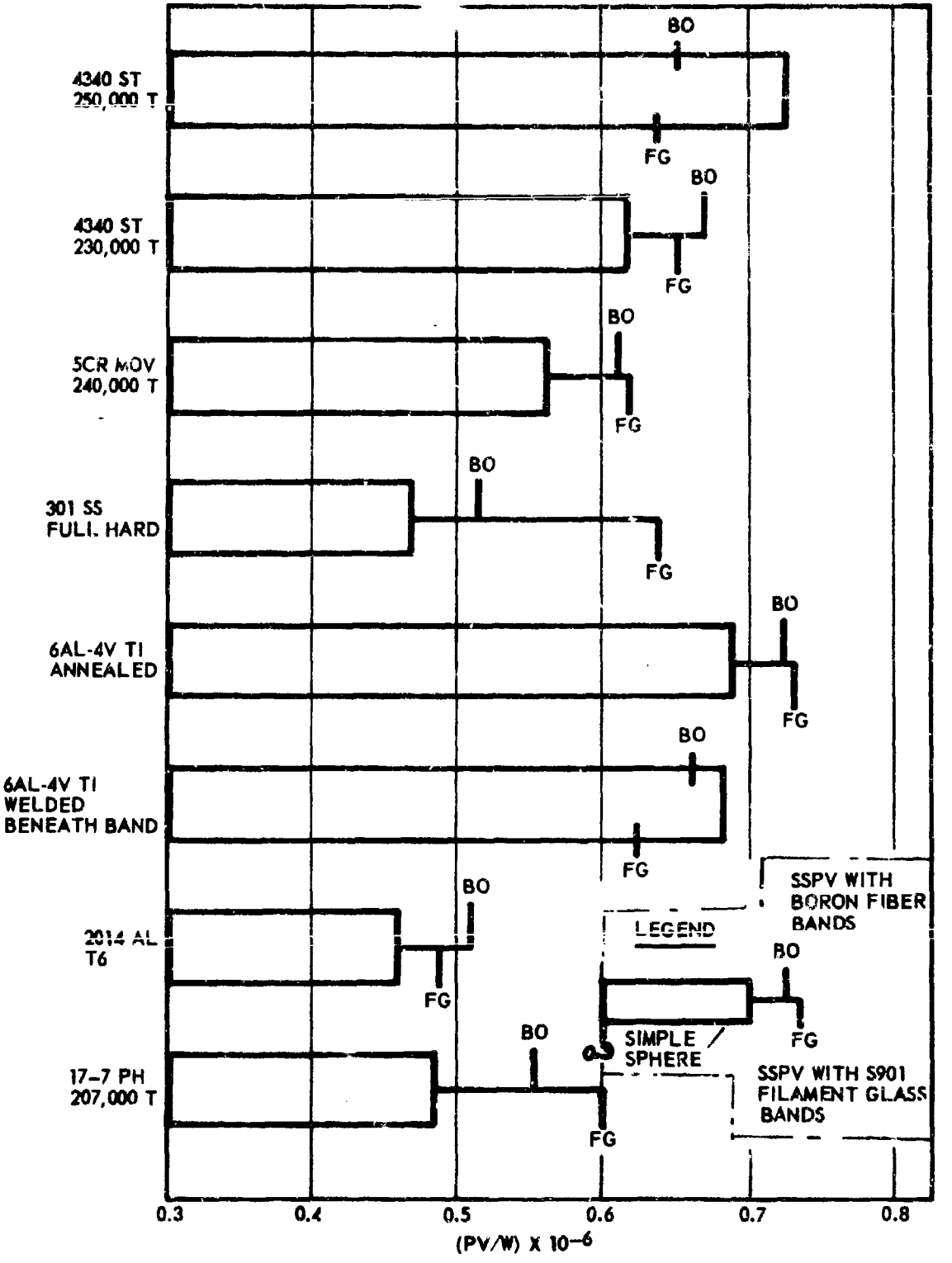

FIGURE 1 COMPARISON OF MATERIAL PRESSURE VESSEL EFFICIENCIES

TABLE III - FRACTURE TOUGHNESS OF SHELL MATERIALS

Material	Condition	1:1 Biaxial Stress F_{tu} (ksi)	Fracture Toughness K_{Ic} (ksi $\sqrt{in.}$)	Pressure Vessel Flaw Tolerance Index K_{Ic}/F_{tu}^{2} ($\sqrt{in.}$)
6AL4V,Ti(1)	Annealed	168	160	.96
301,Stainless(1)	Full Hard	230	190	.82
5CR4V,Steel(2) H-11	H.T.	280	50	.17
5CR4V,Steel(2) H-11	H.T.	250	80	.32
2014,Aluminum(2)	T-6	66	60	.90
4340,Steel(3)	H.T.	250	111	.44
AM 355,Stainless(3) 17-4 Stainless	H.T. & Aged	235	160	.68
Maraging Steel(4) 18N-CO-MO	H.T.	305	120	.39
Maraging Steel(4) 18N-CO-MO	H.T.	280	150	.53

(1) RTD-TDR-63-4094
(2) ASD-TDR-62-401
(3) NAEC-AML-2111
(4) ASM-SIA Q26,1-54

Inquiries were made to four prominent pressure vessel vendors on time and cost of supplying hemispheres or welded spherical vessels in a size near 12 and 18 inch diameters. Exact dimensions were left open to the vendor for adaptation of existing tooling. All vendors declined bidding on delivery of dimensioned hemispheres. Only one vendor indicated an interest in manufacturing spherical vessels to customer drawings.

Inquiries were also made to vendors on supplying forged hemispheres. Such forgings would be machined to thin shells at MSD-T. Again exact dimensions of forgings were to be decided by existing vendor tooling in the 12 to 18 inch diameter range. One vendor made an acceptable time cost quote on the basis of available tooling. However, in follow up to consumate a firm bid this vendor escalated delivery time and costs beyond the scope of this study. The choice of buying components was reduced to possible procurement of welded spheres from one vendor.

e. Modular Design

During a preliminary design study, modules in the form of purchased spherical vessels was considered undesirable due to the need of cutting equator welds, fabricating a node joint and rewelding equators in the process of assembling Phase II SSPV systems.

Design requiring circumferential weld joints at the node location caused low pressure vessel efficiencies. It then became certain that new design of shell components was justified and producibility would be greatest by employing basic shell modules. An hour glass module was attractive since the node would be part of the integral shell. Also, the same module could be trimmed to assemble both in-line and toroidal systems.

f. Design Study Parameters

Tables I and IV present the independent variables pertinent to parametric study of SSPV designs. This data includes the particular values pertinent to the selection of materials and geometry for study hardware.

The matrix of Table I defines the Design Criteria variations in materials, geometry and load.

Table IV identifies dimension parameters which must be optimized to achieve a pure membrane stress state in the shells.

3. MANUFACTURING CONSIDERATIONS

a. Formability

A review of previous MSD-T formability studies showed candidate materials (Reference Table I) were acceptable for SSPV fabrication. A ranking of materials in the expected order of increased forming difficulty was:

TABLE IV MATRIX OF DIMENSION PARAMETERS

		PHASE II DESIGNS (1)		PARAMETRIC STUDY
		CLASS I – II	CLASS III	
MATERIAL	GENERAL			✓
	6AL 4V TI	✓	✓	
	17–7 STAINLESS STEEL	✓	✓	
LOAD RANGE	ELASTIC	✓	✓	
	PLASTIC	✓		
GEOMETRY r/R, Y/R	GENERAL			✓
	ARBITRARY	✓		
	OPTIMUM		✓	
SHELL LOAD MAGNITUDE t/R	GENERAL			✓
	SPECIFIC	✓	✓	
BAND LOAD MAGNITUDE A_b, F_O	GENERAL			RANGE GIVEN IN TABLE III
	OPTIMUM	✓	✓	

NOTES:

(1) PHASE II DESIGN CONFIGURATIONS ARE PRESENTED IN SECTION II FIGURES 4, 5, AND 6.

- o 301 stainless steel
- o 17-7 PH stainless steel
- o Maraging Steel
- o 2014 aluminum alloy
- o 4340 steel
- o E-11 tool steel
- o 6AL-4V titanium alloy

301 stainless was the most ductile but was least desirable because the high strength phase required cold working after assembly. Titanium was rated most difficult because prior MSD-T experience in forming 6AL-4V alloy hemispherical pressure shells (Reference 3) established a need to work the material at temperatures above 900°F. Also, LTV explosive forming studies showed 6AL-4V titanium to be a difficult to work material due to the ratio of yield to ultimate stresses near unity. This caused springback and a susceptibility to rupture.

Considered forming processes relevant to metal parts were ranked in the order of increasing risk as follows:

Hemispheres

- o Machine from forged hemispheres
- o Draw form
- o Shear form from pancake forging

Cylindrical Blank for Nodal Shell

- o Extrude
- o Rolled and seam joined sheet by solid state bonding or fusion welding
- o Shear form from pierced forging

Nodal Shell

- o Expand to female die by explosive forming
- o Reduce to male die by shear forming
- o Reduce to male die by capacitor discharge
- o Stretch form segments of circle and seam weld.

Shear forming was considered undesirable due to prior experience wherein extensive time and materials were required to develop critical controls unique to each design. In addition, a 60 day procurement time for special pancake and pierced forgings was unacceptable because possible forging changes during part development would require reorders.

Extrusion of cylindrical blanks was investigated and found attractive for aluminum and titanium materials. However, a six month delay entailing development of special extrusion dies made the process unsuitable for this program.

Reduction of cylinder diameter, at the nodal section, by shear forming on a male die was considered. This method entailed a high risk of metal fatigue because of tendency to chase a compression wave ahead of the forming rolls.

Reduction of cylinders by high energy forming through capacitor discharge appeared well suited to the desired nodal shape. However, the process was not currently available as a ready production method.

Machining hemispheres from forgings was recognized as a low risk method primarily suited to small production quantities, contingent upon existence of suitable forging dies. Vendors with existing tools in the 12 and 18 inch diameter range could not be found.

Solid state bonding of rolled sheet was attractive but required development expenditures beyond the scope of this study. Fusion welding could be applied as a fore-runner of solid state bonding.

The above considerations eliminated all but the following:

- o Draw form hemispheres
- o Roll and seam weld cylindrical blanks
- o Explosive form nodal shell for Class II
- o Draw form circular segments of the nodal band for Class III and seam weld.

b. Material Weldability

Considered fusion welding methods were Hand TIG, Automatic Machine TIG and Electron Beam Welding. A single preference for a candidate shell material could not be decided on the basis of weldability. MSD-T's successful experience with all of the materials has shown need for equally stringent process control and inspection procedures.

Solid state or diffusion bonding was investigated both for study hardware and future SSPV production. Investigation of vendor sources for electron beam service led to the conclusion that application to SSPV designs was feasible. However, necessary development of special equipment and experimentation to optimize time-temperature-pressure relation placed the process in applied research and beyond the schedule and cost allowances of this study. The present state-of-the-art does justify retention of the process in production plans for maximal performance SSPV designs. With this long range objective in mind, 6AL-4V titanium becomes singularly attractive because of its low temperature response to solid state bonding.

c. Tooling Considerations

Regarding forming of shell components by shear forming, draw forming and explosive forming, all pertinent tooling was ordinary to MSD-T tool design fabrication activities. Shear form and draw forming tools on hand

could be adapted to the SSPV designs. A successful explosive die design was on hand from previous manufacture of SSPV shells in a 6.0 diameter range. Consequently, a larger scale copy of that design offered a minimum effort minimum risk approach. The only uncertainty concerned the explosive forming of seam welded titanium tubing. It appeared probable that tooling complications would develop such as provision for explosively forming at elevated temperatures.

All anticipated trim and weld fixtures were of conventional nature.

Methods of winding filament bands on the toroidal vessel (Class II design for Phase II) presented a new problem. The existing winding lathe had insufficient throw to wind the torus in all hand winding positions.

Straightforward solutions considered:

- o Development of a multi positioning fixture in combination with a gap lathe.
- o Development of a planetary winding device.

Novel approaches were:

- o Prewind bands and position on module blank before explosive forming.
- o Wind modules after explosive forming but prior to welding into the vessel assembly.

The first and fourth method appeared to offer minimum development risks. Feasibility of the fourth method would depend on trials wherein attempts be made to protect the band from over heating during welding. Critical location would be at the inside torus radius where weld and band center lines nearly converge, (Reference Figure 5).

4. DESIGN SELECTION

a. Material Properties

The pressure vessel efficiency index for annealed 6AL-4V titanium alloy in combination with S-901 filament glass is in the highest bracket between .7 and .8 (Reference Figure 1).

Whether an efficiency gain would result from heat treatment of the titanium is uncertain. Biaxial stress strain data for the 6AL-4V in the high strength phase was not available for application to the mathematical models. However, it is expected that reduced elongation would penalize the band weight more than enough to offset the small decrease in shell weight. Less desirable is the tendency toward brittle failure in pressure vessel usage when material elongation is less than 3 percent. A marginal situation appears to have already been reached with the annealed condition when one considers that under 1:1 biaxial loading a measured maximum elongation of 3.5 percent is a significant drop from the 13 percent measured under uniaxial stress.

Pressure vessel manufacturers have felt the impact of this phenomenon of large ductility loss under biaxial load conditions, in experiences of unreliable strength due to extreme sensitivity to vessel surface scratches and minute manufactured imperfections.

A survey of pressure vessel vendors conducted during this study suggests a practical upper limit of 180 ksi uniaxial ultimate tensile for 4340 and 200 ksi for maraging steels. At these strengths steel is not weight wise competitive with titanium in SSPV designs. These values would correspond to approximate 1:1 biaxial values of 218 ksi and 230 ksi respectively. The values of biaxial UTS of 253 ksi for 4340 and 305 ksi for maraging steels used in this study represent the more optimistic opinions of the industry. At these levels steels are competitive with titanium but they must be recognized as high risk materials.

Maraging steel displays another strain characteristic which appears to be unsuited to thin wall pressure vessels. The distinction between thin and thick wall designs is important because the material was developed as a pressure vessel material where deep hardening characteristics are important. A peculiar property of this material is observed in its stress strain diagram. Once ultimate tensile is reached the material strength continues to drop off with increased elongation (Reference Figure 2). These post ultimate stresses are measurable only under laboratory conditions where the applied load is also proportionally reduced. This is the loading situation of a tensile testing machine where the mechanism introduces a steady strain rate. Under dead weight loading of a tensile coupon the specimen would give way at the instant ultimate stress was reached. The dead weight example is analogous to the steady pressure loading of a thin shell. This rationalization is supported by 1:1 biaxial stress strain curve for maraging steel shown in Figure 3, where plastic elongation is very small relative to the uniaxial strain as shown in Figure 2.

The above considerations led to the selection of 6AL-4V as the preferred material for SSPV hardware for this study.

b. Material Availability

A preliminary survey of titanium suppliers indicated that heat treated 6AL-4V sheet, in standard gages between .063 and .125 could be located in warehouse stocks and delivered within 3 to 4 weeks from ordering date. The desired annealed condition could only be procured by mill order with a 3 to 4 month normal delivery time.

It was therefore planned in the Phase I effort to anneal received material and requisition Phase II material with sufficient lead time to permit mill order.

In the course of the design development the required sheet thicknesses was frozen at .071 and .100 inches.

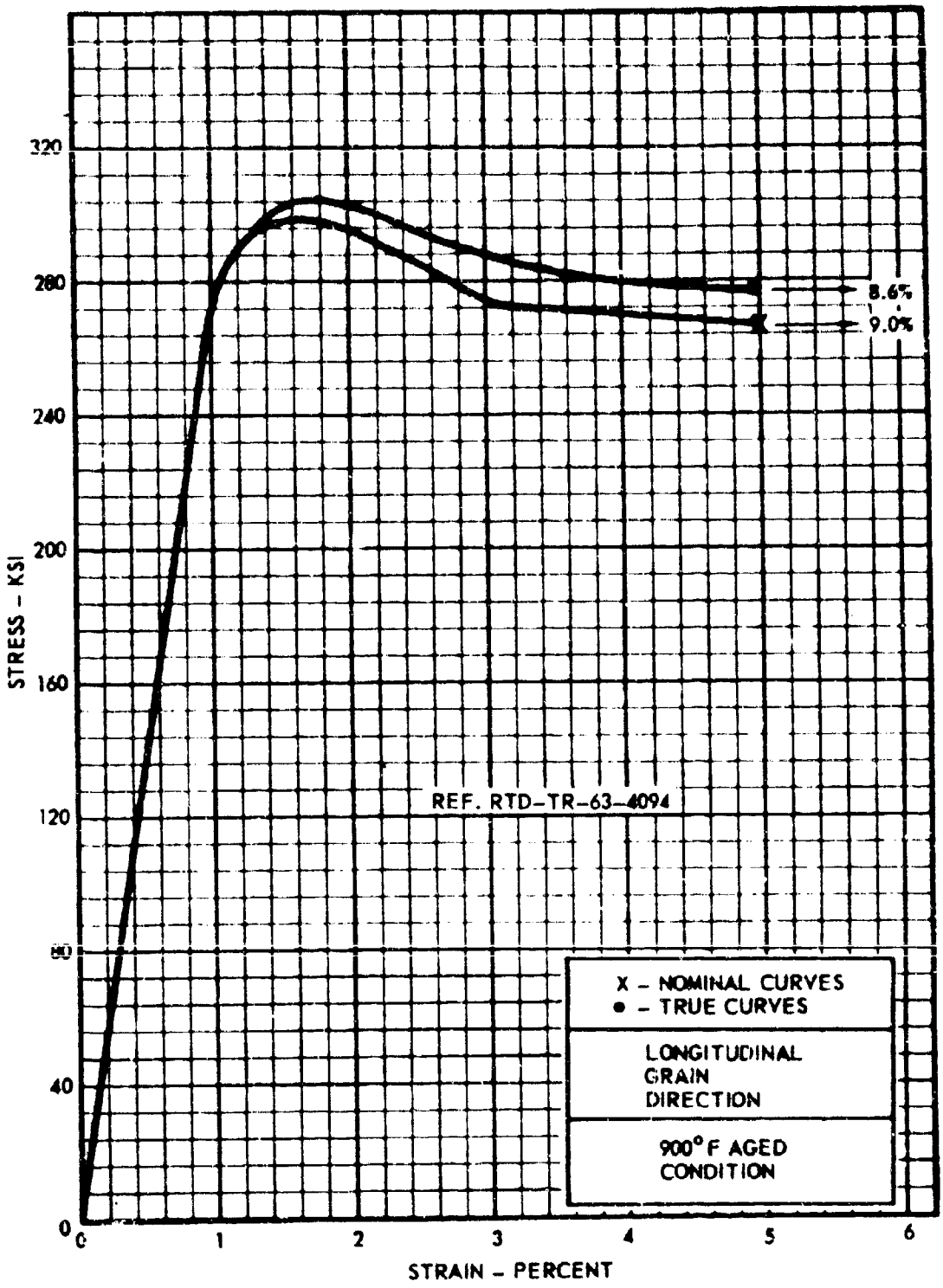

FIGURE 2 MARAGING STEEL UNIAXIAL STRESS–STRAIN CURVES

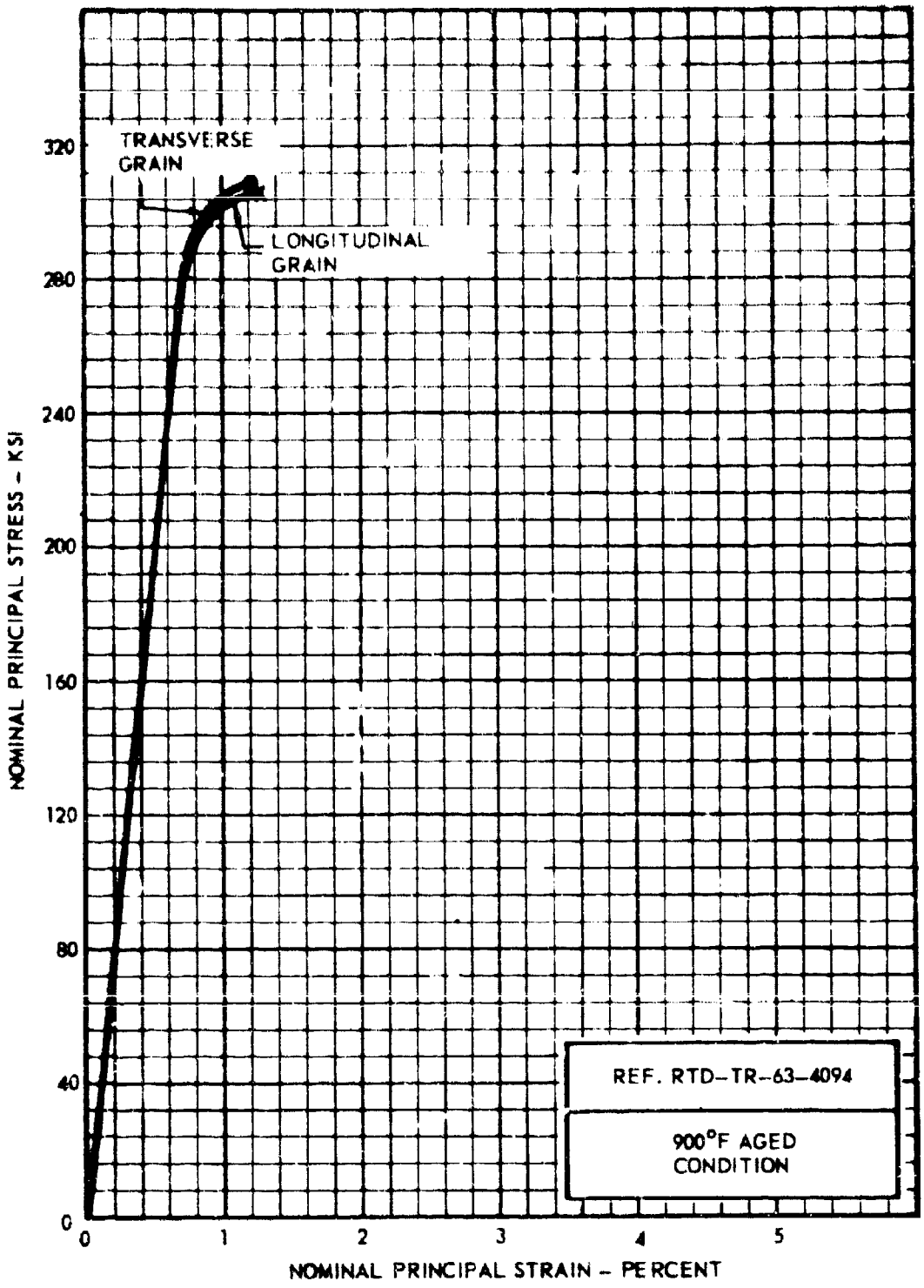

FIGURE 3 MARAGING STEEL STRESS RATIO BIAXIAL STRESS–STRAIN CURVES

A sufficient supply of .071 material was collected by series of small shipments which barely kept pace with development test and fabrication requirements.

However, early orders on .100 sheet remained unfilled. There was no prospect of the situation changing. This procurement problem affected the Class III configuration hardware only. Fabrication planning was then shifted to machining the Class III 17 inch shells from hemispherical forgings on the strength of an eight week delivery quote by one vendor. Other sources were prohibitive due to large time and cost provisions for fabrication of forging tools. Confirmation was asked and received with the vendors statement that proper forging dies were on hand. However, upon receipt of MSD-T's purchase order the vendor revised costs and schedules in a manner incompatible with this study. The vendor could not deliver because tooling would have to be developed after all.

At this point it was clear that a material change was necessary if the study was to benefit from Class III engineering model design and fabrication experience. A preliminary analysis indicated a reasonable engineering facsimile of the titanium Class III vessel could be produced by using 17-7 PH steel sheet and by dropping the gage one step. This material was readily available and was accordingly introduced into the Class III engineering model design.

c. Design Producibility Considerations

An important evaluation in the design feasibility study concerned the producibility of SSPV hardware. The design philosophy should give credence to practical manufacturing methods, few components and well controlled tolerances.

A second criterion - avoidance of circumferential welds underlying the band - came about as a result of material efficiency comparisons with mathematical models.

Preliminary design studies demonstrated that a large family of systems of constant diameter could be assembled from two basic modules. These are an explosive formed shell in the shape of an hour glass and a hemisphere end closure. Class I and II vessels of this study are included in that family. Variations in trimming these explosive-formed-modules provides versatility in shape of the system. Modules would be welded to each other such that their intersections describe a great circle. This would allow a choice of assembly shapes. System centerline could be axis symmetric, disjointed or follow any curve. Yet in this assembly each segment operates in the stress state of a simple sphere.

The end closure of these systems would be accomplished by use of a frustrum of a hemispherical shell. This intersection need not be on a great circle.

Ideally the cylindrical blank for this explosive formed module would be provided as extruded seamless tubing or as rolled sheet solid state bonded at the seam. As an intermediate approach it would be expeditious to fusion bond rolled sheet.

The Class III system did not lend itself as well to so few parts. In theory, membrane conditions could be achieved by simply intersecting and joining two different size spherical shells provided the nodal band restraint could be concentrated as a line load in the intersection plane. Since the physical band occupies a finite width it appeared advisable to provide a transition section. This transition section could be a ring with a cross section profile forming a valley and medium line of the sides sloping to a point of tangency with each adjoining sphere. These points of tangency would define the intersection joints.

This transition ring could be easily shaped in cross section by shear spinning or by explosively forming a short length of seamless tubing. Seamless tubing being unavailable within the time span of this contract made it necessary to resort to sheet stock and one or more seam welds. The simplest method was judged to be that of stretch forming two arc sections of the transition ring and joining by fusion welding.

From a producibility viewpoint it would be highly advantageous to filament wind bands on the explosive formed segments before welding into the assembly. This approach would standardize the winding method for the entire family which included Class I and II systems. Further, the reinforcing bands of complete toroids could be wound without need of special planetary or shuttle winding machines. This method could be adapted to Class III vessels by increasing the width of the transition section beyond the tangency points with the adjoining spheres. This would cause the weld joint to be displaced from the band which for structural reasons is bounded in width by the tangency locus. However, widening the band would increase severity of the cross section forming to a degree possible only by shear forming or explosively forming seamless tubing. It was therefore planned that Class III vessels fabricated in this study would be wound after weld assembly.

d. Vessel Configurations

The three basic SSPV configurations to be designed and tested were defined by the Air Force as:

- o Class I Longitudinally Symmetric System (Reference Figure 4)
- o Class II Toroidal System (Reference Figure 5)
- o Class II Combined System (Random) (Reference Figure 6)

Size for the basic spherical segments was selected through manufacturing considerations as: 12 inch diameter for Classes I and II, 12 and 17 inch diameters for Class III. Definitive details to be found by analyses and design studies were:

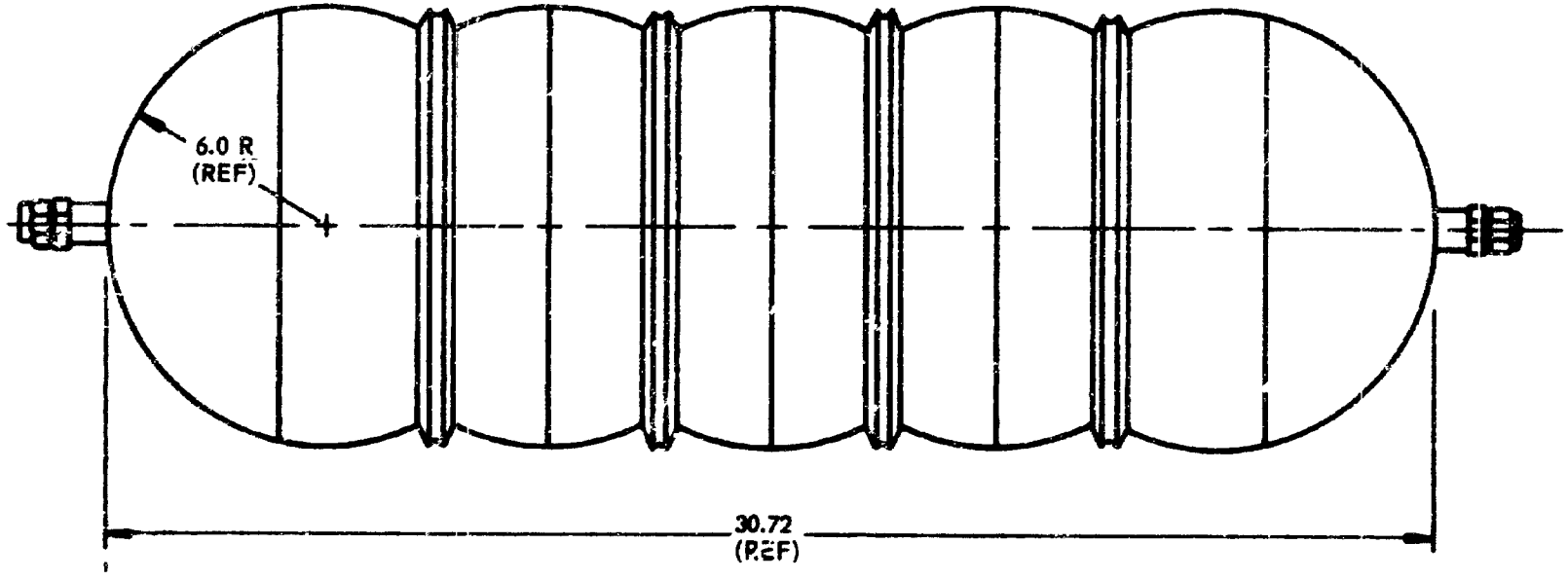

FIGURE 4 CLASS I VESSEL GEOMETRY

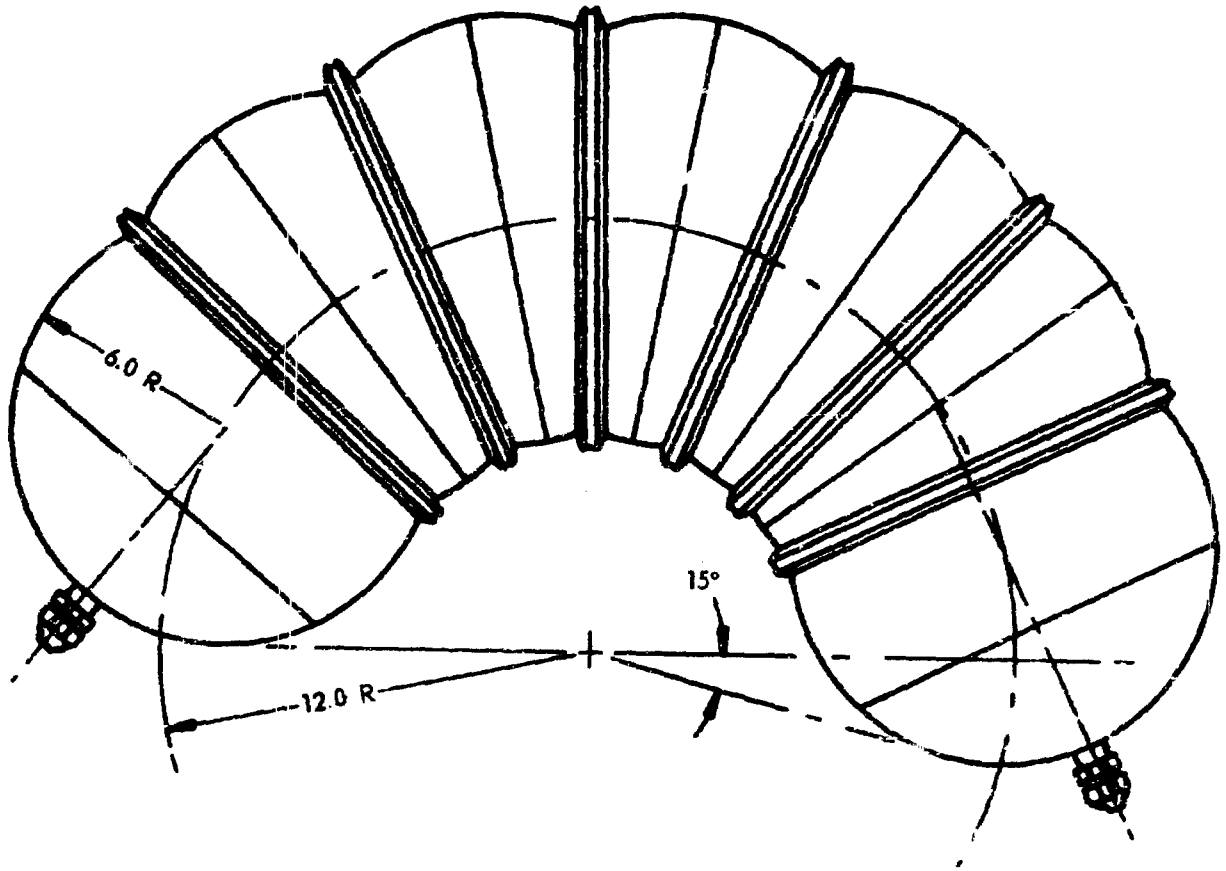

FIGURE 5 CLASS II VESSEL GEOMETRY

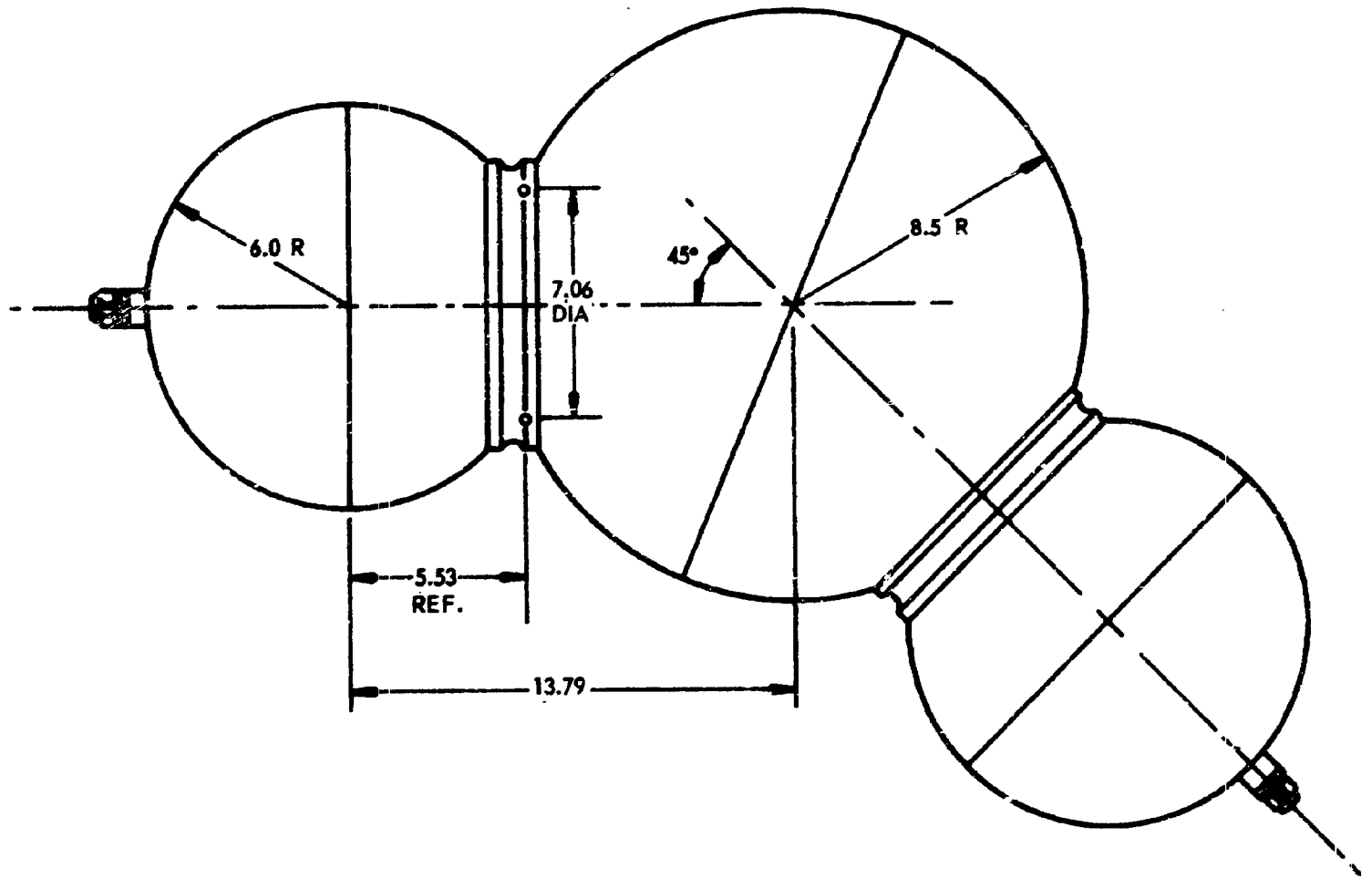

FIGURE 6 CLASS III VESSEL GEOMETRY

- o Ratio of transition ring radius to spherical radius
- o Shape and size of nodal transition section (Y/R)
- o Shape and size of the filament wound reinforcing band
- o Magnitude of the filament band preload
- o Major radius of torus (Class II system)
- o Necessity of weld lands

Preliminary mathematical nodal data showed pressure vessel efficiency increased with increased segment angle (α), where: $\alpha = \sin^{-1}(Y/R)$. Small improvement in efficiency was shown for segment angles greater than 65 degrees. On this basis $\alpha = 65°$ was selected as an approximate design condition for Class I and II systems. The precise value was determined by design lay-out studies. A nodal radius of 1.0 inch was used since smaller radii appeared to be too severe for explosive forming.

Selection of the segment angle for the Class III vessel required layout study to establish the influence of (α) on the physical properties of the transition section. It was desirable for structural reasons to develop a transition section which would be tangent to both the 12 and 17 inch sphere at the same cylindrical radius. The particular transition geometry chosen for the Class III design was one of several known to satisfy the common cylindrical radii condition.

Band area was determined by two analysis methods. It is clear from both methods that the band width should stop at the tangency loci between the transition section and the adjoining spheres. Equations have been developed in the AMC method defining how band depth should vary along the transition zone width in order to preserve membrane stress conditions. These equations were the source of band shape definition for all three class systems.

By analyses, the required band cross section area decreased as prestress increased. Selection of the filament band preload was decided at 40 to 45 ksi filament tension. It was believed this represented an upper limit beyond which filament fraying would be troublesome during winding. However, fraying did not develop as a problem. No evidence of shell buckling was observed for engineering models wound at the 40 ksi prestress. In so far as maximum working stress of the S-901 filament glass, a prestress of 90 ksi could be used before band ultimate allowable stress would be approached under combined condition of prestress and design burst pressure.

The major radius of the torus design for Class II systems was based on a minimum for 12 inch spherical segments which would provide sufficient space for chill bars to protect the bands against overheating during welding of the prewound segments.

It was uncertain whether lands would be required along the seam welds of the tubular blank to avoid weld failure during explosive forming. This decision was left to development tests wherein weld lands were found not required for forming purposes. To achieve uniform vessel strength,

weld lands are commonly used to compensate for strength loss in the heat affected zone. However, since localized thinning of unknown amount would occur during forming of the shells, design of the lands was delayed until completion of engineering model thickness measurements.

e. Engineering Models

The engineering models were configured to duplicate the segment joints and the nodal zone details for the three design configurations.

It can be assumed that adjoining sections, wherein each section is taken with the band centered, have identical stress fields. Therefore, one such section with hemispherical end closures represents the complete structure of the larger system.

Engineering model Class (I and II) was designed as a prototype of the axis symmetric and toroid systems. Engineering model Class III represented the combined or random system. (Reference Figures 7 and 8)

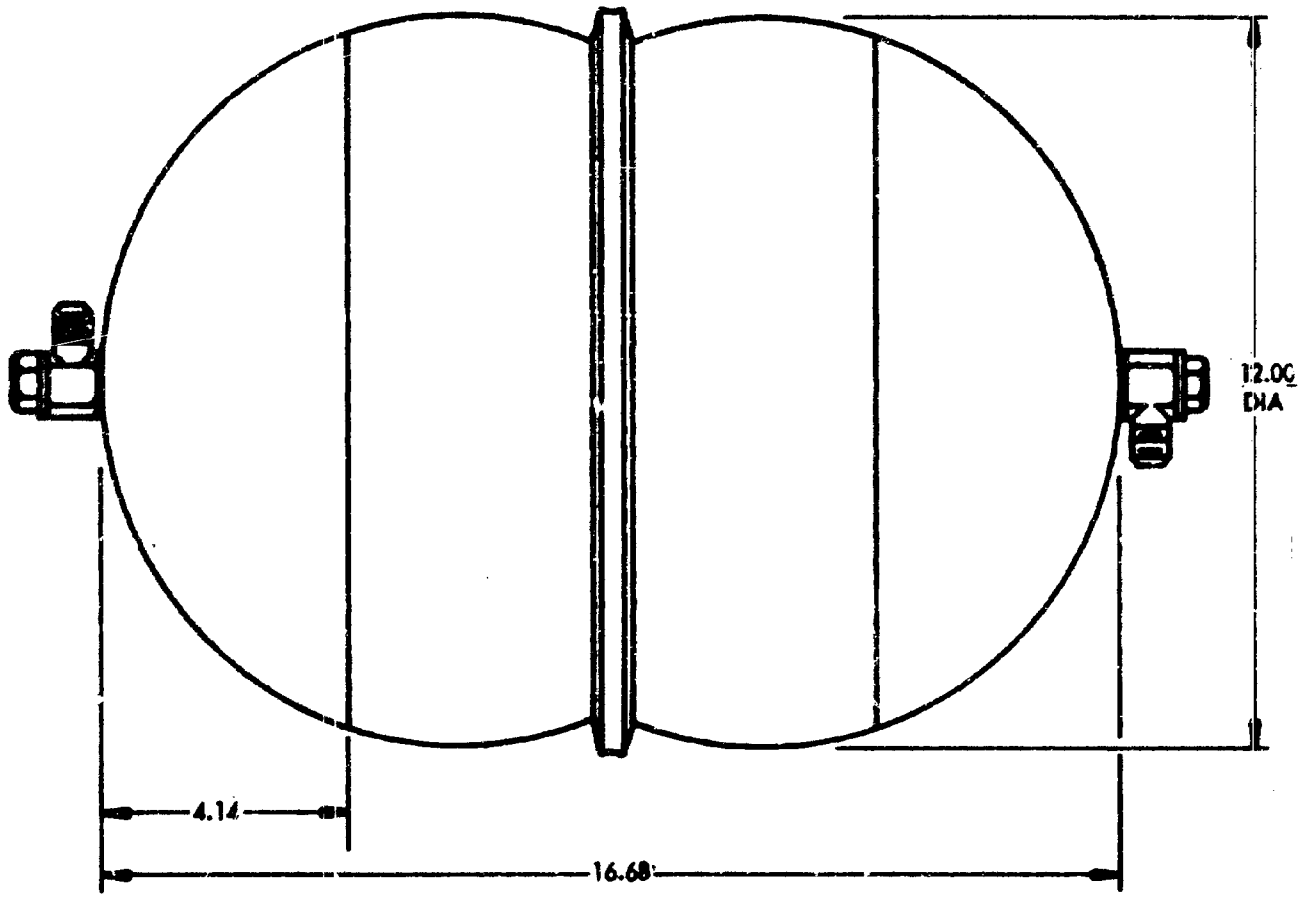

FIGURE 7 CLASS I - II ENGINEERING MODEL

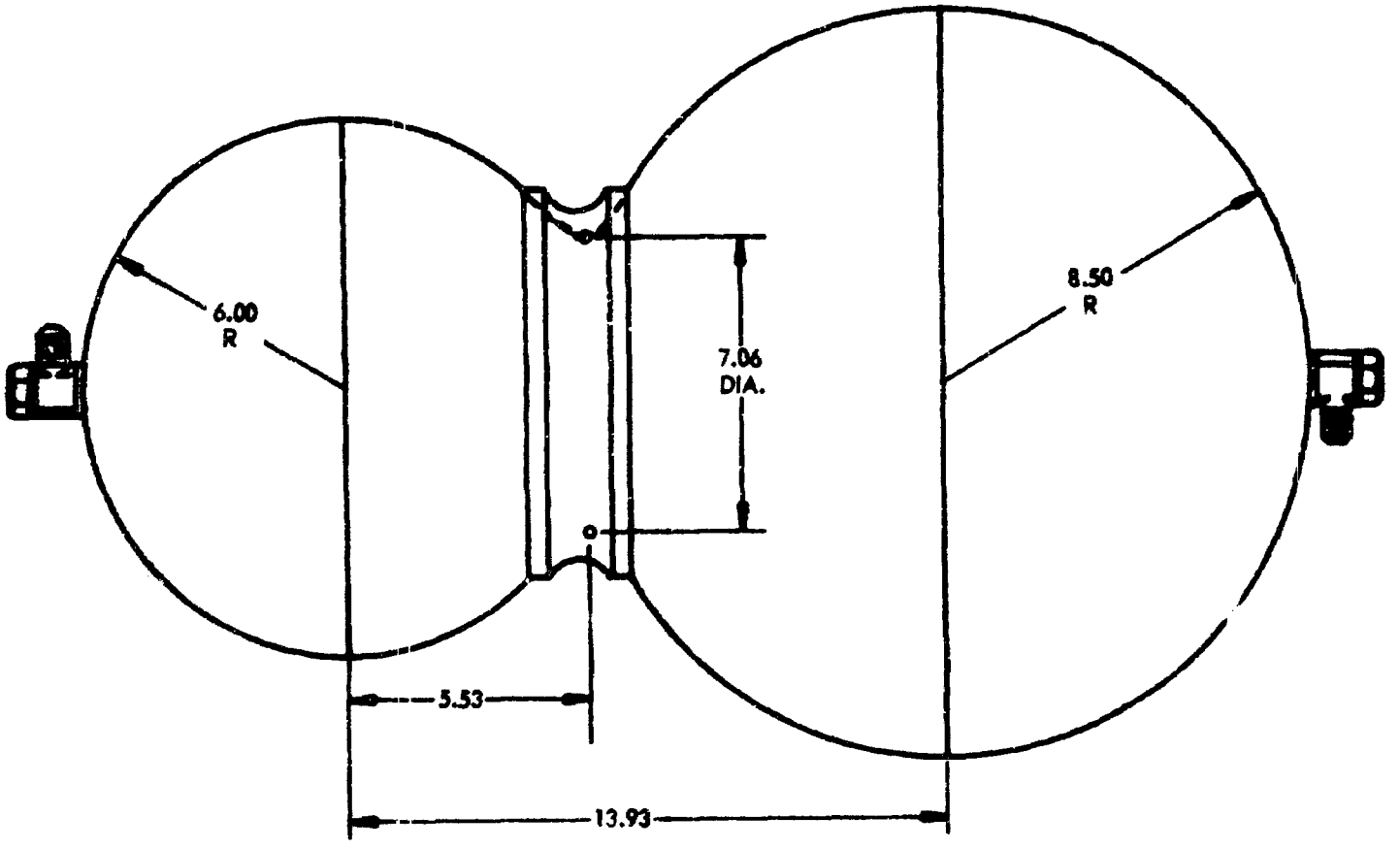

FIGURE 8 CLASS III ENGINEERING MODEL

SECTION III

DESIGN OF ENGINEERING MODELS

1. DESIGN OPTIMIZATION BY AMC METHOD (REF. SECTION VII, PAR. 3.0)

a. Band Load Distribution

The ratio of band pressure to internal pressure is computed by use of Equation 1.1 from Section VII paragraph 3.

$$f/P = \frac{1}{2}\left(2 + (r/R)^{-1} - \frac{\cos\phi}{(1 + r/R)\,Y/R - r/R\,\cos\phi}\right) \qquad (1.1)$$

Governing geometric parameters for the Class (I and II) vessel, given in Figure 9, are:

$Y/R = 0.9450$ $\quad r/R = 0.1666$ $\quad$ Maximum = 19.5°

Applicable parameters for Class III vessels are based on geometry of Figure 10, which are:

Large Segment	Small Segment
$Y_1/R_1 = 0.4848$	$Y_2/R_2 = 0.6867$
$r_1/R_1 = 0.1666$	$r_2/R_2 = 0.2739$
ϕ_1 max = 60°	ϕ_2 max = 46.6°

b. Design of Engineering Models

A. Class (I - II)

Using 6AL-4V titanium annealed shell material and the S-901 fiber glass wound band, the following conditions are used in the analysis for the design:

F_o = 40,000 psi

t (nominal) = 0.070 in.

t (min) = 0.060 in

$$P_B = \frac{2\,t\,(min)\,\sigma_U}{R} = \frac{(.120)\,(168{,}000)}{5.9615}$$

$$= 3381.7 \text{ psi (no reduction for inefficiencies)}$$

$$\varepsilon_P^{Sb} = \sigma_Y^S\,(1 - u)/E^S + 0.002$$

$$= ((152 \times 0.7) - 17)\,10^{-3} + 0.002$$

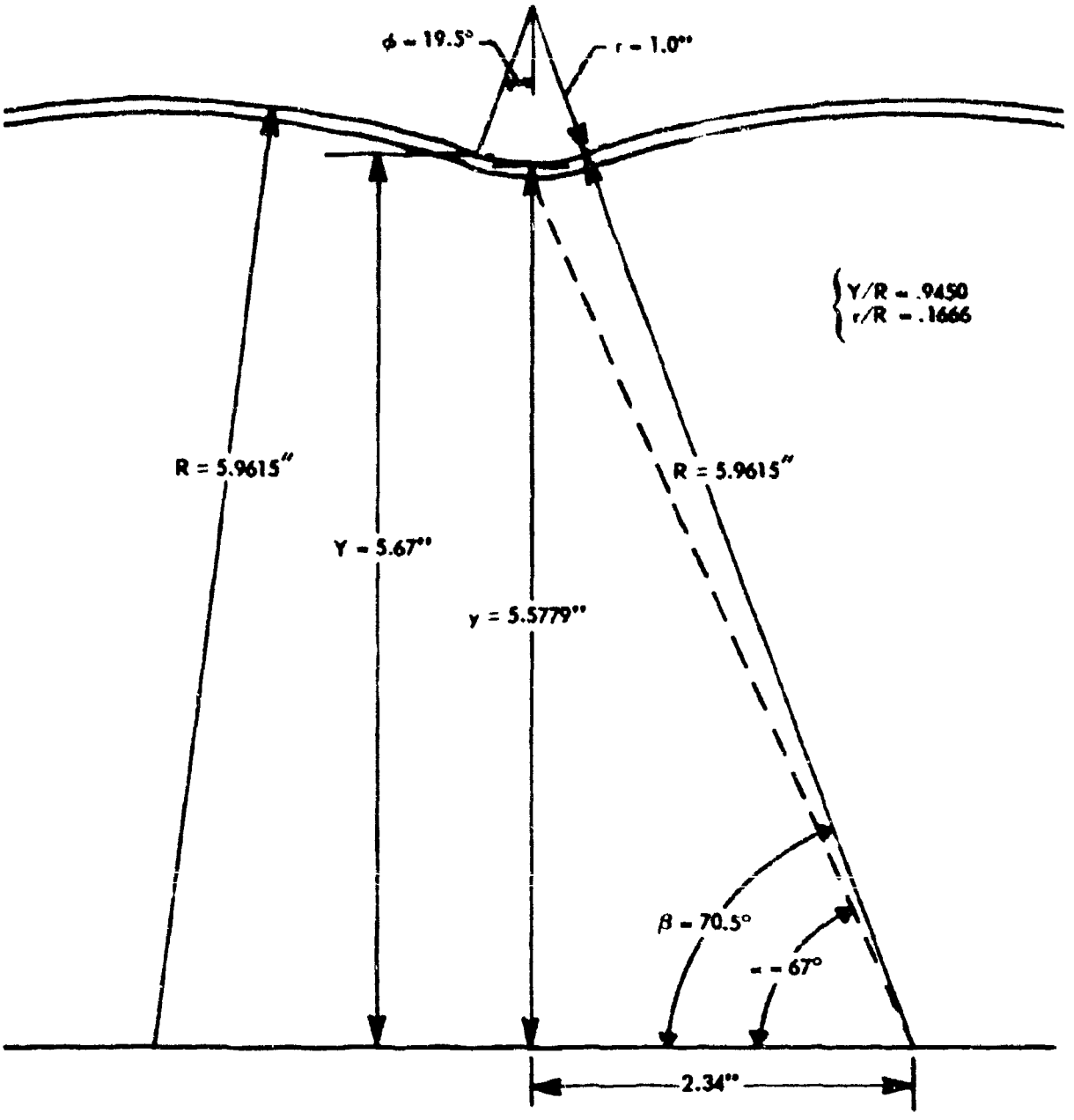

FIGURE 9 CLASS(I - II) ENGINEERING MODEL GEOMETRY

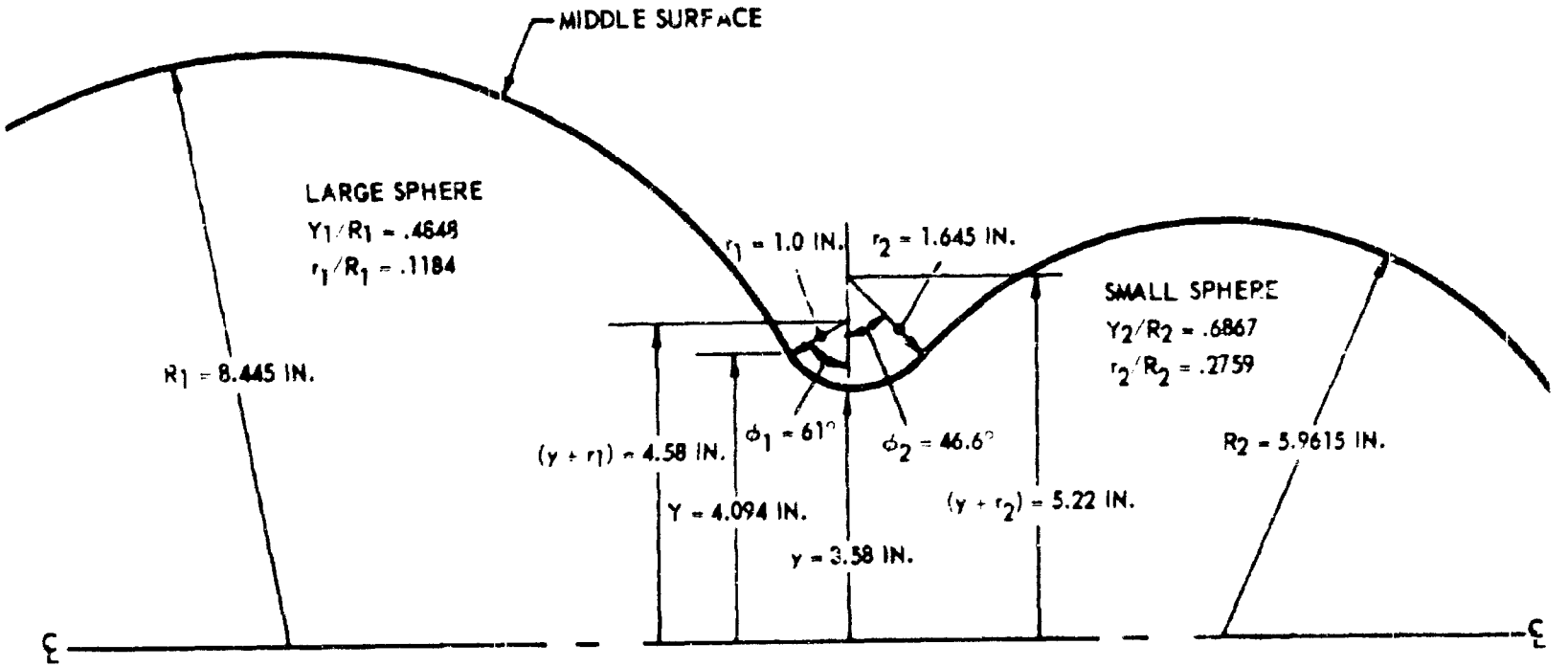

FIGURE 10 CLASS III ENGINEERING MODEL GEOMETRY

$$= \quad 0.00825$$

$$n_p/n_B \quad = \quad 0.565$$

Based on these conditions and the geometry given in Figure 9, the band load for membrane conditions is calculated using the following relation:

$$\sigma^b \; A^b = 2\int_0^{19.5^\circ} (r\, f \cos\phi \, d\phi)\,(y + r) - r\cos\phi$$

$$\sigma^b \; A^b = 2\, r^2\, f \int_0^{19.5^\circ} \left(\left(\frac{y + r}{r}\right)\cos\phi - \cos^2\phi\right) d\phi \qquad (1.2)$$

Where the band to internal pressure ratio is taken to be,

$$f/P = 3.47 \qquad \text{(Ref. Figure 11)} \qquad (1.3)$$

Substitution of values into Equation (1.2) yields:

$$\sigma^b \; A^b = 3.7387\, f \qquad (1.4)$$

Substitution for f yields:

$$\sigma_B^b \; A_B^b = (3.7387)\,(3.47)\,(3381.7)$$

$$= 43{,}871.77 \text{ lbs.} \qquad (1.5)$$

Based on proof pressure, the stress is:

$$\sigma_P^b = F_o + \frac{Sb}{F} \; E^b$$

$$= 40{,}000 + (.00825 \times 9 \times 10^6) \qquad (1.6)$$

$$\sigma_P^b = 114{,}340 \text{ psi}$$

Then, the stress at burst pressure is:

$$\sigma_B^b = 114{,}340 \div n_p/n_B = 171{,}680 \text{ psi} \qquad (1.7)$$

Using the value for σ_B^b in Equation 1.5, the band area required for the burst condition is:

$$A_B^b = \frac{43{,}871.77}{\sigma_B^b} = \frac{43{,}871.77}{171{,}680} = 0.2555 \text{ sq. in.} \qquad (1.8)$$

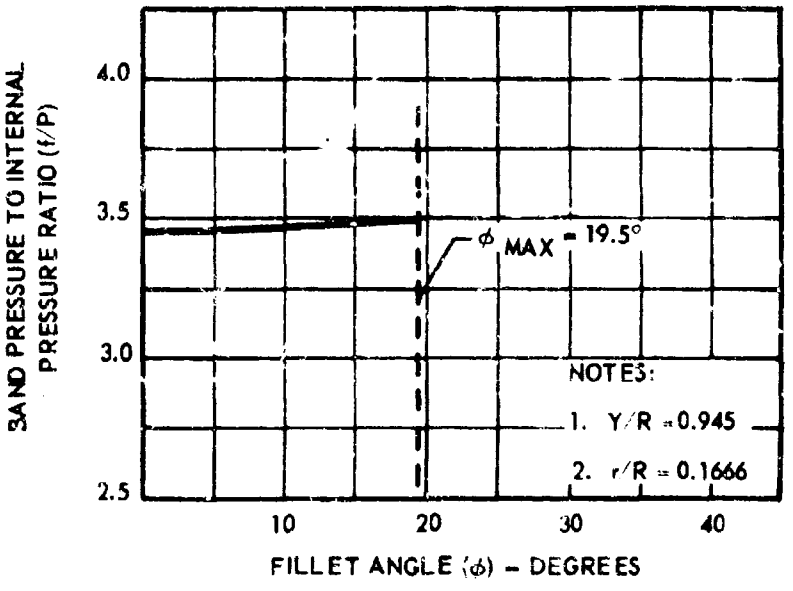

FIGURE 11 PRESSURE RATIO VERSUS FILLET ANGLE FOR CLASS (I – II) ENGINEERING MODEL

B. Class III

The Class III vessel is made of 17-7 PH steel with S-901 fiber glass band. The design analysis is divided into two parts, each segment being one part.

The large segment design is based on the following conditions and the geometry given in Figure 10.

F_o = 40,000 psi

n_p/n_B = 0.666

t (nominal) = 0.09 in.

t (min.) = 0.077 in.

$$P_B = \frac{2t\ (min)\ \sigma^{\S}_U}{R} = \frac{.154 \times 185{,}000}{8.445} = 3373.59 \text{ psi}$$
(no reduction for inefficiencies)

$$\varepsilon^{Sb}_P = \sigma^S_Y\ (1 - u)/E^S + .002 = ((150 \times .7) - 30)\ 10^{-3} + .002 = 0.0055$$

The band load equation for a membrane condition is:

$$\sigma^b\ A^b = r_1^2 \int_0^{61^\circ} \left(\left(\frac{y + r_1}{r_1}\right) f \cos\phi - f \cos^2\phi\right) d\phi \qquad (1.9)$$

where the straight line relationship $f = (3.95 + .657\,\phi)\ P$ is an approximation of the distribution given in Figure 12.

Substituting in values and integrating, the band load becomes:

$$\sigma^b\ A^b = 13.67\ P \qquad (1.10)$$

Based on proof pressure, the stress is:

$$\sigma^b_P = F_o + \varepsilon^{Sb}_P\ E^S \qquad (1.11)$$

$$= 40{,}000 + 0.0055 \times 9 \times 10^6$$

$$= 89{,}500 \text{ psi}$$

Then the stress at burst is:

$$\sigma^b_B = (89{,}500 \text{ psi}) - (n_p/n_B) - 134{,}250 \text{ psi} \qquad (1.12)$$

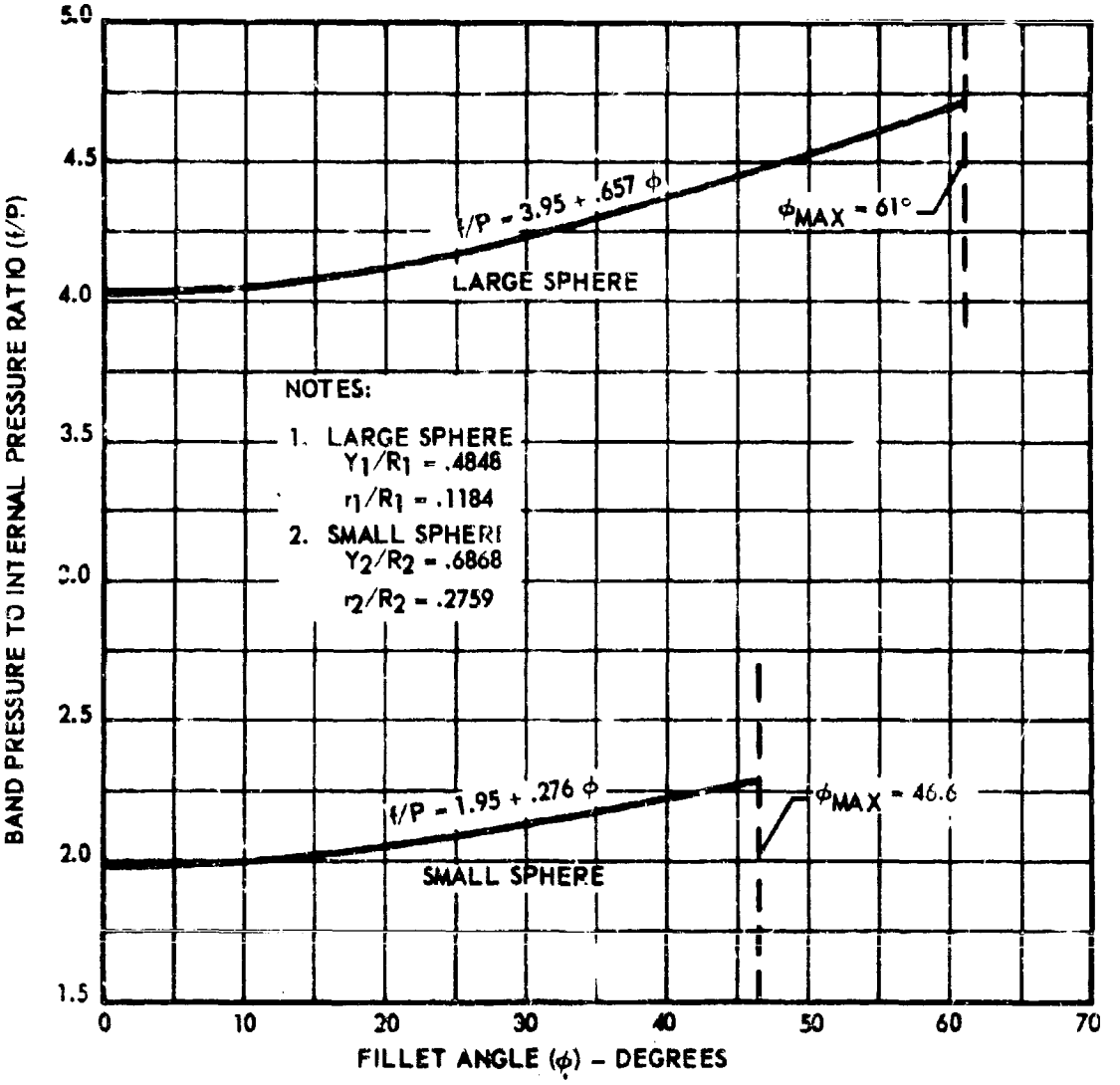

FIGURE 12 PRESSURE RATIO VERSUS FILLET ANGLE FOR CLASS III ENGINEERING MODEL

Using the above value in Equation (1.10), the band area required for the large segment at burst pressure is:

$$A_B^b = \frac{13.67 \times 3373.6}{134{,}250} = 0.3435 \text{ sq. in.} \qquad (1.13)$$

The small segment's geometry, Figure 10, and the following conditions differ from the large segment.

t (nominal) =0.063 in.

t (min) =0.054 in.

$$P_B = \frac{0.108 \times 168{,}000}{5.9615} = 3043.5 \text{ psi (no reduction for inefficiencies)}$$

The band pressure for this segment is given by the straight line relationship:

$$f = (1.95 + .276\,\phi)\,P \text{ (Ref. Figure 12)} \qquad (1.14)$$

Band load for membrane conditions is calculated using Equation 1.9 with only numerical changes due to geometry with the result:

$$\sigma^b A^b = 8.94\,P \qquad (1.15)$$

The stress at burst condition was previously calculated to be 134,250 psi. Substituting this value in Equation (1.15) along with the pressure at burst (P_B), the required band area for the small segment is:

$$A_B^b = \frac{(8.94) \times (3024)}{134{,}250} = 0.2026 \text{ sq. in.} \qquad (1.16)$$

The total band area for both segments at burst condition is:

$$A_B^b = 0.3435 + 0.2026 = 0.5461 \text{ sq. in.} \qquad (1.17)$$

2. ANALYSIS BY PETS DIGITAL ROUTINE

The large number of trial designs which must be made in a comprehensive parametric a alysis of a segmented spherical pressure vessel make it expedient to use a simple membrane analysis in the design procedure. For a given value of internal pressure P, the stress predicted by the membrane theory ($\sigma_m = PR/2t$) will be accurate except in regions of shell bending. Since the individual segments are homogeneous spheres of constant thickness, shell bending will occur only in the neighborhood of the reinforcing band and near points of manufacturing error. The primary purpose of this analysis is to determine the effect of this bending on the design.

a. Solutions on Equal Segment Configurations

This section presents the results of the stress-strain analysis of the equal sphere configurations. As will be indicated in Section VII, the analysis employs the band shell compatibility relations to combine the results of unit load analyses for the reinforcing band and un-reinforced shell to yield solutions for the reinforced shell. The unit load analysis for the un-reinforced shell determines strain, displacement, and stress influence functions directly from the output of digital routine PETS. Two such analyses are required for any shell configuration; one with a uniform internal pressure, P, and one with a uniform band pressure f The influence functions presented in this report were all obtained with P and f equal to 1000 psi = 1 ksi.

Figures 13 and 14 are typical of the stress influence curves which are obtained from unit analysis of the equal sphere configurations. The four stresses represented are:

σ_f^i, σ_f^o : Meridional stress on inside and outside fibers.

σ_ϕ^i, σ_ϕ^o : Circumferential stress on inside and outside fibers.

These stresses are shown as functions of meridional arc length, ξ. The stress distribution is symmetric about the low point of the node (shown as the center line) and the maximum values of stress occur at this point. Figure 13 shows the stress is ksi per ksi of internal pressure and Figure 14 shows the stress in ksi per ksi of band pressure. Both of these curves represent the design case (12 inch diameter sphere, segment angle 67° 58', wall thickness .068 inch, elastic modulus 16 x 10^6 psi, and a 1 inch nodal radius).

b. Design Optimization, 12" to 12" Vessels

In general, shell bending in the neighborhood of the reinforcing band will reduce the safe working range of pressure. The problem considered here is that of minimizing this reduction for a particular choice of materials and shell radii. Explicitly, for given shell and band materials and nodal radii, the optimization procedure is to find a combination of band area, A^b, and prestress force, F_o, which minimizes the effects as the design of shell bending in the neighborhood of the reinforcing band.

For the equal sphere configurations, the problem is simplified by the existence of a pure membrane state for some value of f/P. In such a case, the pressure is obtained by the band area and prestress such that the stress in the shell in its membrane condition is exactly equal to the yield point stress of the material.

We illustrate the procedure by means of the design example.

A. Determination of Design Stress

The first step is to determine which of the four stress

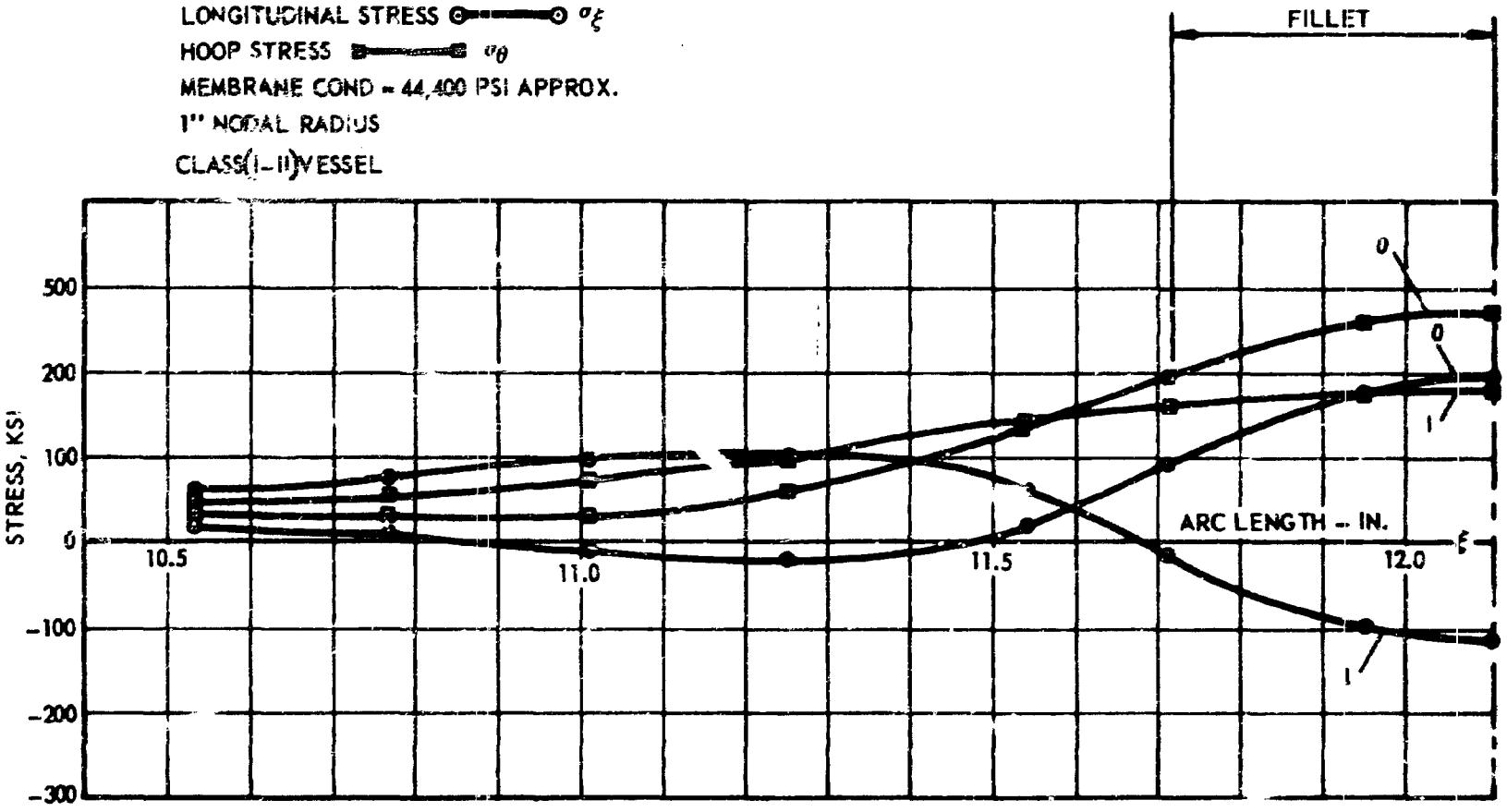

FIGURE 13 NORMAL STRESS VS ARC LENGTH FOR INTERNAL PRESSURE

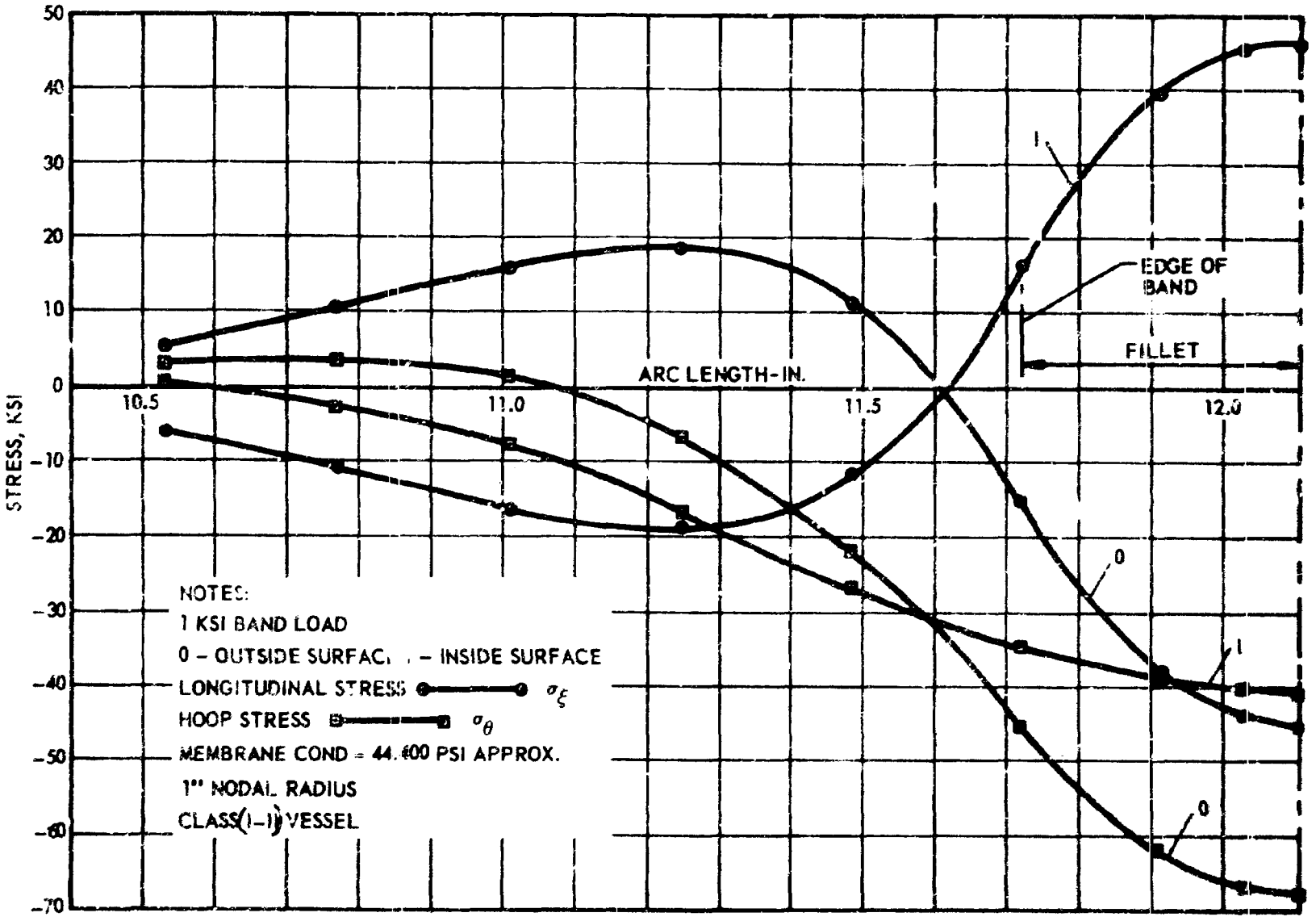

FIGURE 14 NORMAL STRESS VS ARC LENGTH FOR BAND LOAD

functions $\sigma_\phi^o(P)$, $\sigma_\phi^i(P)$, $\sigma_\xi^o(P)$, $\sigma_\xi^i(P)$, is critical at any given value of P. From the unit analyses by digital routine PETS it is found that:

$$\sigma_\phi^o/P = 259.10 - 63.742\ f/P \qquad \sigma_\xi^o/P = 197.39 - 45.67\ f/P$$

$$\sigma_\phi^i/P = 165.37 - 35.876\ f/P \qquad \sigma_\xi^i/P = 115.06 + 47.22\ f/P$$

It is easily verified from these results that the stress σ_ξ^o, σ_ϕ^i, are intermediate stresses for all values of f/P, and

σ_ϕ^o/P is design stress for $3.37 \geq f/P \geq 8.7$

σ_ξ^i/P is design stress for $3.37 \leq f/P \leq 8.7$

where

f/P = 3.37 is the membrane condition.

Now in general,

$$f = Pk_1 + f_o = f/P = k_1 + f_o/P$$

So for a fixed design (F_o, A^b), f/P is a function of P alone and

$$\frac{d}{dp}\ (f/P) = -\ f_o/P^2$$

Thus for $I \geq o$;

σ_ϕ^o is design stress for $P' \geq P \geq P_{mem}$

σ_ξ^i is design stress for $P' \leq P \leq P_{mem}$

where P' corresponds to f/P = 8.7.

B. Optimization

Now f/P = 3.37 eliminates the secondary stress - that is, a membrane state exists at this value of f/P. We wish to maximize the value of P at which f/P equals 3.37 relative to the condition that the shell does not yield under the band load alone. Now the stresses in the shell are:

$$\sigma^s = P\ \sigma_P^s + f\ \sigma_f^s,$$

and in view of the above, we wish to choose f such that, for a yield stress of 150 ksi,

$$150 \geq \sigma^s = P\ \sigma_P^o + f\ \sigma_{\phi f}^o, \text{ for } I \geq P_m \qquad (2.1)$$

$$150 \geq \sigma^s = f_o\ \sigma_f^o, \text{ for } P = o, \qquad (2.2)$$

Subject to the condition that

$$f_m/P_m - 3.37 = k \tag{2.3}$$

In order to maximize the value of the internal pressure, P_m, at which the membrane state occurs, we take

$$\frac{150}{P_m} \geq \sigma_p^\circ + \frac{f_m}{P_m}\,\sigma_f^\circ = \sigma_p^\circ + k\sigma_f^\circ, \tag{2.4}$$

thus

$$P_m \leq \frac{150}{\sigma_p^\circ + k\,\sigma_f^\circ} \tag{2.5}$$

Since,

$$\sigma_p^\circ = 259.1, \qquad \sigma_f^\circ = 63{,}742$$

we get

$$P_m \leq 3{,}38 \text{ ksi},$$

which, as predicted, is the value of pressure at which a single component sphere yields.

C. Choose Band Area and Prestress, F_o

Thus, letting

$$P_m = 3.38, \qquad k = 3.37 \tag{2.6}$$

we obtain

$$f_o = 3.38\,(3.37 - k_1) \tag{2.7}$$

But for no yielding at P = 0, one must have,

$$150 \geq f_o\,\sigma_f^\circ \qquad (63{,}742)$$

which implies

$$f_o \leq 2.35 \tag{2.8}$$

and we note that this is independant of P_m. Combining this with (2.7) yields

$$k_1 \geq 2.675 \qquad (2.9)$$

But in general,

$$k_1 = \frac{\varepsilon_P^s}{\varepsilon_f^b - \varepsilon_f^s} \quad \varepsilon_f^b = \frac{\varepsilon_P^s + k_1 \varepsilon_f^s}{k_1} \qquad (2.10)$$

From unit analyses by routine PETS the ε strains are

$$\varepsilon_P^s = .012493 \qquad \varepsilon_f^s = -.0031276$$

Therefore,

$$\varepsilon_f^b = \frac{\varepsilon_P^s + k_1 \varepsilon_f^s}{k_1} = \frac{.012493 - k_1 (.0031276)}{k_1}$$

and since $k_1 \geq 2.675$ by (2.9)

$$\varepsilon_f^b \leq \frac{.00419}{2.675} = .001565 \qquad (2.11)$$

Now since $f_o \leq 2.35$,

$$\varepsilon_f^b = \frac{SR}{E^b A^b} = \frac{F_o}{f_o E^b}$$

implies

$$\varepsilon_f^b \geq \frac{F_o}{2.35 E^b}$$

Therefore,

$$\frac{F_o}{2.35 E^b} \leq \frac{ER}{E^b A^b} \leq .001565$$

Now S = .733 R = 5.62 SR = 4.11

Thus, for no yielding in the range $0 \leq P \leq P_m$

$$\frac{F_o}{2.35} \leq \frac{4.11}{A^b} \leq .001565 E^b \qquad (2.12)$$

In order to enforce band shell compatibility at P = 3.38 (so that the design stress assumed by inequality (2.12) is correct) we must have:

$$f_o = \frac{F_o A_b}{SR} = P_m (k - k_1) - 3.38 (3.37 - k_1)$$

Thus

$$\frac{F_o A^b}{SR} = 3.38 \left(3.37 - \frac{\varepsilon^s_P}{\frac{SR}{E^b A^b} - \varepsilon^s_f} \right)$$

or, with $\varepsilon^s_P, \varepsilon^s_f$ as before, and SR = 4.11,

$$F_o = \frac{13.9}{A^b} \left(3.37 - \frac{.01249\, E^b A^b}{4.11 + .00313\, E^b A^b} \right) \qquad (2.13)$$

In general, any consideration of E^b A^b and F which satisfy (2.13) and nequality (2.12) is satisfactory for all values of internal pressure in the range $0 \leq P \leq 3.38$ ksi. Figure 15 shows a plot of such combinations for $E^b = 9.1$.

The actual design case does not quite lie on these optimum curves. Figure 16 is helpful in illustrating the consequences of utilizing a non-optimum case. This figure shows the contours of critical shell stress as a function of band area and prestress. For example, the shell yields at P = 0 for $A^b = .270$ if $F_o > 36$ ksi. On the other hand, for $A^b/.270 = .9$, and $F_o < 39.8$, the shell stress just reached yield point at P = 0, but then relaxes and remains less than yield point until P exceeds 3.0 ksi. Of course, every point in the shell will yield when P = 3.38 ksi.

c. Design Optimization, 12" to 1/" Vessels

This solution assumed existence of a single uniform (f/p) value to satisfy membrane conditions on both the large and small segment sides of the nodal section.

The stress distribution from routine PETS for the design case, for a unit internal pressure and a unit band load, are shown in Figures 17 and 18 respectively. These figures clearly illustrate the origin of the residual bending stress. The maximum stress due to the internal pressure occurs (in the node) on the side near the large sphere, and the maximum stress due to the uniform band load occurs (in the node) on the side near the small sphere. Obviously, these can never cancel. From a procedure completely analogous to that derived for the 12-12 inch spheres, it is found that value of f/p which minimizes secondary stress is 3.42 ksi and that the corresponding maximum value of internal pressure, for no yielding is 1.86 ksi. Finally, the basic relations between band prestress, F_o, band A^b, modulus E^b and dimension SR to insure that there is no yielding anywhere in the range of pressure,

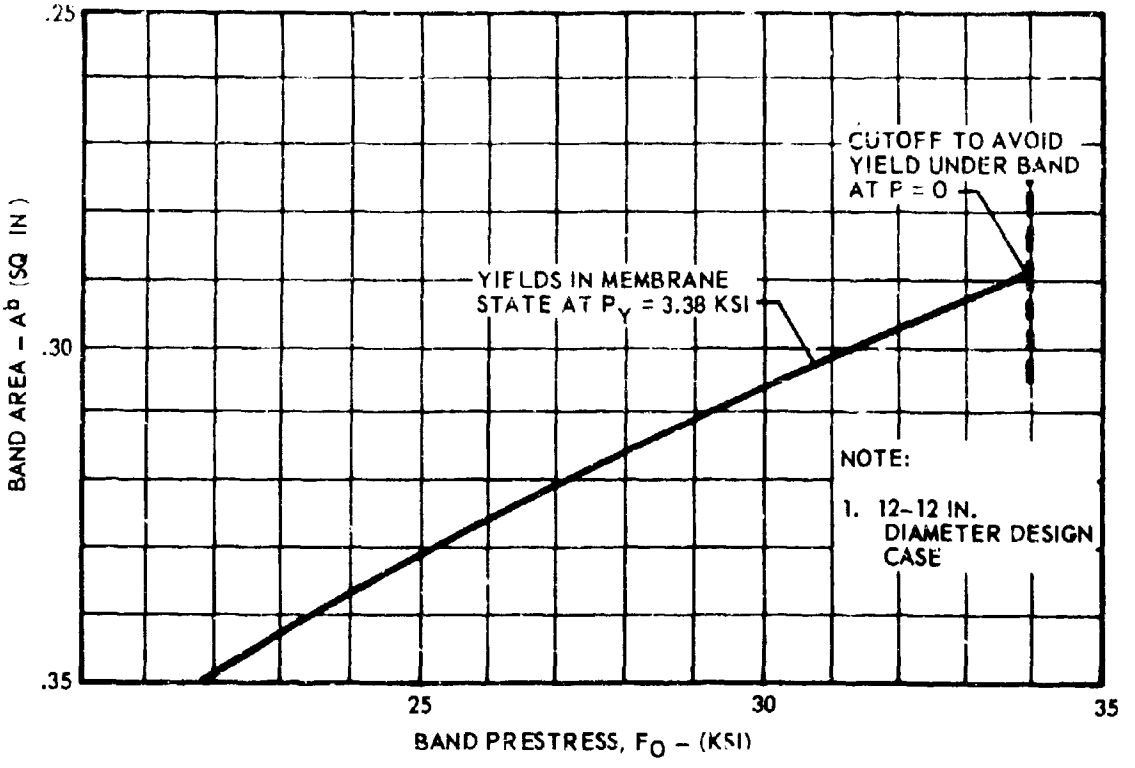

FIGURE 15 BAND AREA – PRESTRESS RELATION TO ACHIEVE THEORETICAL MAXIMUM INTERNAL PRESSURE AT YIELD POINT

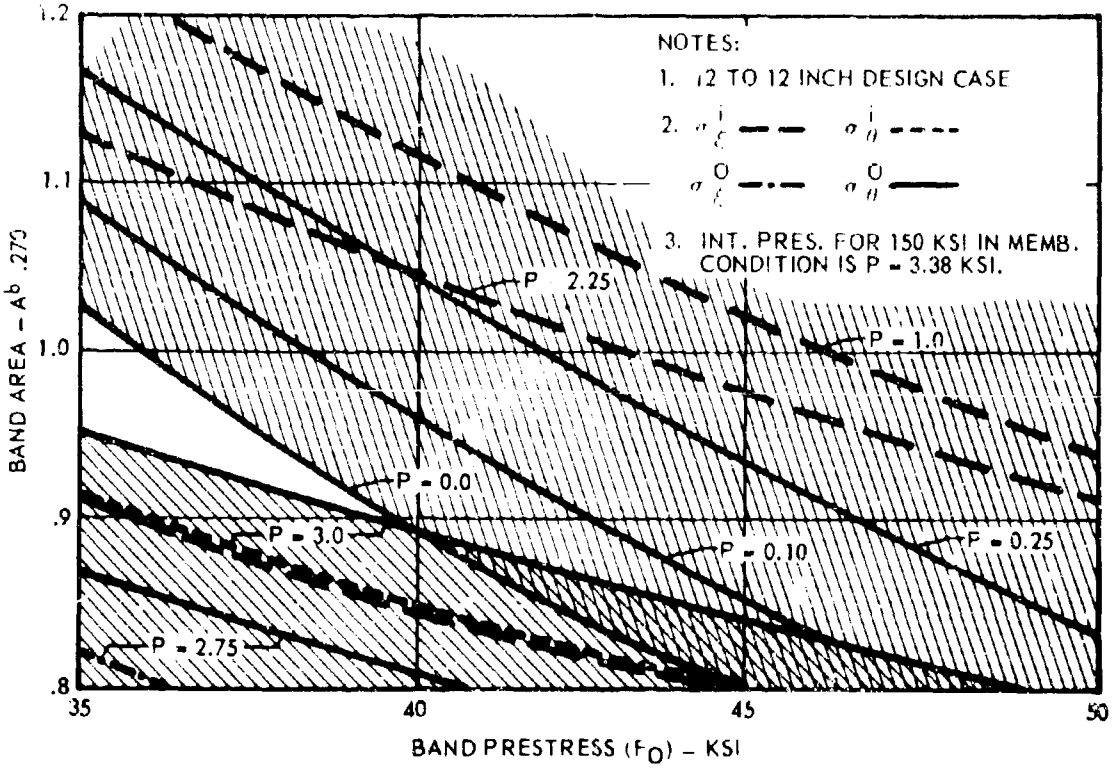

FIGURE 16 150 KSI CONTOURS FOR CRITICAL SHELL STRESS OVER INTERNAL PRESSURE HISTORY

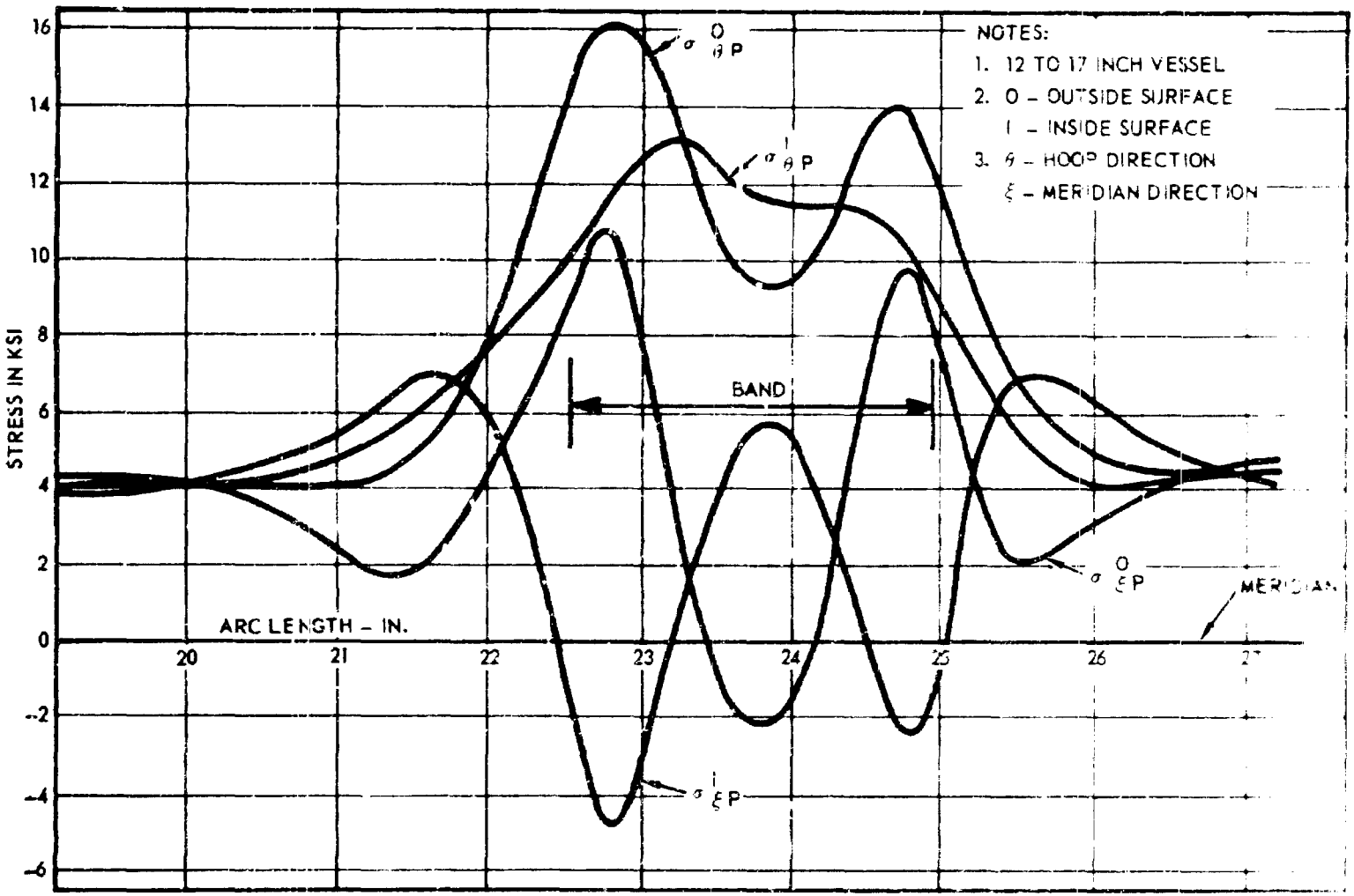

FIGURE 17 STRESS VS ARC LENGTH FOR 1 KSI INTERNAL PRESSURE

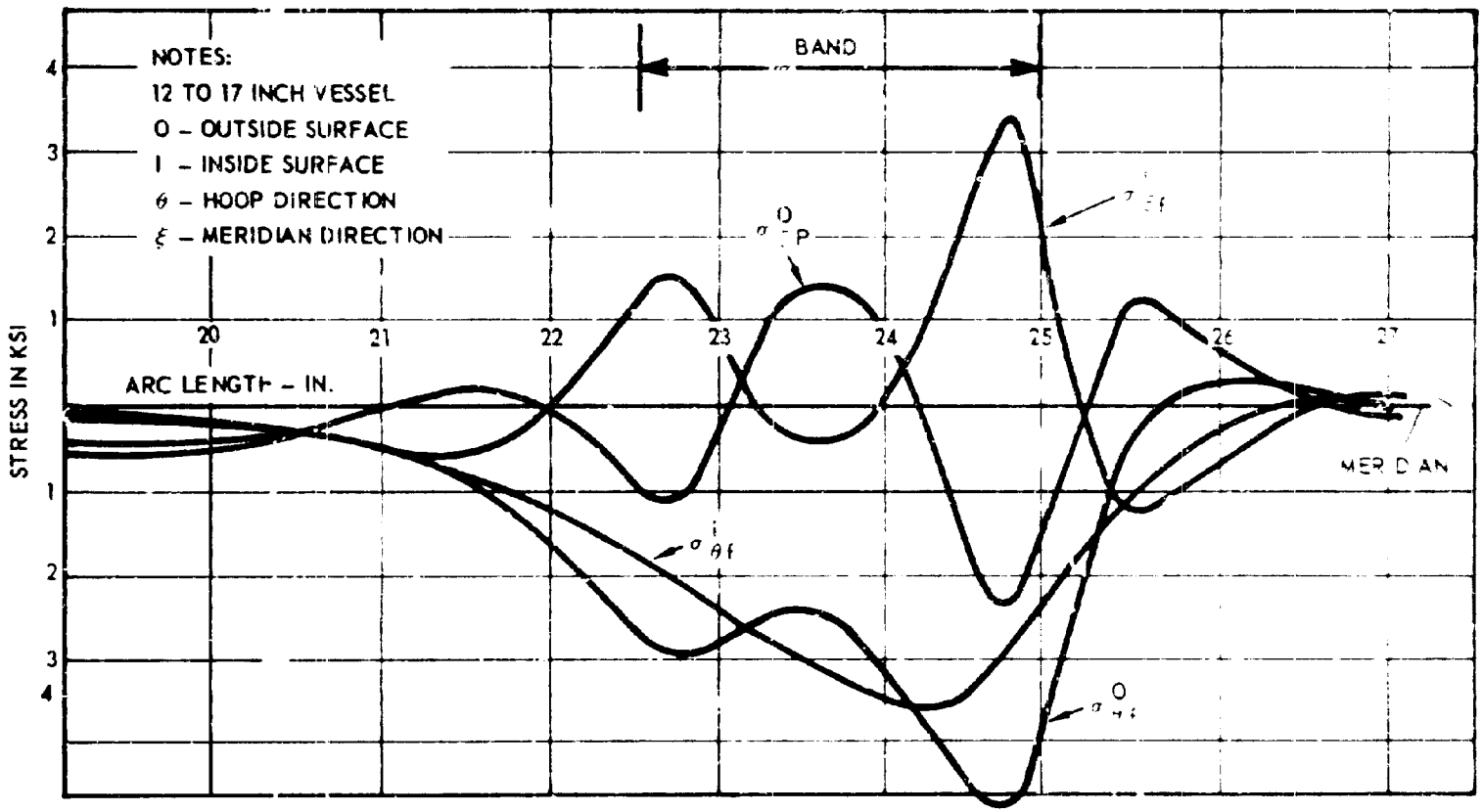

FIGURE 18 STRESS VS ARC LENGTH FOR 1 KSI BAND LOAD

$$0 \leq P \leq 1.9,$$

are found to be

$$\frac{F_o}{2.93\ E^b} \leq \frac{SR}{E^b\ A^b} \leq .001,$$

and

$$\frac{F_o\ A_b}{SR} = 1.86\ \left(3.42 - \frac{.00375\ E^b\ A^b}{SR + .00101\ E^b\ A^b}\right) \qquad (2.14)$$

It is noted that the two (f/P) gradients computed by the AMC method (Ref. Figure 12 have average values of 2.1[illegible] for the small segment side and 4.2[illegible] for the large segment side of the nodal section. These values bracket the value of 3.42 selected by judgment from the PETS data. It is now obvious that the assumption of a single uniform f/p value for the PETS method was a severe compromise on accuracy. However when the PETS results are recognized as an averaging approximation, it provides a good check for the AMC solution.

SECTION IV

LABORATORY EVALUATIONS

1. FULL SCALE BAND TESTS

a. Test Method

Modulus of elasticity values determined by stress-strain measurements on NOL rings were widely variant and significantly lower than values calculated on the basis of volume percentage of filament glass. These disparities were also found in the literature reported data. It was concluded that the standard split disc test method was inaccurate for modulus of elasticity purposes.

A special radial expanding fixture was designed and fabricated to accommodate full scale bands for the Class (I-II) engineering model. The test fixture design employed an expandable steel ring comprised of eight segments. These segments provided the surfaces which applied uniform radial pressure over the entire inner circumference of the SSPV test ring.

The segments were in turn loaded by a system of wedges on roller bearings (Ref. Figure 19). The wedges were arranged to transform linear travel of crossheads on a standard Baldwin Tensile Testing Machine, into uniform radial displacement of the ring fixture. The test set-up is shown in Figure 20.

b. Test Band Fabrication

A total of 10 full scale SSPV filament bands and 12 NOL rings were wound for structural evaluation tests. Two SSPV bands were wound in each of five lots. Several NOL rings were wound of each lot materials and tested to provide a Quality Control Standard.

All specimens were wound with S-901 20 end filament glass and epoxy resin. A typical band cross section is illustrated in Figure 21. A full scale SSPV band is shown in Figure 22.

c. Test Results

Properties of the SSPV filament wound bands and NOL ring, given in Table V, are based on resin-burn-out tests, to determine percentage of glass by volume, and stress strain measurement during tensile testing. Failure mode, reported as cleavage, was experienced in early SSPV tests due to strain reduction of band cross-section causing load concentration at the cross-section center line as illustrated in Figure 23. This was corrected by providing a .0625 inch thick vinyl liner between the fixture and the band to simulate the actual vessel conditions where the thin shell maintains band shape concentricity. SSPV band specimen numbers 23, 24, 29 and 30 failed in pure tension mode. A typical failed ring is shown in Figure 22. Strength data is given in Table V.

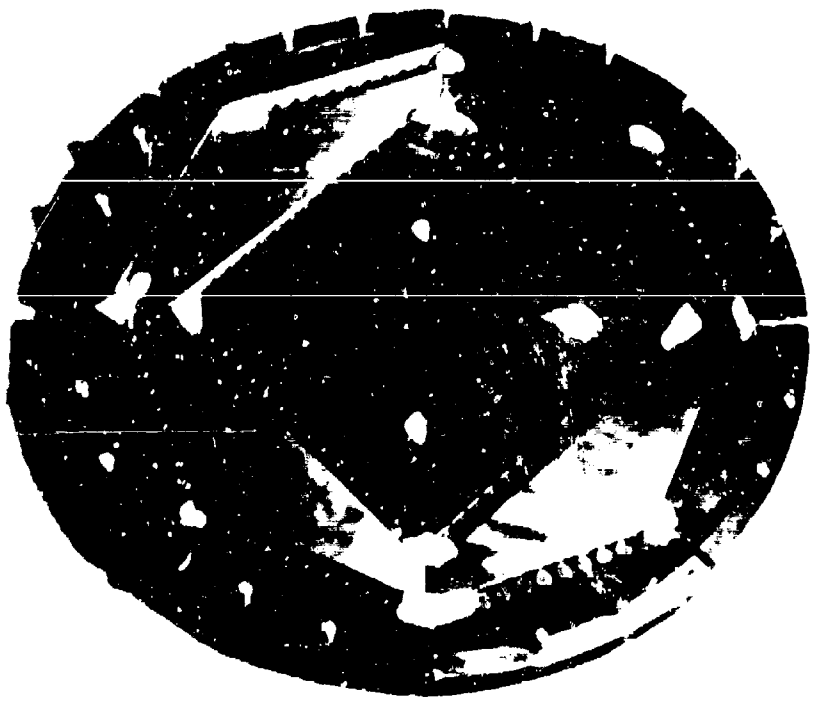

FIGURE 19 BAND TEST FIXTURE

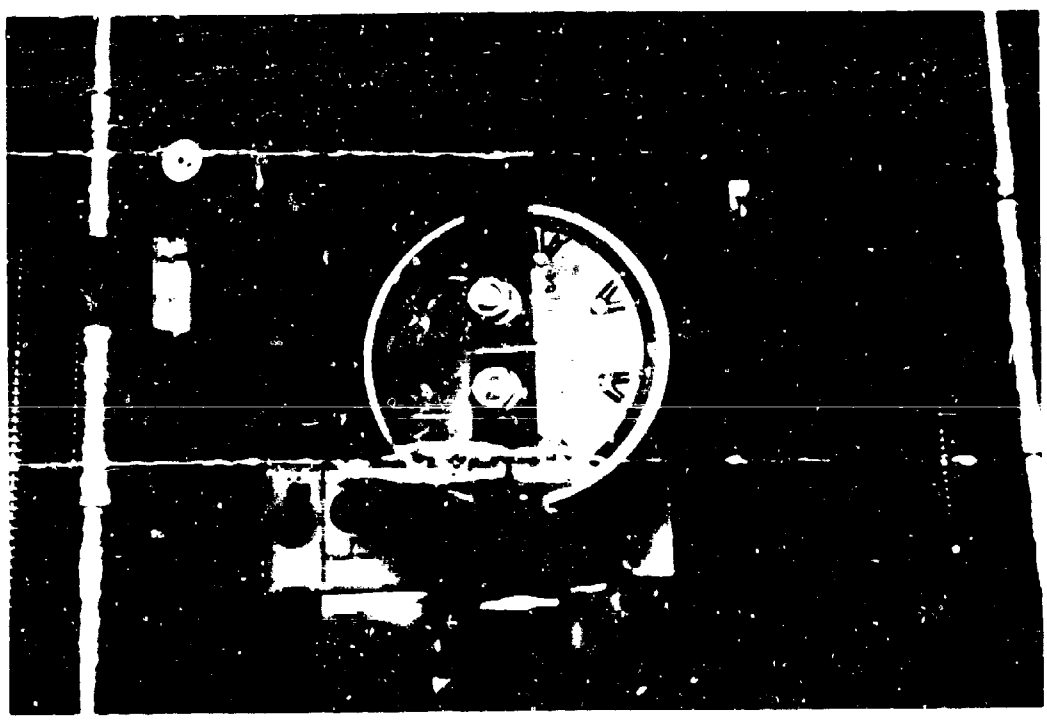

FIGURE 20 BAND TENSILE TEST SETUP

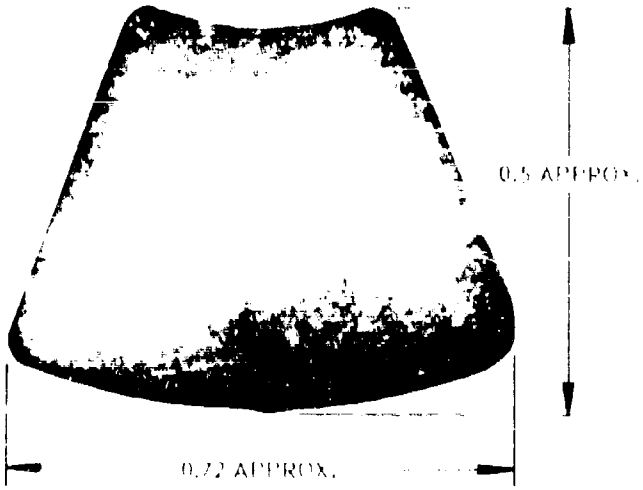

FIGURE 21 BAND CROSS-SECTION

FIGURE 22 FULL SCALE BAND AND TYPICAL FAILURE IN TEST RING

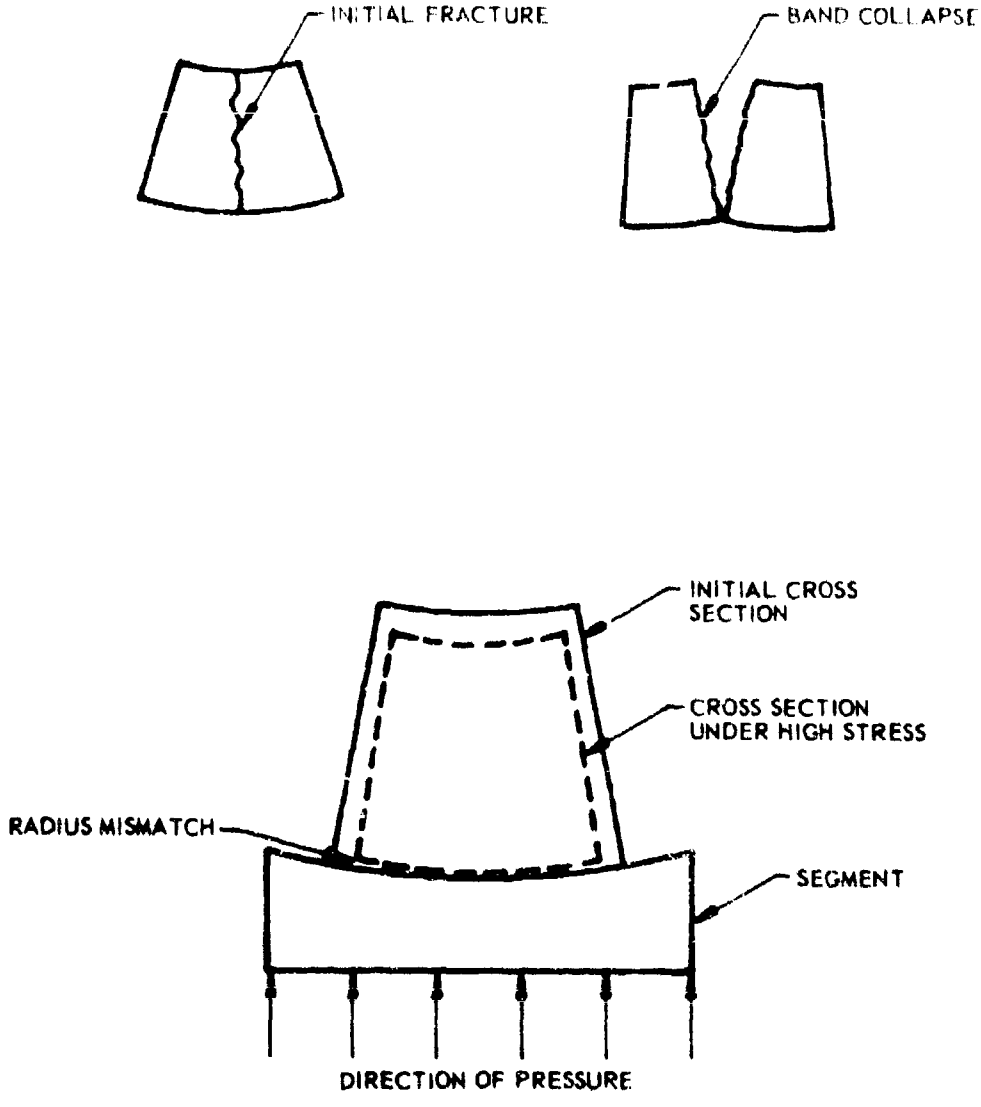

FIGURE 23 CROSS SECTION DISTORTION FROM RIGID FIXTURE

TABLE V TEST DATA AND EVALUATION OF BAND MATERIAL PROPERTIES

TEST GROUP	SPECIMEN NO NOL	SSPV	AREA SQ. IN.	% VOL. FILAMENT	INSTRUMENTED RADIUS (INCHES)	INSTRMT'D. CIRC. / AREA (IN)$^{-1}$	$\left(\frac{\text{TEST LOAD}}{\text{DEFLECTION}}\right) 10^{-3}$ IN	COMPOSITE TENSILE KSI	COMPOSITE MODULUS E x 10^{-6}
II	9		.0175		2.9	520.5	13.56	240.6	7.05
	10		.0186		2.9	489.5	14.27	237.9	6.98
	11		.0176		2.9	517.5	14.27	242.9	[illegible]
	12		.0170		2.9	535.5	14.84	250.0	[illegible]
		13	.277	.6206	6.10	138.34	67.5	151.6	[illegible]
		14	.273	.6[illegible]	5.66	133.97	66.0	158.7	8.83
III		15	.2815	.62	5.66	126.32	72.1	157.0	9.74
		16	.2793	.62	5.66	130.8	70.0	155.3	9.15
	17		.017	.68	2.9	535.5	13.06	250.0	6.99
	18		.0169	.68	2.9	539.0	14.27	261.1	7.69
IV	19		.0175	68	2.9	520.5	14.12	239.5	7.35
	20			.6862	2.9				
		21	.2781	.6293				144.2	
		22	.2806	.6331	5.66	126.7	74.0	156.1	[illegible]
V		23	.2712	.63	6.09	141.0	64.0	199.5	
		24	.2756	.63	6.10	139.0	68.0	195.9	
VI	25		.017	.68	2.9	535.9	13.[illegible]	241.7	
	26		.017	.68	2.9	535.9	13.[illegible]	230.4	
	27		.016	.68	2.9	569.4	15.01	237.8	8
	28			USE FOR RESIN BURNOUT TEST					
		29	.265	.63	6.07	143.77	72.72	203.77	10.42
		30	.250	.63	6.03	151.47	73.52	209.20	11.13

V TEST DATA AND EVALUATION OF BAND MATERIAL PROPERTIES

D ES)	INSTRMT'D. CIRCUM. / AREA (IN)−1	(TEST LOAD / DEFLECTION (# IN)) 10−3	COMPOSITE TENSILE KSI	COMPOSITE MODULUS (E X 10−6)	FIBER TENSILE KSI	TYPE FRACTURE
	520.5	13.56	240.0	7.05		TENSILE
	489.5	14.27	237.9	6.98		TENSILE
	517.5	14.27	242.9	7.38		TENSILE
	535.5	14.84	250.0	7.94		TENSILE
	138.34	67.5	151.6	9.33	244.2	CLEAVAGE & CUTTING
	133.92	66.0	158.7	8.83	255.9	CLEAVAGE & CUTTING
	126.32	77.1	157.0	9.74	253.2	CLEAVAGE & CUTTING
	130.8	70.0	155.0	9.15	250.0	CLEAVAGE & CUTTING
	535.5	13.06	250.0	6.99	367.6	TENSILE
	539.0	14.27	261.5	7.69	383.8	TENSILE
	520.5	14.12	239.4	7.35	352.0	TENSILE
			144.2			CLEAVAGE & CUTTING
	126.7	74.0	156.1	9.37	229.1	CLEAVAGE
	141.0	64.0	199.5	9.02	316.6	TENSILE
	139.0	68.0	195.9	9.45	310.9	TENSILE
	535.9	13.69	241.7	7.33	355.41	TENSILE
	535.9	13.17	230.4	7.05	338.8	TENSILE
	569.4	15.01	237.8	8.54	349.68	TENSILE
T TEST						
	143.77	72.72	203.77	10.45	323.44	TENSILE
	151.47	73.52	209.20	11.13	332.06	TENSILE

2

[illegible] PAGE BLANK--NOT FILMED

2. DEVELOPMENT OF EXPLOSIVE FORM PROCESS

a. Test Specimens

In order to evaluate weld methods and explosive forming controls suited to forming the hour glass shell module, a test plan was prepared for forming half scale cylinders. An explosive die was designed and fabricated to bulge the 6AL-4V seam welded cylinders to 12 percent permanent radial strain. It was reasoned that 12 percent would provide a conservative criterion since the SSPV Class (I-II) design would require less than 8 percent permanent strain. Land configurations are given in Figure 24 with considered weld material processes listed in Table VI.

b. End Load and Explosive Forming Process

The greatest risk in explosive forming the SSPV modules was associated with the presence of the TIG welded seam. It was known from previous MSD-T formability studies that 6AL-4V titanium did not respond well to high energy forming methods. In search of the cause it was observed that 6AL-4V annealed material lost 75 percent of uniaxial elongation when subjected to biaxial tensile strain. It was reasoned that introduction of an axial compressive preload would help move material in the radial direction and tend to restore uniaxial elongation capabilities. Therefore, the test die was designed with end plates and bolts which could be torqued to introduce a controlled axial preload.

c. Test Results

Test experience conclusively demonstrated end loading caused a significant improvement in formability of 6AL-4V titanium in explosive forming. At the beginning of testing, four identical specimens were formed two with and two without end loading (Ref. Figure 25). In order to achieve full form with the unloaded specimens it was necessary to increase the primacord charge at the second and final stage. In the end load tests the charge was held constant and the axial load retorqued to the original level after each firing. Metallurgical examination of the unloaded specimens showed considerable necking and surface tearing of the welds as a result of explosive forming. No deleterious effects were found in the end loaded specimens after explosive forming. Continuation of testing to evaluate weld processes, was made with end load of 75 ft. lbs. bolt torque and 8 inches of 100 grains per foot primacord. Test results showed satisfactory formability with 6AL-4V titanium rod without weld land provisions. No significant difference could be found between specimens with and without weld lands. As a result of this favorable experience the requirements for electron beam welded specimens was cancelled. A thickness survey of explosive formed specimen was taken and is shown in Figure 26. Design instructions were issued to provide end loading features for the full scale explosive die. Engineering model design proceeded with useage of 6AL-4V weld rod and no provisions for weld lands prior to explosive forming.

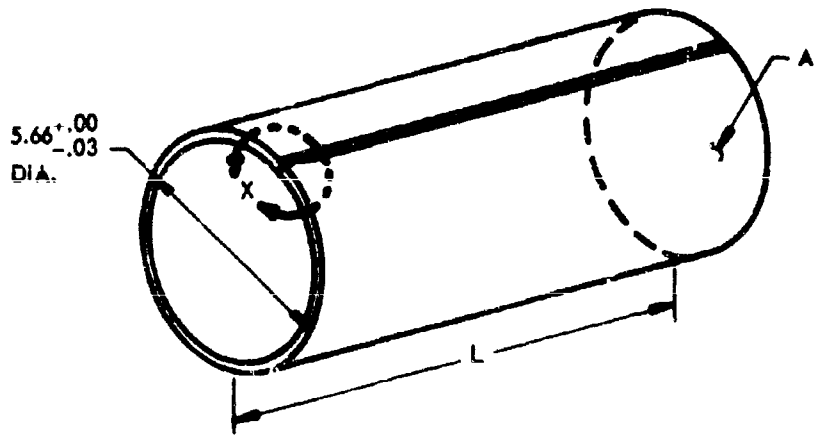

-10, -11, -12, -13, -14, -15, & -16
WELD SPECIMEN

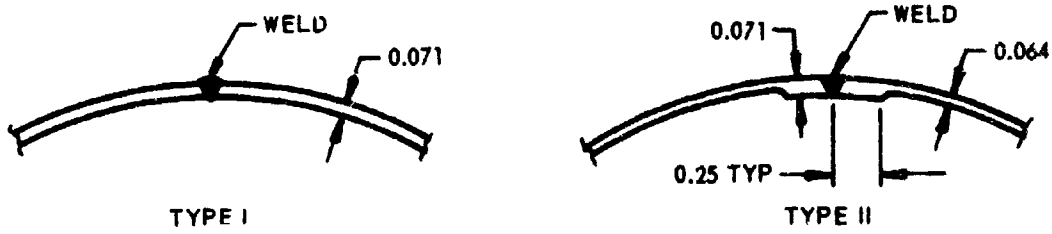

TYPE I TYPE II

DETAIL X - WELD TYPE

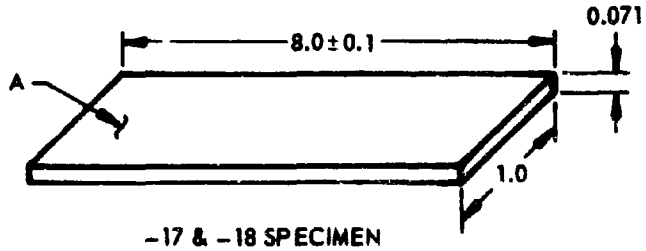

-17 & -18 SPECIMEN

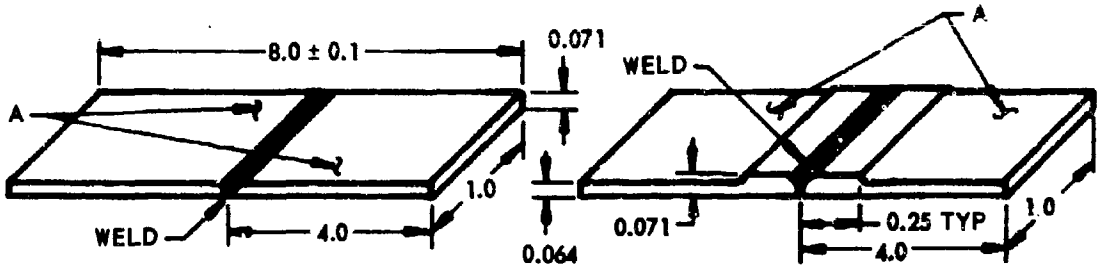

-19, -20, -21, & -22
WELD SPECIMEN

-23 & -24
WELD SPECIMEN

FIGURE 24 WELD LAND CONFIGURATIONS FOR TEST SPECIMEN

TABLE VI EXPLOSIVE FORM TEST SPECIMEN PLAN

TABULATION							
DASH NO.	WELD TYPE	"A" MAKE FROM	"L" DIM.	TY. REQD.	WELD METHOD	WELD ROD	GRAIN DIRECTION
-10	I	-1	$4.62^{+0.00}_{-0.10}$	4	TIG	6 AL-4V	LONG.
-11	I	-1	$4.62^{+0.00}_{-0.10}$	4	TIG	COM-MERCIAL PURE TI	LONG.
-12	I	-6	$4.67^{+0.04}_{-0.00}$	2	TIG	6 AL-4V	LONG.
-13	I	-6	$4.67^{+0.04}_{-0.00}$	2	TIG	COM-MERCIAL PURE TI	LONG.
-14	II	-6	$4.67^{+0.04}_{-0.00}$	2	TIG	COM-MERCIAL PURE TI	LONG.
-15	I	-6	$4.67^{+0.04}_{-0.00}$	2	ELECTRON BEAM	-	LONG.
-16	II	-6	$4.67^{+0.04}_{-0.00}$	2	ELECTRON BEAM	-	LONG.
-17	-	-2	-	8	-	-	LONG.
-18	-	-3	-	8	-	-	TRANSV.
-19	-	-5	-	8	TIG	6 AL-4V	LONG.
-20	-	-4	-	8	TIG	6 AL-4V	TRANSV.
-21	-	-5	-	8	TIG	COM-MERCIAL PURE TI	LONG.
-22	-	-4	-	8	TIG	COM-MERCIAL PURE TI	TRANSV.
-23	-	-5	-	8	TIG	COM-MERCIAL PURE TI	LONG.
-24	-	-4	-	8	TIG	COM-MERCIAL PURE TI	TRANSV.

FIGURE 25 EXPLOSIVE FORM TEST SPECIMEN

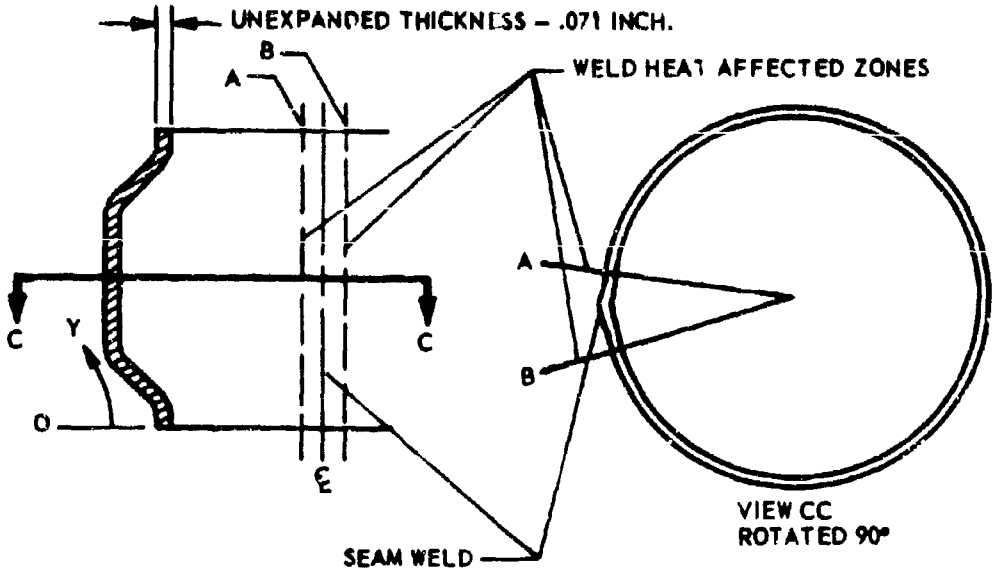

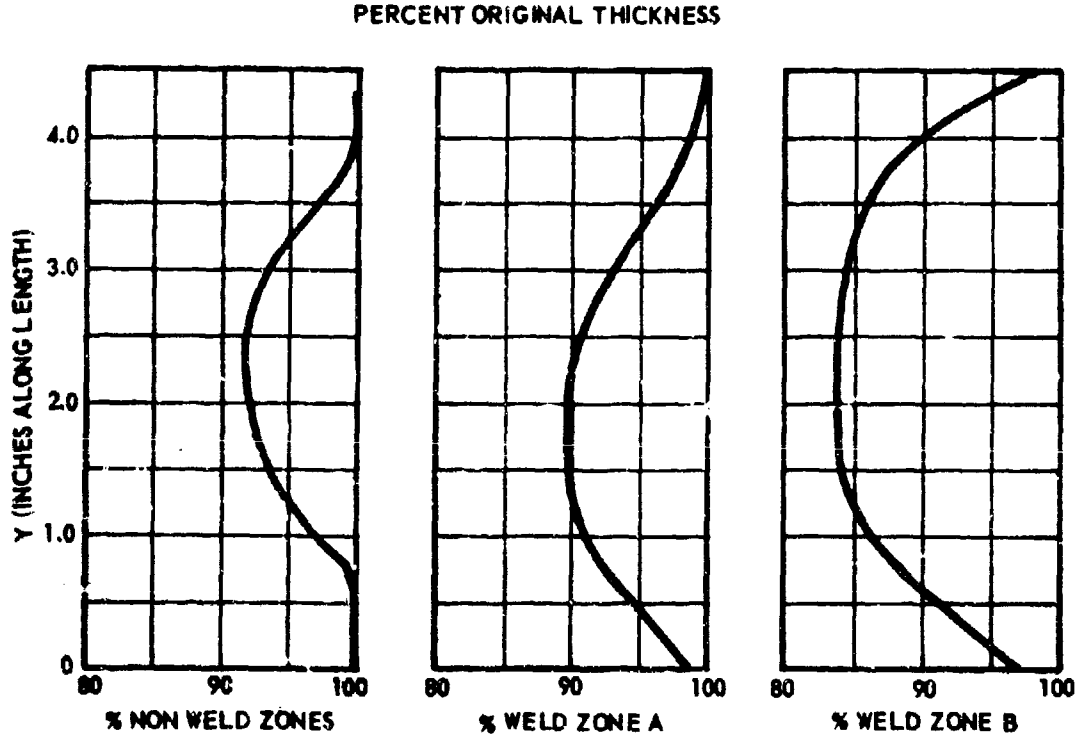

FIGURE 26 EXPLOSIVE FORM WELD TEST SPECIMEN – THICKNESS REDUCTION FOR 12% EXPANSION (SHEET 1)

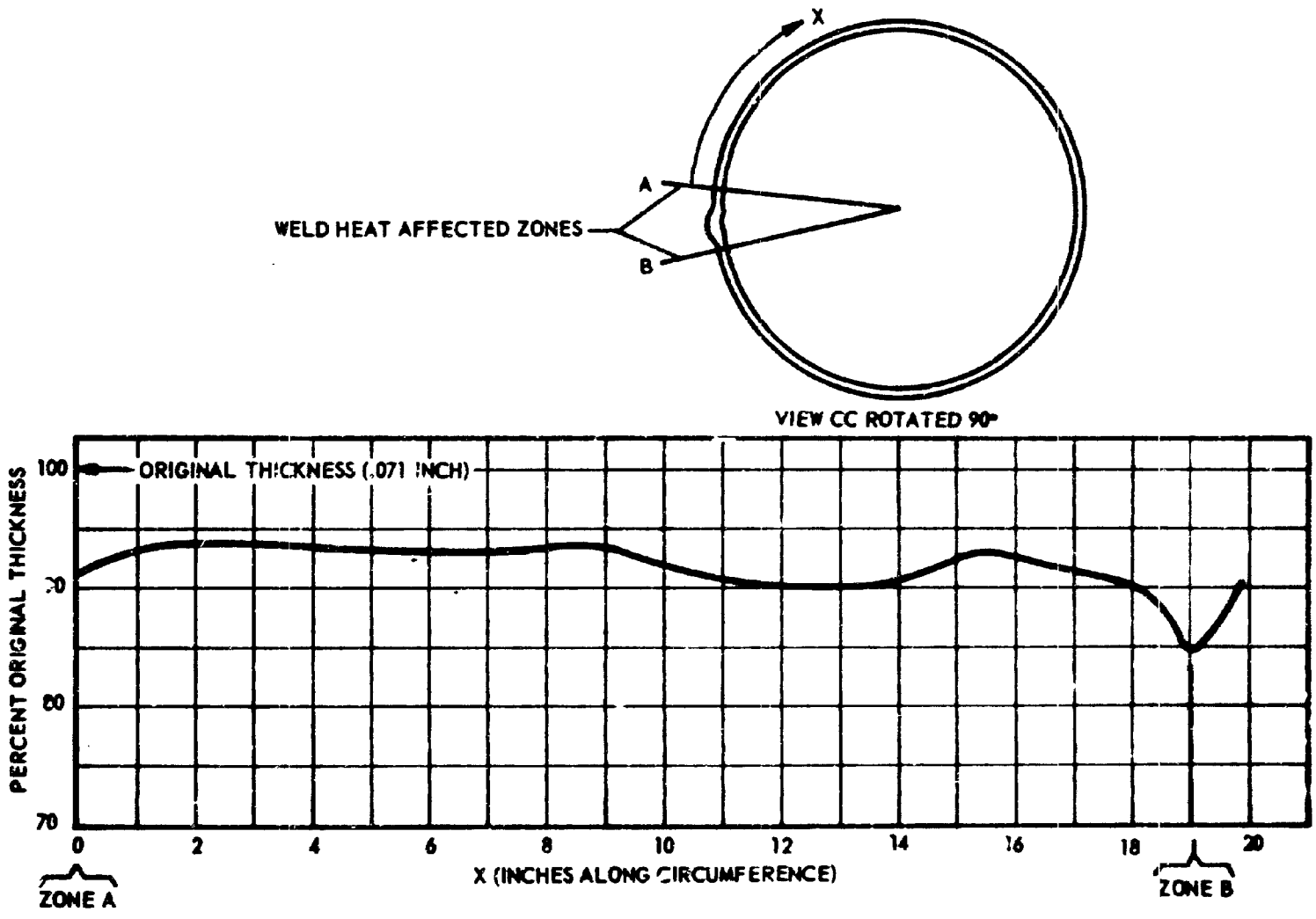

FIGURE 26 EXPLOSIVE FORM WELD TEST SPECIMEN – THICKNESS REDUCTION AT MAX. DIA. FOR 12 PERCENT EXPANSION (SHEET 2)

3. WELD AND HEAT TREATMENT EVALUATION TESTS OF TITANIUM 6AL-4V ALLOY

a. Test Specimens

Tensile coupons were type 211 given in Federal Test Specification 151. Tests were conducted at a strain rate of .005 in/in/sec. Coupons were cut from flat sheet, butt welded by the methods given in Table VI and Figure 27. Specimen numbers -2, -3, -11b, -12b, -2m, -3m, D-1 and D-2 (Ref. Figure 28) were received in the solution treated condition. Heat treat procedures used in preparing test specimens are described in Table VII.

Argon protective atmosphere was used. Specimen numbers MPA-1 and MPA-2 (Ref. Figure 28) were obtained from mill annealed stock.

Specimens for metallurgical evaluation, numbers 11w and 12w of Figure 29, were cut from explosively formed test cylinders. Specimens -20c and -21d of Figure 29 were cut from flat tensile coupons.

b. Test Evaluation

Study results of 6AL-4V titanium weld evaluations are as follows:

Sections of flat tensile specimens and explosively formed 6 inch diameter test cylinders (8% expansion) were obtained for metallographic examination of the weld beads, fusion zone, and heat affected areas. Samples were prepared from weld joints made with commercially pure and 6AL-4V titanium alloy filler wire.

Evaluation disclosed specimens cut from explosively formed cylinders had wider heat affected and fusion zones due to inadequate contact with the copper backup bar. A notable reduction of zone width is shown for flat sheet tensile specimens where intimate contact with the backup bar provided good chilling. Comparison of Figure 29 sheet 1 with sheet 2 and comparison of Figure 29 sheet 3 with sheet 4 shows 6AL-4V filler wire provided a more uniform grain size distribution across the weld, finer grains within the heat affected zone, and greater ductility than the commercially pure filler metal.

c. Test Results

As a result of these test and observations during explosive form test, 6AL-4V alloy weld rod and anneal temperature of 1500°F was selected for study hardware. Detail instructions on weld and heat treat processes were written and issued in LTV Engineering Department Specification Code 11813, No. 308-17-6.

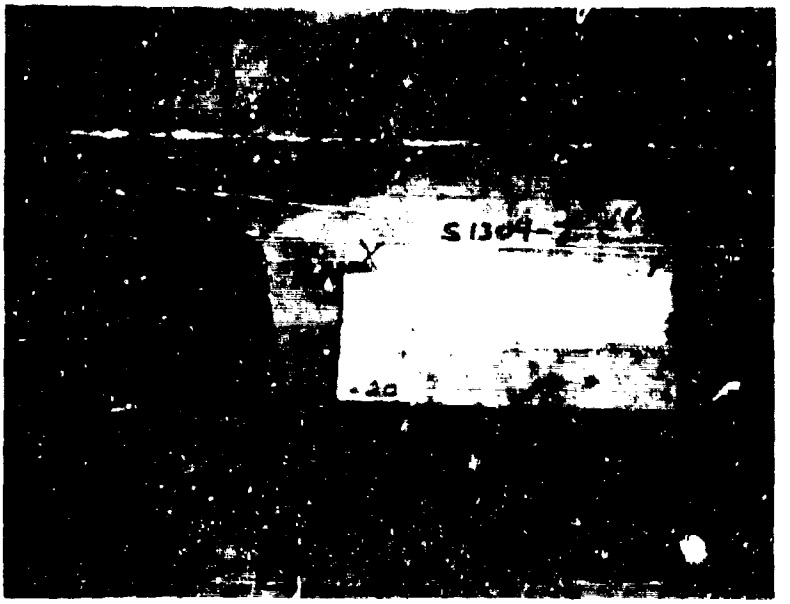

FIGURE 27 TITANIUM WELD EVALUATION CYLINDER AND BUTT WELDED SHEET

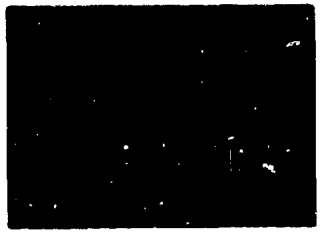

-2, LONGITUDINAL
R_c30.5

-3, TRANSVERSE R_c32
SOLUTION TREATED
+ 1350° F ANNEAL–VACUUM–
1 MICRON

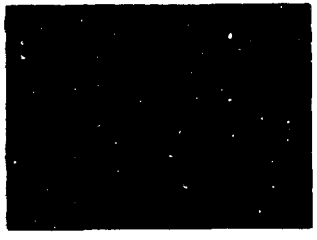

-11b, LONGITUDINAL
R_c32.5

-12b, LONGITUDINAL R_c32
SOLUTION TREATED
+ 1350° F ANNEAL–ARGON,
EXPLOSIVE FORMED TO 8%
EXPANSION

3m, LONGITUDINAL R_c29

2m, LONGITUDINAL R_c32
SOLUTION TREATED
+ DOUBLE 1350° F ANNEAL

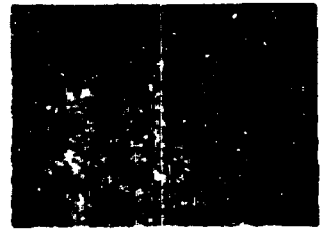

D–2, TRANSVERSE R_c31

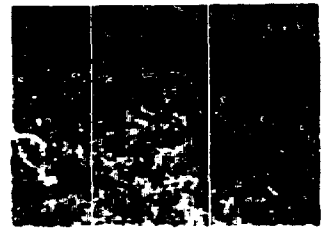

D–1, LONGITUDINAL
R_c29 SOLUTION TREATED
+ 1500° F ANNEAL–ARGON

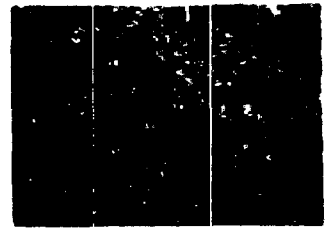

MPA–1, LONGITUDINAL
R_c34.5

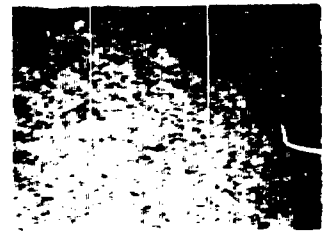

MPA–2, TRANSVERSE
R_c32.5 MILL, PURCHASED
ANNEALED

FIGURE 28 6AL–4V TITANIUM HEAT TREATMENT

TABLE VII

6AL-4V TITANIUM HEAT TREATMENT - SSPV PROGRAM

Specimen No.	Condition	Hardness Value	Remarks
-2 Longitudinal	Solution Treated + 1350° anneal in vacuum of 1 micron	R_C 30.5	Microstructure similar to "Solution Treated and Aged" condition, but hardness and elongation values indicate partially annealed properties.
-3 Transverse		R_C 32	
-11b Longitudinal	Solution Treated + 1350° in argon (-80°F dewpoint) and explosively formed to 3% expansion in 6" diameter cyls.	R_C 32.5	Similar to -2 and -3 microstructure, with slight elongation of grains due to cold work of explosive forming.
-12b Longitudinal		R_C 32	
-2m Longitudinal	Solution Treated + double 1350°F anneal in argon (-80°F dewpoint)	R_C 32	Double 1350°F anneal tended to increase grain size and slightly increase elongation values.
-3m Longitudinal		R_C 29	
D-1 Longitudinal	Solution Treated + 1500°F anneal in argon (-80°F dewpoint)	R_C 29	Increased annealing temperature caused dissolution of grain boundaries and intermetallic precipitates which increased formability of domes.
D-2 Transverse		R_C 31	
MPA-1 Longitudinal	Mill purchased in annealed condition, no LTV heat treatment performed.	R_C 34.5	Grain boundaries and precipitates partially dissolved, but still evident, with slightly higher hardness values.
MPA-2 Transverse		R_C 32.5	

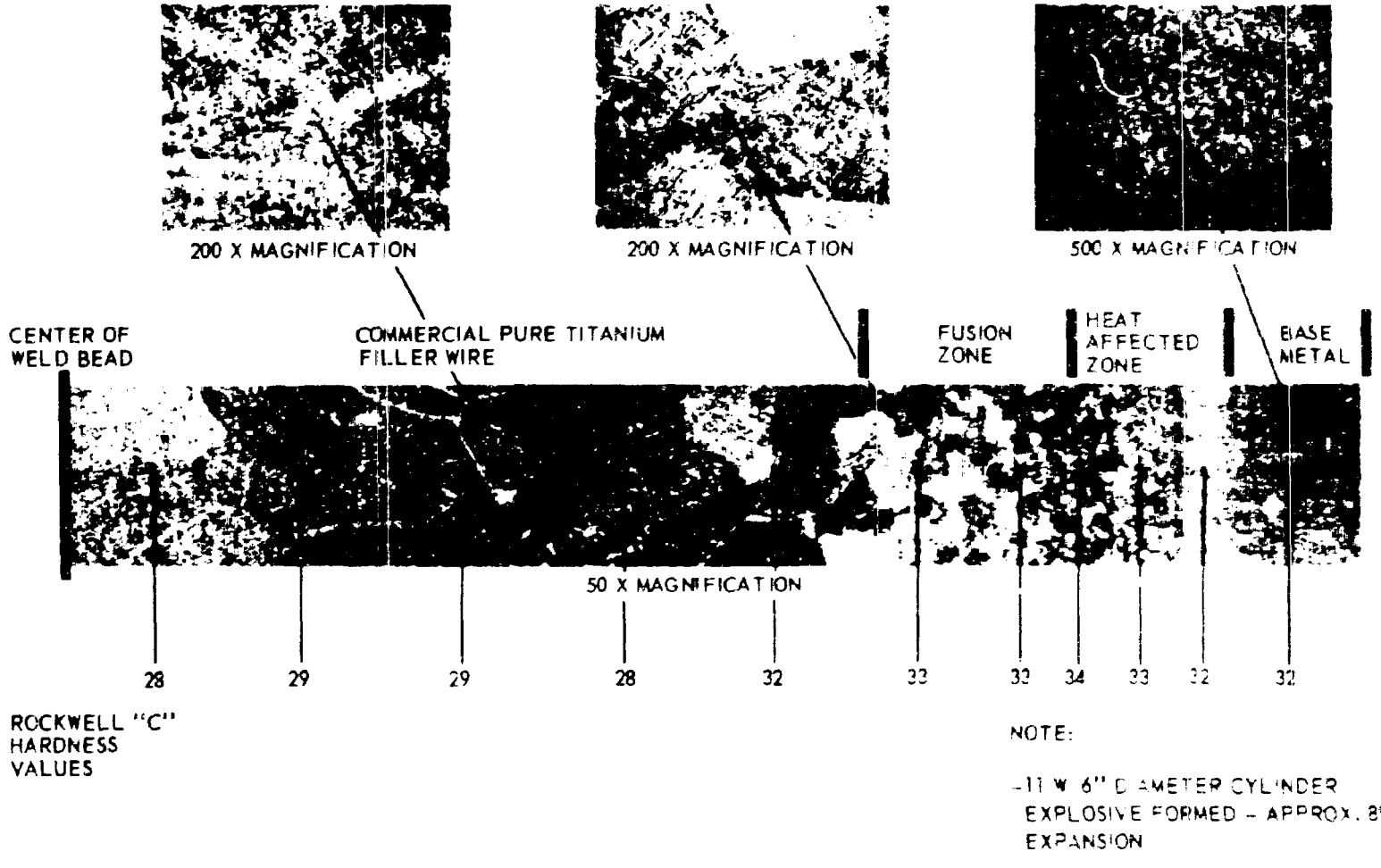

FIGURE 29 HEAT TREAT EFFECTS ON 6AL-4V TITANIUM ALLOY (SHEET 1)

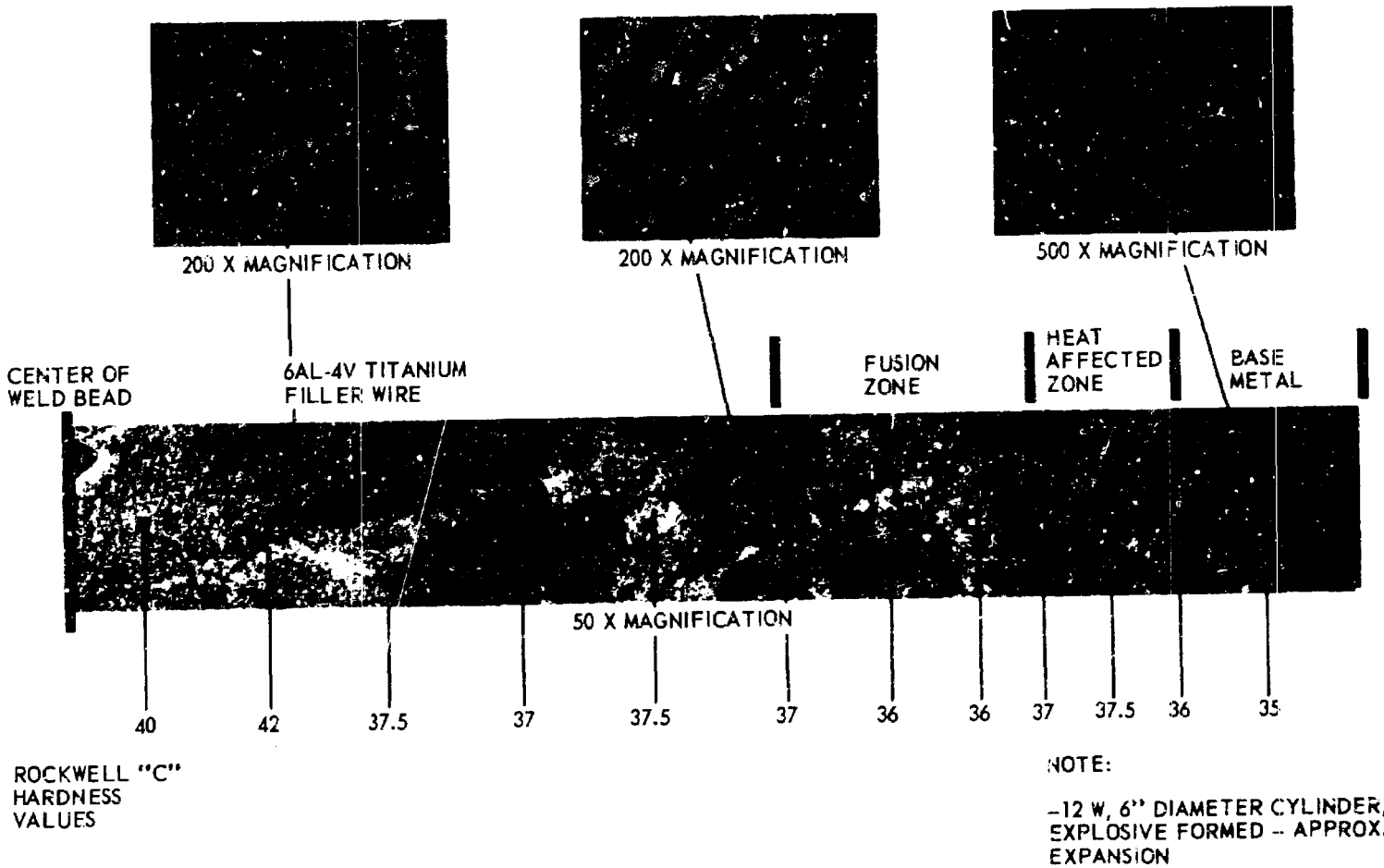

FIGURE 29 HEAT TREAT EFFECTS ON 6AL-4V TITANIUM ALLOY (SHEET 2)

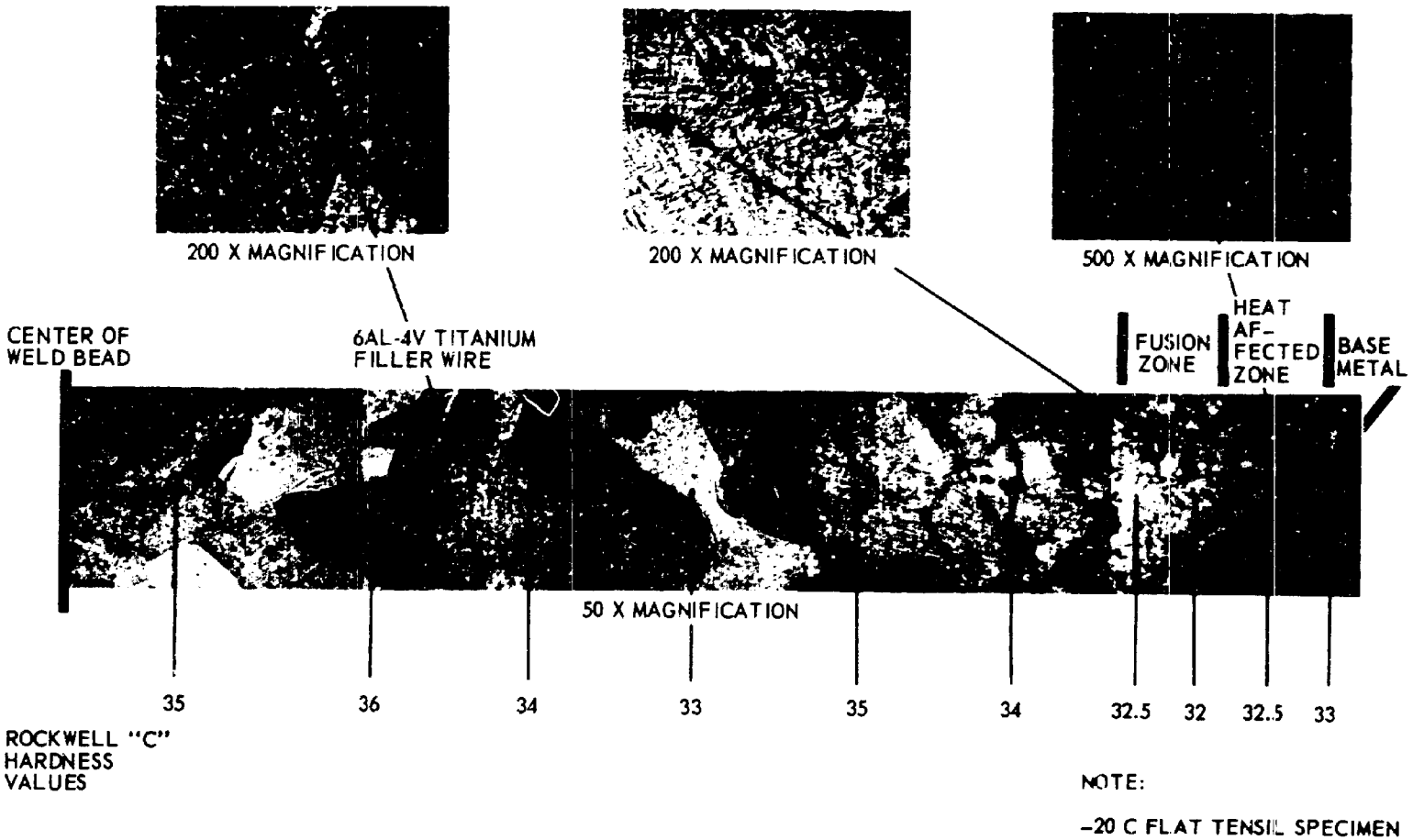

FIGURE 29 HEAT TREAT EFFECTS ON 6AL-4V TITANIUM ALLOY (SHEET 3)

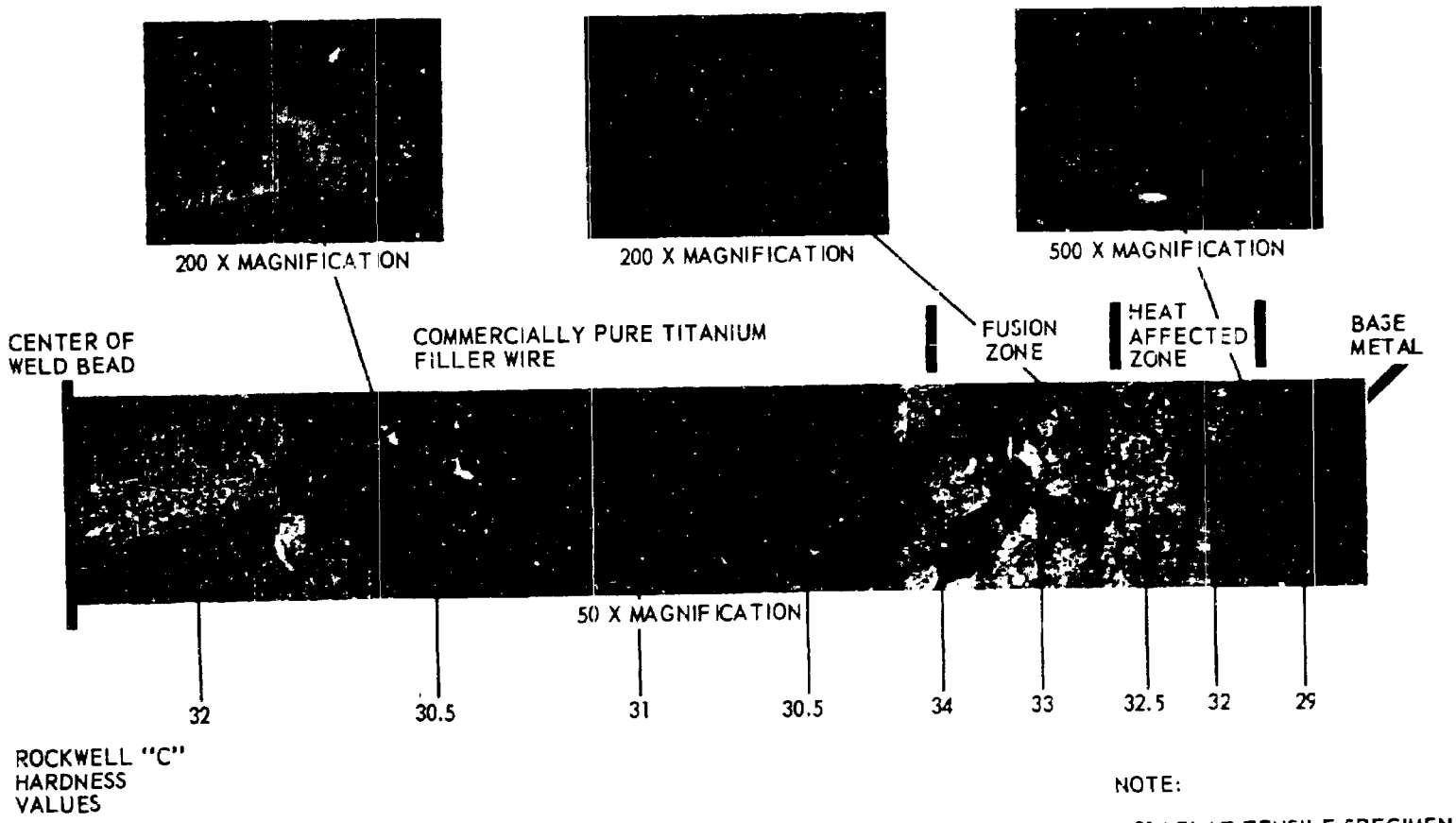

FIGURE 29 HEAT TREAT EFFECTS ON 6AL-4V TITANIUM ALLOY (SHEET 4)

4. STRUCTURAL MOCKUP TESTS

a. Structural Mockup Design

The structural mockup was designed to provide a means of measuring radial deflection of the engineering model Class (I-II) shell under band preload. An actual explosive formed shell component was fitted with a spindle and four internally located dial gages. The gages were supported from the spindle at 90 degree angular spacing, with radial alignment of sensor rods. The sensor rods contacted the inside surface of the shell at the centerplane of the MODE. Access holes were provided through the spindle end plates to allow initial setting and reading of the gages at any band winding stage. (Ref. Figure 30)

The method of mounting the shell on the spindle allowed free deflection of the MODE area. Consequently, the mockup also served as a test structure for observing any exceedance of shell buckling strength under band preload.

b. Test Procedure

A winding tensioning schedule was prepared for end conditions of 15,000, 25,000, 35,000 and 40,000 uniform pretension. Deflection readings were called for at each 10 percent increment of area. For this purpose trial runs were made to establish the number of turns to build the ring to full depth. A photograph showing the winding setup is shown in Figure 31.

c. Test Results

Deflection readings of the dial gages was converted to strain per psi of normal band load, which was known from cumulative filament turns at known tensions. A foundation modulus of 3.49×10^{-6} (in/psi-normal) was determined for the Class I and II shells. This value was in excellent agreement with calculated value by the PETS computer routine.

There was no indication of yielding or buckling of the shell under the constrictive band load from a 40,000 psi winding tension.

FIGURE 30 STRUCTURAL MOCKUP SPINDLE FOR CLASS I-II VESSEL

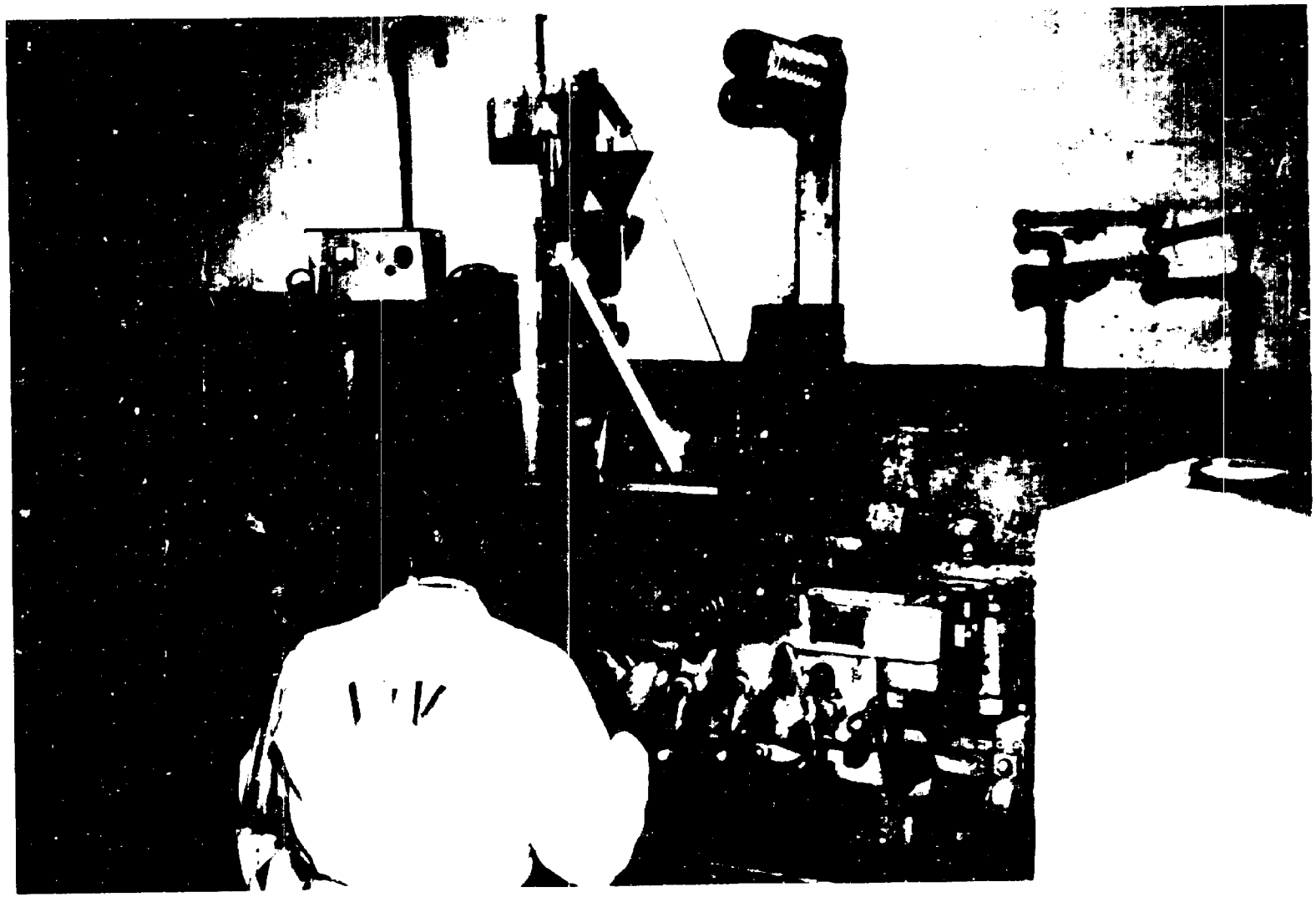

FIGURE 31 STRUCTURAL MOCK-UP OF WINDING SETUP

SECTION V

FABRICATION

1. EXPLOSIVE FORM PROCESS

a. Fabrication of Die

The explosive form die was designed as an inner split female die, an external cylinderical case and two end loading collars. All parts were machined from heavy wall steel pressure vessel tubing of SAE 335 PL alloy.

The split die was internally machined to the contour described in Figure 9. An interference fit between the external surface of the die and its restraining case was assured by a two degree diametrical taper. Axial preload of the cylindrical titanium blank was provided by sixteen bolts through each collar and threaded into the end faces of the case. By means of prescribed bolt torques, a controlled compressive force was developed between the collars and the end faces of the cylindrical blank.

Early trials showed a tendency to over-form the node radius. The axial preload on a partially formed part caused an inward radial load at the nodal plane. This effect was negated by installing an internal support ring in the nodal plane. Ring installation was made after firing the second explosive charge.

b. Forming Procedure

Beginning of the explosive forming operation is shown in Figure 32 as the placement of the cylindrical blank into the split die. Figure 33 shows the die completely assembled and in process of end loading the cylindrical blank. Figure 34 shows the primacord explosive charge suspended along the cylindrical axis. An explosive formed specimen is shown being removed from the die in Figure 35.

Forming was accomplished in three stages. After each firing, the end loading dropped off since radial expansion caused shortening of the part. Staging the forming operation allowed retorqueing to maintain a high end load during the application of the explosive pressure wave. Optimum procedure was found to be 75 foot pounds of bolt torque and an explosive charge of 50 grains per foot. The part was annealed after each firing.

c. Inspection

Distribution of wall thickness in the completely formed part is given in Figure 36. Maximum reduction occurred in the seam weld. X-ray and dye penetrant inspection disclosed several half inch long cracks in two of six parts, within the fusion weld zone inner surface, at the location of maximum expansion. In these cases the cracks were approximately .005 inches deep and were removed by localized grinding and polishing. Final ground thickness exceeded minimum thickness from forming so repair by local re-welding was not required.

FIGURE 32 LOADING CYLINDER BLANK IN EXPLOSIVE FORM DIE

FIGURE 33 LOADING AXIAL PRECOMPRESSION

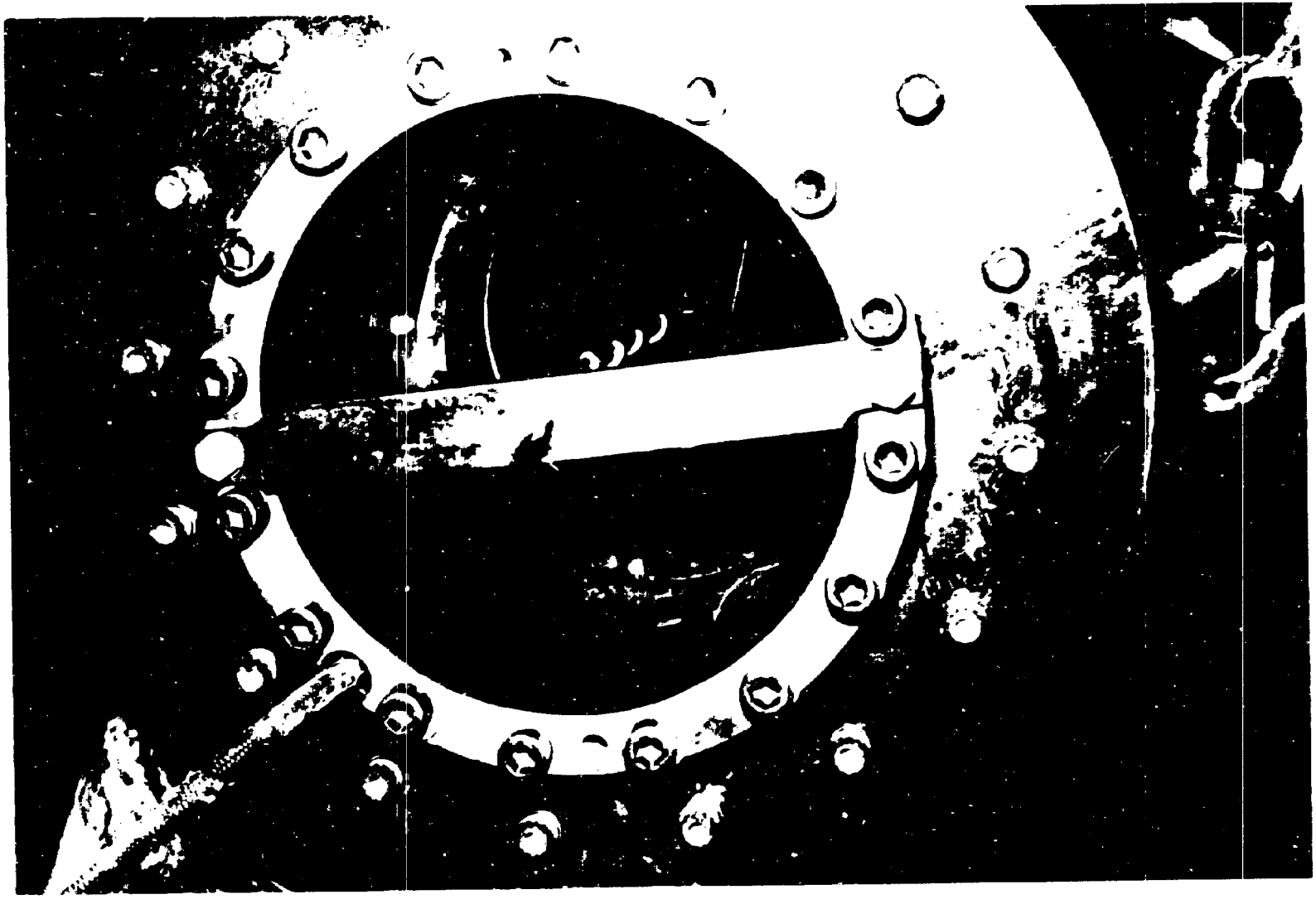

FIGURE 34 PRIMACORD AND MODE SUPPORT RING INSTALLED

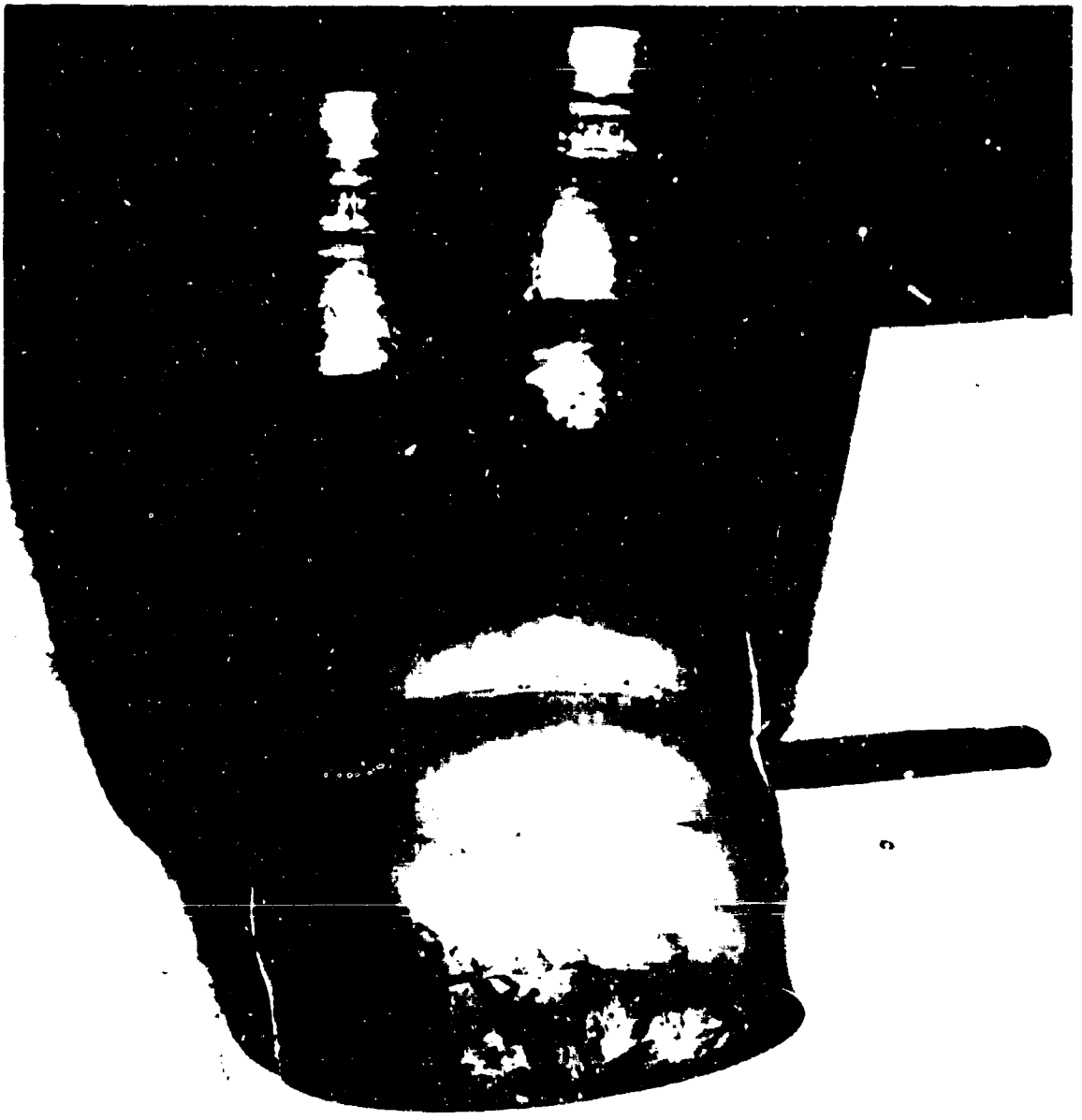

FIGURE 35 REMOVAL OF EXPLOSIVE FORMED PART

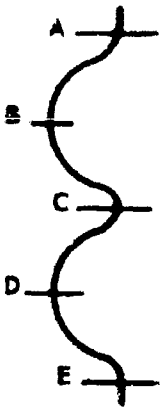

REFERENCE POINTS

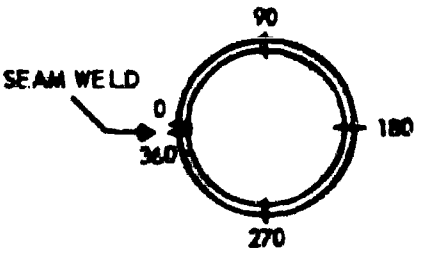

TYPICAL CROSS SECTION

NOTE: NOMINAL THICKNESS 0.070 IN.

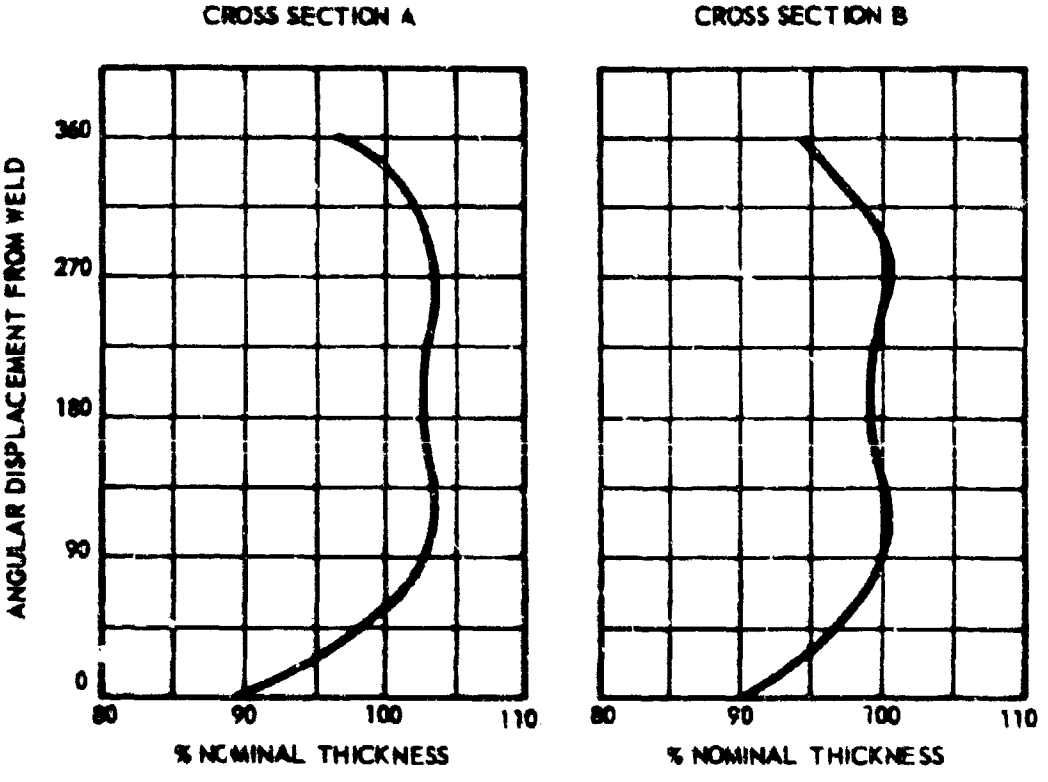

FIGURE 36 THICKNESS SURVEY OF EXPLOSIVE FORMED PART (SHEET 1)

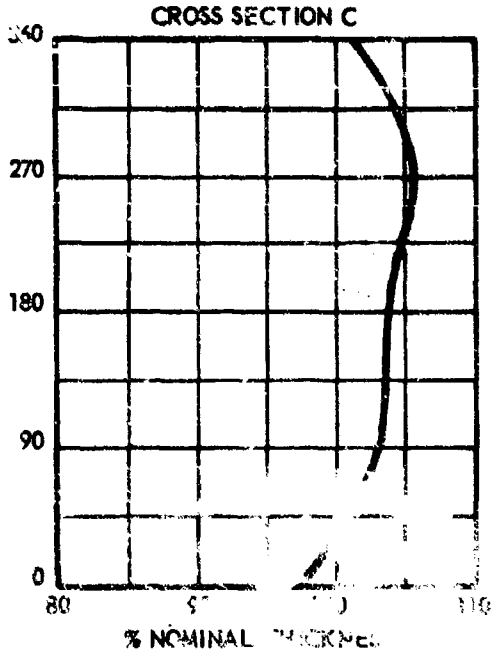

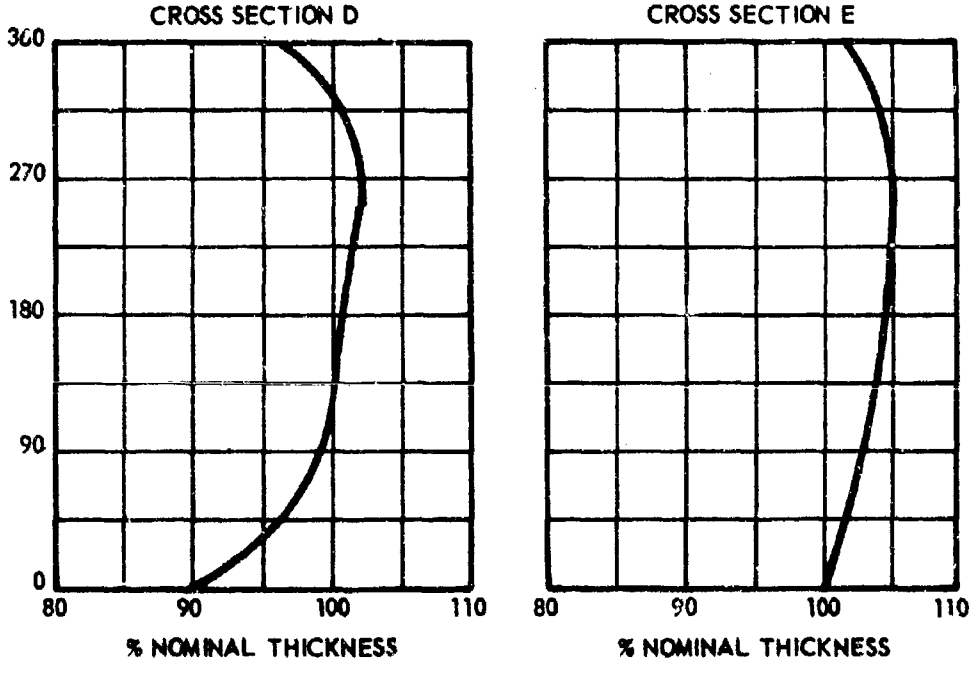

FIGURE 36 THICKNESS SURVEY OF EXPLOSIVE FORMED PART (SHEET 2)

2. FORMING PROCESSES

a. Titanium Hemispheres

The 6AL-4V titanium alloy hemispherical end closures for the Class (I-II) engineering models were draw formed from annealed sheet cut into 20 inch diameter blanks. For this purpose an existing punch and draw ring was modified and equipped with gas jets and manifolds for forming at elevated temperatures. Gas flames applied to the outer diameter of the draw ring and pressure plate was used to maintain a 1200°F temperature. A punch temperature of 1000°F was maintained by radiation from the draw ring and pressure plate. Temperature measurement was made by four thermocouples at 90 degree spacing in the draw ring and two thermocouples inserted in the top of the punch.

The draw operation was made in three stages. Three .125 inch thick blanks of 301 CRS were initially stacked above the titanium blank. When the draw progressed to the point of interference between the stock and the draw ring, the top cover blank was removed and the draw continued to the next position of interference. The cover blank adjacent to the part was retained through the complete draw in order to minimize scouring of the titanium surface.

Maximum thinning of the part occurred at the apex. Variation in thickness of a typical part is shown by the measurement survey in Figure 37.

b. 17-7PH Steel Hemispheres

The 12 and 17 inch diameter hemispheres for the Class III engineering model were draw formed from annealed sheet at room temperature. The high ductility of annealed 17-7PH material permitted complete draw in one stage.

c. 17-7PH Nodal Section

The nodal section was stretch formed at room temperature. Due to the small diameter of the part, the grips of the radial-draw-form machine interfered with each other at 140 degrees of segment angle. This machine limitation required three segments to make up the 360 degrees of the nodal section.

3. WELDING METHODS

a. Titanium

All titanium welds assembling the Class (I-II) vessels were in accordance with MSD-T Engineering Specification Code Identification No. 11813. 6AL-4V titanium welding wire was used in all joints. Special holding fixtures were fabricated for adaptation to an automatic TIG welding machine. These fixtures provided copper rings and an internal inert gas atmosphere. Weld schedules were established by trial welds of real assemblies and evaluation of welds by x-ray and dye penetrant inspection and metallurgical measurement of the heat affected zone.

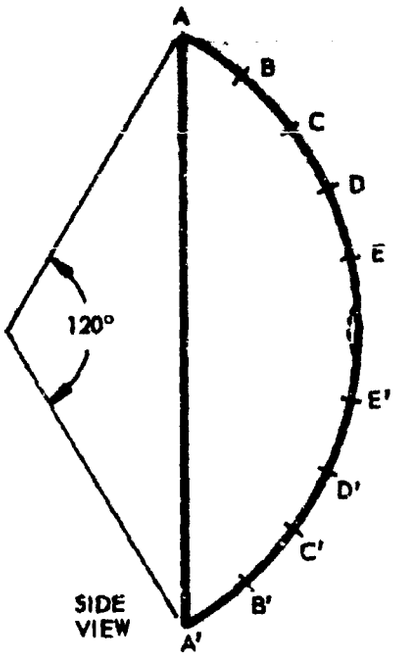

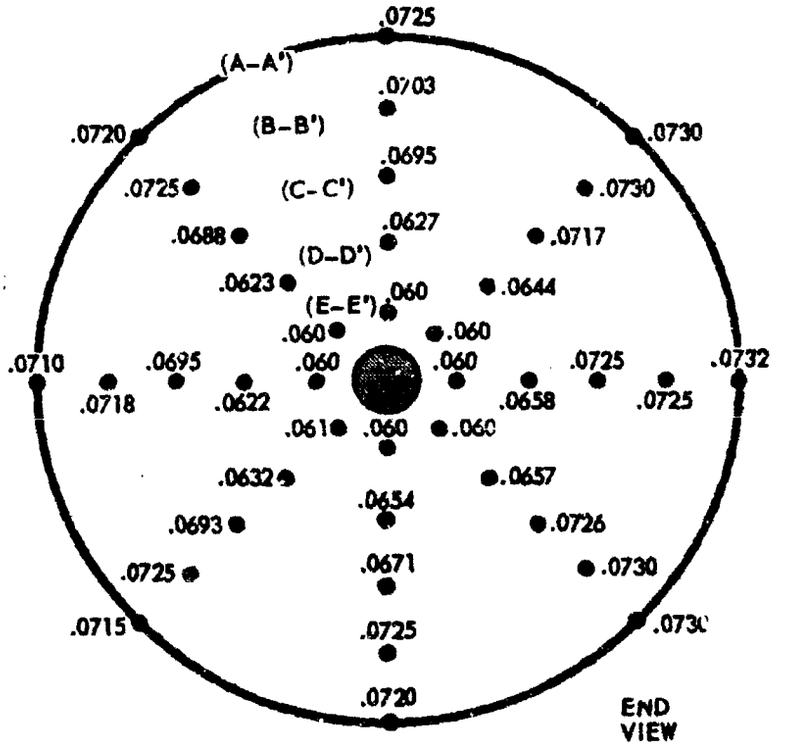

FIGURE 37 THICKNESS SURVEY OF DRAW FORMED PART

b. 17-7PH Steel

All steel assemblies were hand TIG welded with 17-4 stainless steel rod in accordance with specification MIL-W-8611. Special fixtures were used to provide dimensional alignment and an internal inert gas atmosphere (Ref. Figure 38). The assembled shell is shown in Figure 39.

c. Weld Inspection

Titanium and steel weldments were inspected to equivalent requirements of acceptance specification MIL-R-11-486, Weld Standard II. Since all phase I hardware was for test purposes, minor defects were bought off by engineering examination and notation to assure their consideration during evaluation of test results.

Temperature measurements were made during a trial weld of a Class II Vessel Joint with a wound band in place. Temperatures developed at the band location were given in Figure 40. This test proved feasibility of welding prewound modules.

4. WINDING PROCEDURE

a. Winding Equipment

Reinforcement bands were wound with 20-end S901 filament glass at a constant 20 lb. tension. This corresponds to a filament tensile prestress of 37,000 psi. Tensioning load during winding was controlled by an Entec Model 728 electrical controlled tensioning device.

b. Class (I-II) Engineering Models

A special winding fixture was developed to provide side plates so the angled sides of the band could be wound to finished dimensions. This winding set up is shown in Figure 41. A finished machine cut was made on the outside surface after cure in order to provide a concave surface to final dimensions.

c. Class III

This band was wound in two steps without use of mold plates. A fifty percent excess of filament wraps was required to provide a leveled fill of sufficient depth to allow machining a concave surface to final dimension. To avoid risk of buckling the shell under the high culmative preload of the total wraps, half depth was wound and cured before winding the remainder. The winding operation is shown in Figure 42.

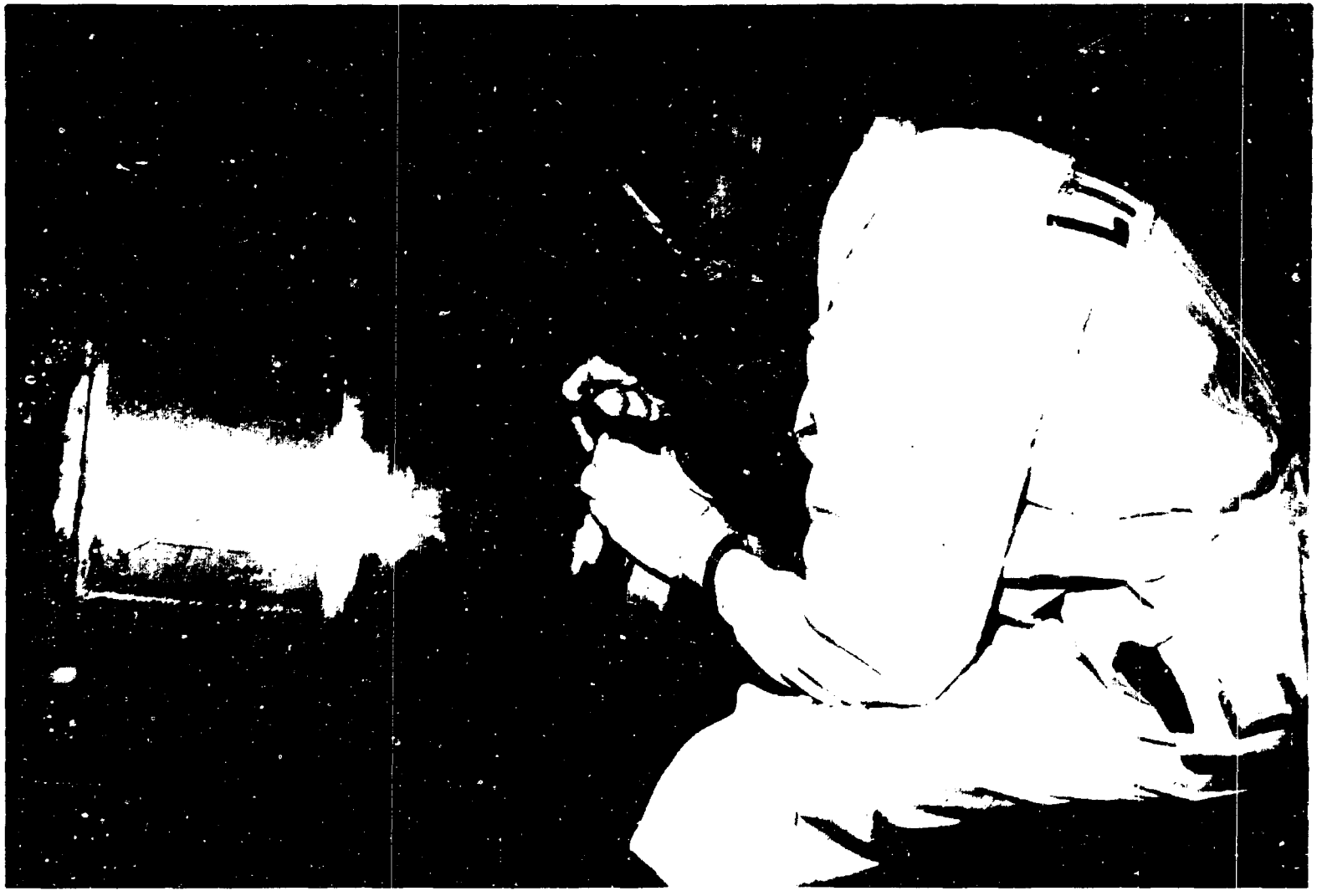

FIGURE 38 ENGINEERING MODEL CLASS III IN WELD FIXTURE

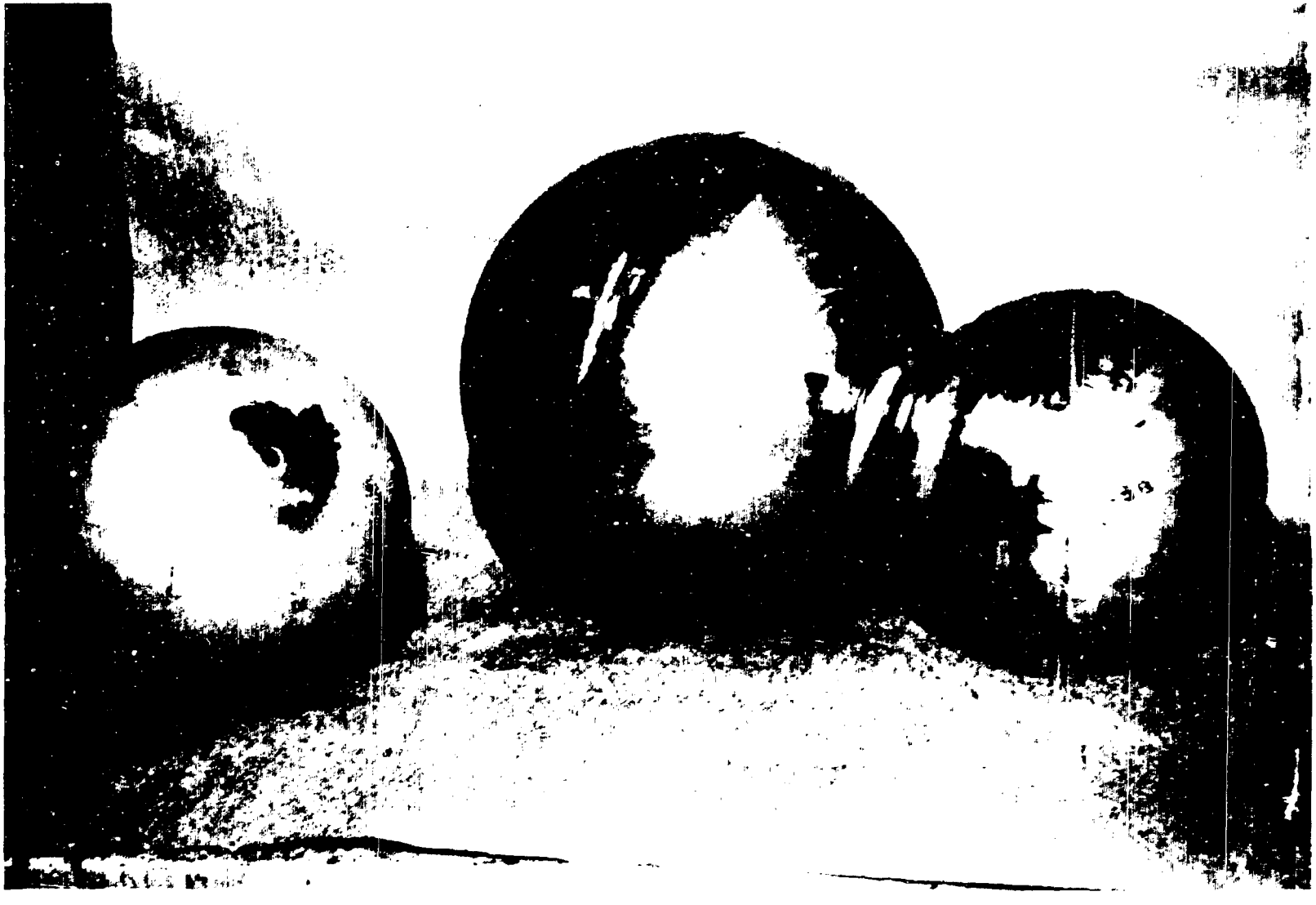

FIGURE 39 ENGINEERING MODEL SHELL CLASS III

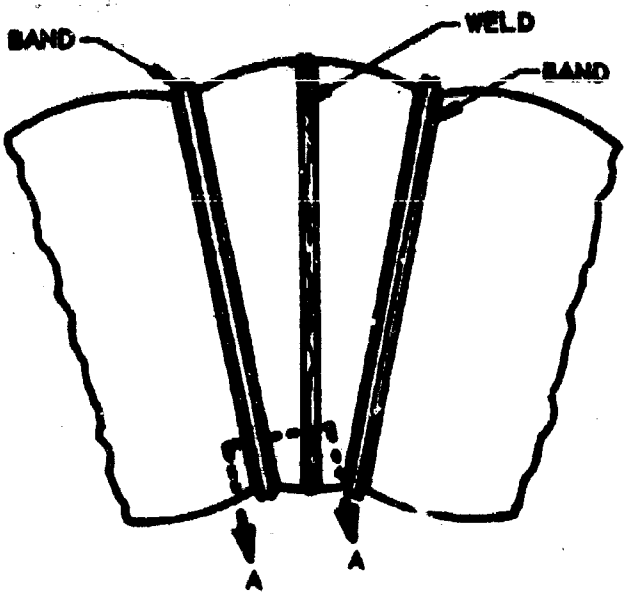

TEST SPECIMEN

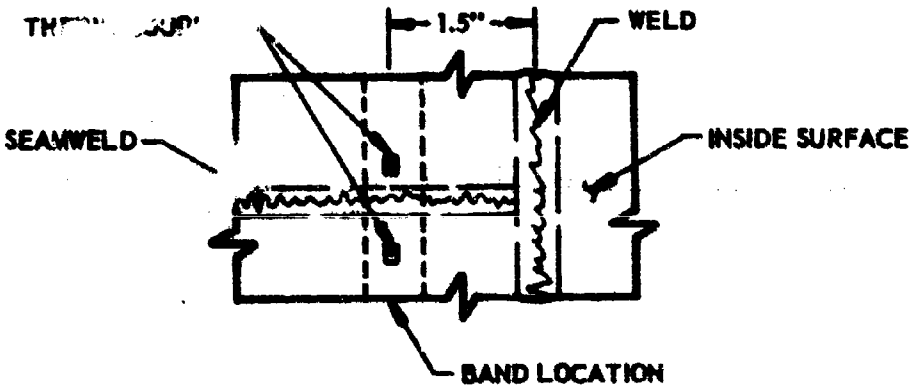

SECTION A–A

FIGURE 40 WELD TEMPERATURE MEASUREMENT – CLASS II VESSEL (SHEET 1)

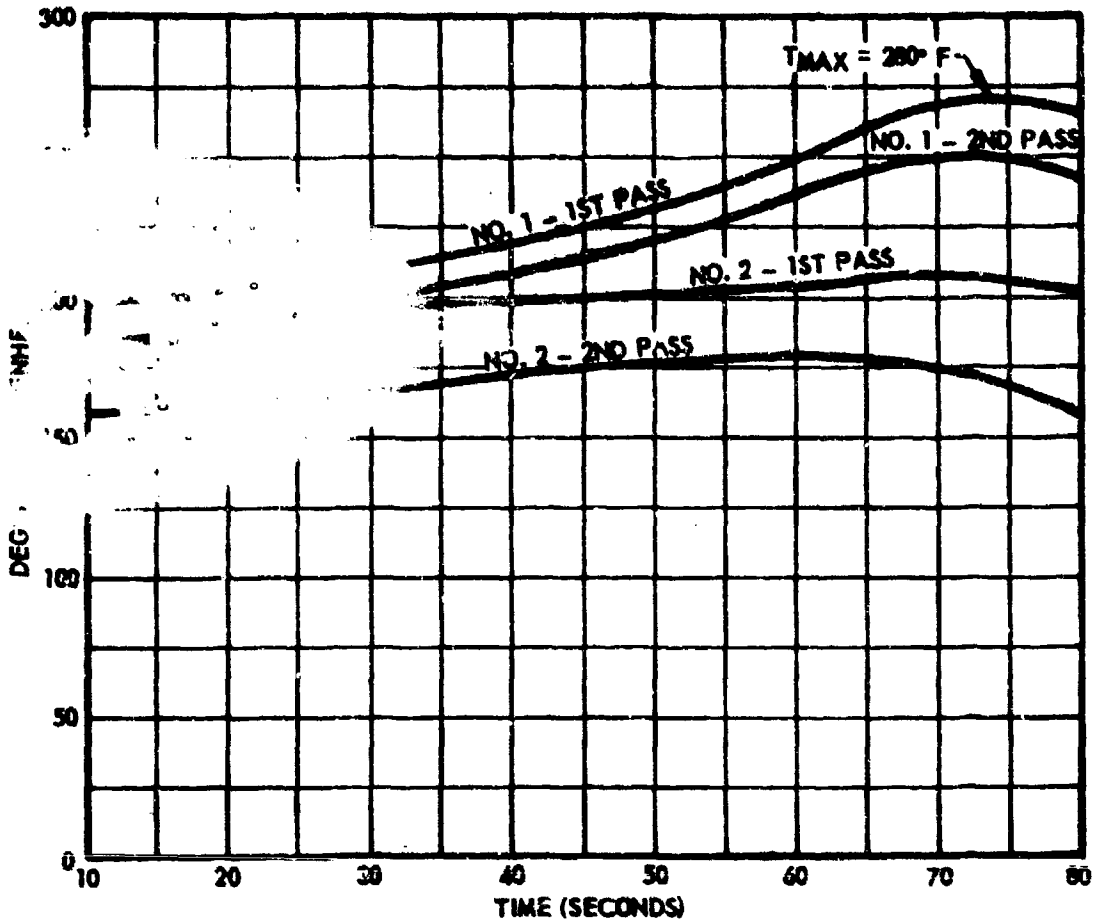

FIGURE 40 WELD TEMPERATURE MEASUREMENT – CLASS II VESSEL (SHEET 2)

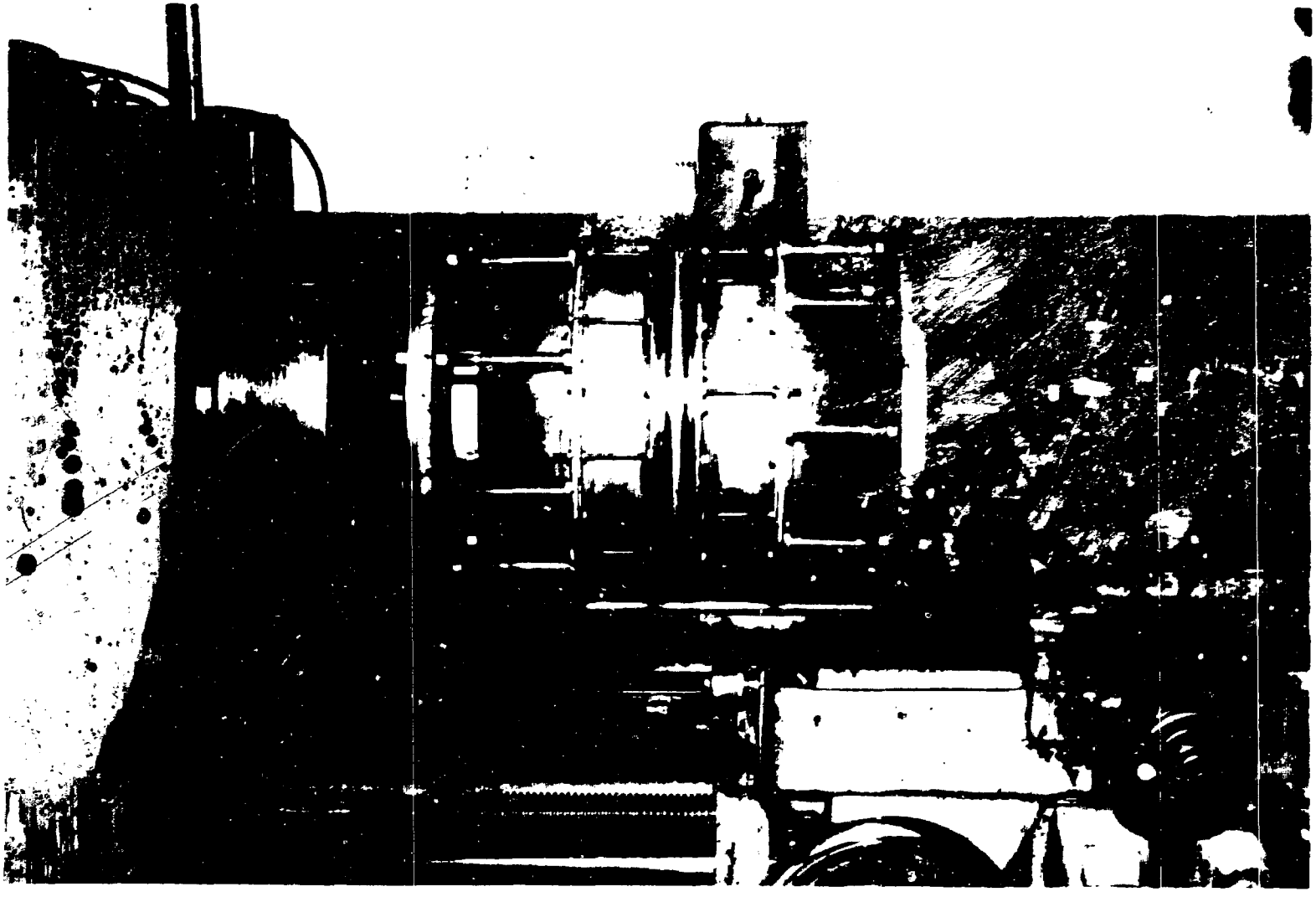

FIGURE 41 ENGINEERING MODEL CLASS(1 – II)IN WINDING LATHE

FIGURE 42 WINDING OF ENGINEERING MODEL CLASS III

SECTION VI

PRESSURE TESTS

1. OBJECTIVE

The objective of the test was to measure deflection and strength of SSPV Engineering Models.

2. TEST SPECIMENS

Specimens consist of two Class (I - II) Engineering Models and two Class III Engineering Model pressure vessels. The Class (I - II) Engineering Model was made of 6AL-4V titanium with a S-901 fiber glass filament wound band (Ref. Figure 43). The Class III Engineering Models were made of 17-7 PH corrosion resistance steel with the S-901 filament band. Series I and II in the following discussion designates the order of vessel manufacture for each class.

3. TEST SETUP

An optical comparator was used to make point and profile deflection measurements. This machine projects a low power magnification of the test specimen profile and is equipped to measure deflection displacement by use of a vertical and horizontal micrometer drive of the test specimen support base. The apparatus is shown in photographs of Figures 44, 45 and 46. Hydraulic fluid was used as a pressurization medium.

4. TEST PROCEDURE AND RESULTS

Each vessel was proof tested prior to placement on the comparator for deflection measurements. For safety purposes, vessels were proof tested to pressures 300 to 400 psi greater than maximum pressure to be applied during deflection measurements.

a. First Specimen

The Engineering model designated Series I, Class I, failed during proof test on 19 June 1967. Test pressure of 1500 psi was sustained for 30 minutes. The test proof pressure of 1650 psi was then sustained for 20 minutes, at which time the vessel failed. Failure occurred in the weld as shown in photographs of Figures 47 and 48. Metallographic examination and hardness traverse survey of the weld determined failure was due to atmospheric contamination of the weld. Hardness readings indicated gross atmospheric pickup of oxygen, nitrogen and possibly hydrogen due to loss of inert gas shielding.

b. Second Specimen

Engineering model Series I of Class III was tested on 21 June 1967. During proof test pressurization at 200 psi, an abnormally small increase in pressure with each pumping stroke was characterisitc of shell failure under the band, although leakage was not visible. Pressure was stabilized after

FIGURE 43 ENGINEERING MODEL CLASS I -- II

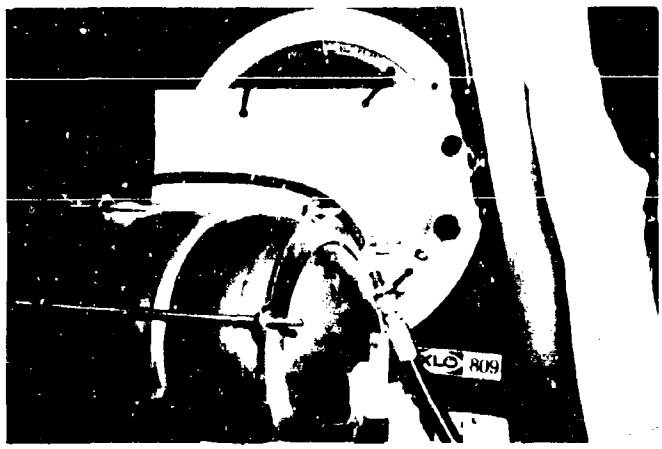

FIGURE 44 TEST VESSEL POSITIONED ON OPTICAL COMPARATOR

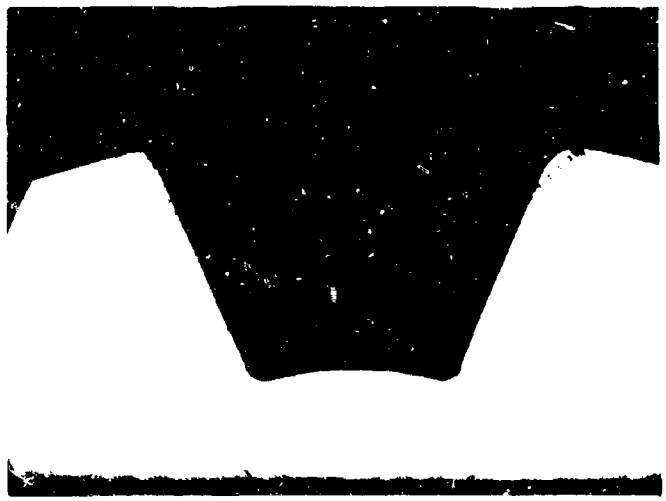

FIGURE 45 MAGNIFIED IMAGE OF TEST VESSEL BAND

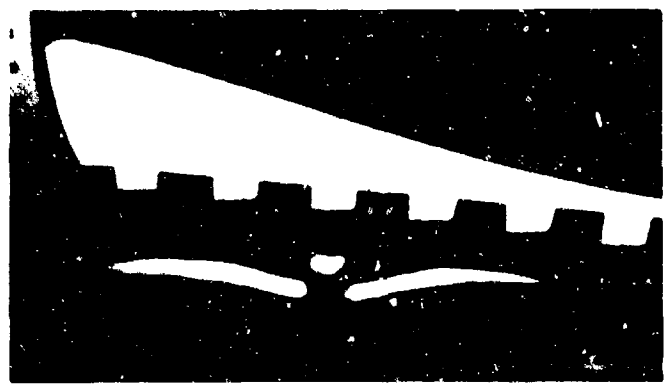

FIGURE 46 MAGNIFIED IMAGE OF TEST VESSEL PROFILE AND ADJACENT NOTCHED SCALE

FIGURE 47 FIRST TEST VESSEL AFTER BURST FAILURE

FIGURE 48 LOCATION OF INITIAL FAILURE IN FIRST TEST SPECIMEN

buildup due to blockage of flow through the fracture. At 1200 psi the fluid began to leak from underneath the band. Examination of the vessel (band removed) disclosed a half inch crack across the weld joining the 12 inch sphere to nodal band. The crack was normal to the circumferential direction of the band. Attempts to repair the failure by welding were unsuccessful. Tests were discontinued.

c. Third Specimen

The Series II, Class I was tested during the period 23-28 June 1967. This vessel was first proof tested for 30 minutes at 1500 psi. Following this proof, the vessel was taken to the comparator for deflection measurements, at 1200 psi. Deflections of the band and maximum sphere were measured adjacent to the fiber glass band. The viewed section extended a distance of 1.5 inches along the surface of the sphere. Measurements were converted to strain by dividing deflection by the original diameters. Pressure vs strain is plotted in Figure 49, sheet 1, 2, 3 and 4. A second proof test pressurization to 1800 psi was next completed after which profile deflection measurements were made up to 1500 psi. A plot using this data is given in Figure 50. A final proof test to 2200 psi was then carried out, followed by deflection measurements to 1800 psi. Test results are given in Figure 51, sheet 1 and 2.

In the subsequent test, pressures were increased to determine burst strength. Burst failure occurred at 2760 psi. Predicted burst failure was 2800 psi based on measured minimum wall thickness and weld strength reduction at the origin of fracture. The point of failure was at a welded pressure fitting. Photographs of the failed vessel are shown in Figures 52, 53 and 54.

d. Fourth Specimen

On 10 July 1967, the Series II vessel of Class III failed at 920 psi, during proof test pressure. Failure was confined to the circumferential weld joining the two larger hemispheres. The nature of the fracture, shown in Figures 55 and 56, indicated weld embrittlement.

e. Fifth Specimen

The failed Series I, Class III vessel (ref. paragraph b above) was salvaged by cutting out the leaking nodal section and welding the segment together to form an angular joint. The vessel was heat treated to the 1075°F condition followed by rewinding the reinforcing band. Burst test was conducted on 25 August 1967. Failure occurred at 1300 psi and appeared to initiate under the band and progressed to the great circle welds of both segments. All fractured surfaces indicated brittle material properties.

f. Sixth Specimen

The Series II, Class III vessel (ref. paragraph d above) was repaired by rewelding the failed great circle weld in the 17 inch segment.

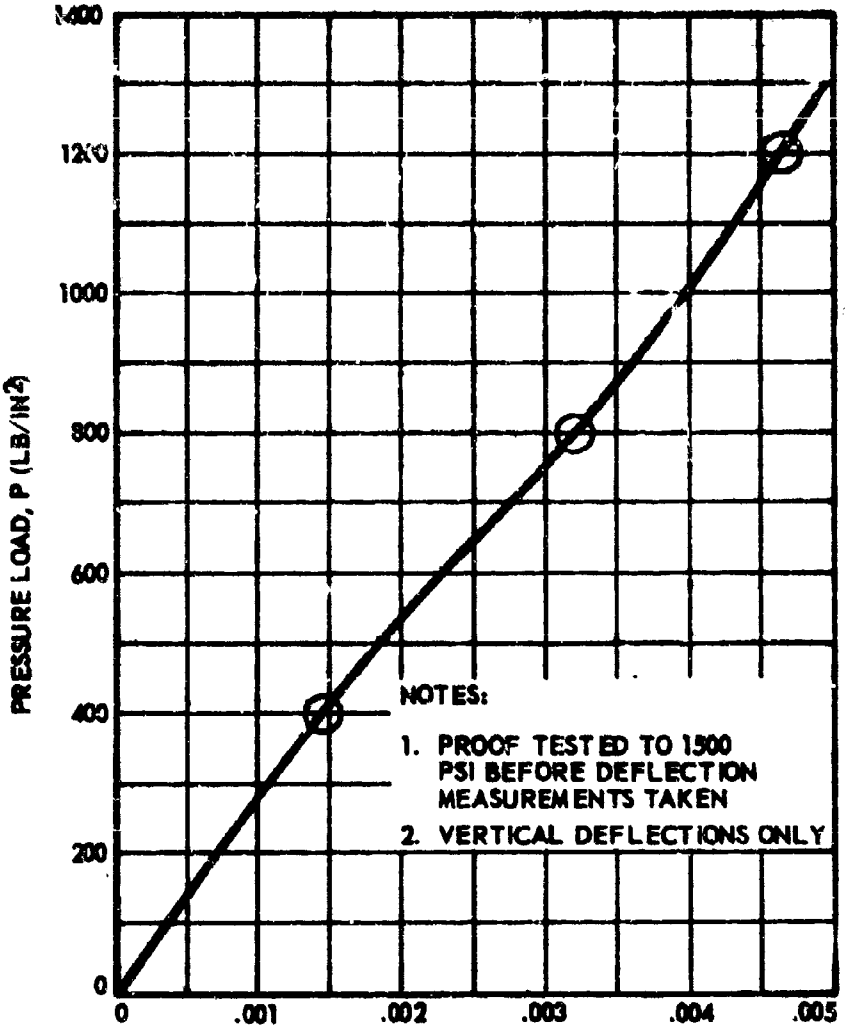

PRESSURE	0	400	800	1200
BAND DEFLECTION	0	.008	.018	.026
STRAIN	0	.00145	.00322	.00463

FIGURE 49 PRESSURE – STRAIN RELATIONSHIP OF AND THIRD SPECIMEN (SHEET 1)

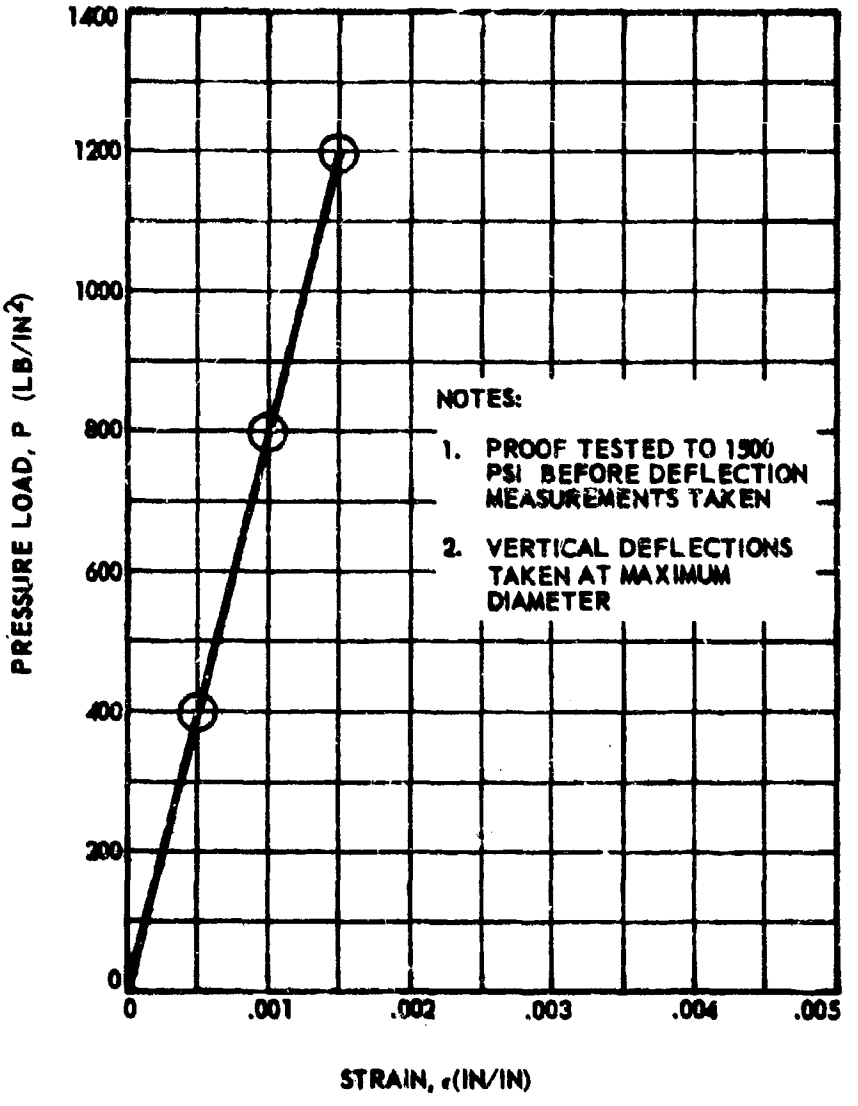

PRESSURE	0	400	800	1200
SHELL DEFLECTION	0	.003	.006	.009
STRAIN	0	.0005	.001	.0015

FIGURE 49 PRESSURE – STRAIN RELATIONSHIP OF SHELL THIRD SPECIMEN (SHEET 2)

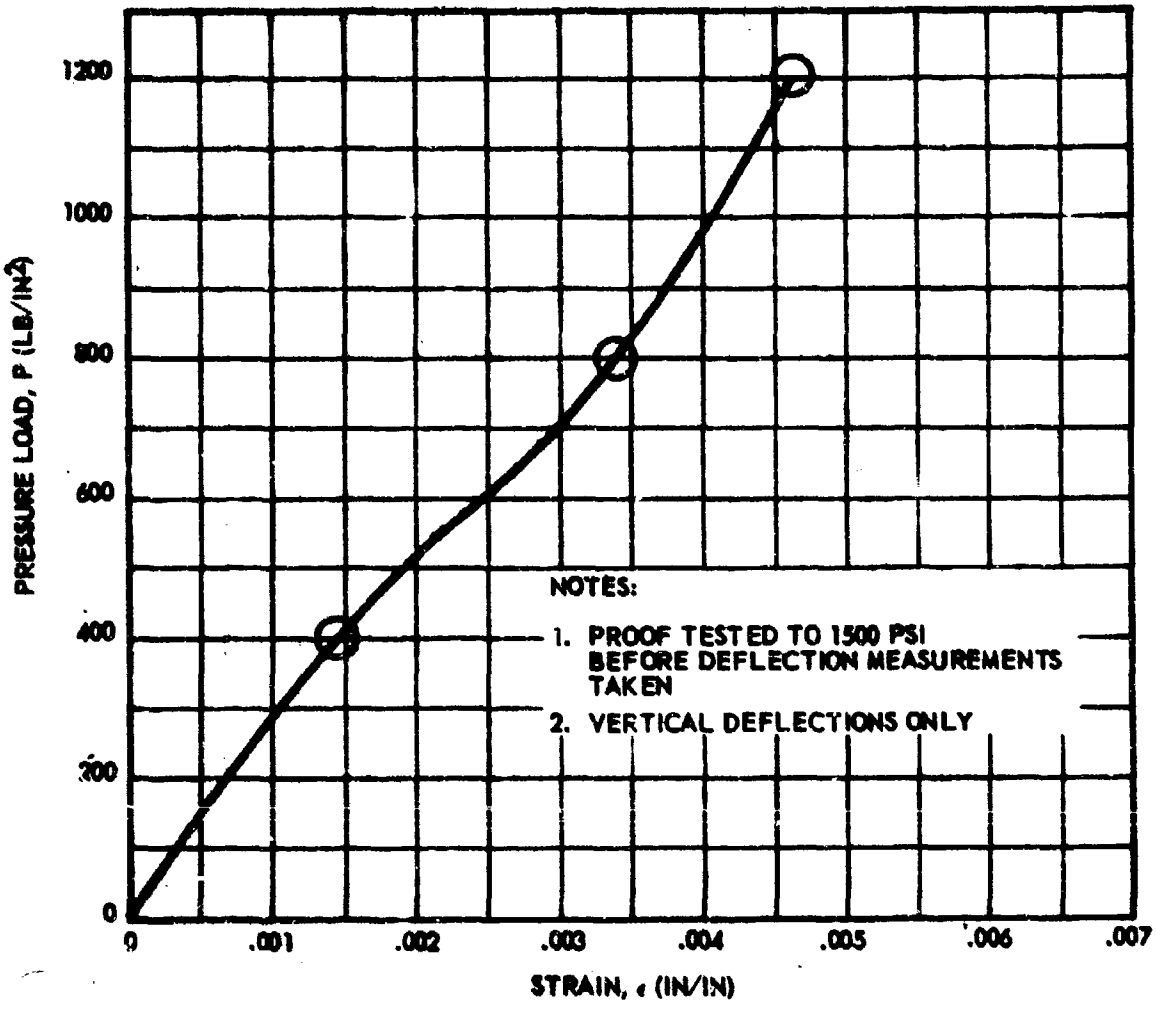

FIGURE 49 PRESSURE - STRAIN RELATIONSHIP AT BAND AND SHELL INTERSECTION THIRD SPECIMEN (SHEET 3)

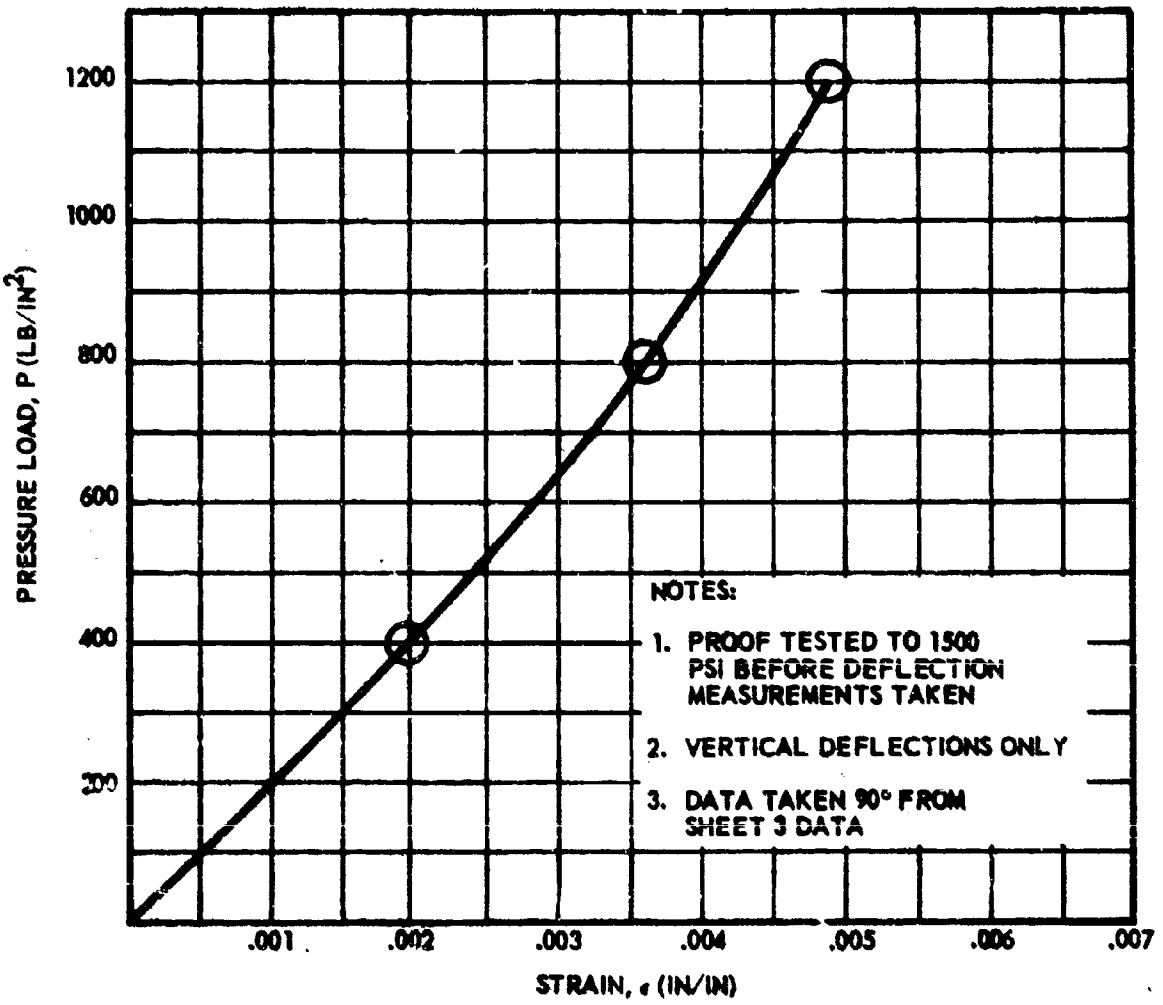

FIGURE 49 PRESSURE – STRAIN RELATIONSHIP AT BAND AND SHELL INTERSECTION THIRD SPECIMEN (SHEET 4)

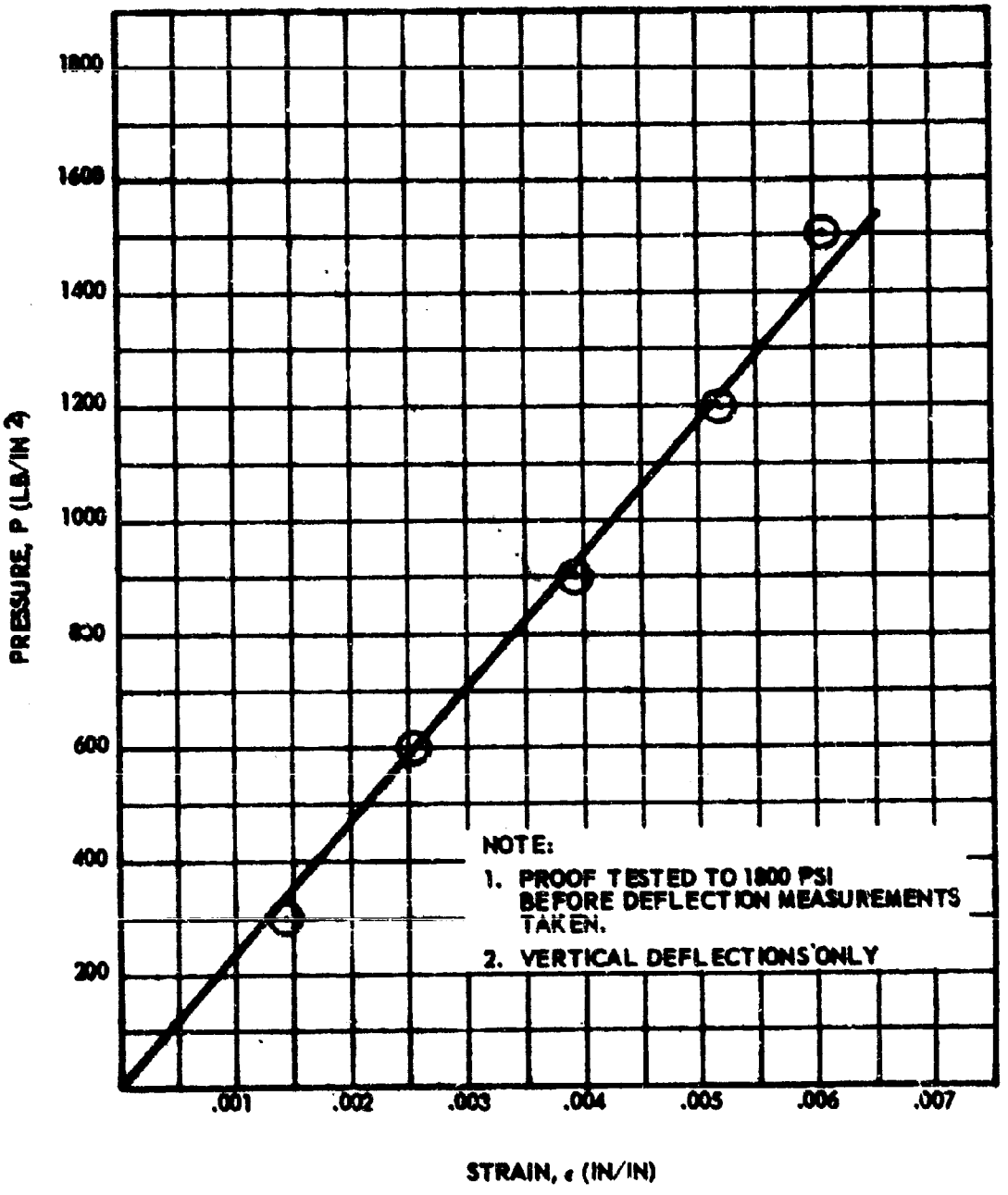

FIGURE 28 PRESSURE VERSUS STRAIN AT BAND AND SHELL INTERSECTION, THIRD SPECIMEN

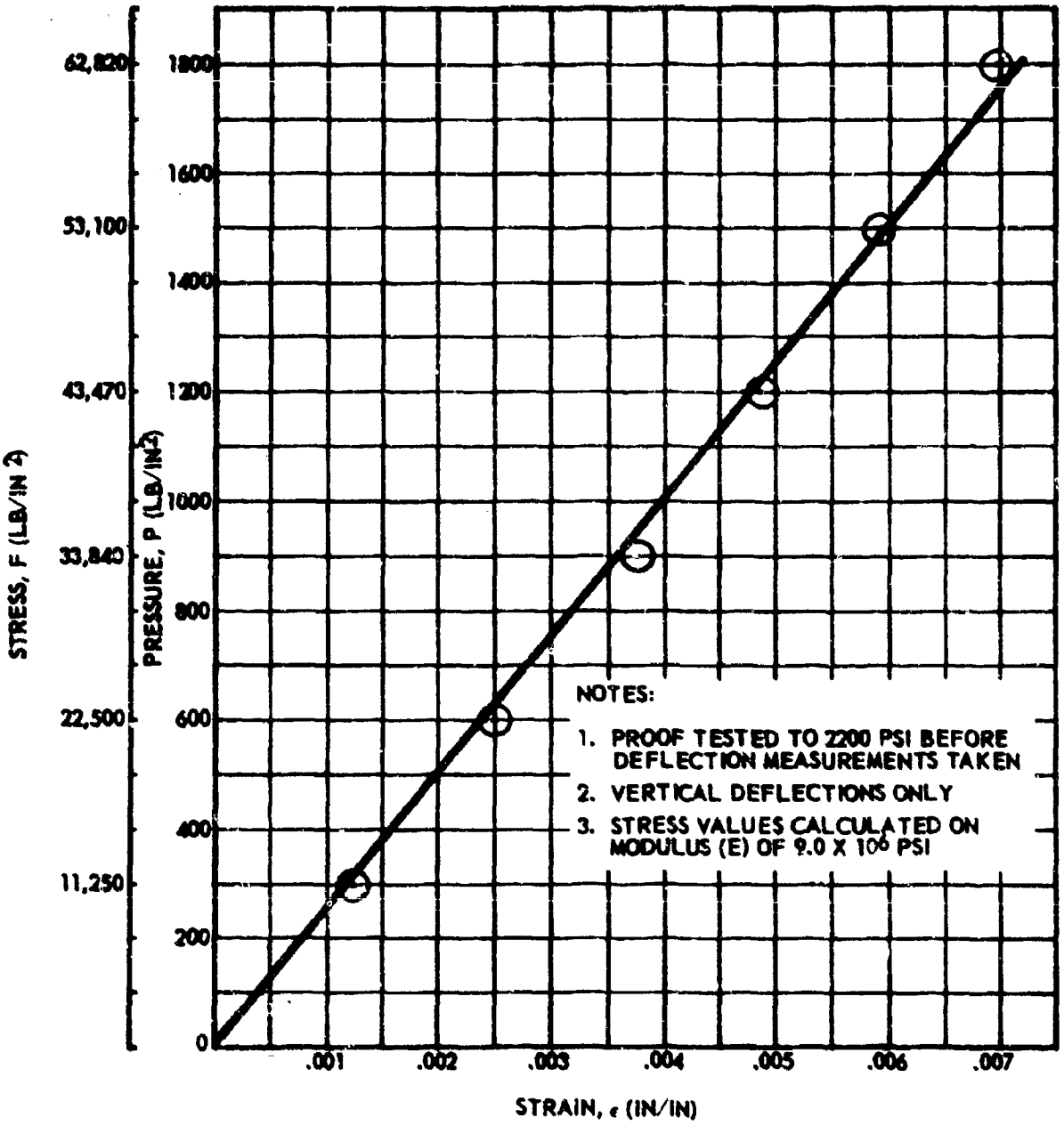

FIGURE 51 STRESS AND PRESSURE VERSUS STRAIN IN BAND THIRD SPECIMEN (SHEET 1)

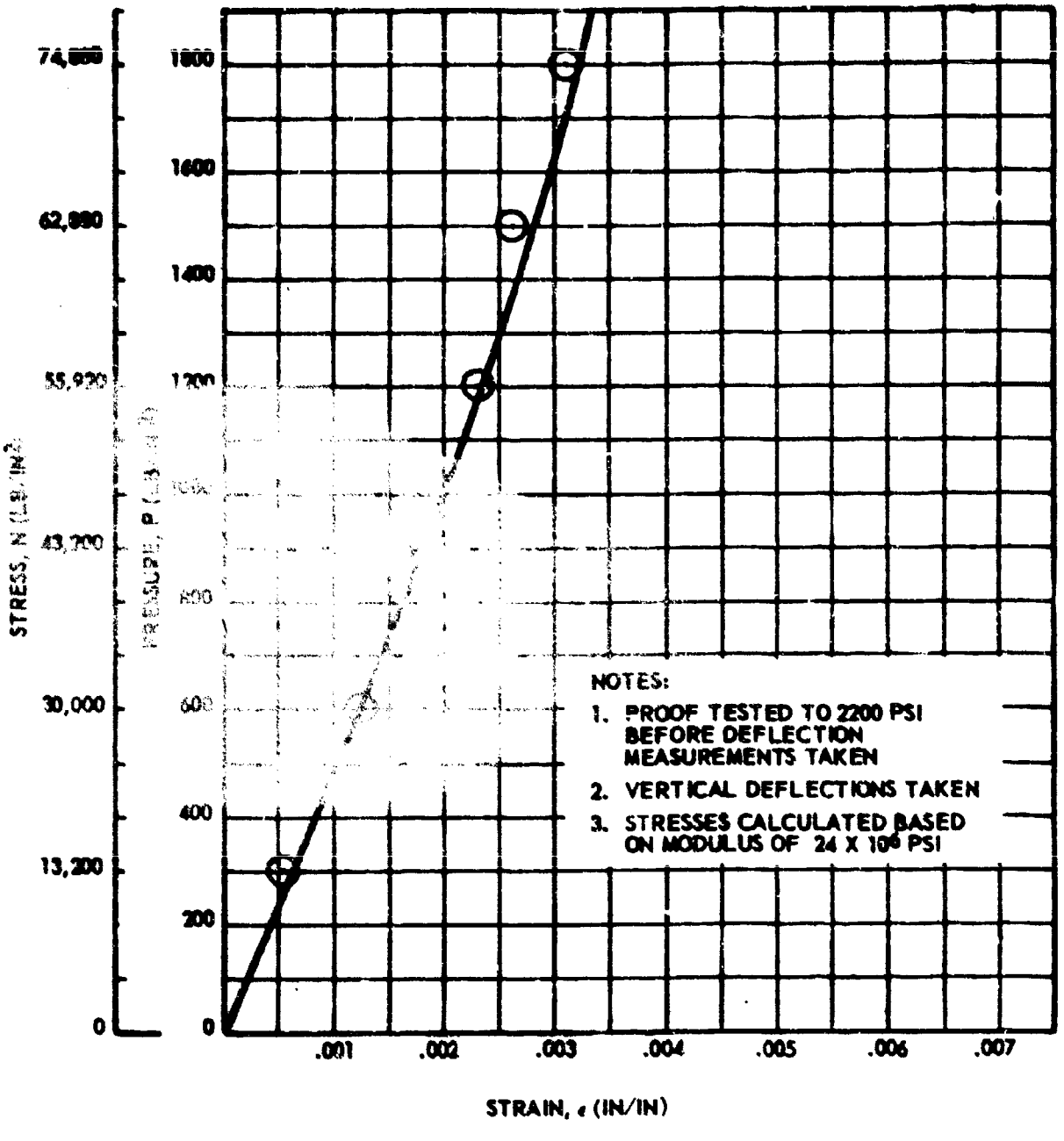

FIGURE 51 STRESS AND PRESSURE VERSUS STRAIN OF MAXIMUM SHELL DIAMETER THIRD SPECIMEN (SHEET 2)

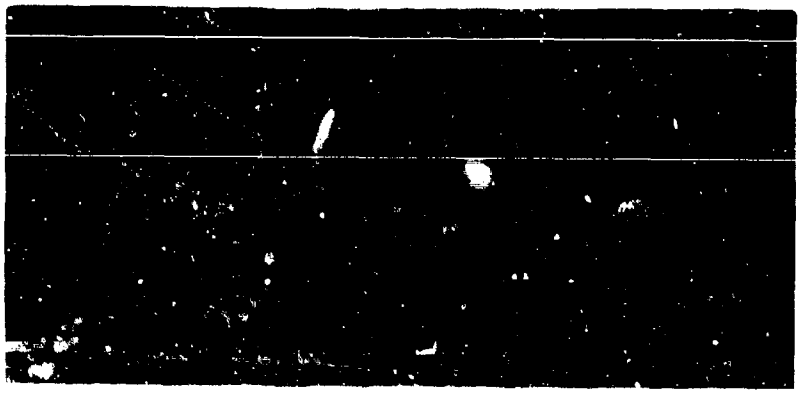

FIGURE 52 THIRD SPECIMEN AFTER BURST FAILURE

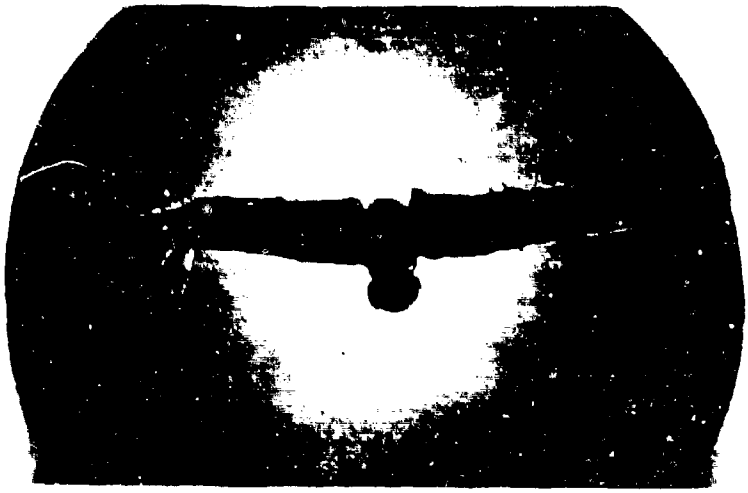

FIGURE 53 THIRD SPECIMEN ORIGIN OF FAILURE

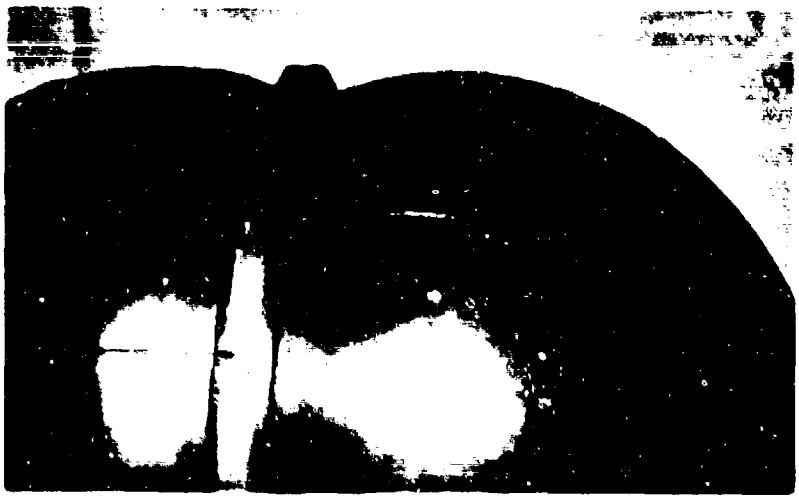

FIGURE 54 THIRD SPECIMEN FAILURE ARREST BY REINFORCING BAND

FIGURE 55 FOURTH SPECIMEN AFTER BURST FAILURE

FIGURE 56 FOURTH SPECIMEN CLOSE-UP OF FAILURE

It was then heat treated to 1075 condition and rewound. Burst test was conducted on 22 August 1967. This test was intended to evaluate differences with and without nodal section. However, failure occured at 1000 psi by brittle fracture of the repaired joint.

5. EVALUATION OF TEST DATA

a. Shell Remote From Band (Class I - II)

Test data was applied to reconstruct design conditions shown in Figure 57. The solid portion of curves 1 and 2 are based on test measurements reported in Figure 51. Curve 1 of Figure 57 shows an elastic stiffness parameter ($\varepsilon^s/f = 17.5 \times 10^6$). When this value is fitted to design formulae:

$$\varepsilon^s/f = \frac{\sigma^s}{\varepsilon^s f} = \frac{R}{2\,t\,E^s} = 17.5 \times 10^{-6}$$

An apparent average shell thickness is calculated as:

$$t = \left(\frac{6}{2 \times 17.5 \times 24} \right) = .0715" \quad \text{(Average)}$$

This is in agreement with measured thicknesses given in Figure 36. An average of 100 percent of nominal (.070 inches) is reported except for a localized zone near the weld seam. Test measurements were made for a diameter 90 degrees to the weld seam.

The extrapolated portion of curve 2 is based on typical 1:1 biaxial stress strain values for a local thickness of .060. This would predict a burst pressure of 3375 psi, neglecting weld effects which correspond to a proof pressure of 3375/1.5 = 2250 psi.

The weakest point is located at the welded port fitting. Shell thickness at this location was measured as .060 inches (Ref. Section V). Applying a weld reduction value of $\frac{135 \text{ ksi}}{168 \text{ ksi}} = .8$. Predicted burst based on analyses is then:

$$P_B = .80 \times 3381.7 = 2705 \text{ psi}$$

This agrees with a measured burst pressure of 2760 psi.

b. Band (Class I - II)

Extrapolating of curve 2 to burst load (point A) shows a maximum measurable strain of 13.75×10^{-3}. This corresponds to an increment band stress of 123,750 psi Total band stress must include the prestress of 40,000 (Curve 3) introduced by filament tension control during winding. Total band stress at burst is then 163,750 psi which is in good agreement with the 171,680 psi based on analysis of Section III.

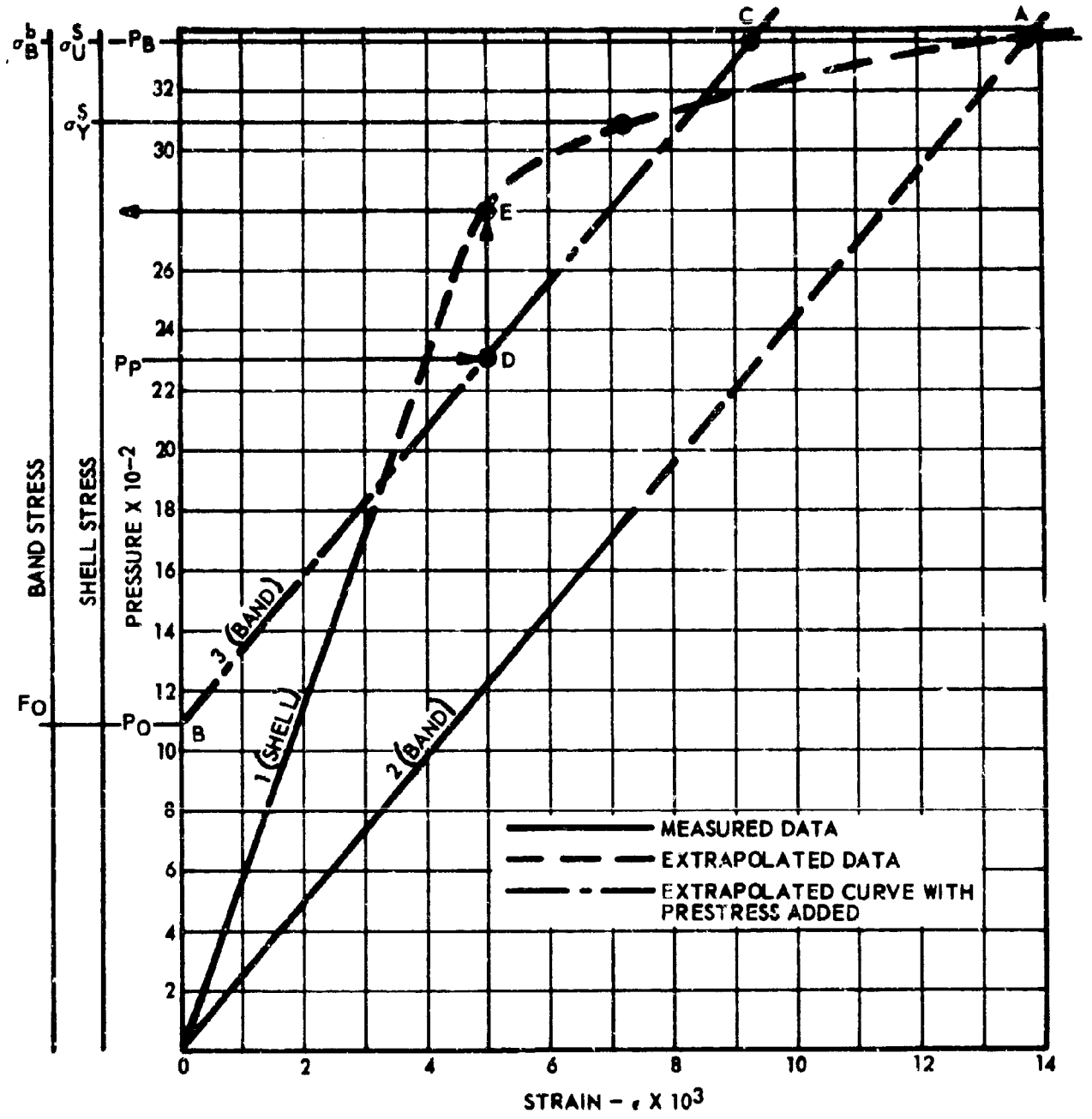

FIGURE 57 DESIGN CONDITIONS BASED ON TEST

c. Shell Local To The Band (Class I - II)

Curve 3 of Figure 57 shows strain relation between the band and the underlying shell. P_o is the pressure at which F_o loading of underlying skin is cancelled. The slope of the measured band strain versus internal pressure is:

$$\epsilon_{b/P} = 4.09 \times 10^{-5}$$

A band prestress of 40,000 psi relates to a prestrain of:

$$\frac{\epsilon_o{}^b}{E^b} = \frac{40 \text{ ksi}}{9 \times 10^6} = 4.44 \times 10^{-3}$$

Then

$P_o = \frac{4.44}{4.09} \times 10^3 = 1085$ psi which is shown as point B on Figure 57.

Underlying shell stress at proof pressure is found by projecting from point (D) on curve 3 to the equal strain point (E) on the shell curve 1. Then projecting horizontally it is shown that shell stress at proof pressure is less than yield value.

d. Evaluation of Test (Class III)

Data from Class III vessel tests allowed no conclusion on effects of the SSPV features. The Second and Fourth Specimens had been heat treated to 1050 condition which corresponds to a biaxial ultimate tensile strength of 230 ksi. Maximum sustained pressure (without leakage) was 900 psi which represented 24 percent of ultimate tensile stress for the shell. The repaired specimens were heat treated to a 1075 condition which corresponds to a biaxial ultimate tensile strength of 210 ksi. Maximum sustained stress was 38 percent of ultimate. In all four tests (paragraph b, d, e, f above) extreme notch sensitivity of the material and the presence of minute manufactured flaws masked any significance to SSPV features. No further attempt was made to improve performance of the 17-7 ph steel since it had been planned to replace it in phase II with the 6AL-4V titanium.

6. CONCLUSIONS

This evaluation of test data on 6AL-4V titanium designs show SSPV structural characteristics can be accurately prediced by the design procedure of Section VII paragraph 3.

Good agreement between load deflection data and theory shows strain compatibility objectives are satisfied by the derived design methodology.

Annealed 6AL-4V titanium SSPV shells will sustain burst pressures corresponding to material ultimate stress when fabricated to developed manufacturing standards.

17-7 PH steel heat treated to uniaxial tensile stress of 105 ksi (210 ksi-1:1 biaxial) entails a high risk pressure vessel material due to excessive notch sensitivity.

SECTION VII

SEGMENTED SPHERE PRESSURE VESSEL DESIGN CRITERIA

1. GENERAL

This criteria furnishes design aids on segmented sphere pressure vessels. Effects and interactions of SSPV design parameters are described by derivation of methodology analyses of variable parameters and data presentation showing design trends for maximizing structural performance.

Design parameters on mechanical and geometric properties, pertinent to the SSPV structural performance, are combined when term consolidation better defines the real design options.

Data handling is simplified by general use of non-dimensional terms. Development of theory and parameter evaluations are treated under three categories of methodology:

- Mathematical Models on Pressure Vessel Efficiency
- Mathematical Models on Band Optimization
- Stress-strain Analyses of Band and Shell Composite Structure

2. MATHEMATICAL MODEL FOR DESIGN PARAMETER OPTIMIZATION(DPO)

This mathematical model (DPO) is written as a digital computer routine.

a. Generalities of Method

Effects of design variables are quantitatively rated by use of the pressure vessel efficiency index:

$$\eta = \frac{P_B V}{(W^s + W^b)} \tag{2.1}$$

Membrane analysis applies to the extent that bending stresses are assumed to be negligible. However, the biaxial stress state at all loads for the shell underlying the band is based on strain compatibility inclusive of Poission's effects, that is:

$$\varepsilon^{bs} = \varepsilon^{b} \tag{2.2}$$

Given a set of quantities for shell and band materials and a set for SSPV geometry, dependent variables need be determined for minimum band weight. These dependent variables are:

- band stress at burst pressure
- band stress at zero pressure
- band cross section area

b. Methods

The theory includes the following boundaries:

- The filament tensioning stress during winding of the band must not exceed a maximum allowable based on fraying of the roving or buckling of the shell.

$$\sigma_o^b \leq F_o^b \tag{2.3}$$

- The band stress at burst pressure, based on strain compatibility condition, must not exceed the band ultimate stress.

$$\sigma_B^b \leq \sigma_U^b \tag{2.4}$$

- The band strain at burst pressure must not exceed maximum elongation of the shell material.

$$\varepsilon_B^b \leq \varepsilon_U^s \tag{2.5}$$

- The shell stress at proof pressure must not exceed shell material yield stress.

$$\sigma_P^s \leq \sigma_Y^s \tag{2.6}$$

$$\sigma_P^{sb} \leq \sigma_Y^s$$

The complete expression for Equation 2.1 is derived in Appendix I and is given in Equation 2.7.

$$\eta = \frac{.0666 \dfrac{f_u^s}{\rho^s}\left(1 + 0.5 \sin^2 \alpha\right)}{\left(1 + 0.25 \dfrac{P_B N_B}{f_u^s}\right)^2 + \psi^{-1}\left\{\sin^2\alpha + 0.5\left[\dfrac{P_B}{F_U^s} + \sin^{3/2}\alpha\left(\dfrac{P_o N_B \cos\alpha}{f_u^b}\right)^{1/2}\right]\right\}} \tag{2.7}$$

where

$$\psi = \frac{\sigma_B^b}{\rho^B} - \frac{\sigma_U^s}{\rho^s} \tag{2.8}$$

The methodology in computing η satisfies all boundary conditions for load-strain compatibility between the band and underlying shell at proof and burst pressure. Strain conditions for the initial trial are:

$$\varepsilon_B^b = \varepsilon_B^{Sb} = \varepsilon_U^S \qquad (2.9)$$

and

$$\varepsilon_P^b = \varepsilon_P^{Sb} = \varepsilon_Y^S \qquad (2.10)$$

Since the stress-strain plot of most filament materials is linear from zero stress to tensile failure, this first set of strain points completely defines the load-strain line for the band as indicated by line (a) of Figure 58. If this line satisfies the conditions of Equations 2.3 through 2.6 the first set of strain points is valid. Otherwise, ε_U^S is discarded. For the case when F_0^B is exceeded its value is used to complete the second trial set of points defining the new band load strain line (b of Figure 58). That is: $\varepsilon_B^b = \varepsilon_0^b$, $\varepsilon_P^b = \varepsilon_Y^S$. It is on this basis the prestress of the band at zero pressure is computed. If Equation 2.3 is violated a third set of points is required That is: $\sigma_o^b = F_o^B$, $\varepsilon_P^b = \varepsilon_Y^S$ (line c of Figure 58). On this basis the maximum band stress σ_B^b is computed. The arrived values of σ_o^b and σ_B^b are sufficient to define the band cross section area. The final value for σ_o^B is entered into Equation 2.8 for computation of the pressure vessel efficiency index (η).

c. Digital Computer Program

The mathematical model logic described is arranged in Figure 59, 60 and 61 as written into 7090 digital computer routine.

d. Data Mode

In the efficiency comparisons it was deemed advisable to group parameters in a manner definitive of real materials. These groupings are given in Table I which also presents the matrix of evaluated band and shell material.

This matrix also shows the manner of varying other vessel load and geometry parameters. These are: design burst pressure, ratio of design proof factor to design burst factor and segment angle which defines the ratio of band inside radius to the exterior shell spherical radius.

3. MATHEMATICAL MODELS FOR ACHIEVEMENT OF MEMBRANE CONDITIONS (AMC)

a. Generalities

Band cross section, required for strain compatibility with the shell, is diminished with increased band prestress. The upper limit on band prestress is set by one of the following:

- Maximum tensioning capability of the winding equipment
- Tension causing fraying of the silament roving

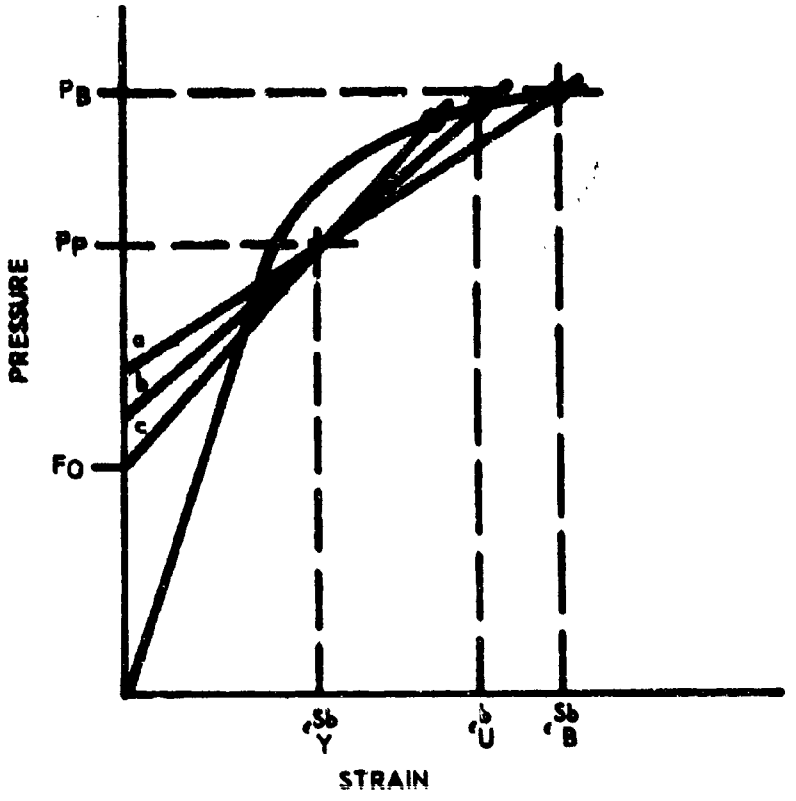

FIGURE 58 SSPV LOAD-STRAIN COMPATIBILITY CONDITIONS

WHEN $\dfrac{F_Y^S}{F_U^S} < \dfrac{n_P}{n_B}$

$$\sigma_P^S = F_Y^S \quad \sigma_B^S = \left(\frac{n_B}{n_P}\right) F_Y^S$$

WHEN $\dfrac{F_Y^S}{F_U^S} > \dfrac{n_P}{n_B}$

$$\sigma_P^S = F_U^S \left(\frac{n_P}{n_B}\right) \sigma_B^S = F_U^S$$

$\epsilon_P = \left[(F_Y^S - \psi\sigma_P^S) \div E^S\right] + .002$

ϵ_U = MAX. ELON. OF SHELL MATERIAL

$\Delta\sigma_P^b = E_b\, \epsilon_P$

$\Delta\sigma_B^b = E_b\, \epsilon_U$

$f_0 = (n_P \Delta\sigma_B^b - n_B\, \Delta\rho) \div (n_B - n_P)$

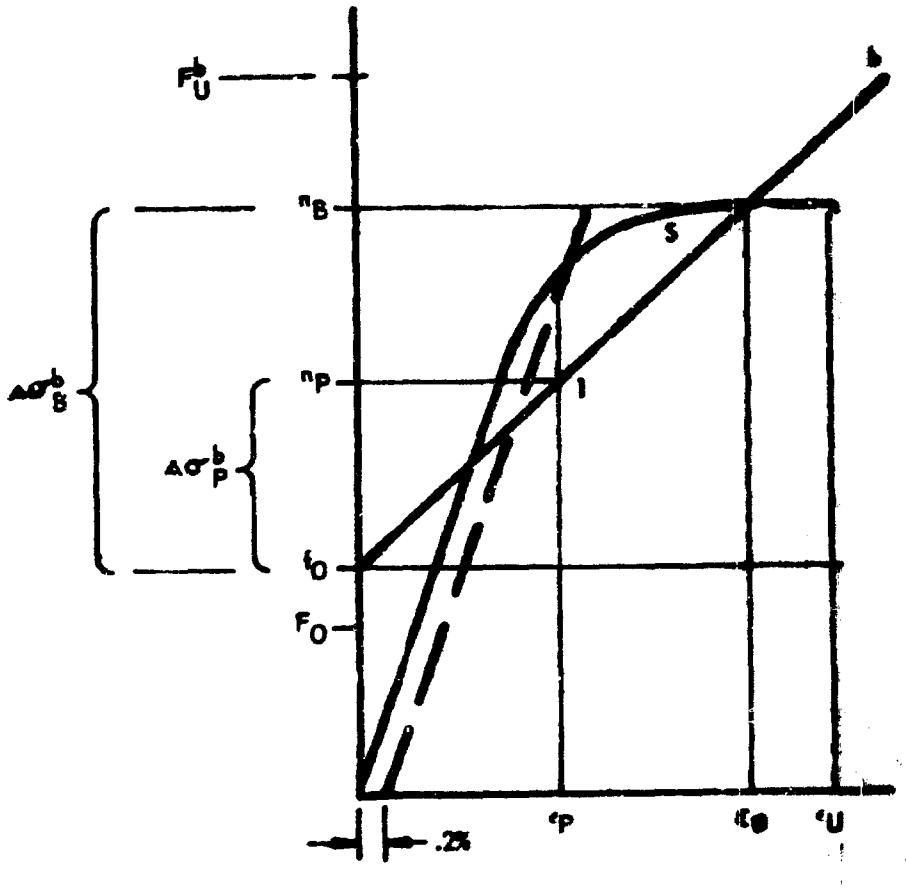

LEGEND:

NOTATION: n = DESIGN FACTORS, F = MATERIAL ALLOWABLE PSI, f = WORKING STRESS
u = POISSON RATIO, E = YOUNGS MODULUS, ϵ = ELONGATION, ρ = DENSITY

SUBSCRIPTS: Y = YIELD, U = ULTIMATE, P = PROOF PRESSURE, B = BURST PRESSURE

SUPERSCRIPTS: S = SHELL MATERIAL, b = BAND MATERIAL

FIGURE 59 MATH MODEL PART 1

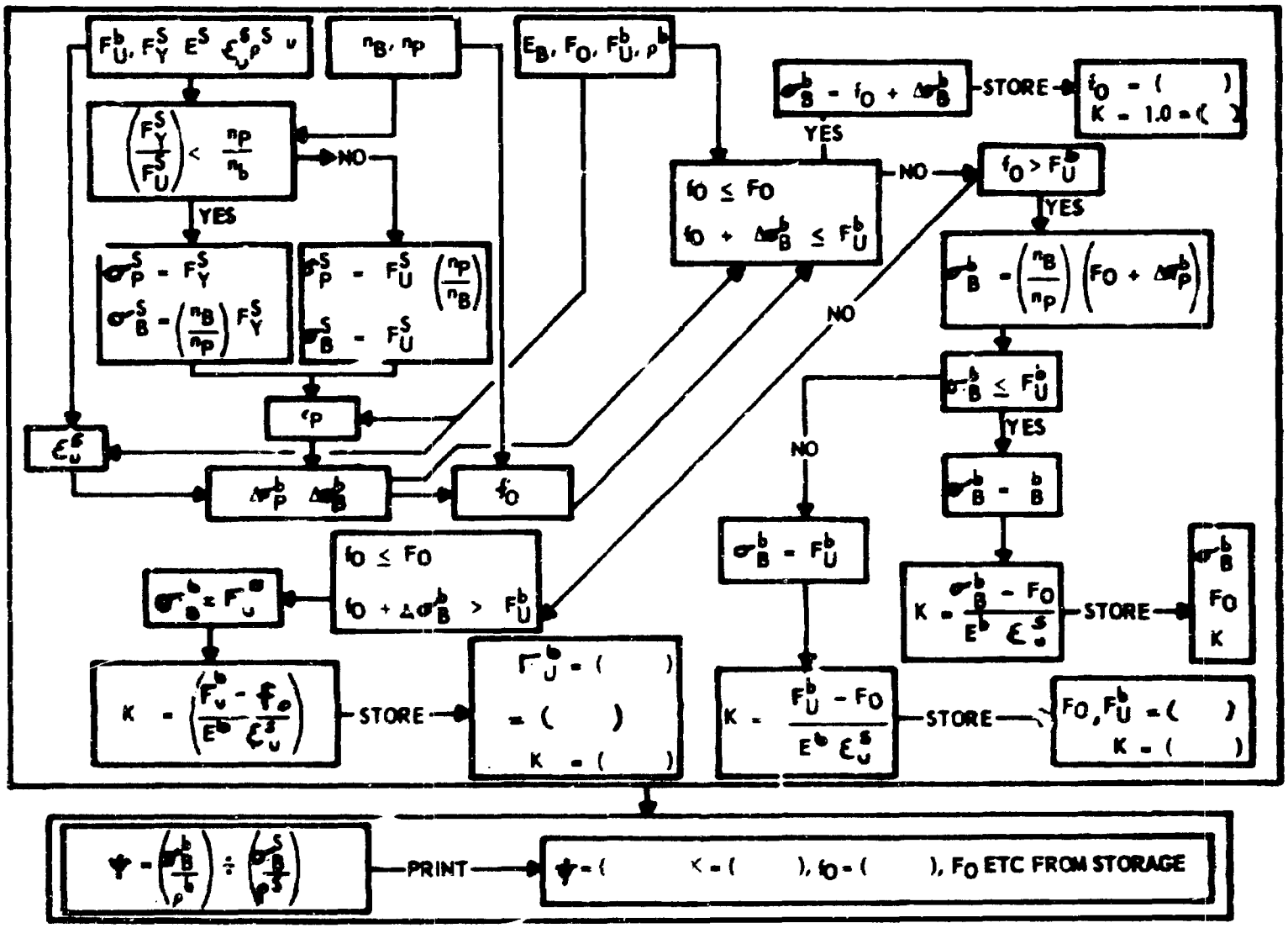

FIGURE 60 MATH MODEL PART I COMPUTER LOGIC

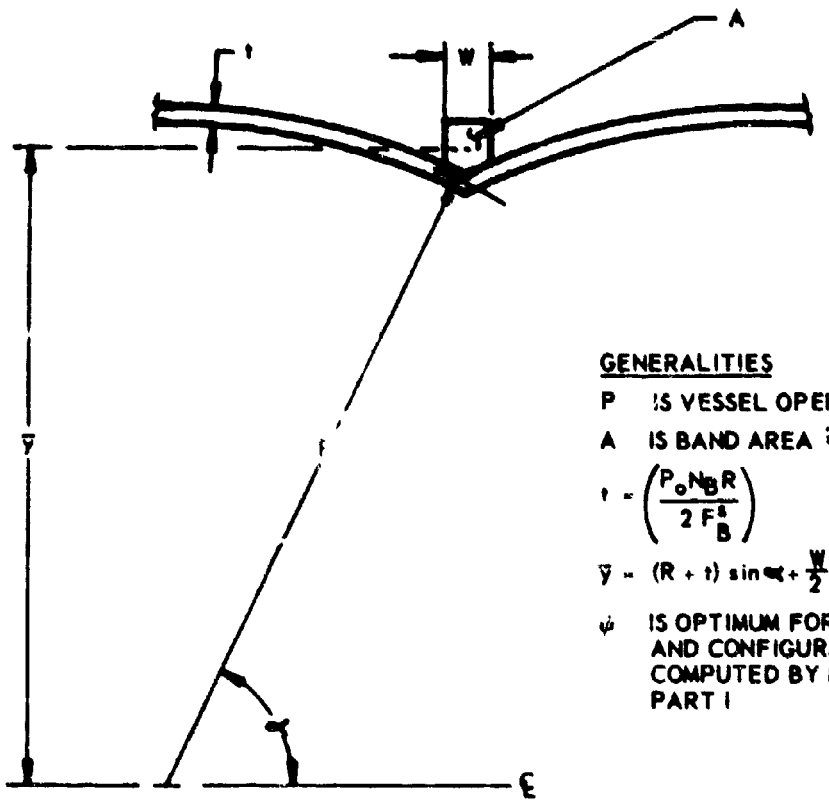

GENERALITIES

P IS VESSEL OPERATING PRESSURE

A IS BAND AREA ≅ W2

$$t = \left(\frac{P_o N_B R}{2 F_B^s}\right)$$

$$\bar{y} = (R + t)\sin\alpha + \frac{W}{2}$$

ψ IS OPTIMUM FOR EACH SET OF MATERIAL AND CONFIGURATION CONDITIONS AS COMPUTED BY MATHEMATICAL MODEL PART I

$$\frac{PV}{W} = \frac{.0666\left(\frac{F_u^s}{\rho_s}\right)(1 + 0.5\sin^2\alpha)}{\left(1 + 0.25\left\{\frac{P N_B}{F_U^s}\right\}\right)^2 + \psi^2\left[\sin^2\alpha + (0.5)\left\{\left(\frac{P N_B}{F_U^s}\right) + \sin^{3/2}\alpha - \left(\frac{P N_B \cos\alpha}{t_B^b}\right)^{\frac{1}{2}}\right\}\right]}$$

FIGURE 61 MATHEMATICAL MODEL PART II

- o Buckling strength of the shell under band preload
- o Ultimate stress in the filament at burst pressure.

An upper limit of 45,000 psi tensile stress is used in this study for S-901 fiber glass based on maximum equipment capability with 20 end roving. Trial winding on Class (I - II) and III shells showed fraying and buckling to be non critical at 40,000 psi and lesser tensioning values.

Independent of the above limiting conditions, maximum pretension and minimum band cross sectional area may be dictated by need to hold band strain at Design Burst Condition to a value not greater than maximum shell elongation.

Membrane conditions as used herein refers to achievement of 1:1 biaxial loading and stress levels for all points in the shell node equivalent to the pure membrane state in the spherical shell remote from the band.

When the reverse curvature of the node is described by a constant radius there exists a band pressure which eliminates any stress anomolies in the pure membrane state.

An object of this analyses is to establish band dimensions which achieves pure membrane conditions at the specific load corresponding to design burst condition. It is at this load that shell strains have least reserve margin for secondary bending stress associated with deviation from 1:1 biaxial stress conditions.

A third design control concerns developed maximum shell stress at proof pressure. Minimal band cross section area objectives are favored by designing for high shell stresses in the load regime below burst condition. The upper limit applied herein gives recognition to common criteria statement that yield stress shall not be exceeded at proof pressure.

b. Methods

Band pressure "f" is applied over the entire node up to the limit ϕ where transition to spherical radius R occurs. "f"is nonuniform over the angular range in the direction of ϕ .

Biaxial 1:1 stresses at level $\sigma^{sb} = \sigma^{s} = \frac{PR}{2t}$ is achieved by satisfying Equation 3.1 which is derived in Appendix II.

$$f/P = \frac{1}{2}\left(2 + \left(\frac{r}{R}\right)^{-1} - \frac{\cos\phi}{\frac{Y}{R}\left(1 + \frac{r}{R}\right) - \frac{r}{R}\left(\cos\phi\right)}\right) \qquad (3.1)$$

The expression applies to both elastic and plastic strain regimes.

c. Boundaries of Real Configurations

Validity of Equation 3.1 is bounded by two geometric conditions

$$\text{a} \quad r/R > 0 \tag{3.2}$$

$$\text{b} \quad f/P > 0$$

The first condition is defined by:

$$\frac{Y}{R} > \left(\frac{r}{R} + 1\right) \tag{3.3}$$

The second condition requires that the band-shell interface transfers normal compressive loads - never tension. This boundary is demonstrated by the intercepts on Figures 73 and 74 which are discussed later.

4. STRESS-STRAIN ANALYSIS BY DIGITAL ROUTINE (PETS)

a. Generalities

Ideally, the stress strain analysis should develop analytical expressions for the stress and strain at points on a reinforced shell as a function of the internal shell pressure, reinforcing band preload, and the geometric and consittutive parameters of the shell and reinforcing band. Such a complete analysis is impossible at present, for it requires analytical solutions of the differential equations of the problem and no such solutions are known.

In the absence of analytical solutions one must rely on numerical procedures to solve the differential equations. This is the case of the present study. Unfortunately, analyses based on such solutions are necessarily limited in scope. The purpose of this section is to describe, in a general way, the method and limitations of the present analysis.

The basic method is to obtain separate solutions for the band and shell and then to combine these solutions by means of a compatibility relation. The result is a solution for the reinforced shell. Obviously, the value of the final solution depends upon the compatibility relation as well as the component solutions. The digital computer routine used to obtain the solutions for the unreinforced shell is discussed in paragraph b below.

The band to shell compatibility conditions are presented in Appendix III. Paragraphs (c) and (d) below describe the scope of the elastic and plastic analyses in the context of the present application.

b. Methods

Solutions for the unreinforced shell are obtained by use of digital routine "PETS" (Ref. 4), a variation of the LASL "SAD" code (Ref. 5). In turn, the "SAD" code is based on a digital routine developed by AVCO Research and Advanced Development Division, Willimington, Massachusetts (Ref. 6).

These routines are devoted to the solution of the general differential equations of equilibrium of thin shells of revolution subjected to rotationally symmetric pressure and temperature distributions. The motivation for selecting the PETS code over competing solutions using finite cylindrical and conical elements is that it yields a better mathematical model of the present problem. In particular:

- The PETS family has versatility comparable to a finite element approach in that it considers multi-regional shells - a "Region" being defined as a portion of a shell which contains no discontinuities in loading or geometry. Regions are joined together by appropriate "Junction" conditions.

- The integration of the differential equations is carried out for each region by a finite difference approach with a prescribed integration interval on an arbitrarily prescribed middle surface generator (Ref. 6 and 8) (equivalent to a finite element of arbitrary curvature).

- The SAD and PETS versions have the capability of developing internally the geometrical data for regions generated by straight lines (cylindrical and conical elements) and circular arcs.

- Finally, the PETS code allows one to prescribe the generator of the geometrical middle surface and thickness of each region in such a way that the generator of the geometrical middle surface of the complete configuration of interest here (composed of circular arcs) is a continuous curve with a continuously turning tangent and the thickness is a continuous function of the generator's arc length.

- This feature eliminates apparent stress concentration due to imperfections in the geometrical simulation of the undeformed configuration. This is particularly important in the present analysis, since its primary purpose is the evaluation of the secondary (bending) stresses in the vicinity of the reinforcing band.

c. Scope of the Elastic Analysis

For the elastic analysis, it is assumed that both shell and reinforcing band are perfectly elastic for all values of internal pressure up to a well defined yield pressure, Py. It follows therefore that Equation (4.32) of Appendix III, relating the internal pressure to band pressure holds from P = 0 to P = Py and can be rewritten in the form

$$f(P) = k_1^E P + f_o \qquad (4.33)$$

where f_o is the pressure executed by the band where P = 0 and k_1^P is a

constant given by

$$k_1^E = \frac{\varepsilon_{P'}^{AS}}{\varepsilon_{f'}^{Ab} - \varepsilon_{f'}^{AS}}. \tag{4.34}$$

In addition, one can determine the stress, σ^S, at any point in the shell by means of influence coefficients defined at that point. That is,

$$\sigma^S = \sigma^S (P, t) = P \sigma_{P'}^S + f \sigma_{f'}^S \tag{4.35}$$

Where $\sigma_{P'}^S$ denotes the stress at the point due to a unit uniform internal pressure P', and $\sigma_{f'}^S$ denotes the stress at the point due to a unit uniform external pressure, f', applied to the band-shell interface.

For a compatible band and shell, Equations (4.33) and (4.35) are combined to yield

$$\sigma^S = P \sigma_{P'}^S + (P k_1^E + f_o) \sigma_{f'}^S \tag{4.36}$$

So that the stress in the shell is a function only of the internal pressure, P, and the value of the pressure, f_o, exerted by the band on the shell initially (i.e., when P = 0).

The stress is in the reinforcing band, σ^b is assumed to be uniform hoop tension resulting from the application of a uniform pressure, f. Explicity

$$\sigma_\theta^b = f \sigma_{f'}^b = f \left(\frac{S\bar{R}^b}{A^b} \right) \tag{4.37}$$

Where A^b is the cross sectional area of the band, and S and $\bar{R}^b$ measure the length and distance from the axis of symmetry of the band chord. The corresponding uniform hoop strain of the band is

$$\varepsilon_\theta^b = f \varepsilon_{f'}^b = f \left(\frac{S \bar{R}^b}{E^b A^b} \right) \tag{4.38}$$

Where E^b is the elastic modulus of the band.

Since the hoop strain in the shell at point "A" (the low point of the node) under this assumption is

$$\varepsilon_\theta^{AS} = P \varepsilon_{P'}^{AS} + f \varepsilon_{\theta f'}^{AS} \tag{4.39}$$

one can combine Equations (4.37) and (4.38) and the strain compatibility Equation (4.25), to yield, for the conditions at P = 0,

$$f_o = \varepsilon_\theta / \left(\varepsilon_{f'\theta}^b - \varepsilon_{\theta f'}^{AS} \right) = \sigma_o^b / \left(\bar{SR}^b / A^b \right). \tag{4.40}$$

Equations (4.36), (4.37), (4.38) and (4.40) define the state of stress in the shell in terms of the shell pressure, P, and reinforcing band prestress, σ_o^b. This is the form in which the equations are used in the design procedures described in Section VII.

The influence coefficients for the stresses and strains in the shell are determined by unit analysis of the unreinforced shell under the appropriate loading condition using the digital routine described in Appendix III. For example, the coefficient $\varepsilon_{\theta_P}^{AS}$, is obtained directly from the numerical solution of digital routine PETS for the problem of a shell of the particular material and geometry of interest loaded by a uniform internal pressure, P. The coefficient $\varepsilon_{\theta_f}^{Ab}$ is obtained in the same way for a uniform external pressure, f, acting on the band-node interface.

Examination of the equations of equilibrium solved by digital routine PETS (References 3,4) make it clear that although one can combine different solutions for the same shell, one cannot indiscriminately superimpose on the solution of a standard problem, the effects of variations in, say, Young's modulus and shell radius, to arrive at a meaningful solution for a new problem. For while Equations (4.3) and (4.4) of Appendix III are linear differential equations, they are not linear in the geometric and constitutive parameters of the shell - so that in general, their solutions will not be linear in these parameters.

This is obviously a severe limitation, for it requires a completely new analysis for every change in the geometric and constitutive parameters of the shell. As a result, the design data presented in Section III are, in general, meaningful only for the particular configuration and material for which they were computed. There is, however, one exceptional configuration for which limited generalizations are possible.

In particular, it was found that the stresses in a configuration employing identical spheres are independent of Young's modulus, E. Hence the influence functions relating shell stress to internal and band pressures (P, f) are the same for a given configuration, regardless of the value of E, and the strain influence functions for this configuration are inversely proportional to E. It follows that the stress-strain relations for a given family of shells is determined providing these relations are known for one value of E.

Of even greater importance is the existance of a pure membrane state of stress in the identical sphere configuration. That is, it is possible to find a value of the ratio f/P of band pressure to internal pressure at which a pure membrane state of stress exists. Moreover, the stress in the configuration under this condition is the same as that of a single sphere (identical to one of component spheres) loaded only by the internal pressure, P. Explicitly, at the critical value f/P, a uniform "hydrostatic" two dimension state of stress exists ($\sigma_\theta = \sigma_\phi = \sigma^S$), and the magnitude of the stress is

$$\sigma^S = PR/2t. \qquad (4.41)$$

If the material is linear and isotropic, the strains are given by

$$\varepsilon_\theta = \frac{1}{E^S}(\sigma_\theta - \mu^S \sigma_\gamma), \quad \varepsilon_\gamma = \frac{1}{E^S}(\sigma_\gamma - \mu^S \sigma_\theta)$$

and it follows that $(\sigma_\theta = \sigma_\gamma = \sigma^S) > (\varepsilon_\theta = \varepsilon_\gamma = \varepsilon^S)$,

where

$$\varepsilon^S = \frac{(1 - \mu^S)}{E^S} \sigma^S \tag{4.43}$$

d Scope of Plastic Strain Analysis

A general plastic analysis of the segmented sphere configuration is not attempted here. On the contrary, this analysis applies only to the individual sphere configuration and amounts to an extension of the elastic analysis by another linear analysis which also satisfies the band-shell compatibility relations

It is assumed that the shell material has a stress strain curve such as is shown in Figure 62. The values $(\sigma_Y, \varepsilon_Y)$, $(\sigma_U, \varepsilon_U)$ refer to the yield point and ultimate stress conditions respectively for the pure biaxial state of stress

$$\varepsilon = \frac{(1 - \mu\phi)}{E\phi} \sigma \tag{4.44}$$

The linear constitutive parameters $(E\phi_1, \mu\phi_1)$, $(E\phi_2, \mu\phi_2)$, $(E\phi_3, \mu\phi_3)$ are called the elastic, reduced, and plastic moduli respectively. For simplicity, we take $\mu\phi_1 = \mu\phi_2 = \mu\phi_3$. In this case, the influence coefficients for the shell corresponding to $E\phi_2$ and $E\phi_3$ are immediately determined from those of $E\phi_1$.

It is valid to represent the band as remaining elastic up to its ultimate stress. It is therefore elastic up to ultimate strength of the shell. Thus, if the yield point in the shell actually occurs in a membrane state, then $f/P = f_Y/P_Y$ and the band pressure internal pressure plot will have the form shown in Figure 63. That is, in the elastic range,

$$f = P k_1^E + f_0 \tag{4.45}$$

and in the plastic range

$$f'' = P'' k_3 \tag{4.46}$$

where k_3 is as in Equation (4.33),

$$f'' = f - f_Y, \quad P'' = P - P_Y, \tag{4.47}$$

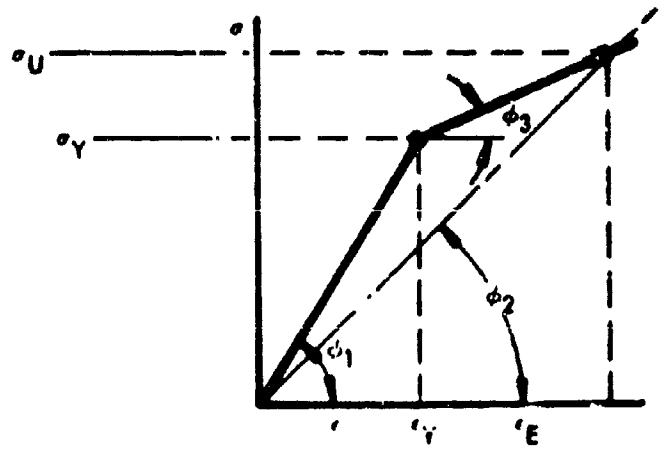

FIGURE 62 MODEL OF SHELL MATERIAL STRESS STRAIN CURVE

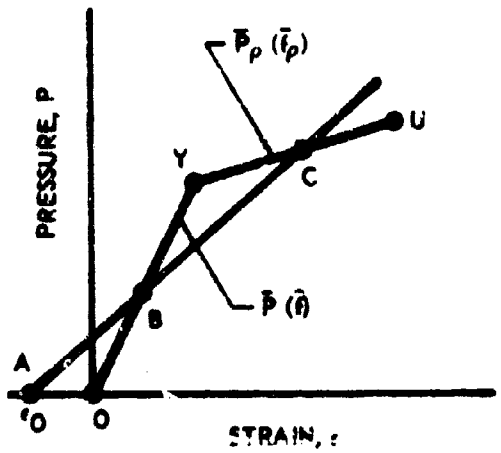

FIGURE 63 MODEL OF LOAD STRAIN CURVE

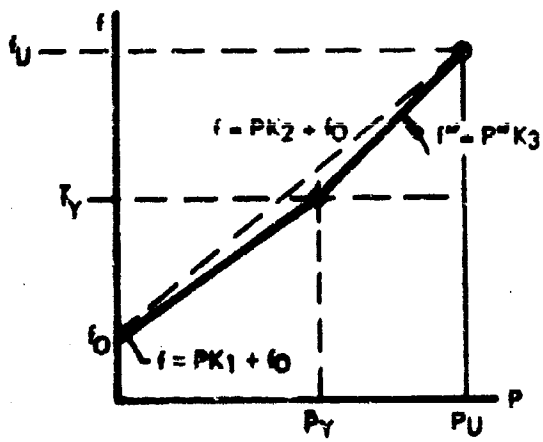

FIGURE 64 BAND PRESSURE VS. INTERNAL PRESSURE

and

$$k_3 = \frac{\varepsilon^{AS\,D}_{\bullet P}\,\phi_3}{\varepsilon^{b}_{r\bullet} - \varepsilon^{AS\,E}_{\bullet r'}\,\phi_3}.$$

With this result, the stress, strain and displacement in the plastic state are obtained by superposition of the values obtained for f", P" from the plastic influence coefficients on the values of these parameters for f_Y, P_Y from the elastic coefficients For example

$$\sigma^S = \sigma_Y + P''\,\sigma^S_{P'} + f''\sigma^S_{f'} \qquad (4\ 48)$$

$$\varepsilon^S = \varepsilon_Y + P''\,\varepsilon^{S\,E}_{P'}\,\phi_3 + f''\varepsilon^{S\,E}_{f'}\,\phi_3$$

If the shell is not in a membrane state at the onset of yielding, then the compatibility condition, Equation (4 46), does not hold over the entire plastic range Rather, Equation (4 46) holds only for pressures, P, in the range $P_Y \leq P \leq P_U$ where P_Y is the pressure at which the shell becomes fully plastic, and P_U is the ultimate pressure

One can still use a simple analysis, however, by working from a fully plastic membrane state. Let $(f_\rho, P_\rho, \sigma_\rho, \varepsilon_\rho)$ denote such a state. Since the value of $\bar{f}/\bar{P}$ for the membrane state is independent of E, one must have

$$f_\rho / P_\rho = \bar{f}/\bar{P}. \qquad (4.49)$$

But hoop shell compatibility requires

$$\frac{f_\rho}{P_\rho} - f_o/P_\rho = k_2 \qquad (4.50)$$

where k_2 corresponds to the reduced modulus E_ρ :

$$k_2 = \frac{\varepsilon^{A\,B\rho}_{\bullet P'}}{\varepsilon^{b}_{\bullet r'} - \varepsilon^{A\,B\rho}_{\bullet r'}}, \qquad (4\ 51)$$

Hence,

$$P_\rho = \frac{f_o}{(\bar{f}/\bar{P} - k_2)}. \qquad (4\ 52)$$

Now the stress and strain in this membrane state are given by

$$\sigma_\rho = P_\rho \left(\sigma^S_{P'} + \bar{f}/\bar{P}\, \sigma^S_{f'}\right) \tag{4.53}$$

$$\varepsilon_\rho = P_\rho \left(\varepsilon^{S\rho}_{P'} + \bar{f}/\bar{P}\, \varepsilon^{S\rho}_{f'}\right).$$

But since this is a pure biaxial state, one must also have

$$\varepsilon_\rho = \frac{(1-\mu)}{E_\rho}\sigma_\rho \tag{4.54}$$

so therefore,

$$\varepsilon^{A\,S}_{P'} = \frac{(1-\mu)}{E_\rho}\sigma^{A\,S}_{P'}, \quad \varepsilon^{A\,S}_{f'} = \frac{(1-\mu)}{E_\rho}\sigma^{A\,S}_{f'} \tag{4.55}$$

The reduced modulus, E_ρ, corresponding to this membrane state can be determined graphically (or by the equivalent analytical analysis) as follows: Let the curve O, Y, U represent the strain vs pressure plot for a single sphere which is identical to the component spheres, Figure 64. Thus points on this curve between O and Y represent ideal elastic membrane strains in a family of multisphere configurations and points on the segment Y and U represent ideal plastic strains. Let the line A, B, and C represent the strain vs pressure plot of the elastic band which is compatible with the deformation of the shells of the family represented by O, Y and U. Then these curves will intersect at the points B and C. These points represent the conditions under which a pure membrane state can exist in the reinforced shell. Once either of these points is chose, the other one is determined immediately from the graph. For a given design, point B is determined from the elastic analysis and point C from the graph. The strain corresponding to point C defines the reduced modulus E_ρ.

The definition of the parameters specifying the plastic membrane condition enables one to work from this condition as a standard, using the plastic modulus $E_{\phi\beta}$. Thus as in Equation (4.46)

$$f''' = P''' k_3 \tag{4.56}$$

Where k_3 is defined in Equation (4.47) and

$$f''' = f - \bar{f}, \quad P''' = P - \bar{P}. \tag{4.57}$$

The stresses, strains, and displacements in the plastic state are determined as in Equation (4.48)

$$\sigma^S = \sigma_\rho + P'''\, \sigma^S_{P'} + f'''\, \sigma^S_{f'}$$

$$\varepsilon^S = \varepsilon_\rho + P'''\, \varepsilon^{S\,E\phi 3}_{P'} + f'''\, \varepsilon^{S\,E\phi 3}_{f'} \tag{4.58}$$

5 GENERAL DESIGN INFORMATION BASED ON DPO ANALYSES

a General

Optimization of design parameters was investigated by use of the mathematical model computer routine described in Section III, Par 2 The value of the analysis results is to show efficiency trend caused by changing one or more design variables These results are shown in the graphs of Figure 65 thru 72 Efficiencies of segmented sphere vessels is compared with simple sphere vessels for like material and load conditions The generalizations of these analyses do not accountfor weight increments from welds and fittings

b Material Properties

The most influential set of design parameters is contained in the set of physical properties describing an applied structural material Figure 65 (Sheet 1-7) compares pressure vessel efficiency expected from use of many feasible combinations of shell and band materials, all other variables being constant Since there is no standard design criteria on the ratio of proof to burst pressure, a range of 0 5 to 0 66 is used to bracket vessel efficiencies associated with each combination of specific materials. In general, the upper limit of efficiency is associated with $P_P/P_B = 0.5$.

c Band Pressure

The effects of varying design pressure is given in Figure 66, sheet 1 thru 4.

In all cases the pressure variable is defined as operating pressure and is associated with a design burst factor of 2 25 Should the designer prefer use of burst pressure as a variable, the operating pressure scale can be converted by simply multiplying its values by 2.25 The trend shows decreasing efficiency for increasing design pressures

d Band Prestress

Figures 67, 68, and 69 show the effect of band prestress for several highly efficient material combinations Vessel efficiency always increases with increase in band prestress However, an upper limit on prestress is dictated by one of the following:

- Excessive fiber fraying from high winding tensions
- Buckling of the shell under band preload
- Exceeding band allowable tension stress at burst pressure

The designer will be required to establish maximum winding tension by trial using materials of interest and shop winding equipment.

Experience of this study showed S-901 filament glass could be tensioned to 40,000 psi with the Entec device without fraying The engineering model shells displayed no buckling tendencies under these

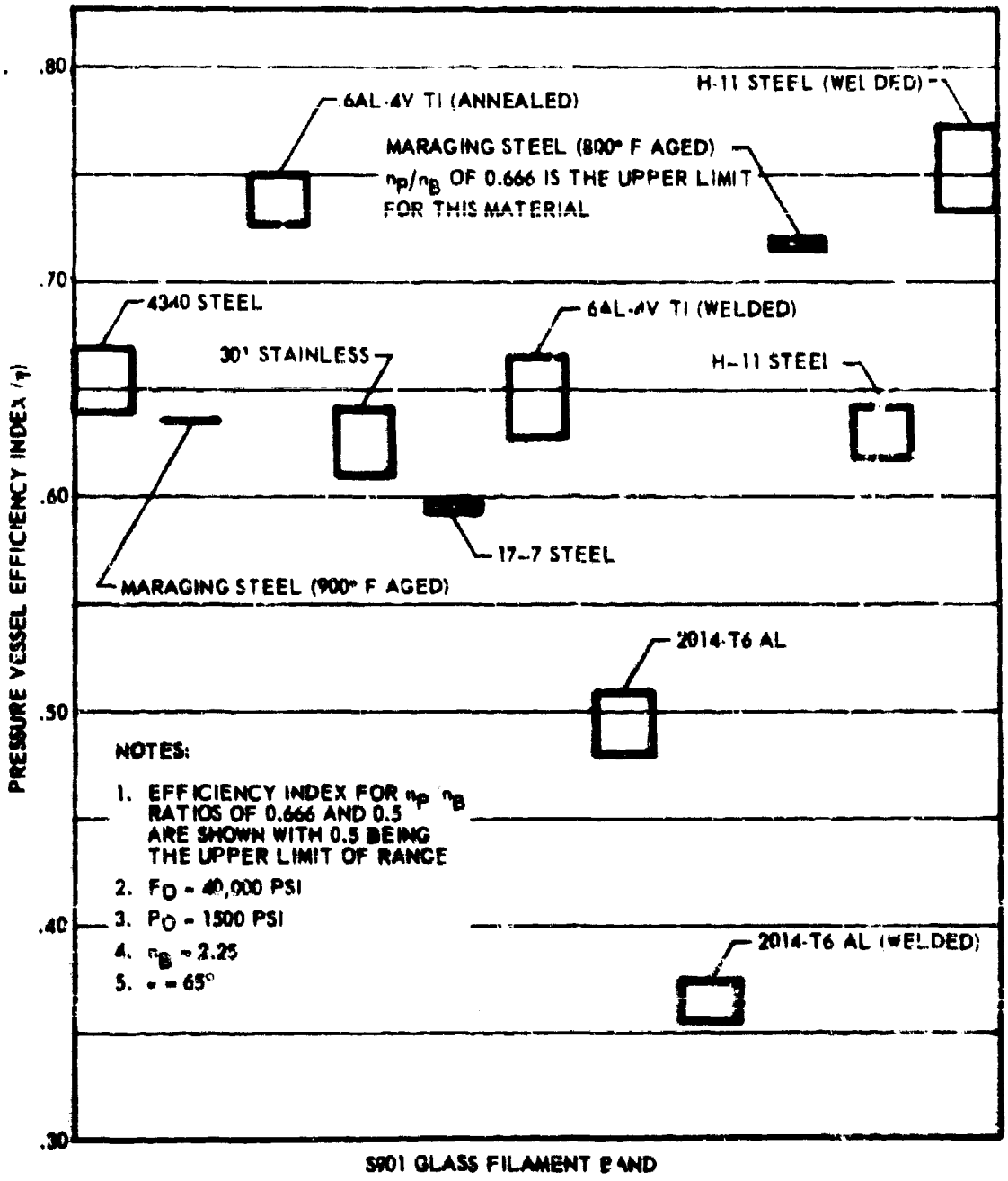

FIGURE 65 PRESSURE VESSEL EFFICIENCY INDEX VERSUS BAND – SHELL MATERIAL SELECTION (SHEET 1)

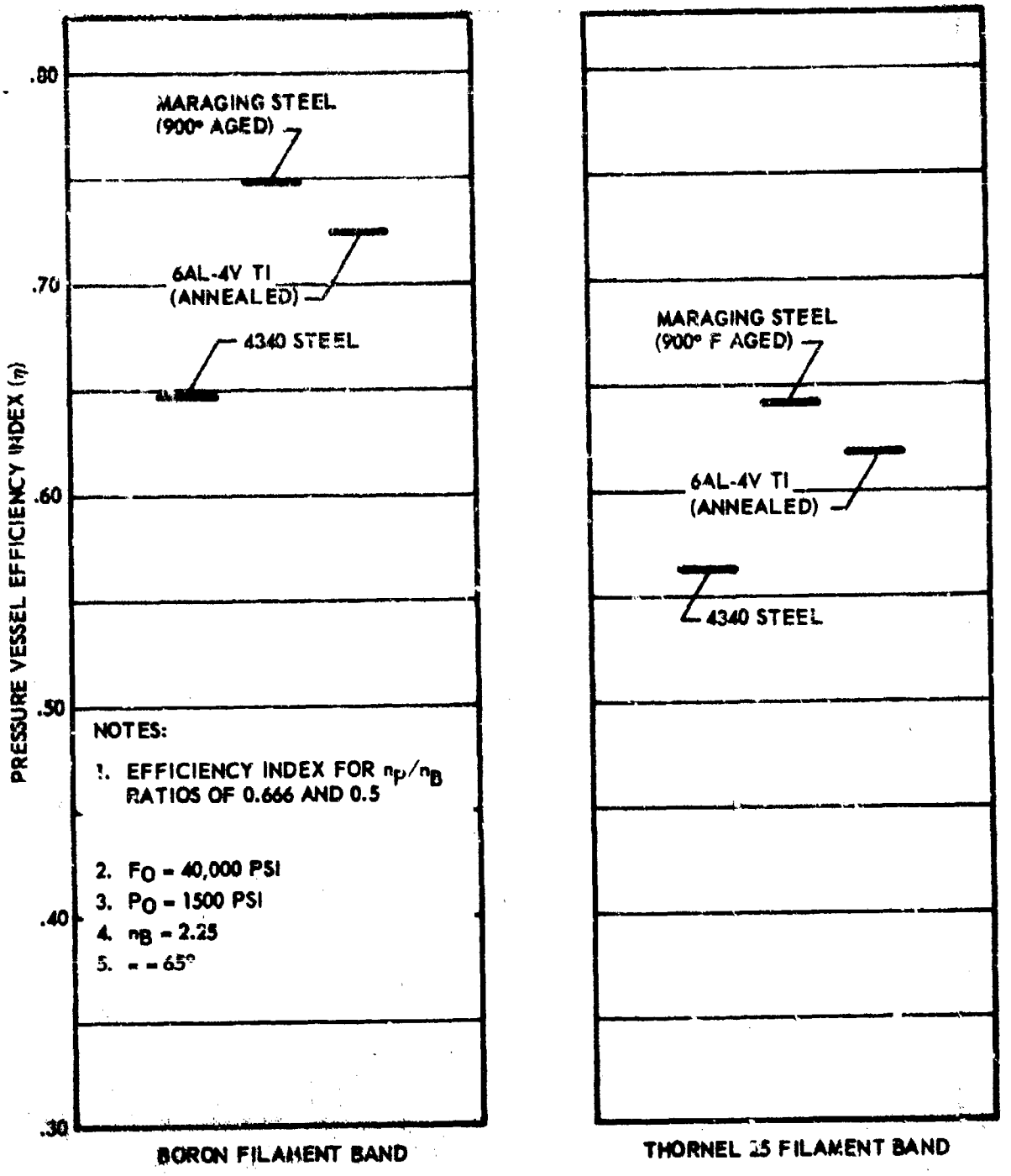

FIGURE 69 PRESSURE VESSEL EFFICIENCY INDEX VERSUS BAND - SHELL MATERIAL SELECTION (SHEET 2)

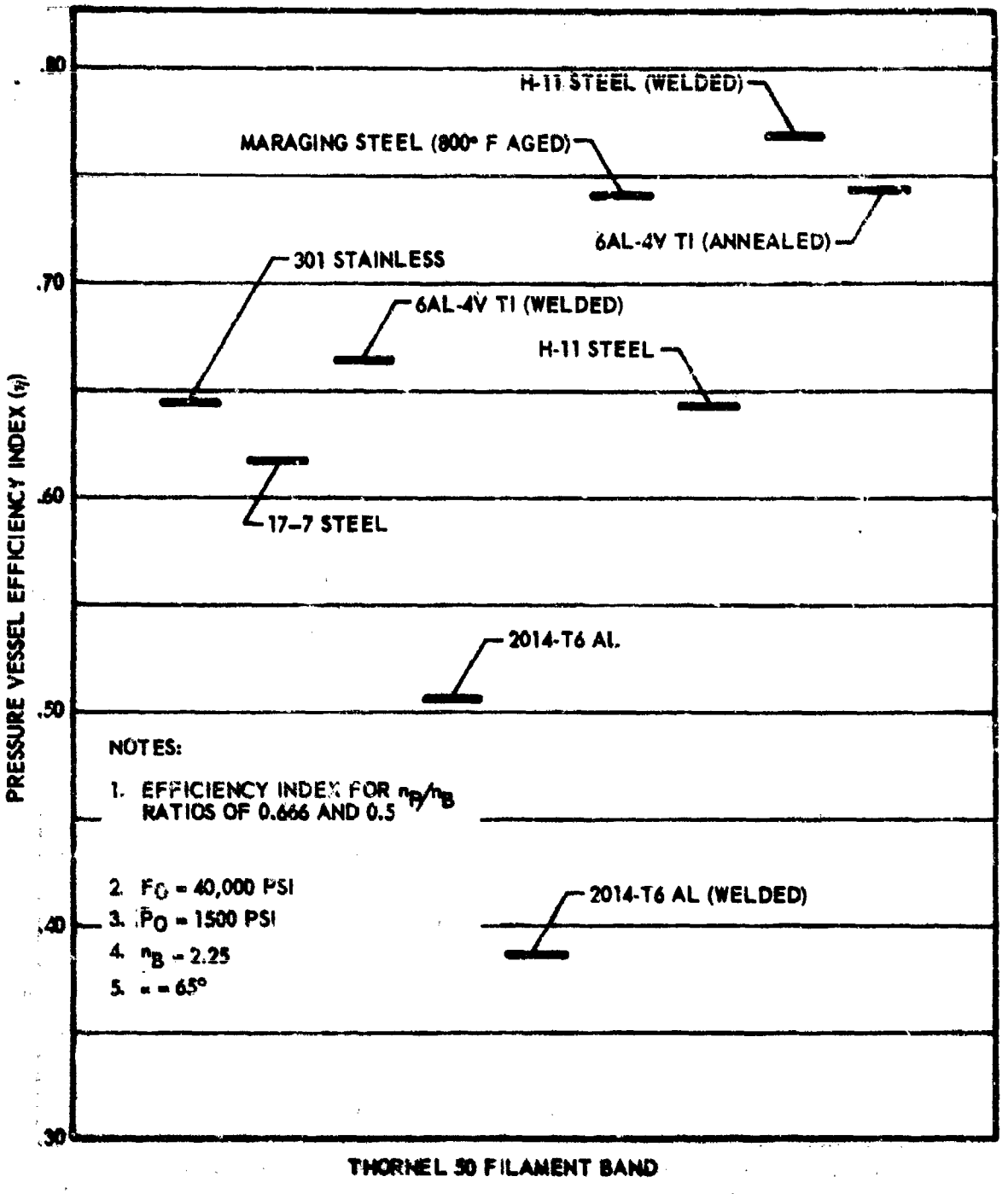

FIGURE 65 PRESSURE VESSEL EFFICIENCY INDEX VERSUS BAND – SHELL MATERIAL SELECTION (SHEET 3)

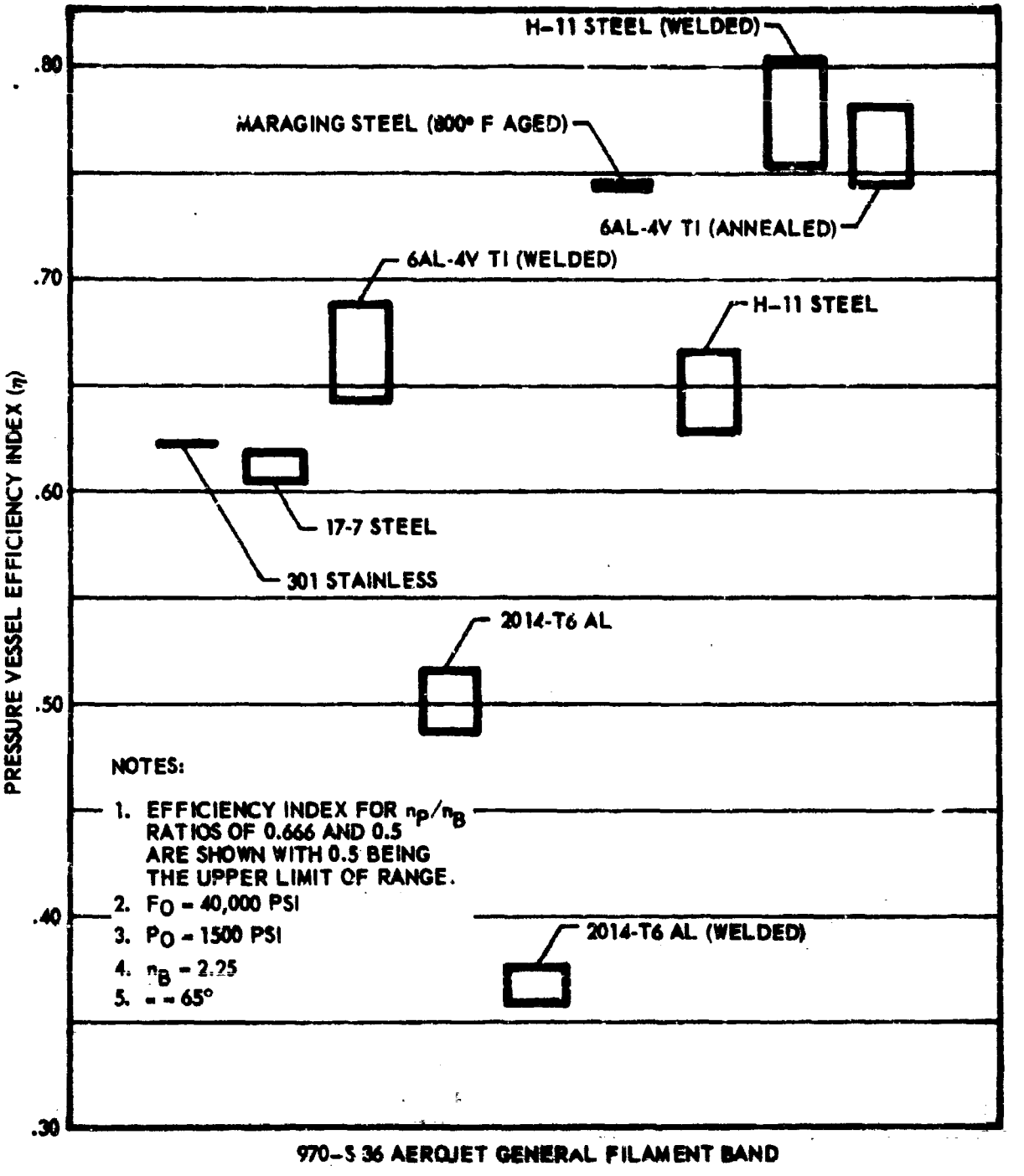

FIGURE 65 PRESSURE VESSEL EFFICIENCY INDEX VERSUS BAND - SHELL MATERIAL SELECTION (SHEET 4)

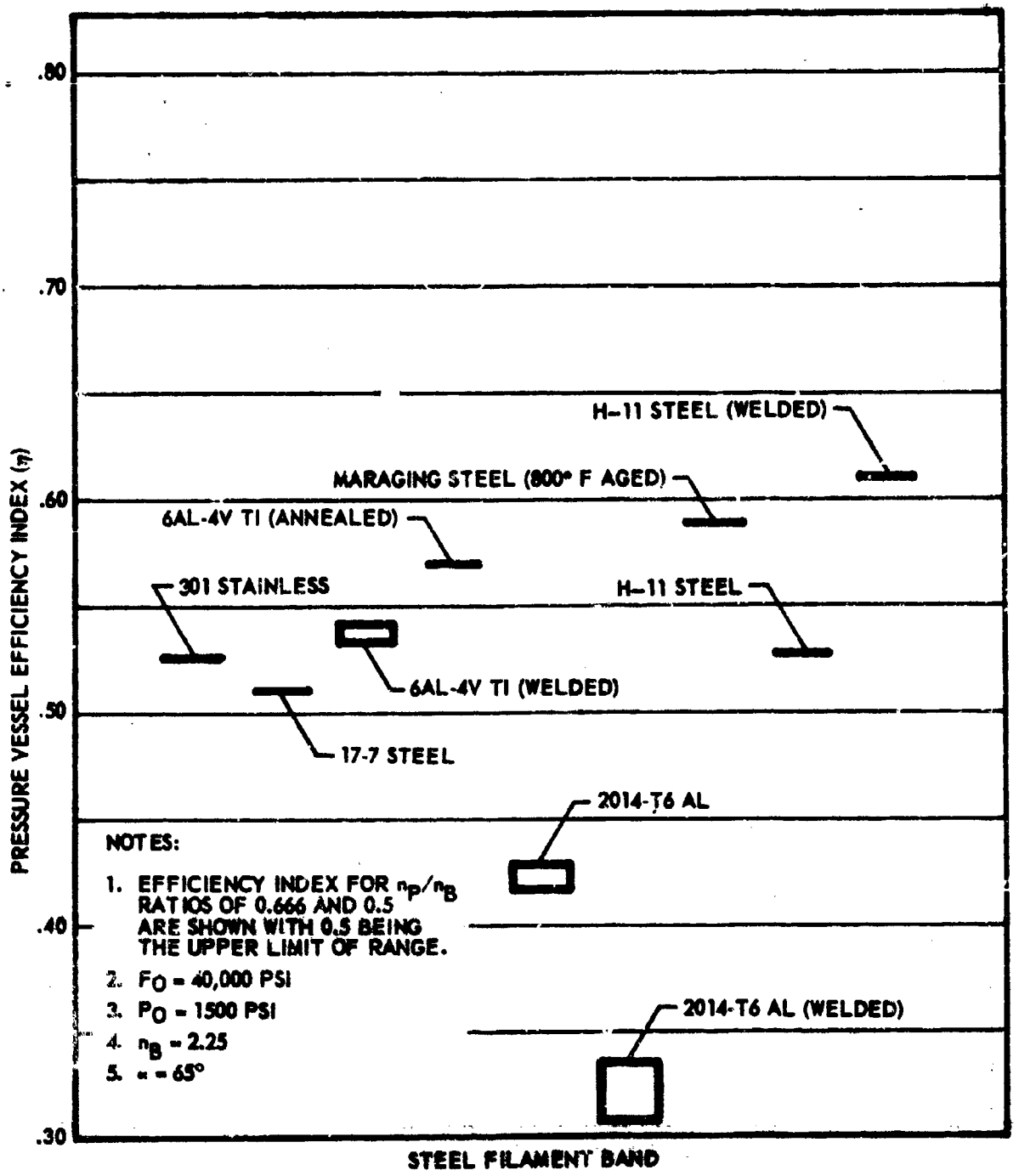

FIGURE 65 PRESSURE VESSEL EFFICIENCY INDEX VERSUS BAND – SHELL MATERIAL SELECTION (SHEET 5)

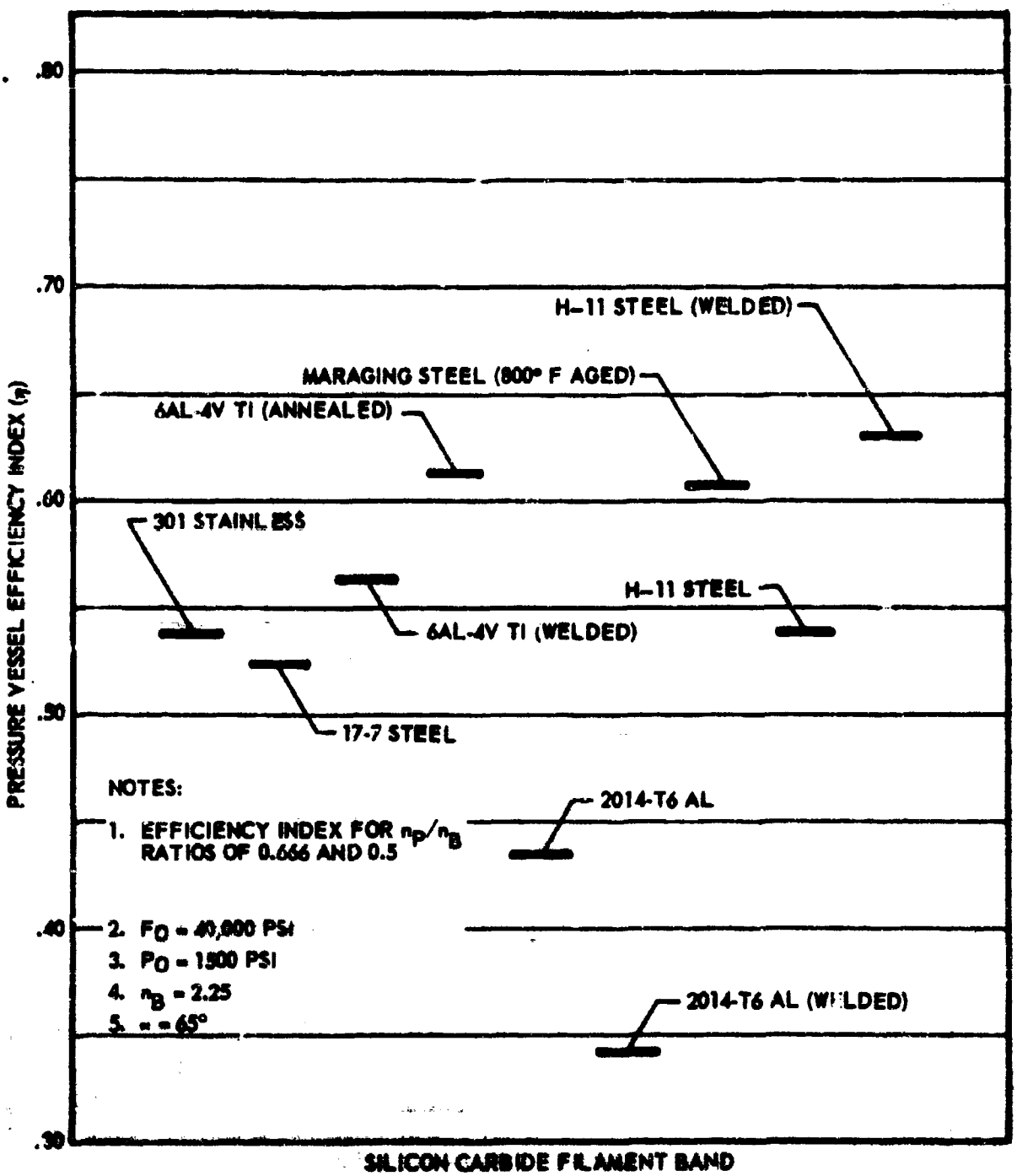

FIGURE 40 - PRESSURE VESSEL EFFICIENCY INDEX VERSUS BAND - SHELL MATERIAL SELECTION SHEET 6)

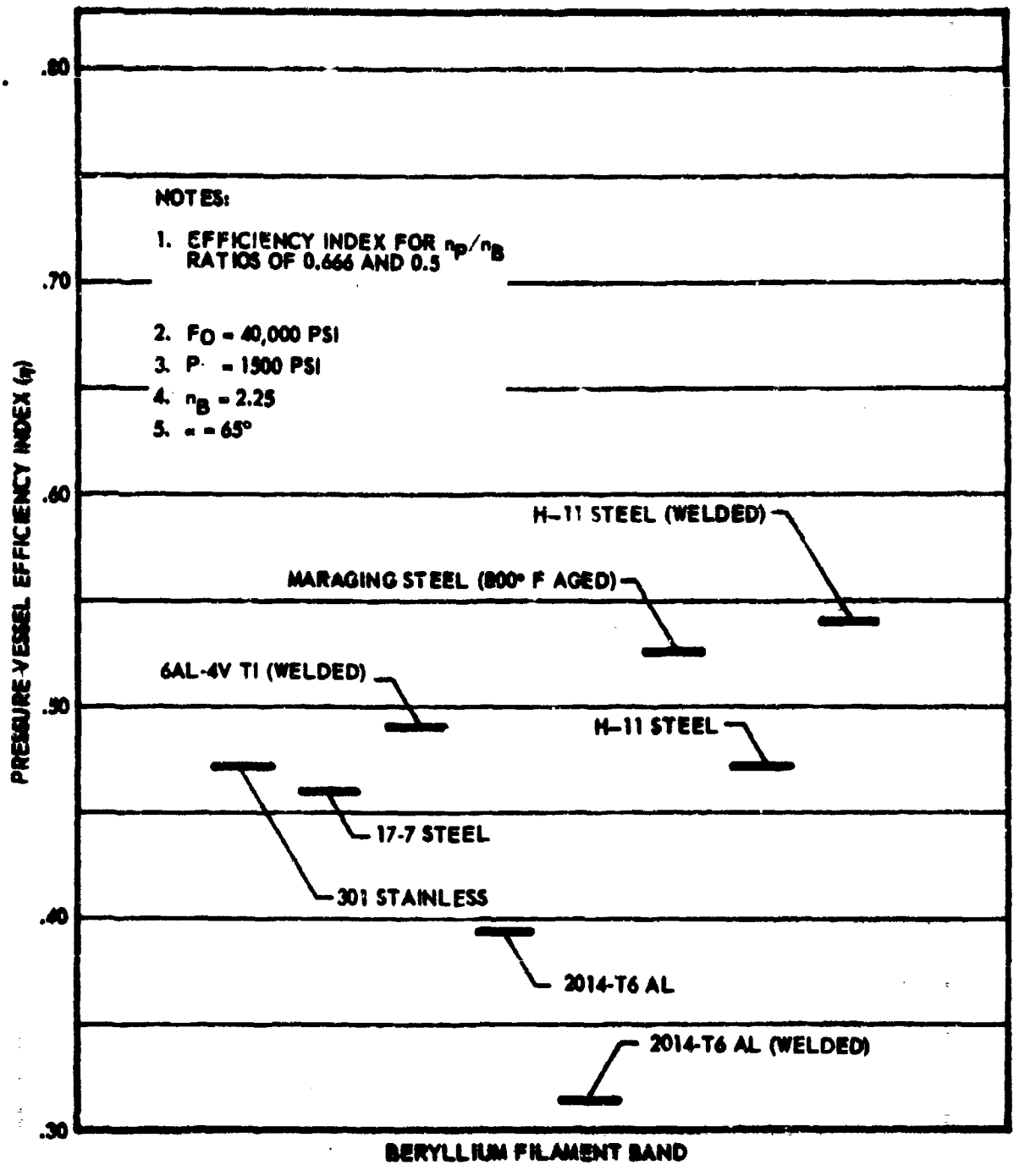

FIGURE 46 PRESSURE VESSEL EFFICIENCY INDEX VERSUS BAND – SHELL MATERIAL SELECTION (SHEET 1)

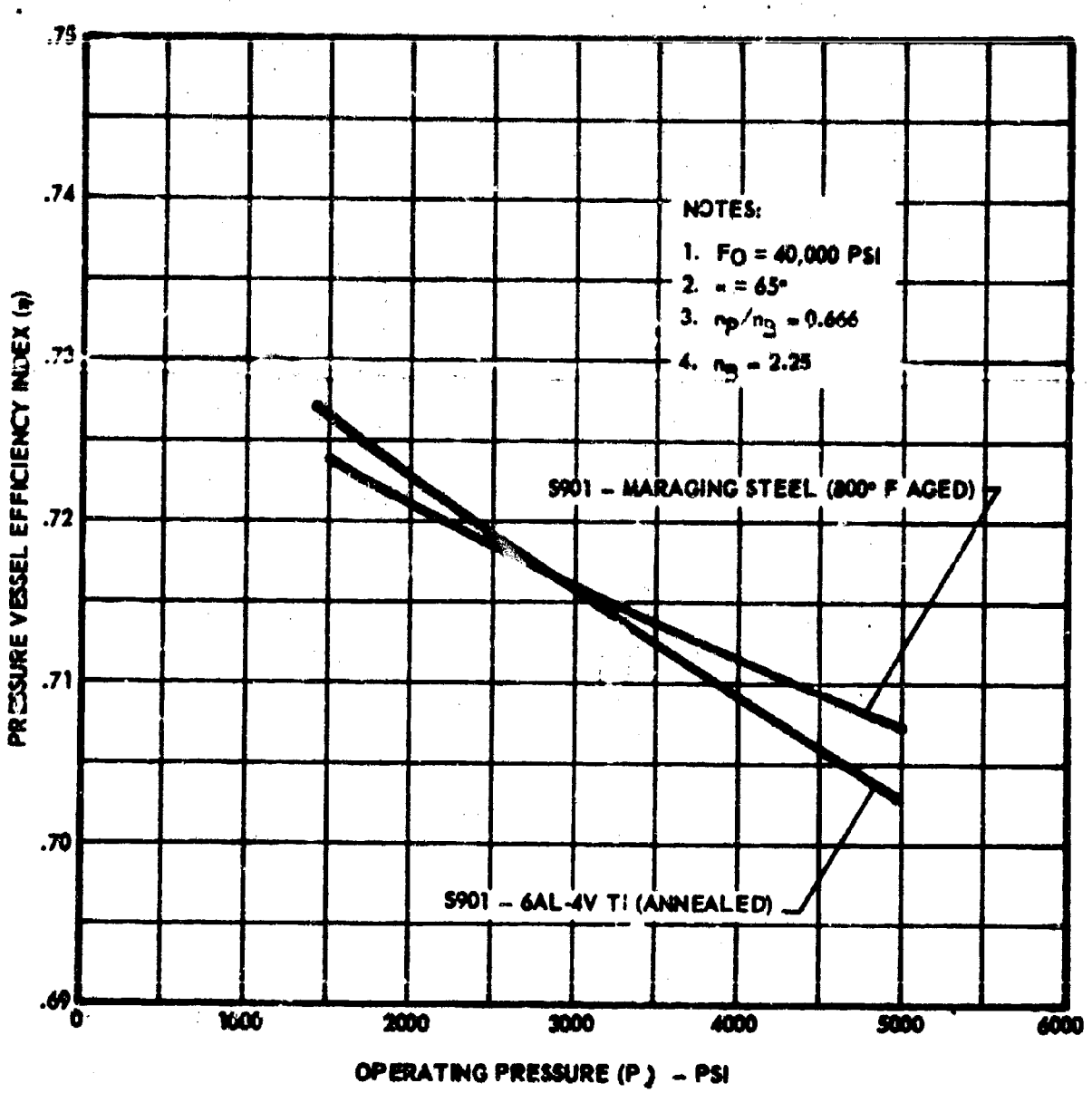

FIGURE 46 EFFICIENCY INDEX VERSUS OPERATING PRESSURE FOR VARIOUS MATERIAL COMBINATIONS (SHEET 1)

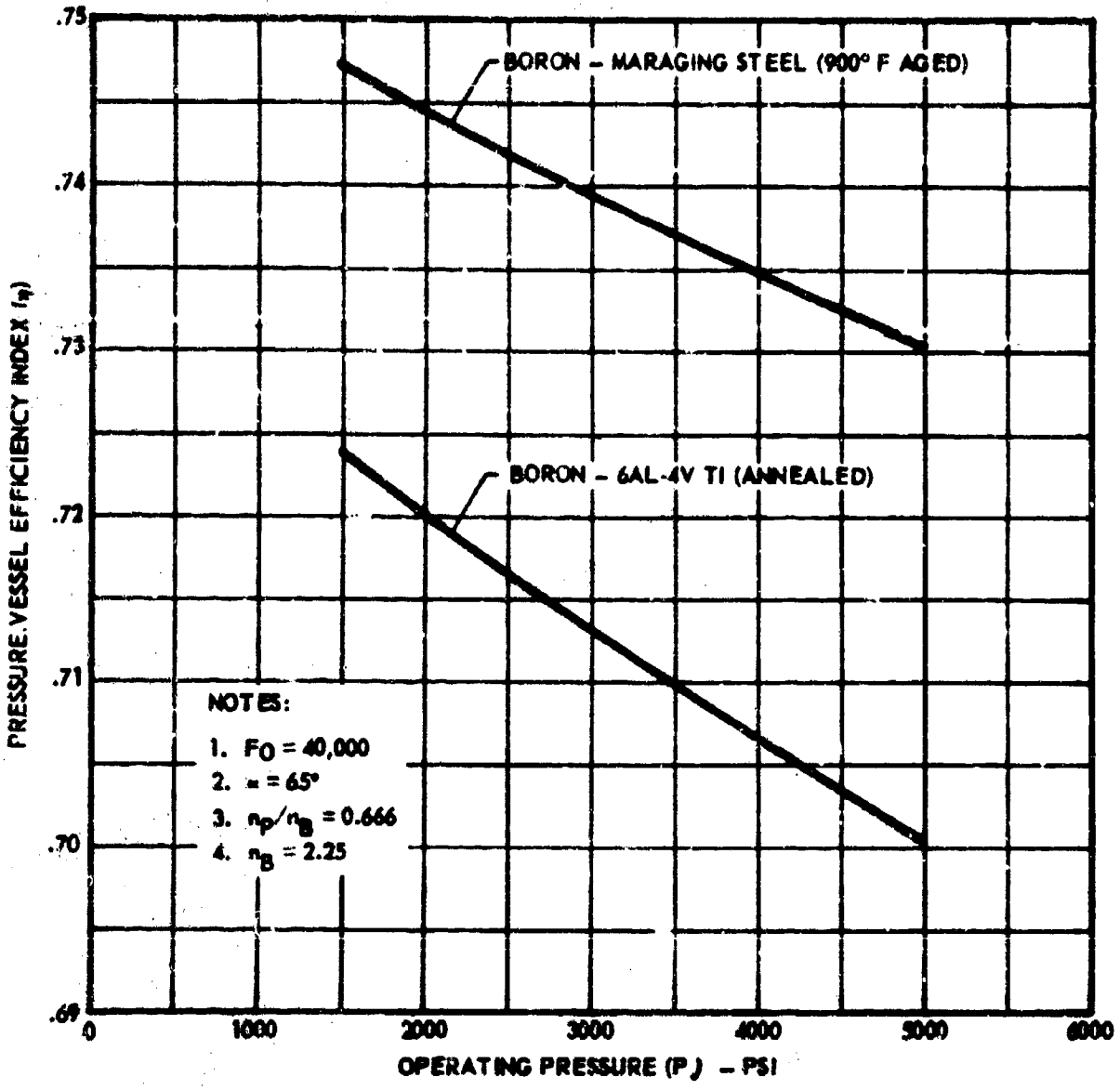

FIGURE 66 EFFICIENCY INDEX VERSUS OPERATING PRESSURE FOR VARIOUS MATERIAL COMBINATIONS (SHEET 2)

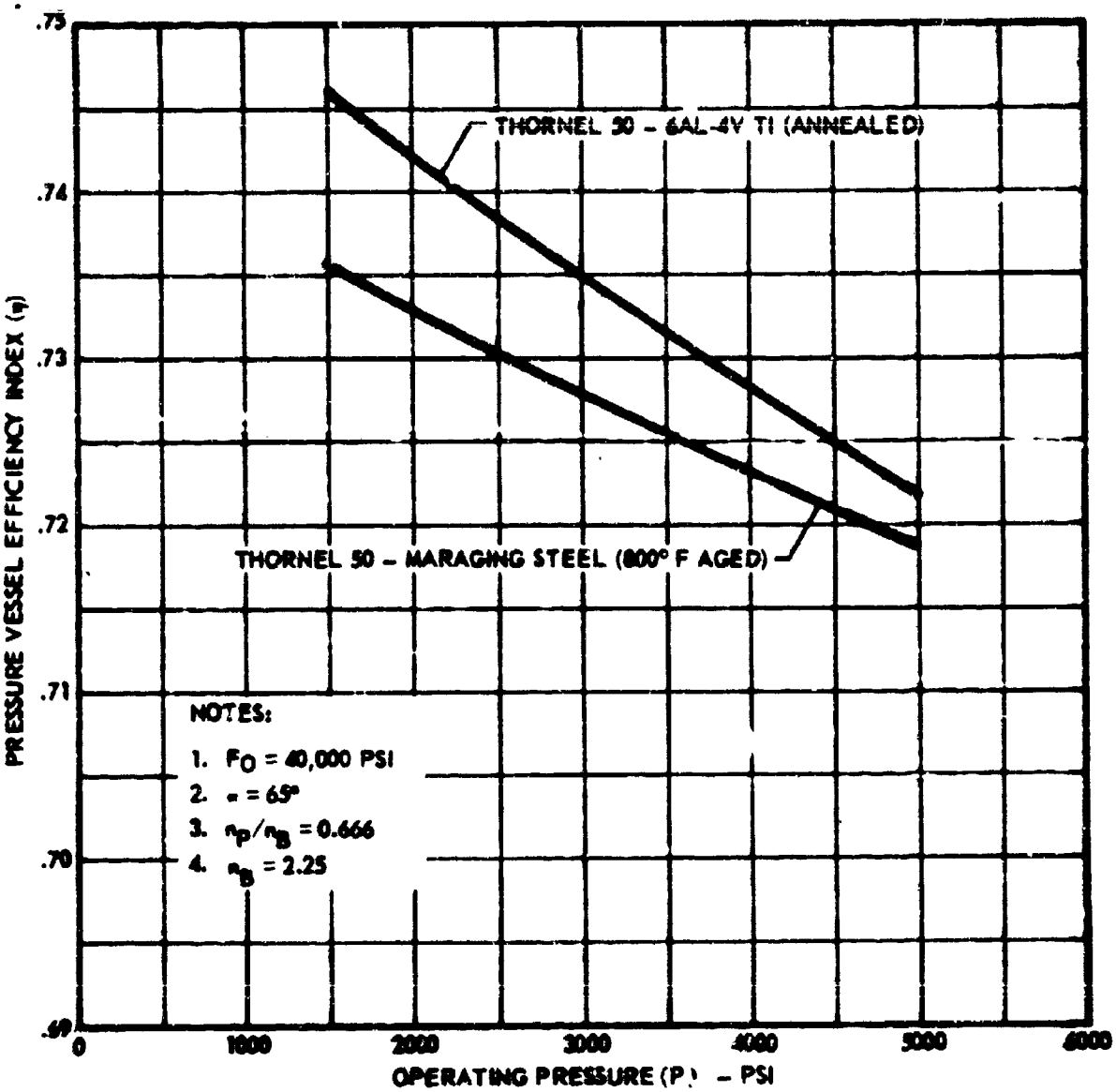

FIGURE 66 EFFICIENCY INDEX VERSUS OPERATING PRESSURE FOR VARIOUS MATERIAL COMBINATIONS (SHEET 2)

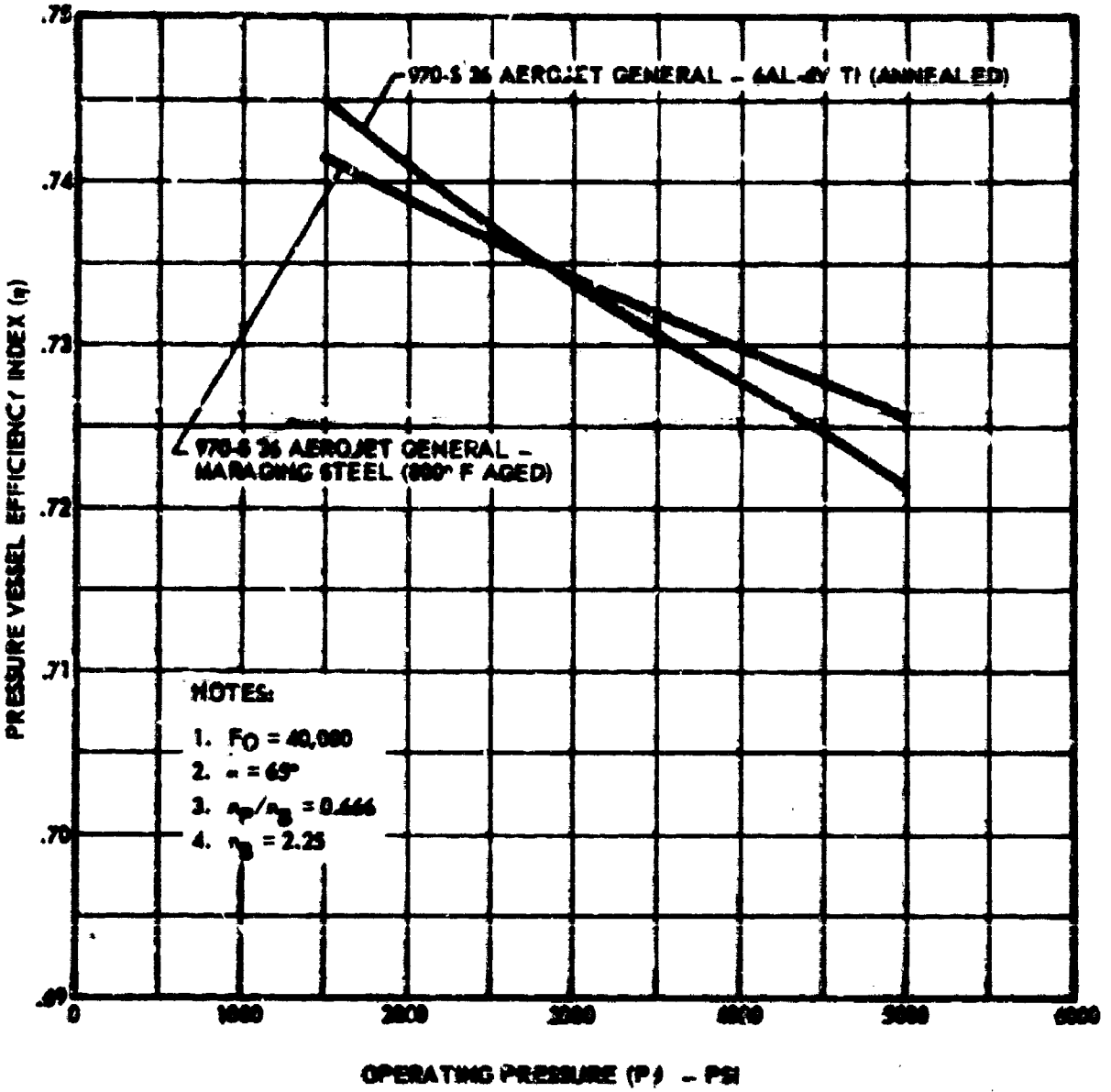

FIGURE 46 EFFICIENCY INDEX VERSUS OPERATING PRESSURE FOR VARIOUS MATERIAL COMBINATIONS (SHEET 4)

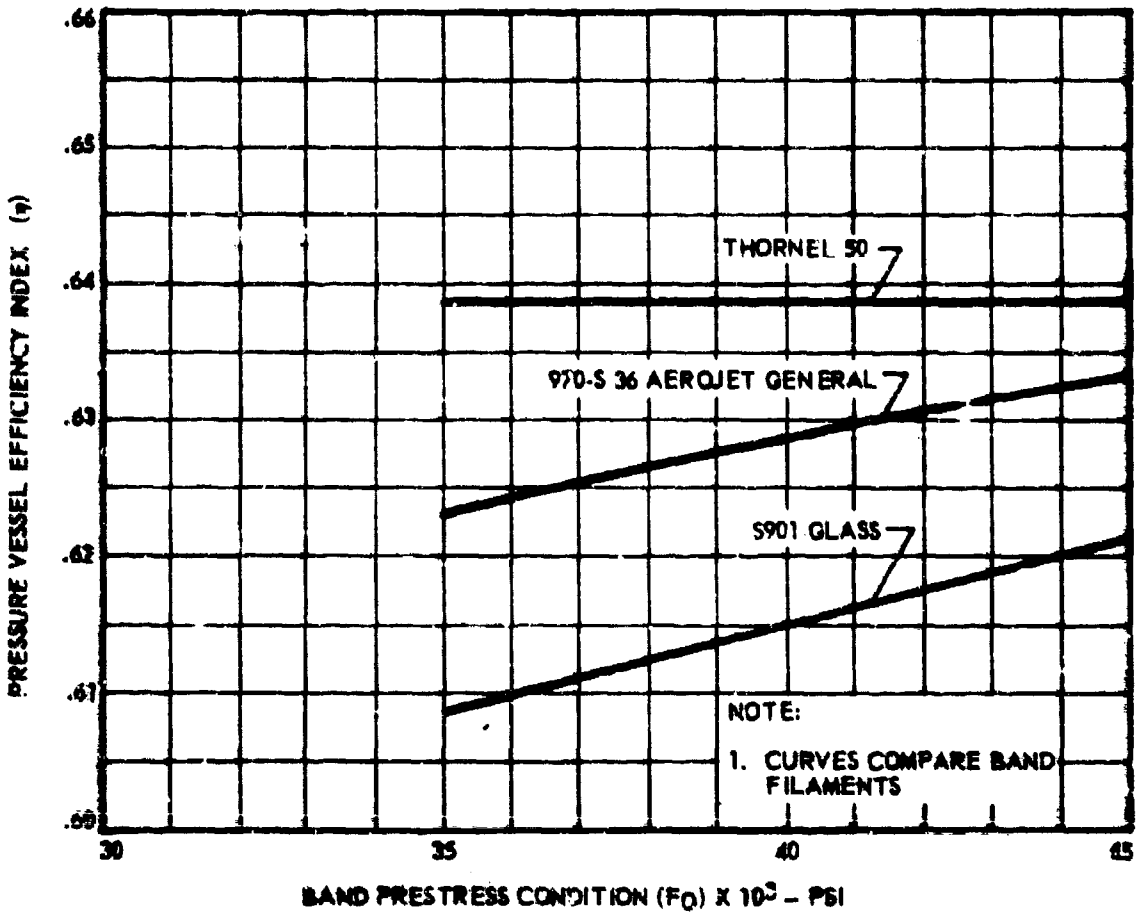

FIGURE 67 EFFICIENCY INDEX VERSUS BAND PRESTRESS – 5 CR MO V (M – 11) STEEL SHELL MATERIAL

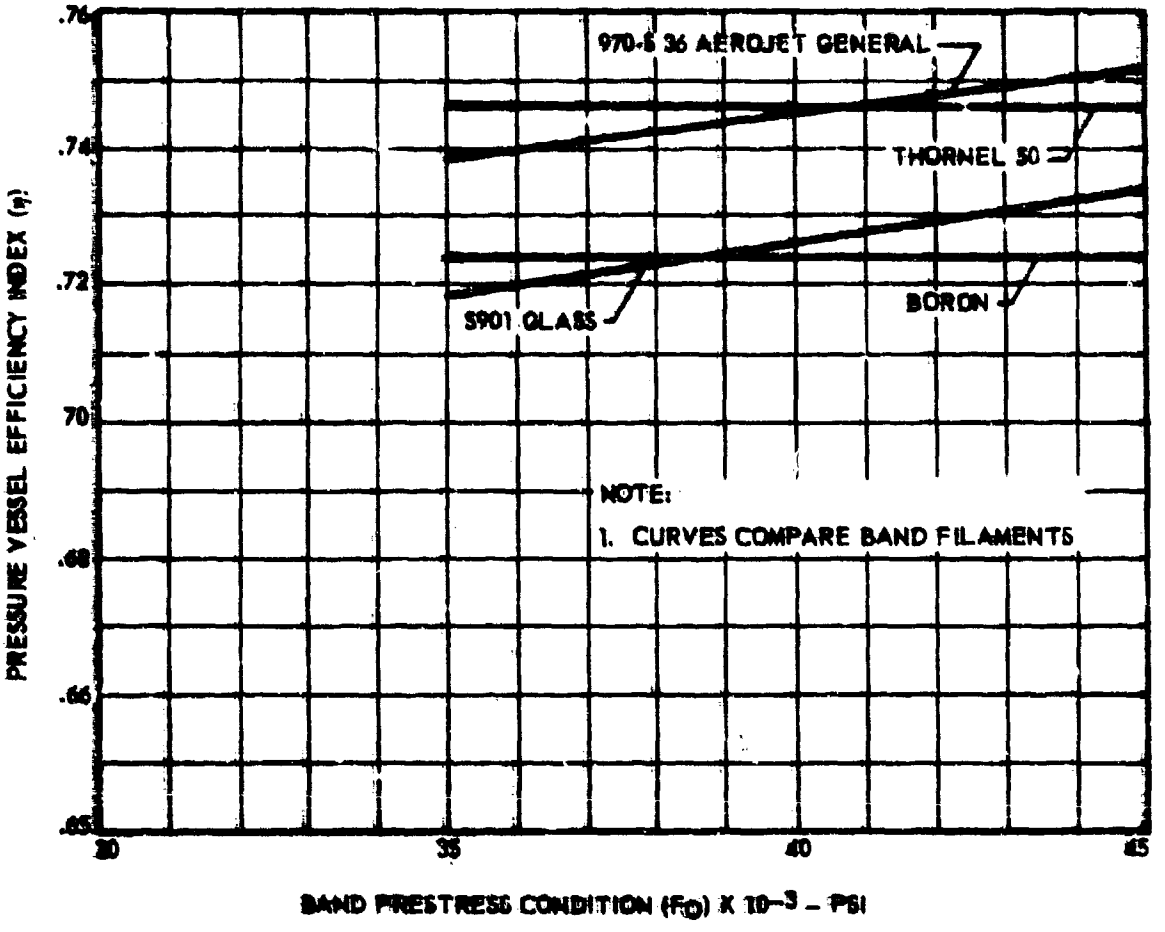

FIGURE 48 EFFICIENCY INDEX VERSUS BAND PRESTRESS-6AL-4V (ANNEALED) SHELL MATERIAL

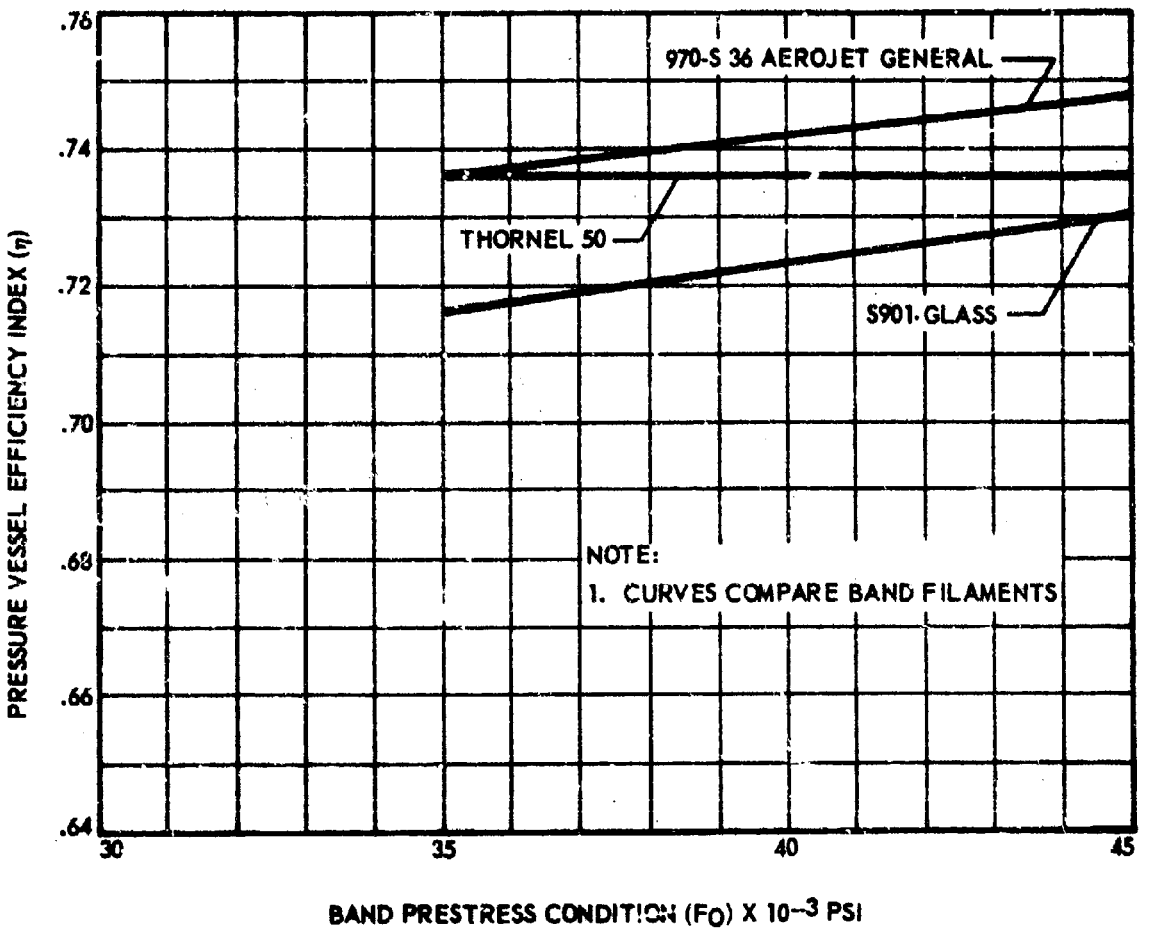

FIGURE 69 EFFICIENCY INDEX VERSUS BAND PRESTRESS–MARAGING STEEL (800° F AGED) SHELL MATERIAL

preloads Therefore, a prestress range of 30 to 45 KSI is included in the graphs as feasible design values.

e Segment Angle

A comparison is made in Figure 70 between a simple sphere and segmented sphere vessels with segment angle (α) approaching 90 degrees There is no distinction between a simple sphere and a segment angle of 0.0 degrees Improvement factor shown is the ratio of segmented to simple sphere efficiency The trend shows increasing efficiency which corresponds to a uniformly wrapped cylinder However, a buckling cut off is expected since deterioration of stability derived from the node cusp will prevent high filament prestress essential to efficient use of available filament materials.

Figures 71, sheets 1 thru 3, present quantitative effects of increasing segment angle as a function of burst pressure.

f. Shell Thickness Considerations

Shell thickness may be of interest as an alternate of design pressure For this purpose t is normalized with respect to the spherical radius. R Effect of t/R on the efficiency is given for several shell materials in Figure 72 (sheets 1-4). The results are similar to those in Figure 66 because of the linear relationship between operating pressure and the thickness The data in either the form of Figure 66 or Figure 72 can be applied to estimate the effect of thickness tolerance on pressure vessel efficiency. For example, assume a system has a nominal thickness t and a minimum thickness t'. An efficiency η is found for t/R. However, η must be reduced since the actual pressure is limited by t'. Then

$$\eta' = \frac{P'V}{W} = \frac{P(\frac{t'}{t})V}{W} = \eta \frac{t'}{t}$$

This data can also be applied to estimate the effect of (t/R) mismatch between two segments For example, if segments. not necessarily of the same radius, are mismatched such that $(t/R)_1 < (t/r)_2$; that is, $P_1 < P_2$; and the design weights of each segment are W_1 and W_2 respectively, then from Figure 72, η_1 and η_2 are readily found. Since net efficiency is

$$\eta = P_1 \frac{(V_1 + V_2)}{W_1 + V_2} = \frac{\frac{P_1V_1}{W_1}}{1 + W_2} + \frac{\left(\frac{P_2V_2}{W_2}\right)\left(\frac{P_1}{P_2}\right)}{1 + W_1}$$

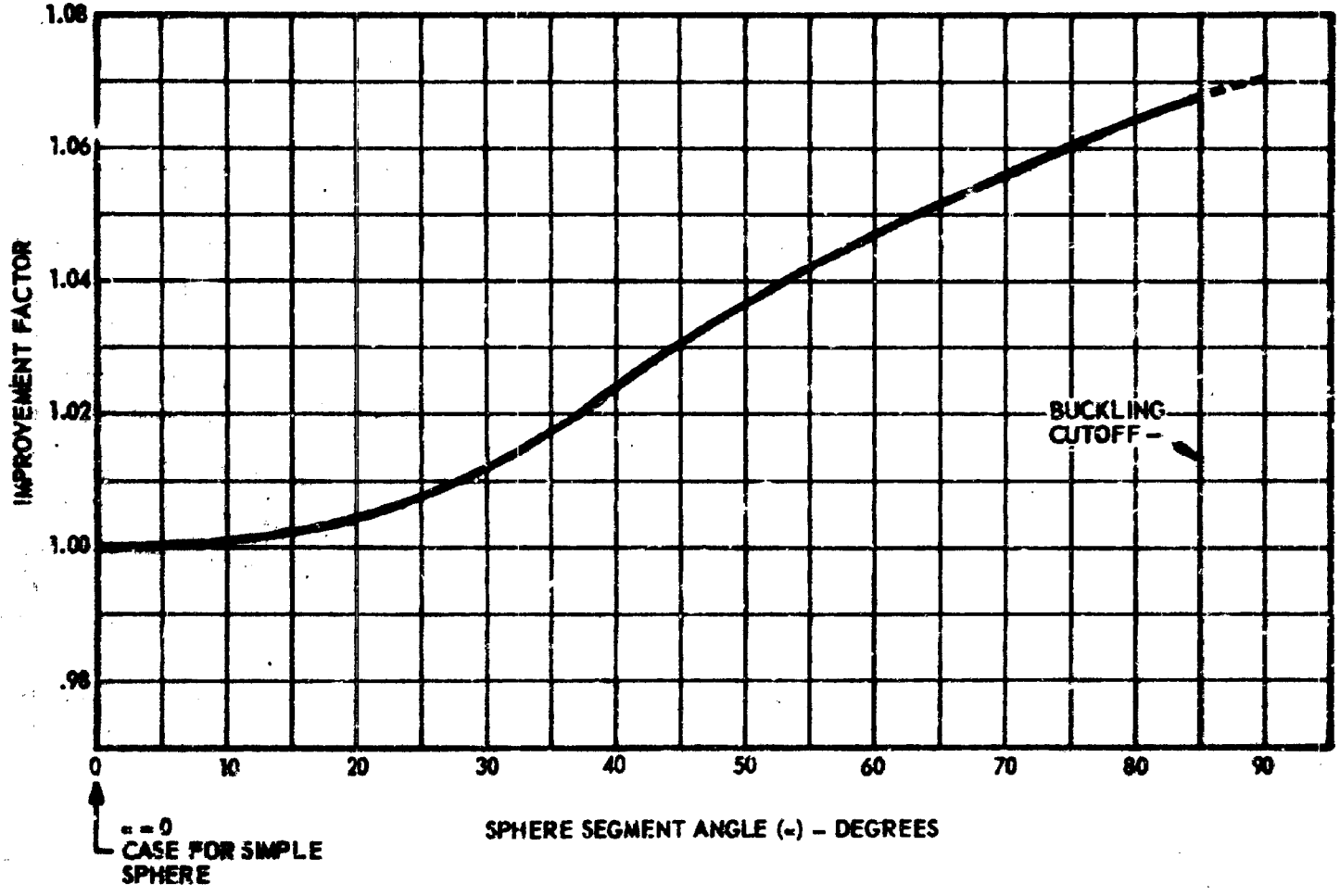

FIGURE 70 SEGMENTED SPHERE IMPROVEMENT OF η FOR SIMPLE SPHERE

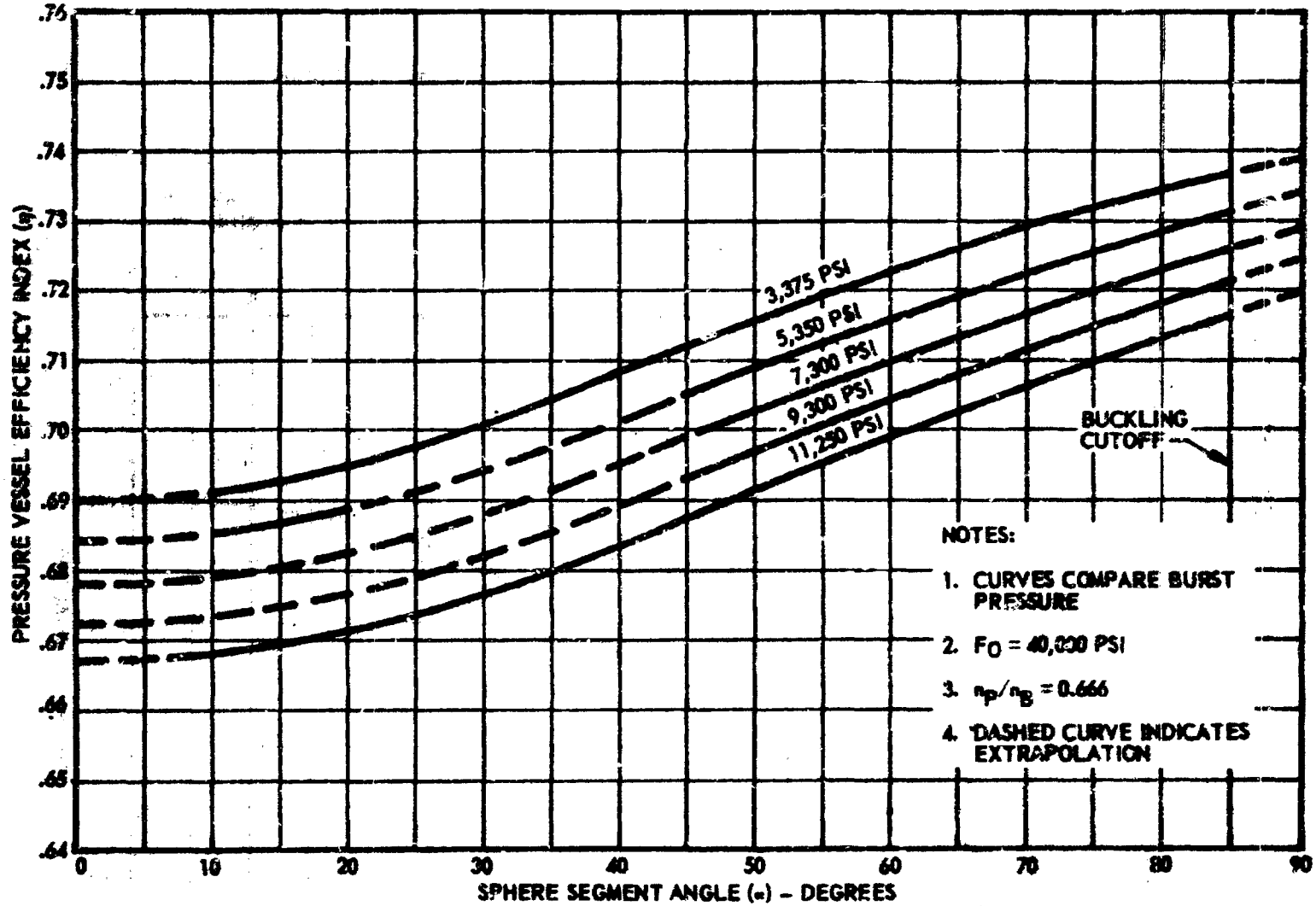

FIGURE 71 EFFICIENCY INDEX SEGMENT ANGLE [5901 GLASS–6AL-4V TI (ANNEALED) VESSEL] (SHEET 1)

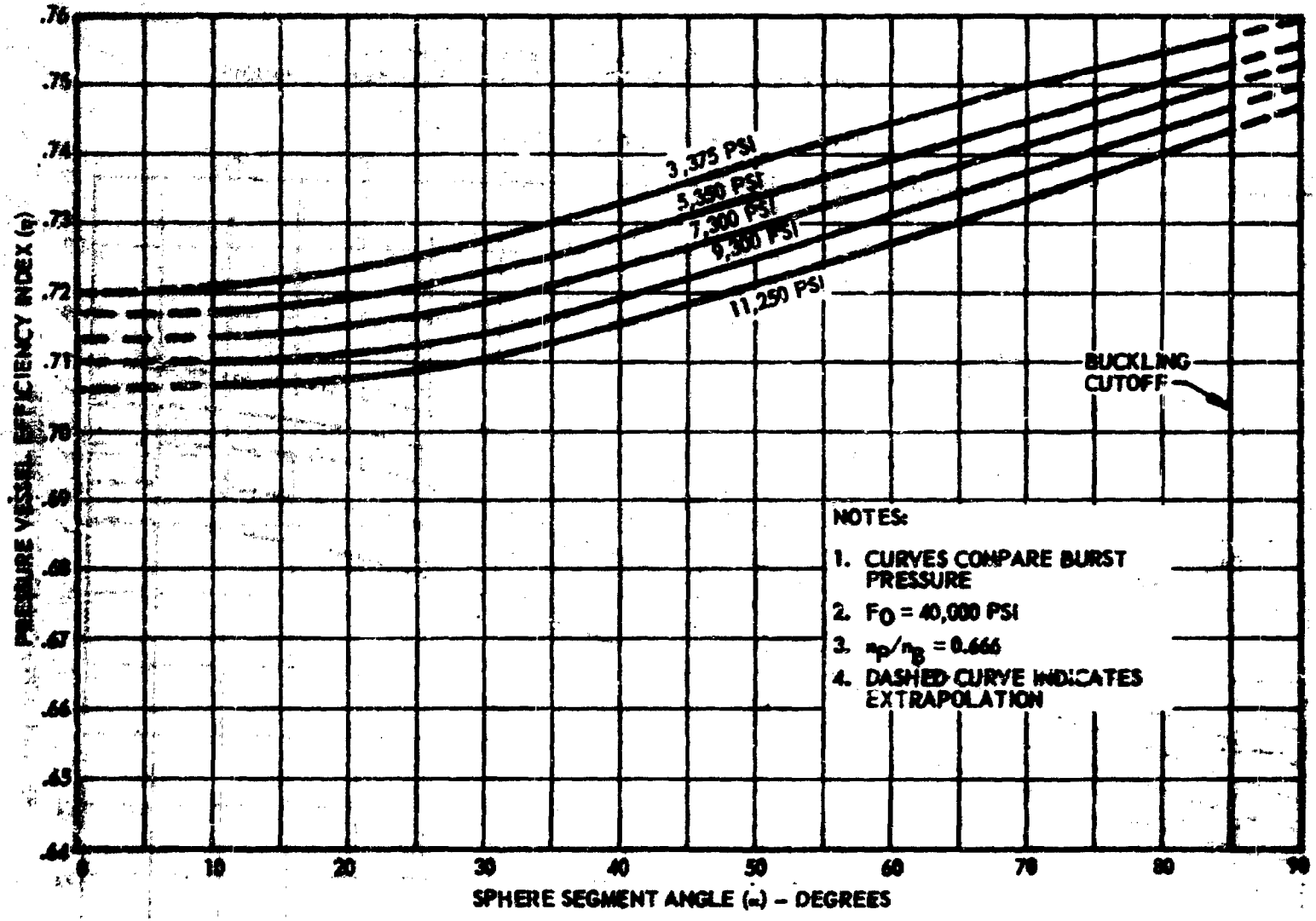

FIGURE 71 EFFICIENCY INDEX VERSUS SEGMENT ANGLE [BORON – MARAGING STEEL (900) VESSEL] (SHEET 2)

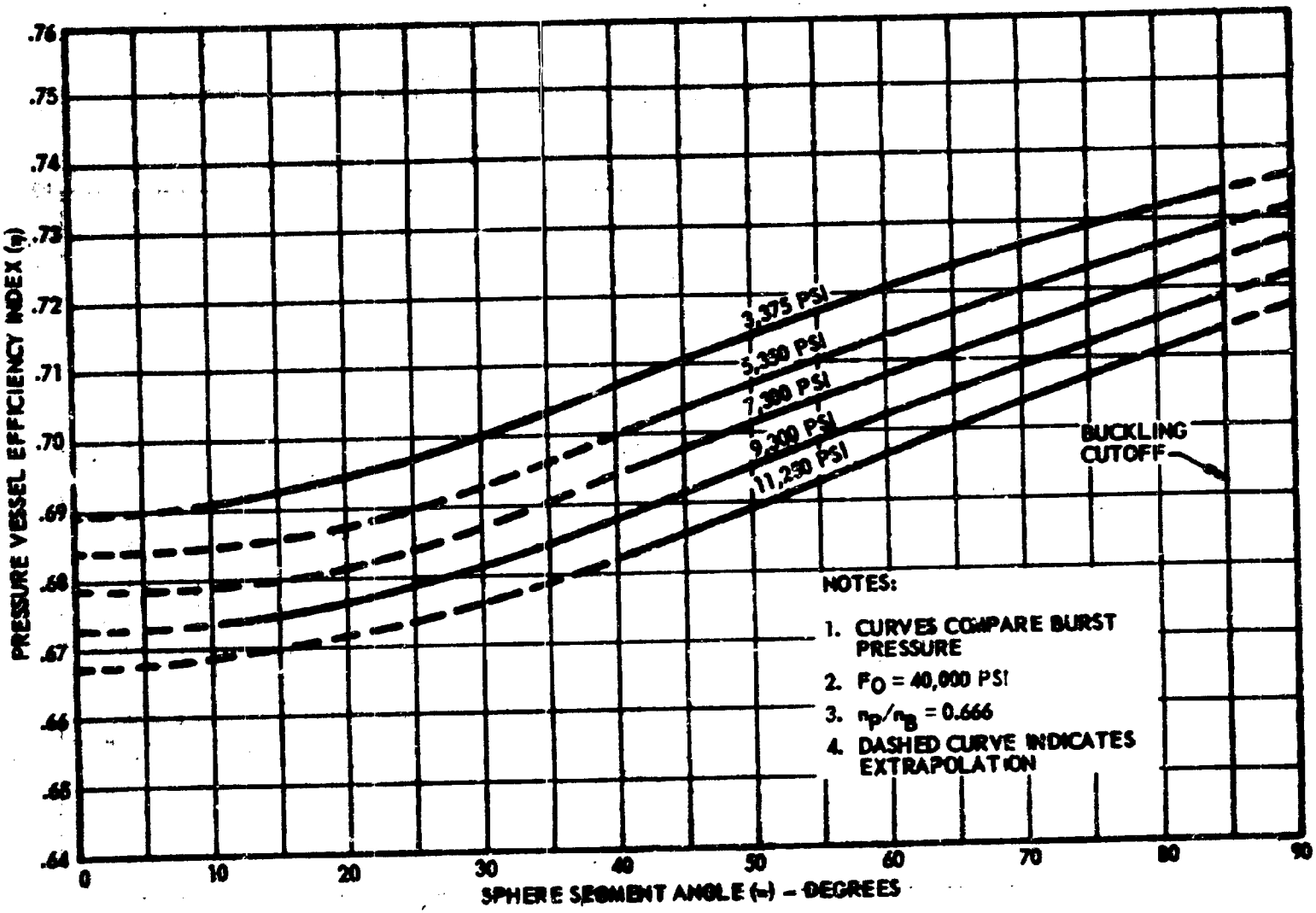

FIGURE 71 EFFICIENCY INDEX VERSUS SEGMENT ANGLE [BORON FILAMENT – 6AL-4V TI (ANNEALED) VESSEL] (SHEET 3)

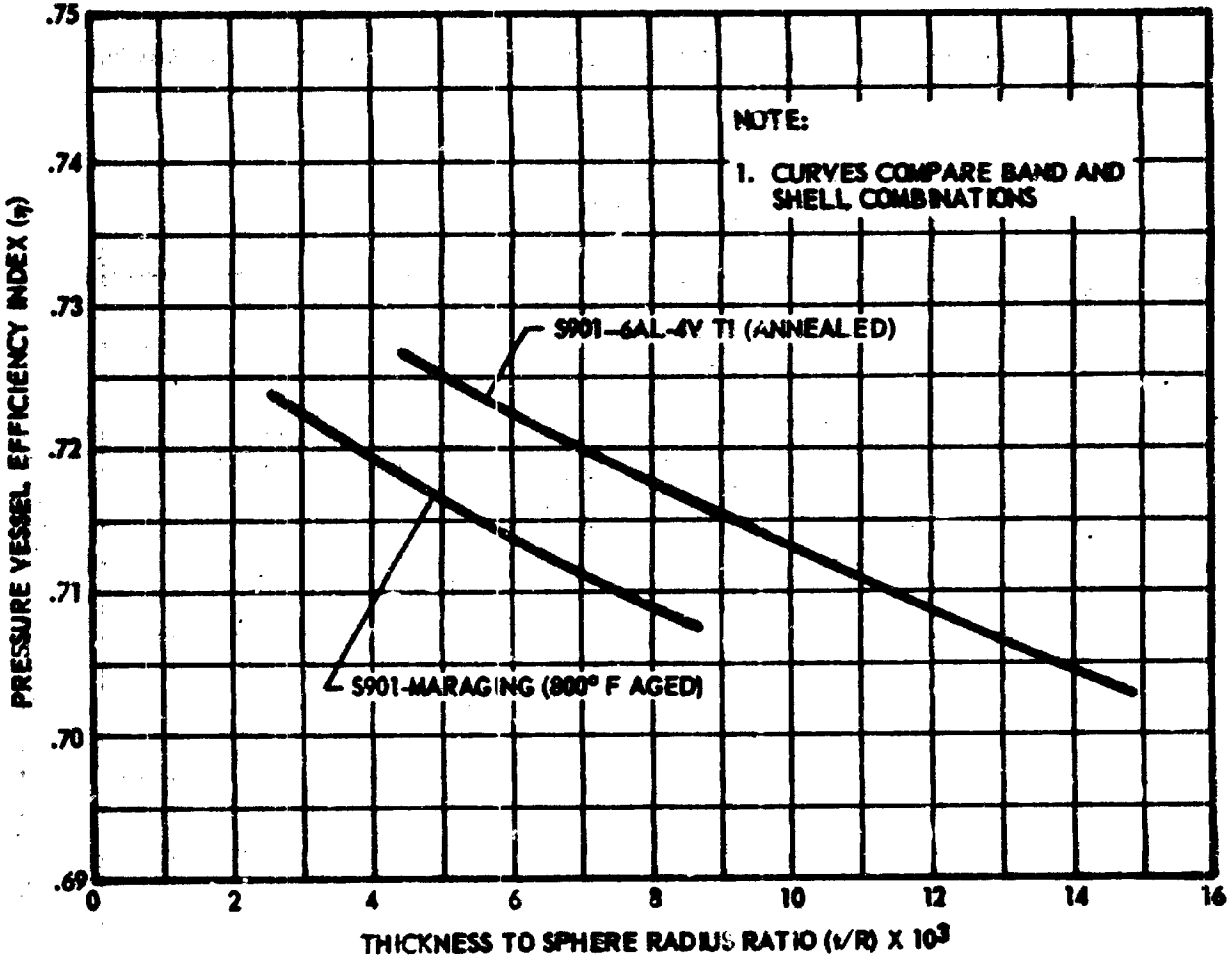

FIGURE 72 EFFICIENCY INDEX VERSUS THICKNESS TO SPHERE RADIUS RATIO (SHEET 1)

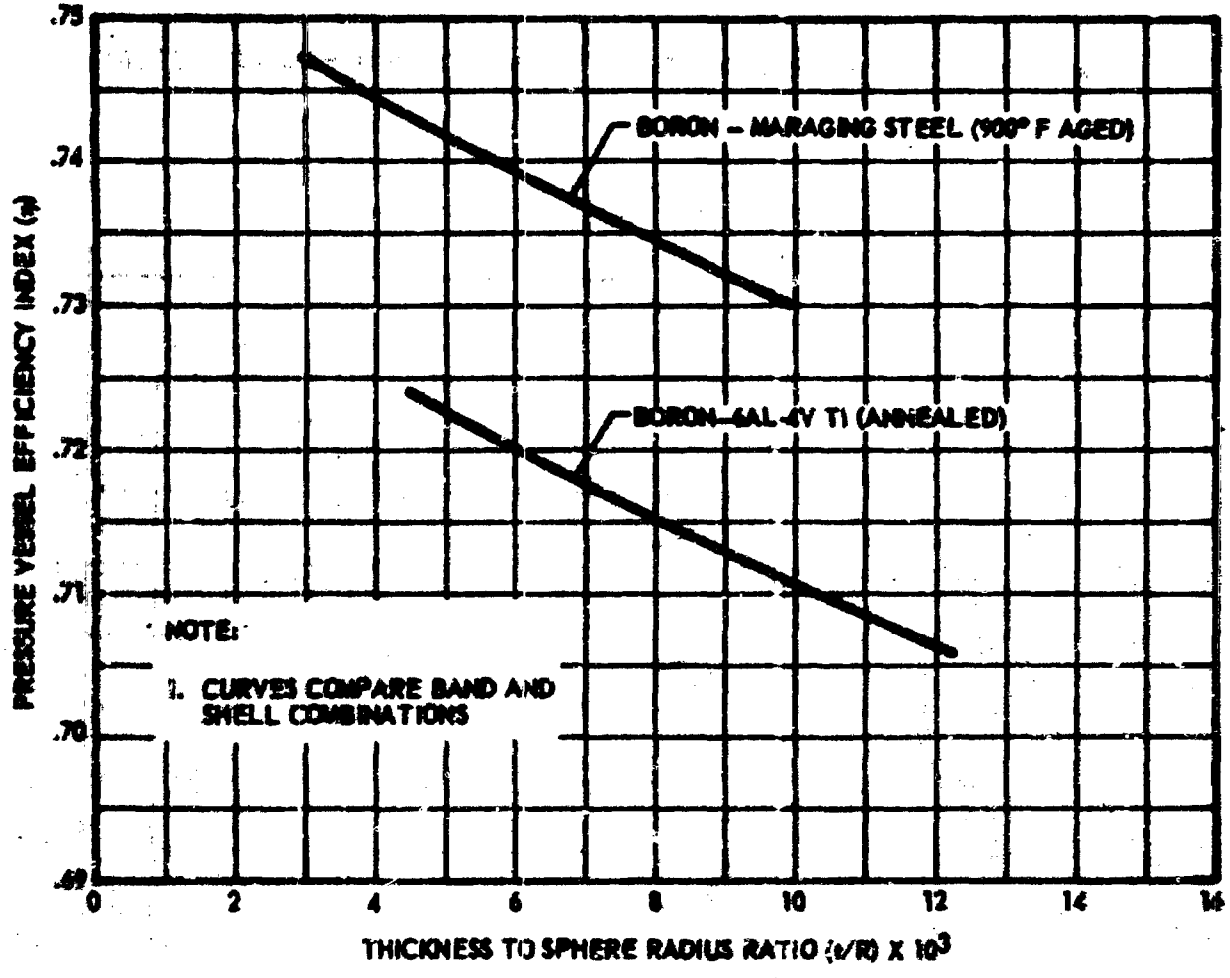

FIGURE 72 EFFICIENCY INDEX VERSUS THICKNESS TO SPHERE RADIUS RATIO (SHEET 2)

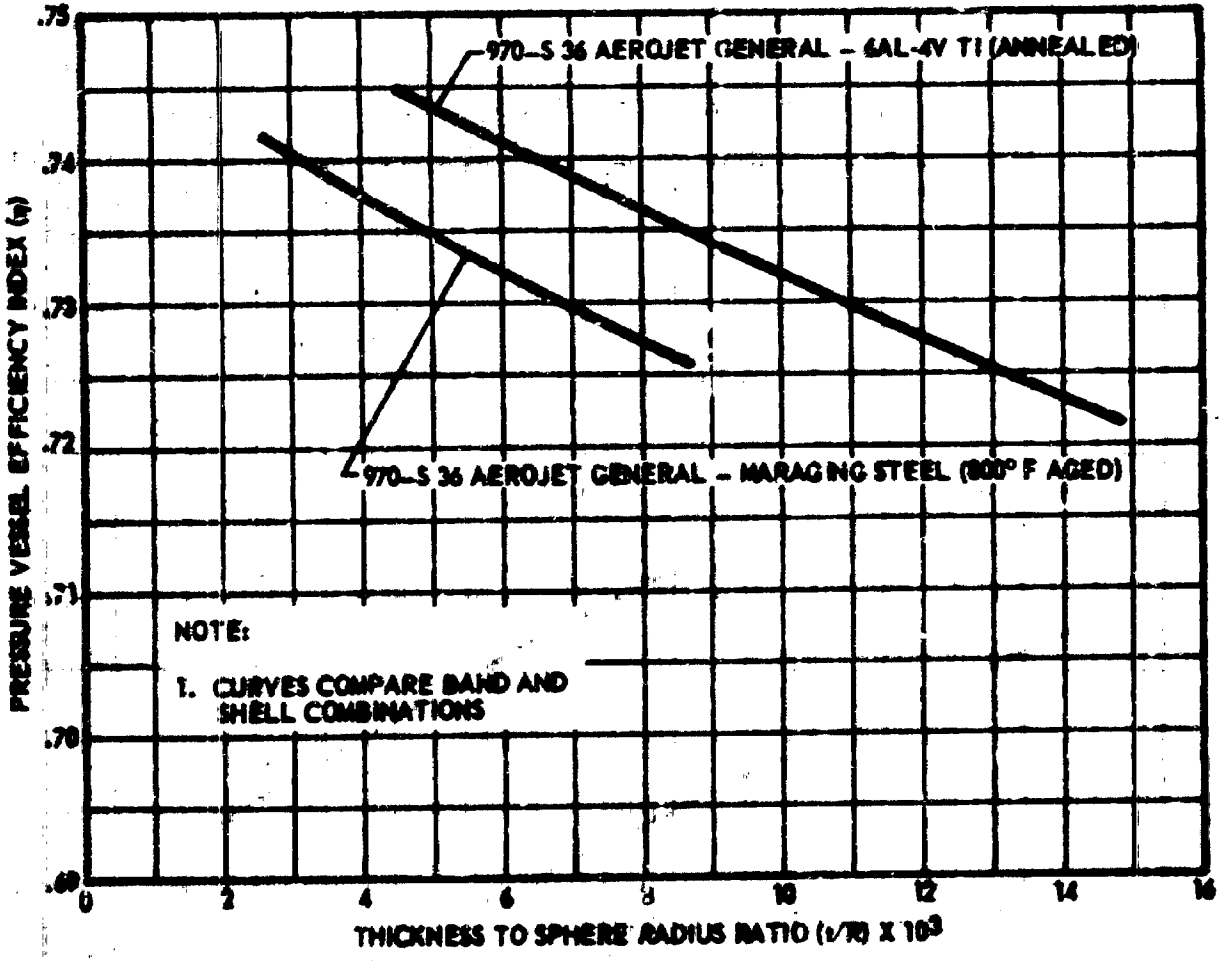

FIGURE 72 EFFICIENCY INDEX VERSUS THICKNESS TO SPHERE RADIUS RATIO (SHEET 2)

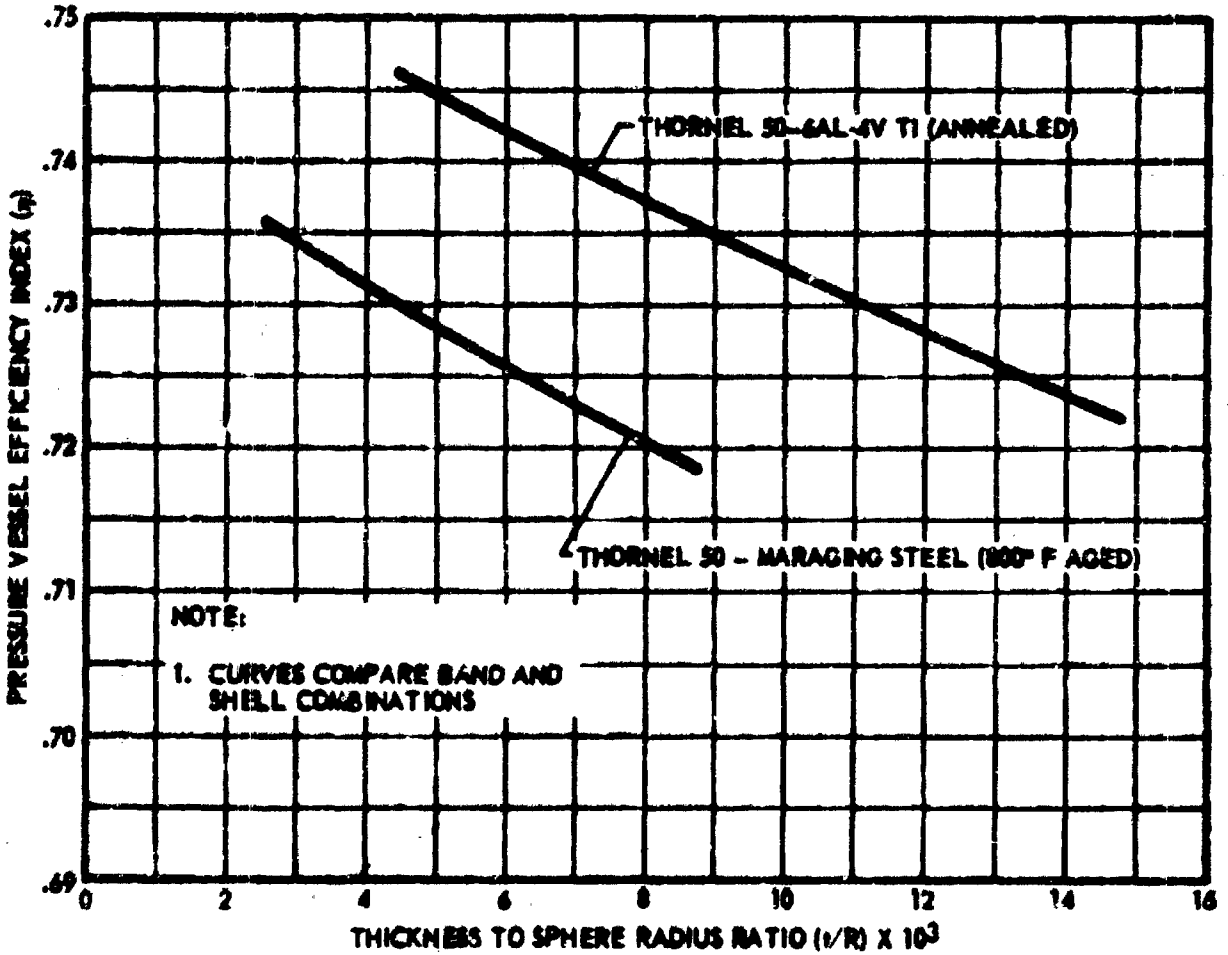

FIGURE 72 EFFICIENCY INDEX VERSUS THICKNESS TO SPHERE RADIUS RATIO (SHEET 4)

or,

$$\eta = \frac{\eta_1}{(1 + W_2)} + \eta_2 \frac{(t/R_1) \div (t/R_2)}{(1 + W_1)} .$$

The general relation for net efficiency of a system of j segments where $(t/R)_m$ is the least value, is:

$$\eta_j = \sum_1^j \frac{\eta_i}{(1 + \sum_1^j W - W_i)} \left[\left(\frac{t}{R}\right)_m \div \left(\frac{t}{R}\right)_i \right]$$

6. GENERAL DESIGN INFORMATION BASED ON AMC ANALYSIS

To achieve membrane conditions throughout the nodal area, the stresses must be known in order to make proper use of the band. Shell stress amplification factors A_ϕ and A_θ were derived (see Appendix IV) as functions of configuration parameters Y/R and r/R. The amplification factor is the ratio of the actual stress to that of a pure membrane stress which is the objective condition. Meridian amplification, A_ϕ, and circumferential amplification, A_θ, versus parameters Y/R and r/R are plotted in Figures 73 and 74. The stresses were calculated at a point where fillet angle, ϕ, is zero. From these plots one can see that the circumferential stress is the crucial one at this point.

Band pressure to internal pressure ratio, f/P, versus fillet angle, ϕ, is shown plotted in Figure 75 (Sheets 1-4). Each curve is for a given configuration specified by Y/R and r/R. The maximum fillet angle is the angle formed by a vertical radius line and a radius line to the point of tangency of sphere and fillet. From such data, the amount of band pressure (and/or band area) required for membrane conditions may be determined. An example is given in Section III. Figure 75 indicates that for all values of Y/R and r/R, the band pressure increases as ϕ increases to maintain membrane conditions. To indicate general requirements, an average value of band pressure is given in Figure 76 as a function of Y/R and r/R.

7. GENERAL DESIGN DATA BASED ON FATS ANALYSIS

In view of the limitation of the computer time analysis which was mentioned above, there are really only a very few parameters which can be generalized to cases other than the design examples. However, in the case of equal sphere configurations, some generalizations of data can be made.

For the purposes of a general design, the data presented in Figure 77 are sufficient to assess the effects of secondary stress. Assuming r, R, and t are known, the membrane state for the segmented sphere is defined by

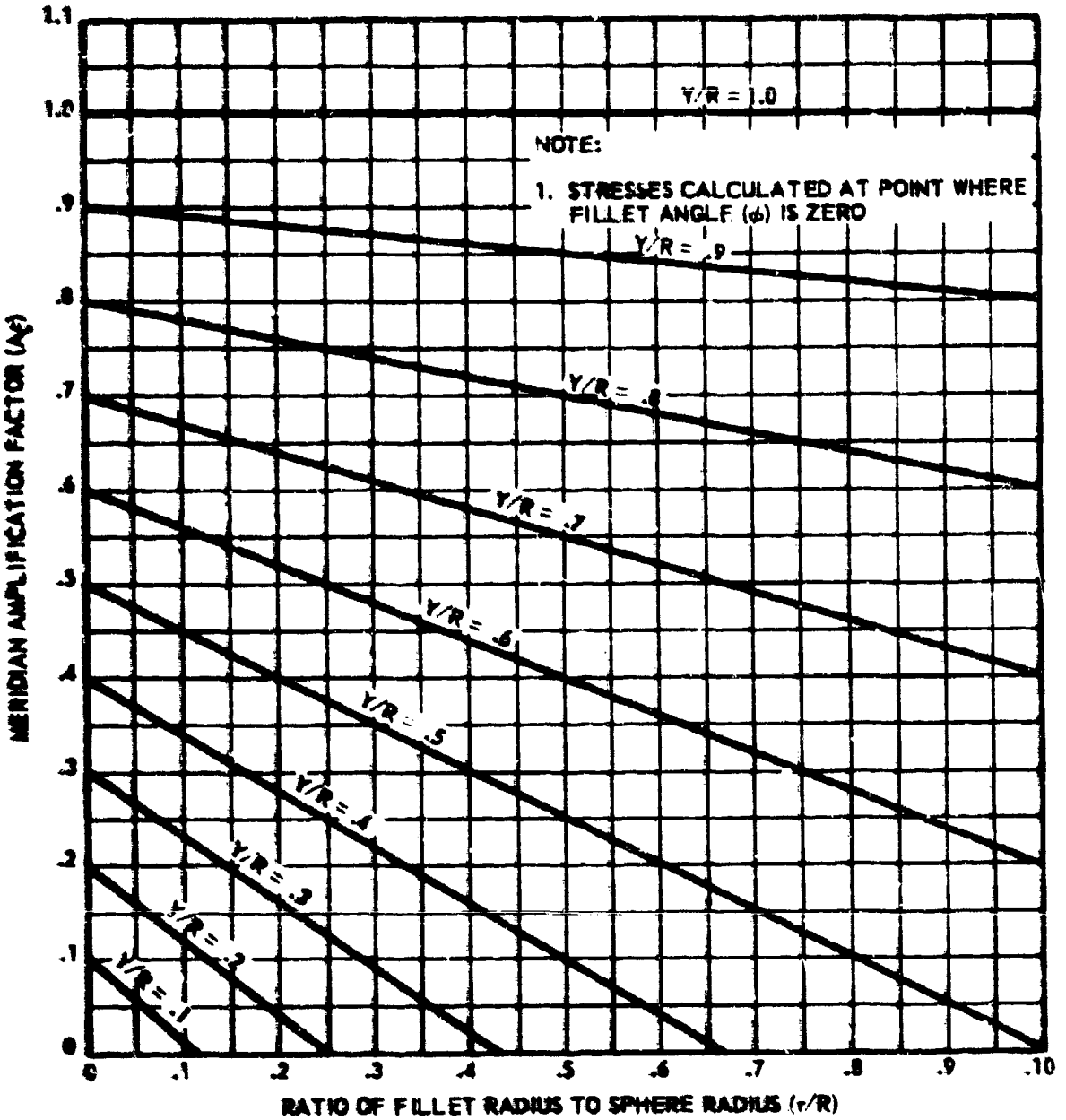

FIGURE 73 K_ϕ AMPLIFICATION FOR HB BAND VERSUS CONFIGURATION PARAMETERS: Y/R, r/R

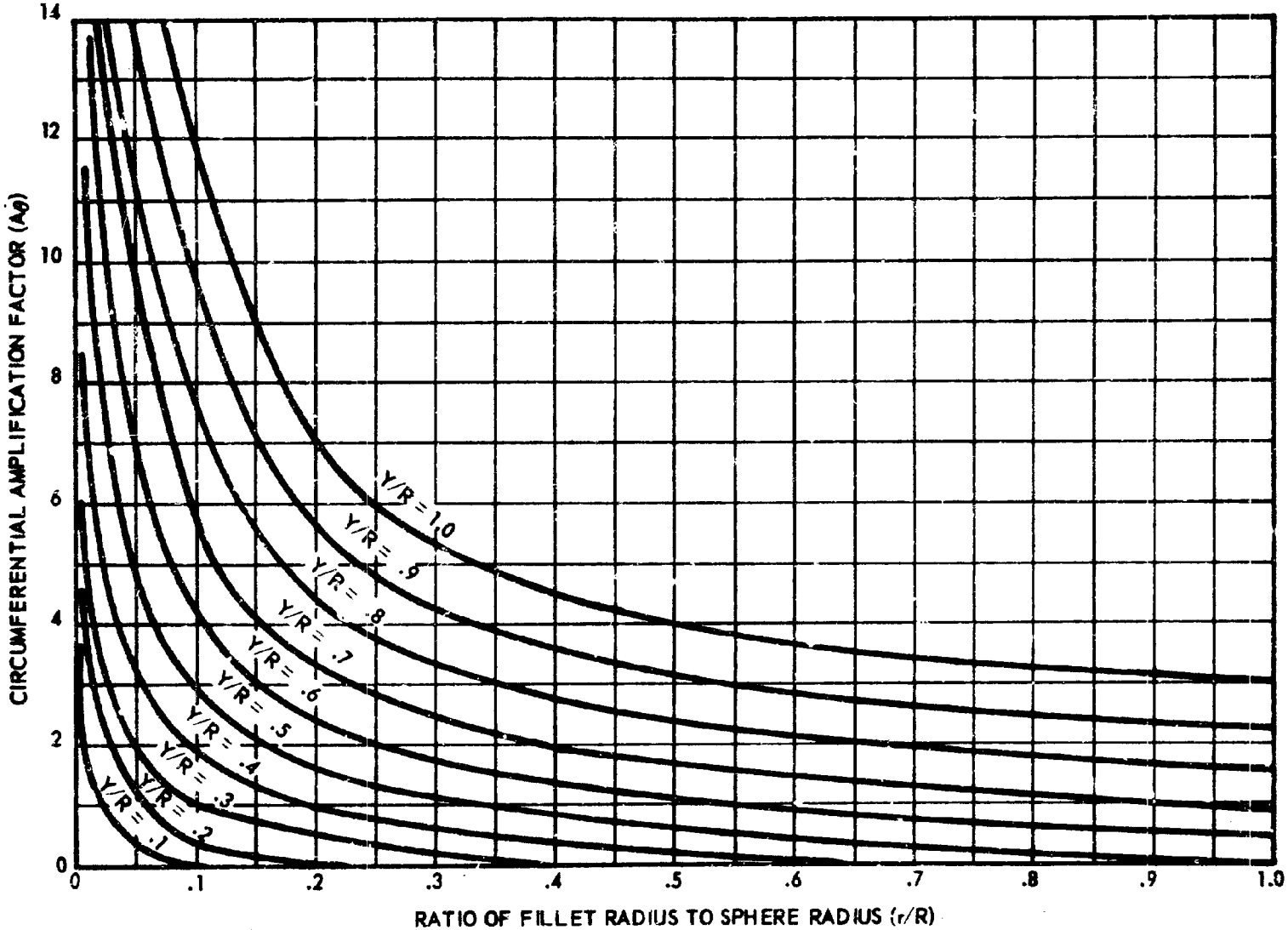

FIGURE 74 N_θ AMPLIFICATION FOR NC BAND VERSUS CONFIGURATION PARAMETERS: Y/R, t/R

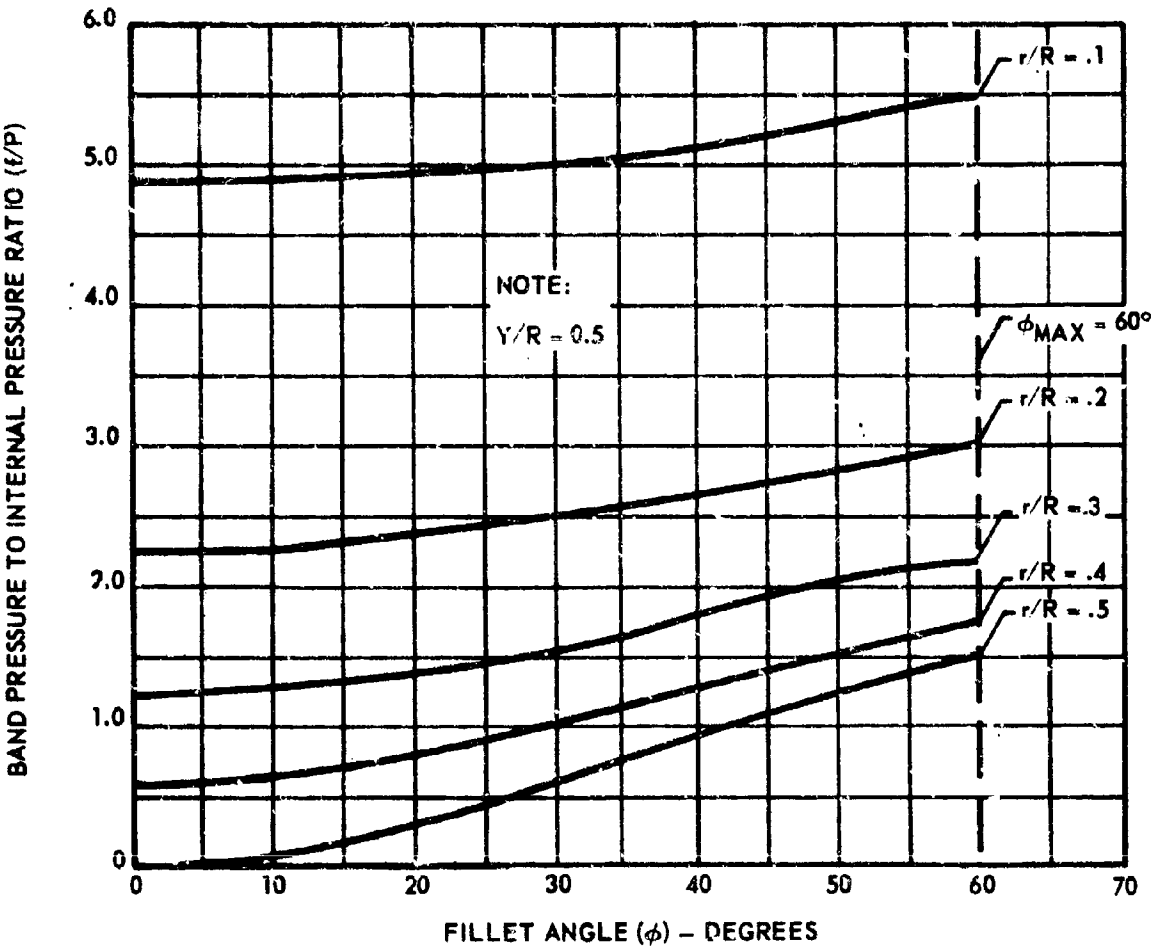

FIGURE 75 BAND PRESSURE TO INTERNAL PRESSURE RATIO VERSUS FILLET ANGLE ϕ (SHEET 1)

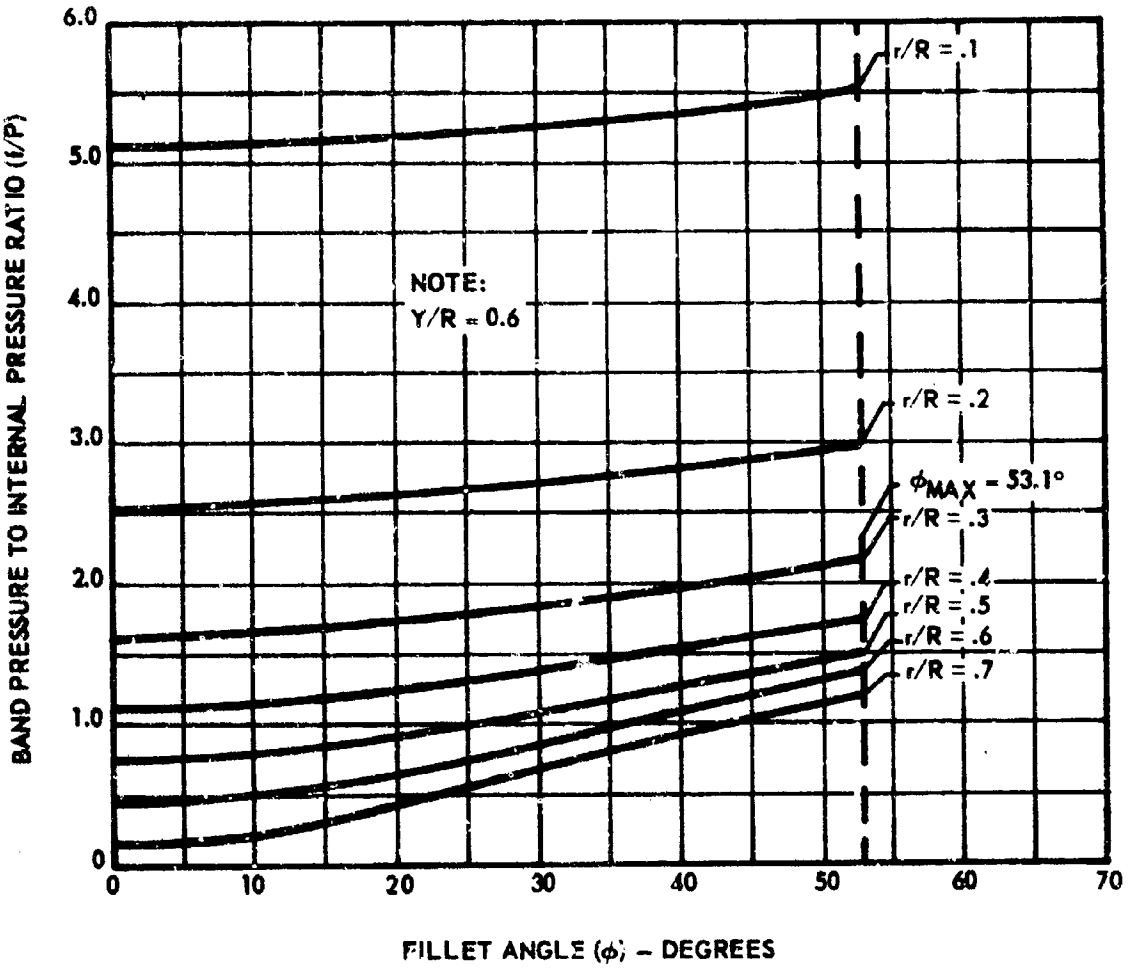

FIGURE 75 BAND PRESSURE TO INTERNAL PRESSURE RATIO VERSUS FILLET ANGLE ϕ (SHEET 2)

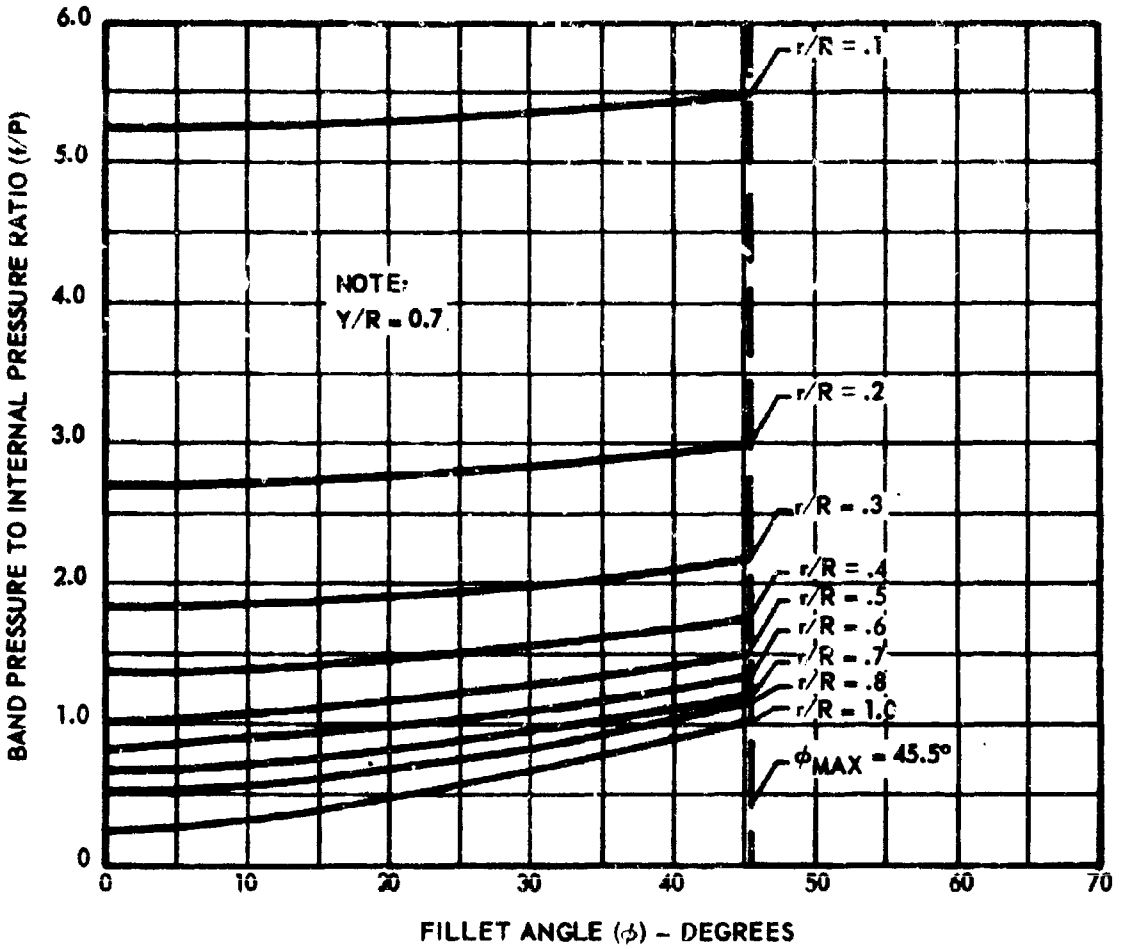

FIGURE 75: BAND PRESSURE TO INTERNAL PRESSURE RATIO VERSUS FILLET ANGLE ϕ (SHEET 3)

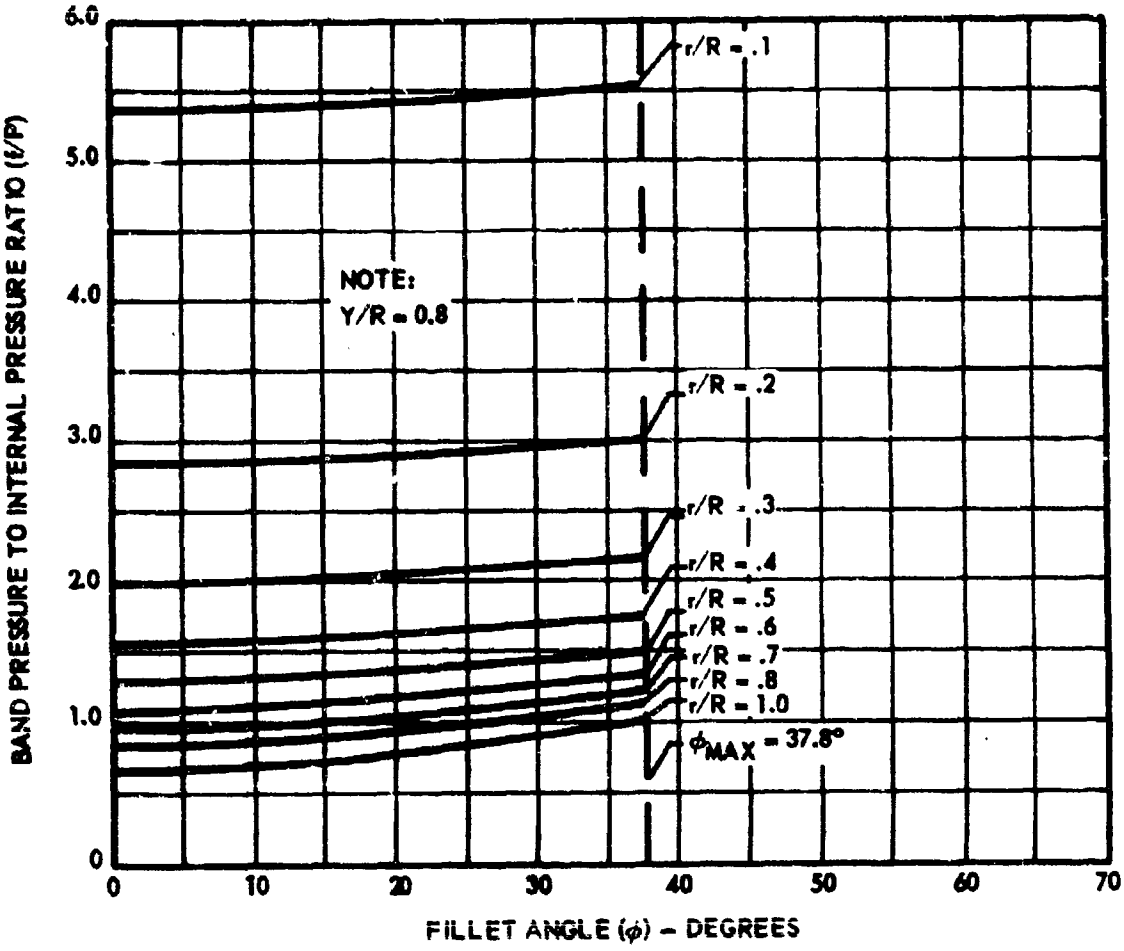

FIGURE 75 BAND PRESSURE TO INTERNAL PRESSURE RATIO VERSUS FILLET ANGLE ϕ (SHEET 4)

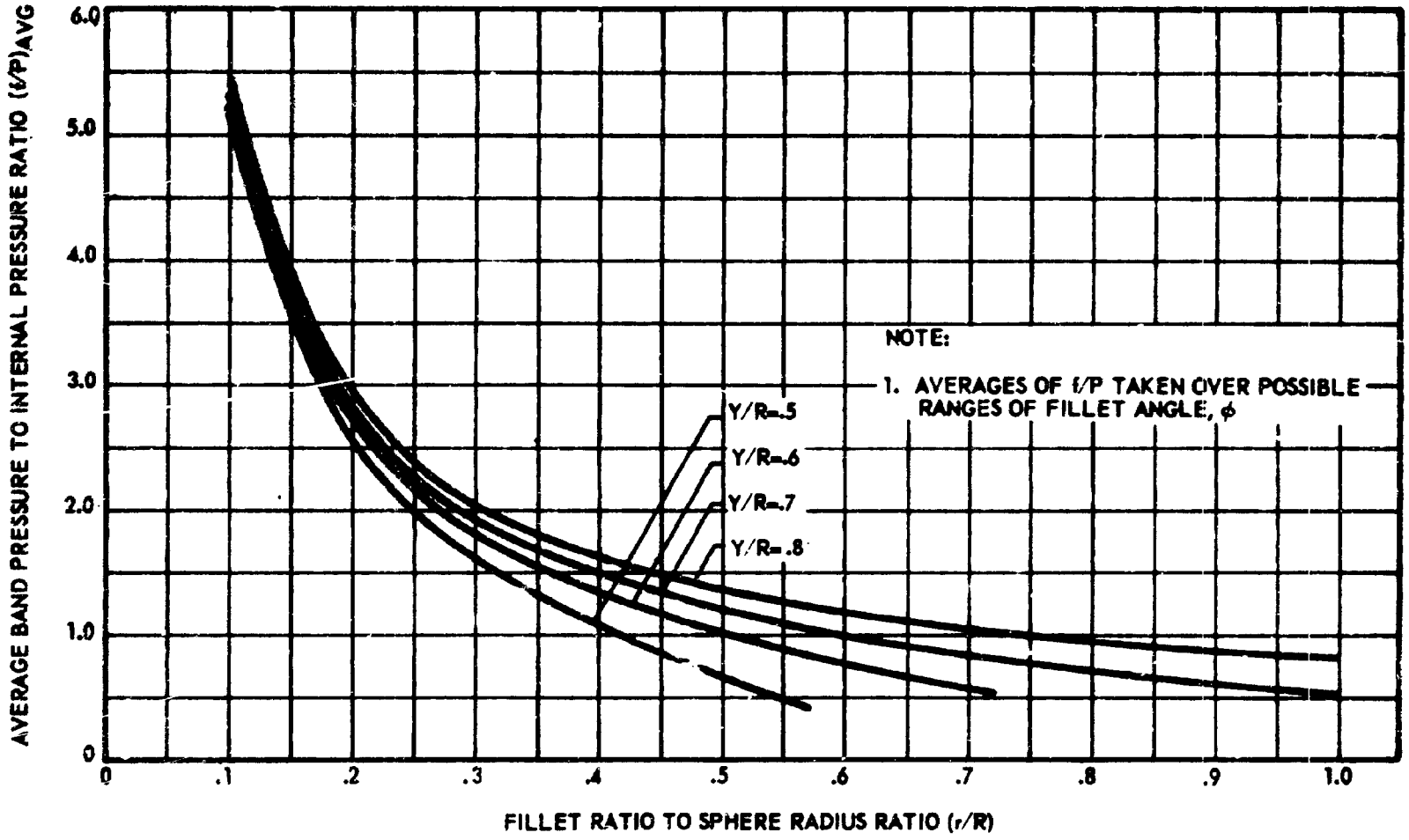

FIGURE 76 AVERAGE BAND PRESSURE TO INTERNAL PRESSURE RATIO VERSUS CONFIGURATION PARAMETERS: Y/R, r/R

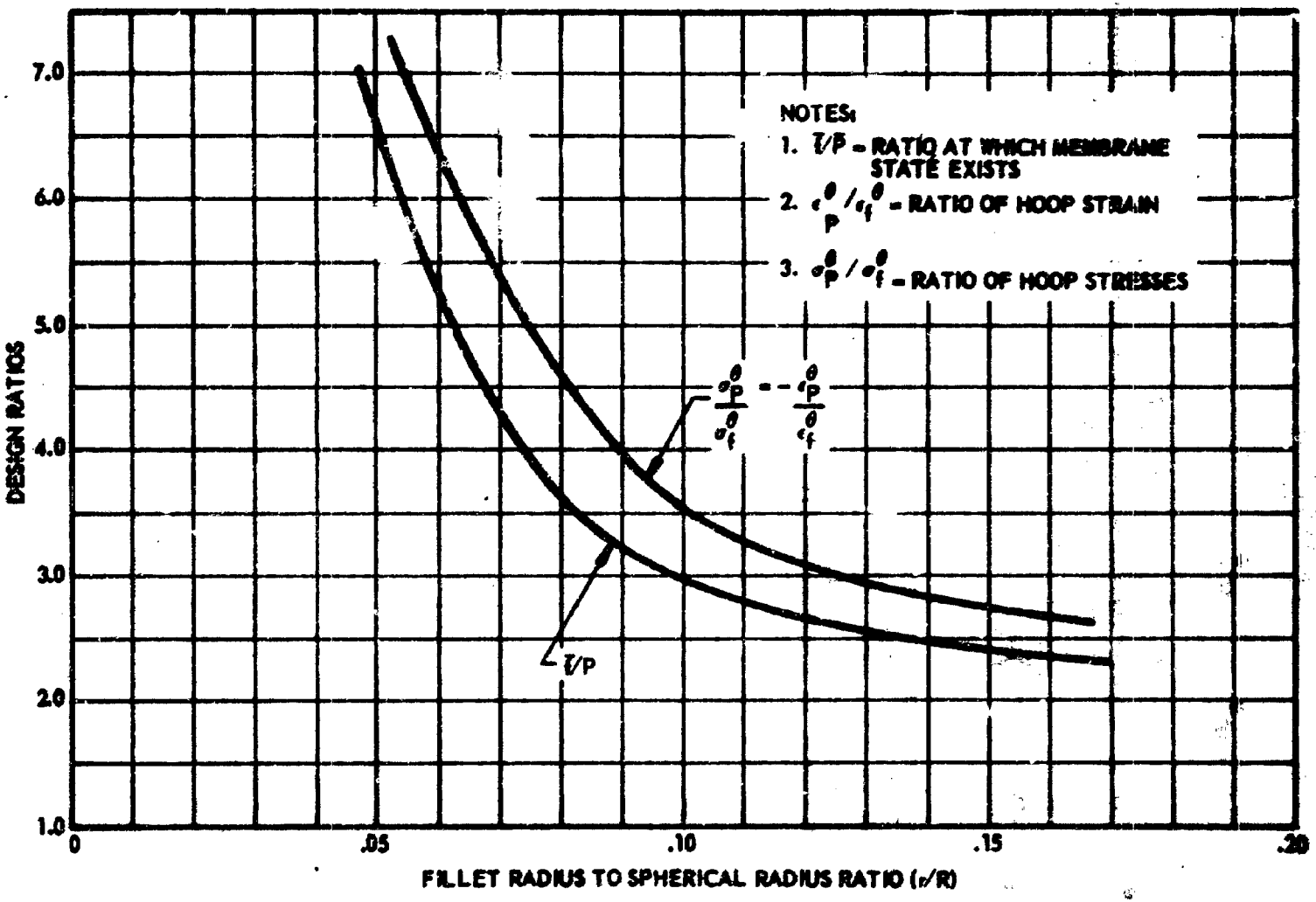

FIGURE 77 DESIGN PARAMETERS BASED ON PETS ANALYSIS

$$R/2t = \sigma^{\bullet}_{p} + \frac{f}{p}\sigma^{\bullet}_{f}$$

Then from R/r, we can obtain f/p and $\sigma^{\bullet}_{p}/\sigma^{\bullet}_{f}$ from Figure 78. It follows that $\sigma^{\bullet}_{p}$ and $\sigma^{\bullet}_{f}$ may be determined. If the pressure p_m which the membrane state is derived is known, then f is determinate from f/p and therefore;

$$\varepsilon^{\bullet}_{f} = \left(\frac{1+\mu^{\bullet}}{E_s}\right)\left(\frac{P_m}{2t}\frac{R}{f}\right),$$

Where $\mu^{\bullet}$ is Poissons' ratio - knowing $\varepsilon^{\bullet}_{f}$, one can determine $\varepsilon^{\bullet}_{p}$ from the known ratio $\varepsilon^{\bullet}_{p}/\varepsilon^{\bullet}_{f}$. Hence all the information required for the analysis is determinate from Figure 77. Finally it is noted that the effects of shell segment thicknesses are easily generalized by referring to a membrane stress. This result is shown in Figure 78

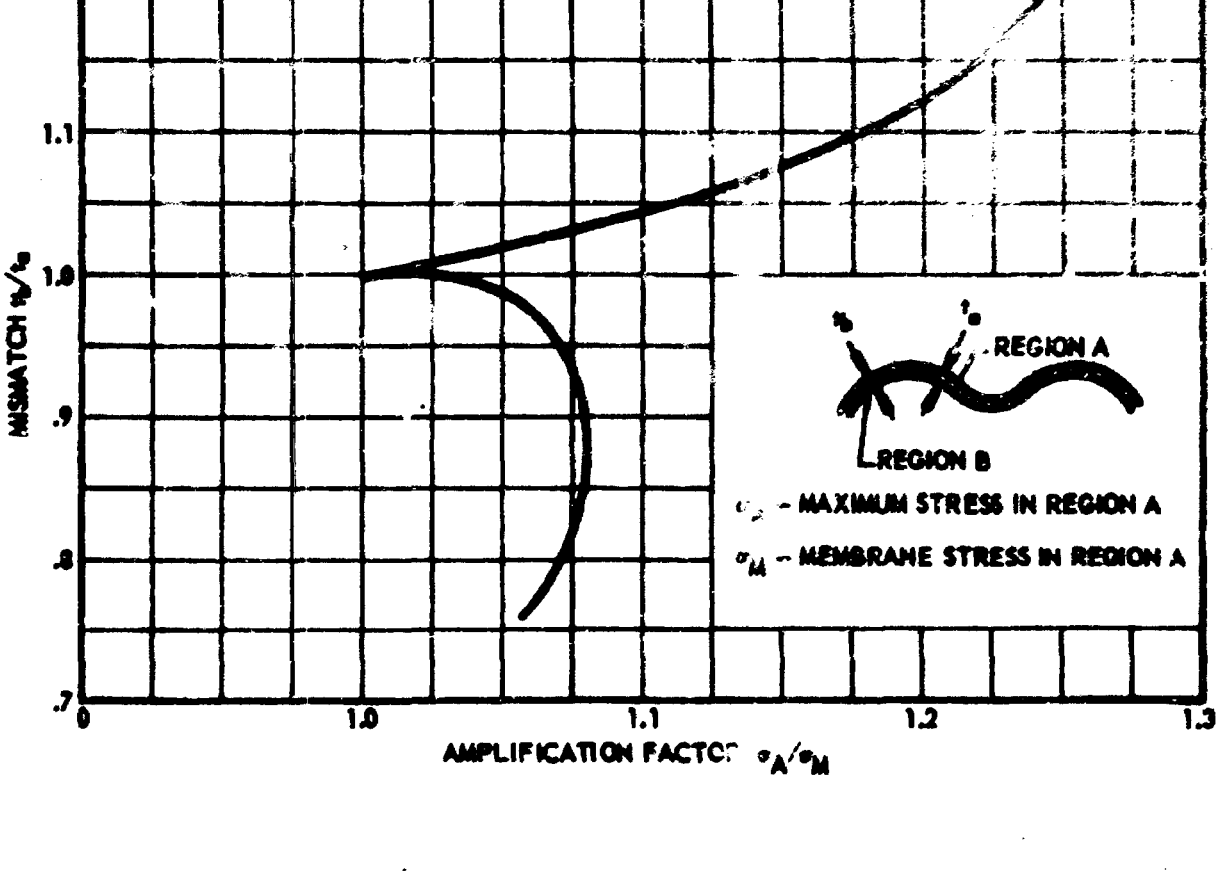

FIGURE 78 AMPLIFICATION OF MEMBRANE STRESS IN REGION A DUE TO MISMATCH WITH REGION B

SECTION VIII

BAND DESIGN FOR PHASE II VESSELS

1. GENERAL

In the Class III configuration the 17-7 PH stainless steel will be replaced by 6AL-4V titanium. A design parameter of n_p/n_B equal to .5 will be used for all systems in order to demonstrate an efficiency improvement over the engineering model designs based on $n_p/n_B = .666$. In addition, final shell thickness will be chem-milled to eliminate variations caused during forming.

2. DESIGN OPTIMIZATION BY ANC METHOD

The band load distribution equations and geometry parameters for Classes I, II and III vessels are the same as Phase I (Ref. Section III). The distribution equation and parameters are listed below:

$$f/P = 1/2 \quad 2 + (r/R)^{-1} - \frac{\cos \phi}{(1 + r/R)\, Y/R - (r/R) \cos \phi}$$

Class I and II (ref. Figure 9)

$Y/R = 0.9450$
$r/R = 0.1666$
ϕ Max $= 19.5^\circ$

Class III (Ref. Figure 10)

$Y_1/R_1 = 0.4848$ $\quad Y_2/R_2 = 0.6867$
$R_1/R_1 = 0.1666$ $\quad r_2/R_2 = 0.2759$
ϕ_1 Max $= 61^\circ$ $\quad \phi_2$ Max $= 46.6^\circ$

3. DESIGN

a. The following properties apply to the Classes I and II vessel:

6AL-4V Ti - shell material

S-901 Fiber Glass - band material

$F_o = 25{,}000$ psi

$n_p/n_B = 0.5$

$f/P = 3.47$

t (nominal) = 0.055

t (minimum) = 0.05 in.

$$P_B = \frac{2\, t\, (\text{min})\, \sigma_U^S}{R} = \frac{0.1\, (168{,}000)}{5.9613} = 2818 \text{ psi}$$

$$\varepsilon_P^{Sb} = \sigma_Y^S\, (1 - U)/E^S + 0.002 = 0.0082588$$

A band prestress (F_o) of 25,000 psi, compared to 40,000 psi for Phase I vessels, is required in order not to exceed an ultimate allowable of 200,000 psi for the composite band at burst pressure (Ref. Equation 3.4).

The band load equation for membrane conditions

$$\sigma^b \; A^b = 2 \, r_1^2 \int_0^{19.5^\circ} \left[\frac{(y + R)}{r} \; f \cos \theta - f \cos^2 \phi \right] d\phi \tag{3.1}$$

was previously used (Ref. Section III, paragraph 2.) in Phase I design. This equation gives the following result for the Phase II design

$$\sigma^b \, A^b = 36,569 \quad \text{lbs.} \tag{3.2}$$

Based on proof pressure, the stress in the band is

$$\sigma_P^b = F_o + \xi_P^{Sb} \; E^b \tag{3.3}$$

$$= 25,000 + .0082598 \; (9 \times 10^6)$$

$$= 25,000 + 74,329$$

$$= 99,329 \quad \text{psi}$$

With a n_P/n_B ratio of 0.50, the band stress at burst condition becomes

$$\sigma_B^b = \frac{\sigma_P^b}{n_P/n_B} = \frac{99,329}{0.5} = 198,658 \quad \text{psi} \tag{3.4}$$

$$\text{M.S.} = \frac{200000}{198,658} - 1 = .01$$

Substitution of the above value in Equation (3.2) yields a required band cross section area at burst condition of

$$A_B^b = \frac{36,569}{198,658} = 0.1840 \text{ sq. in.} \tag{3.5}$$

b. Class III

The following properties apply to the large segment of the Class III vessel:

6 Al-4V Ti - shell material

S-901 Fiber Glass - band material

F_o = 25,000 psi

$n_p/n_b = 0.5$

t (nominal) = 0.078 in.

t (minimum) = 0.073 in.

$f/P = (3.95 + .657\ \phi)$

$$P_b = \frac{2t\ (\min)\ \sigma^s_U}{R} = \frac{(0.146)\ (368{,}000)}{8.445} = 2904 \text{ psi}$$

$$\varepsilon^{sb}_p = \varepsilon^s_Y\ (1 - u)/E^s + 0.002$$

$$\varepsilon^{sb}_p = \left[(152 \times .7) \div 17\right] \times 10^{-3} + 0.002$$

$$\varepsilon^{sb}_p = 0.0082588$$

A maximum band prestress (F_o) of 25,000 psi is required in order not to exceed ultimate tensile allowable for the composite (Ref. Equation 3.13).

The band load equation for this segment is

$$\sigma^b A^b = r_1^2 \int_0^{61^\circ} \left[\frac{y + r_1}{r_1} f \cos\phi - f \cos^2\phi\right] d\phi \quad (3.6)$$

which upon substitution and integration yields

$$\sigma^b A^b = 39{,}703 \text{ lbs.} \quad (3.7)$$

Based on proof pressure, the stress in the band is

$$\sigma^b_p = F_o + \varepsilon^{sb}_p E^b \quad (3.8)$$

$$= 25{,}000 + .0082588\ (9 \times 10^6)$$

$$= 25{,}000 + 74{,}329$$

$$= 99{,}329 \text{ psi}$$

with the stress at burst condition

$$\sigma^b_B = \frac{99{,}329}{0.50} = 198{,}658 \text{ psi} \quad (3.9)$$

Substitution of this value into Equation (3.7) yields a required area for the large segment of

$$A_B^b = \frac{39,703}{198,658} = .200 \text{ sq. in.} \qquad \text{M.S.} = .01 \tag{3.10}$$

The small segment design is governed by the following conditions:

6AL-4V Ti - shell material

S-901 Fiber Glass - band material

$F_o = 25,000$ psi

$n_P/n_B = 0.5$

t (nominal) = 0.055

t (minimum) = 0.05

$f/P = (3.95 + .657\ \phi)$

$$P_B = \frac{2\ t\ (\text{min})\ \sigma_U^S}{R} = \frac{0.1\ (168,000)}{5.9615} = 2818 \text{ psi}$$

$$\varepsilon_P^{Sb} = \sigma_Y^S\ (1 - U)/E^S + 0.002$$

$$\varepsilon_P^{Sb} = (152 \times .7/17) \times 10^{-3} + 0.002$$

$$\varepsilon_P^{Sb} = .0082588$$

The band load equation yields

$$\sigma^b\ A^b = r_2^2 \int_0^{46.6^\circ} \left[\left(\frac{y + r_2}{r_2} \right) f \cos \phi - f \cos^2 \phi \right] d\phi \tag{3.11}$$

$$= 25,193 \text{ lbs.}$$

The stress at proof pressure is

$$\sigma_P^b = F_o + \varepsilon_P^{Sb}\ E^b \tag{3.12}$$

$$= 99,329 \text{ psi}$$

By extrapolation of the stress strain curve and utilizing the assumed relationship $n_p/n_B = 0.5$, the stress at burst condition is:

$$\sigma^b_B = \frac{\sigma^b_P}{n_p/n_B} = \frac{99,329}{0.5} = 198,658 \quad \text{psi} \tag{3.13}$$

Then, the band area for the small segment that will satisfy the burst condition becomes

$$A^b_B = \frac{25,193}{198,658} = .1268 \text{ sq. in.} \tag{3.14}$$

The total area of band for the Class III vessel is sum of the large and small segment areas which is:

$$A^b_B = 0.3268 \text{ sq. in.} \tag{3.15}$$

APPENDIX I

DERIVATION OF PRESSURE VESSEL EFFICIENCY INDEX

The efficiency index indicates a comparison between different vessels. The variables pressure, volume, and weight define the index η. The approximate values for these variables are given in the equations as follows:

(1) Vol. $= \pi R^3/3 \left[3\left(1 + \sin^2\alpha\right) + \cos^2\alpha\right]\cos\alpha$

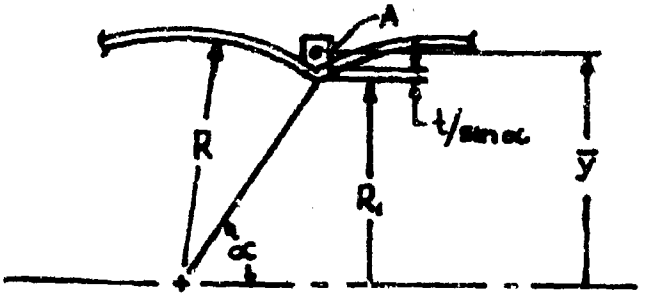

$$y = \left(R\sin\alpha + t/\sin\alpha + \sqrt{A}\ /2\right)$$

where the cross section area is given as

$$A = \left(\frac{2\, f_B^s\, t^s\, R\cos\alpha\sin\alpha}{f_D^b}\right)^{\frac{1}{2}} = \left(\frac{PR^2\cos\alpha\sin\alpha}{f_P^b}\right)^{\frac{1}{2}} = R\left(\frac{P\cos\alpha\sin\alpha}{f_B^b}\right)^{\frac{1}{2}}$$

Weight of Bank $= 2\pi y\, A\rho^b$

$$w^b = \frac{(2\pi\rho\, b)\,(2f_B^s\, t^s\, R\cos\alpha\sin\alpha)\,(R\sin\alpha + t/\sin\alpha + \sqrt{A}\ /2)}{f_B^b}$$

Weight of shell $(w^s) = 4\pi\left(R + t^s/2\right)^2 t^s \rho^s \cos\alpha$

Letting $P = 2\left(t^s\, f_B^s/R\right)$

Then

$$\eta = \frac{P_o}{W} = \frac{\left(\frac{2t^s f_B^s}{R}\right)\left(\frac{\pi R^3}{3}\right)(3\,(1+\sin^2\alpha)+\cos^2\alpha)(\cos\alpha}{4\pi(R+t^s/2)^2\, t^s \rho^s \cos\alpha + (2\pi\rho^b)(2\, f_B^s\, t^s\, R\cos\alpha\sin\alpha)}$$

$$\frac{}{f_B^b} - - -$$

$$- - - \frac{}{(R\sin\alpha + t^s/\sin\alpha + \sqrt{A}/2)}$$

$$= \frac{(2\pi^s)\,(R^2/3)\,(3+3\sin^2\alpha+\cos^2\alpha)}{4\,(R+t^s/2)^2\rho^s + 4\rho^b\, f_B^s\, R\sin\alpha(R\sin\alpha + t^s/\sin\alpha + \sqrt{A}/2)}$$

$$\frac{}{f_B^b}$$

$$= \frac{2\, f_B^s\,(R^2/3)\,(4+2\sin^2\alpha)}{4\,(R+t^s/2)^2\rho^s + \rho^b\, f_B^s\, R\sin\alpha(R\sin\alpha + t^s/\sin\alpha + \sqrt{A}/2)}$$

$$\frac{}{f_B^b}$$

$$= \frac{R^2\, f_B^s\,(4+2\sin^2\alpha)}{6\left[(R+t^s/2)^2\,\rho^s + \rho^b\, f_B^s\, R\sin\alpha\,(R\sin\alpha + t^s/\sin\alpha + \sqrt{A}/2)\right]}$$

$$\frac{}{f_B^b}$$

$$= \frac{.0666\,(f_B^s/\rho^s)\,(1+0.5\sin^2\alpha)}{\left[1+0.25\left(\frac{P_o R_B}{f_B^s}\right)\right]^2 + \psi^{-1}\left[\sin^2\alpha + 0.5\left(\frac{P_o R_B}{f_B^s}\right) + \sin^{3/2}\alpha\left(\frac{P_o R_B\cos}{f_B^b}\right)^{1/2}\right]}$$

where $\psi = f_B^b/\rho^b \div f_B^s/\rho^s$

APPENDIX II

DERIVATION OF EQUATION RATIO f/p

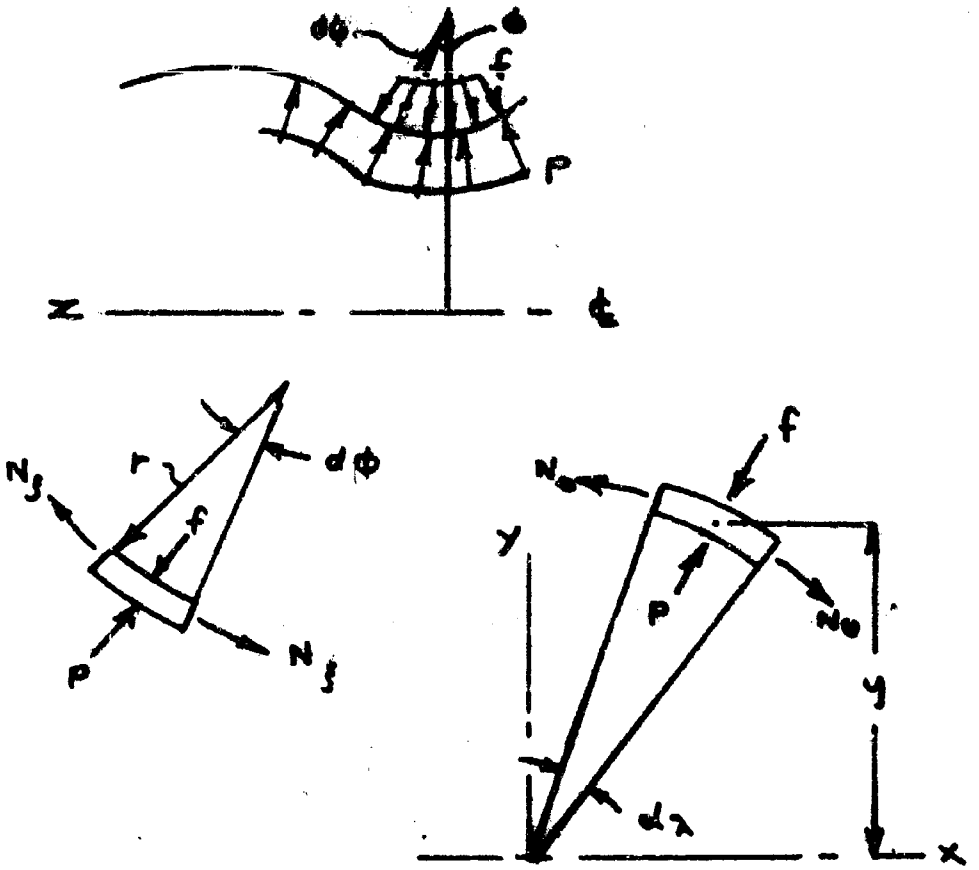

Summing forces in radial direction as shown by arrow, equilibrium requires that:

$$(P - f)\,(y/\cos\phi)\,(d\lambda)\,(r d\phi)$$
$$+ 2N_\phi\,(\sin d\phi/2)\,(y/\cos\phi\, d\lambda)\,(1)$$
$$-2N_\theta\,(\sin d\lambda/2)\,(r d\phi)\,(1) = 0; \text{ and}$$

$$\frac{Pyr}{\cos\phi} + \frac{N_\phi y}{\cos\phi} - Nr = 0.$$

(1) $$Pry = (\cos\phi)\,N_\theta r - N_\phi y$$

Summation of forces in a horizontal direction at a cross section yields

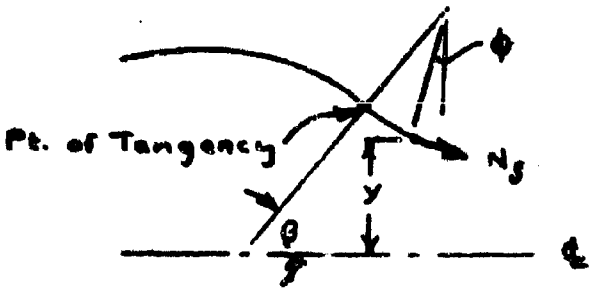

$$(2)\quad N_\xi\ 2\pi y\ \cos\phi = \frac{Py^2\pi}{2} - \int_{\phi}^{\phi\ max} f_\alpha\ r d\phi \cdot 2\pi r_\phi \sin\phi \alpha\phi$$

A third relationship is

$$(3)\quad y = (R + r)\sin\phi - r\cos\phi$$

Three conditions need to be satisfied if membrane conditions are to be met. The first of these is that there be no change in the tangential stress N_ξ.

The first derivative of equation (2) yields

$$N_\xi \left[-\sin\ (R + r\ \sin\phi - 2r\cos\phi)\ + N_\xi\right]\cos\phi\ (R + r)\sin\phi - r\cos\phi = P\ \left\{\left[(R + r)\sin\phi - r\cos\phi\right]\ r\sin\phi\right\} - f\ r\sin\phi(R + r)\sin\phi\ - r\cos\phi\Big]$$

Substitution of equation (3) to simplify

$$N_\xi \left[-\sin\phi\ (y\ - r\cos\phi)\right] = P\ r\ (\sin\phi)\ (y)\ - f\ r\ (\sin\phi)\ y$$

$$N_\xi\ -\sin\phi\ \left(1\ - \frac{r\cos\phi}{y}\right) = P\ (r\sin\phi) - f\ (r\sin\phi)$$

$$N_\xi\ \left(-\frac{\sin\phi}{r\sin\phi}\right)\ \left(1 - \frac{r\cos\phi}{Y}\right) = (P - f)$$

$$(\ )\quad N_\xi\left(\frac{\cos\phi}{y} - \frac{1}{r}\right) = (P - f)$$

A second membrane condition is that the tangential stress be equal to the circumferential stress, ($N_\varphi = N_\zeta$). Substitution of this condition into equation (1) yields:

$$(5)\quad (P - f) = N_\zeta \left(\cos\phi / y - 1/r\right)$$

Comparing equation (4) and (5), the two equations are similar, therefore showing the validity of the derivation.

A final condition for membrane stress is for the tangential stress to be $N_\zeta = PR/2$. The result of subetituting this value in equation (5) is:

$$(P - f) = P/2 \left[-R/r + R/y (\cos\phi)\right]$$

$$P \left\{1 - 1/2 \left[-R/r + R/y (\cos\phi)\right]\right\} = f$$

$$f/P = 1 - 1/2 (-R/r + R/y \cos\phi)$$

Subetitutuion of equation (3) for y yields:

$$(6)\quad f/P = 1 - 1/2 (-R/r + R \cos\phi / (R - r) \sin\phi - r \cos\phi)$$

But $\sin\beta = Y/R$.

$$f/P = 1 - 1/2 (- R/r + R \cos\phi/(R + r)\, Y/R - r \cos\phi)$$

$$(7)\quad f/P = 1/2 \left[2 + 1/(r/R) - \cos\phi/Y/R(1+r/R) - r/R \cos\phi\right]$$

APPENDIX III

DISCUSSION OF "PETS" DIGITAL COMPUTER SOLUTION

The differential equations solved by the PETS routine are based on E. Reissners' (Ref. 6) first order linear approximation to the classical theory of thin elastic shells of revolution.

Refering to Figure 1 let the position of a material point of the deformed middle surface be given by:

$$\begin{aligned} \bar{R} &= \bar{R}_o + \bar{U} \\ \bar{Z} &= \bar{Z}_o + \bar{W} \end{aligned} \tag{4.1}$$

where $\bar{U}$ and $\bar{W}$ are the components of displacement in the R, Z coordinate directions, respectively, and $\bar{R}_o$, $\bar{Z}_o$ is the position of the point in the undeformed configuration. In addition, let denote the difference between the angles of the tangent to the deformed and undeformed surface at the same material point.

$$\omega = \phi_o - \phi \tag{4.2}$$

Finally, let φ (meridional) and θ (circumferential) denote the principal lines of curvature of the middle surface Figure 2. The shell is assumed to remain rotationally symmetric about the Z axis so that all parameters must be taken as functions of φ alone. Parameters which are utilized in subsequent discussions are identified below.

α = AVERAGE COEFFICIENT (ACROSS THICKNESS) OF THERMAL EXPANSION
T = TEMPERATURE CHANGE FROM AMBIENT
$C = \int_h E \, d\zeta$
$D = (1 - \mu^2)^{-1} \int_h E \zeta^2 \, d\zeta$
$N_T = \int_h E \alpha T \, d\zeta$
$M_T = \int_h E \alpha T \zeta \, d\zeta$
P_H = HORIZONTAL PRESSURE COMPONENT
V = VERTICAL STRESS RESULTANT

Subject to the prescription of the foregoing parameters the two simultaneous differential equations which determine the equilibrium state in the PETS routine are:

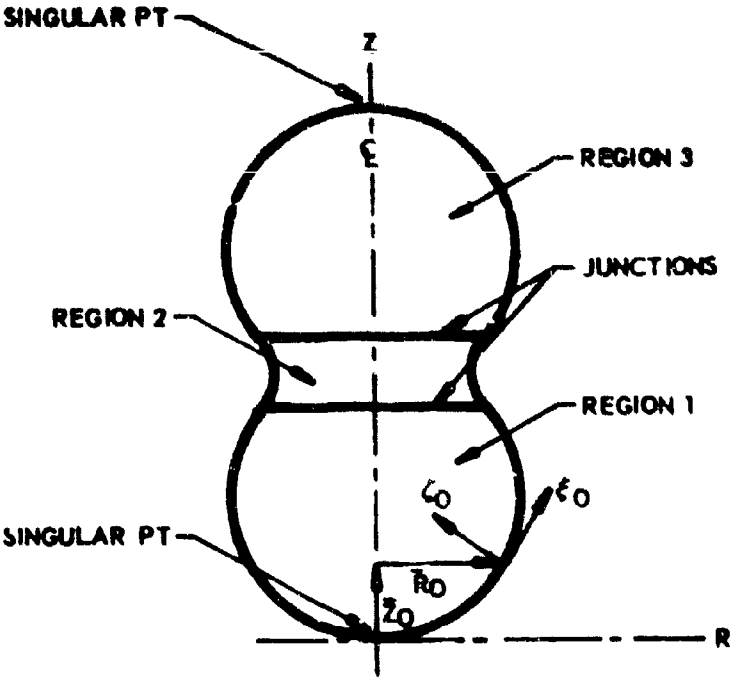

FIGURE 1 REGIONS OF ANALYSIS

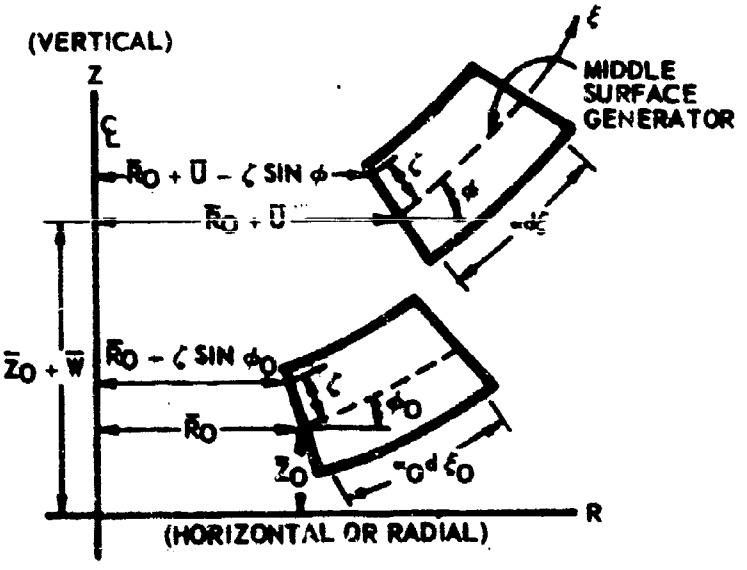

FIGURE 2 SHELL ELEMENT STRAINS

$$\omega'' + \frac{\left(\frac{\bar{R}^2 D}{\bar{R}^2 \bar{R}'_D}\right)'}{\left(\frac{\bar{R}^2 D}{\bar{R}^2 \bar{R}'_D}\right)} \omega' - \left(\frac{\bar{R}'}{\bar{R}}\right)^2 - \frac{\left(\frac{\bar{R}^2 D}{\bar{R}^2 \bar{R}'_D}\right)'}{\left(\frac{\bar{R}^2 D}{\bar{R}^2 \bar{R}'_D}\right)} \omega + \sqrt{\frac{C}{D}} \frac{\bar{z}' \alpha c}{\bar{R}} \psi = X \qquad (4.3)$$

$$\psi'' + \frac{\left(\frac{\bar{R}^2 D}{\bar{R}^2 \bar{R}'_D}\right)'}{\left(\frac{\bar{R}^2 D}{\bar{R}^2 \bar{R}'_D}\right)} \psi + \left\{ 1/2 \left(\frac{CD}{CD}\right)'' - 1/2 \left(\frac{CD}{CD}\right)' \left[1/2 \left(\frac{CD}{CD}\right)' - \frac{\frac{\bar{R}}{C\alpha c}}{\frac{\bar{R}}{C\alpha c}} \left(\frac{\bar{R}'}{\bar{R}}\right)^2 \right] \right\}$$

$$- \frac{u \left(\frac{\bar{R}'}{C\alpha c}\right)'}{\frac{\bar{R}}{C\alpha c}} \psi - \frac{\bar{z}' \alpha c}{\bar{R}} \sqrt{\frac{C}{D}} \omega = Y \qquad (4.4)$$

where

$$Y = \frac{1}{\sqrt{C D}} \left\{ \frac{\bar{R}' \bar{z}'}{\bar{R}^2} + u \frac{\frac{\bar{z}'}{\alpha c C}}{\frac{\bar{R}}{\alpha c C}} \bar{R} V + \frac{u \bar{z}'}{\bar{R}} (\bar{R} V)' - \left[\frac{\left(\frac{\bar{R}}{C \alpha c}\right)'}{\frac{\bar{R}}{C \alpha c}} + \frac{u \bar{R}'}{\bar{R}} \right] \right.$$

$$\left. R \alpha c P_H - (\bar{R} \alpha c P_H)' - \frac{\alpha c}{\bar{R}} C \left[\left(\frac{\bar{R} M_T}{C} \right)' - \frac{\bar{R}' M_T}{C} \right] \right\} \qquad (4.5)$$

$$X = \frac{\alpha c}{D} \left(\bar{R}' V + \frac{M_T}{1 - \alpha} \right) \qquad (4.6)$$

and where the primes denote differentiation with respect to the coordinate. The parameter α is the Lame' parameter connecting the meridional arc length, ds, and the coordinate increment $d\rho_j$. That is

$$(\alpha)^2 = \frac{ds}{d\rho_j}^2 = (\bar{R}')^2 + (\bar{Z}')^2, \tag{4.7}$$

and

$$\bar{R}' = \alpha \cos\phi, \quad \bar{Z}' = \alpha \sin\phi. \tag{4.8}$$

Since the finite difference technique actually employs ρ_j as coordinate, the Lame' parameter is arbitrary, i.e., a scale factor. In particular, we can take $\alpha = 1$.

From the solutions of Equations 4.3 and 4.4 one can determine the stress and couple resultants, stresses, strains, and displacements at points, ρ_j, on the middle surface by means of the following:

$$N_j = \frac{1}{\alpha}\left[\frac{\bar{R}'}{\bar{R}} \sqrt{CD}\,\psi + \frac{\bar{Z}'}{\bar{R}} (\bar{R}\,v)\right], \tag{4.9}$$

$$N_\theta = \frac{1}{\alpha}\left(\sqrt{CD}\,\psi' + \bar{R}\alpha\, p_R\right) \tag{4.10}$$

$$Q = \frac{1}{\alpha}\left[\frac{-\bar{Z}'}{\bar{R}} \sqrt{CD}\,\psi + \frac{\bar{R}'}{\bar{R}} (\bar{R}\,v)\right] \tag{4.11}$$

$$M_j = \frac{D}{\alpha}\left(\omega' + \mu \frac{\bar{R}'}{\bar{R}}\omega\right) - \frac{M_T}{1-\mu}, \tag{4.12}$$

$$M_\theta = \frac{D}{\alpha}\left(\frac{\bar{R}'}{\bar{R}}\omega + \mu\omega'\right) - \frac{M_T}{1-\mu}, \tag{4.13}$$

$$\sigma_j = \frac{E}{1-\mu^2}\left[\frac{1-\mu^2}{C}(N_j + N_T) + \frac{\mu}{D}(M_j + M_T) - \frac{E\alpha T}{1-\mu}\right], \tag{4.14}$$

$$\sigma_\theta = \frac{E}{1-\mu^2}\left[\frac{1-\mu^2}{C}(N_\theta + N_T) + \frac{\mu}{D}(M_\theta + M_T) - \frac{E\alpha T}{1-\mu}\right], \tag{4.15}$$

$$\varepsilon_\phi = \frac{1}{E}\left(\sigma_\phi - \mu\sigma_\theta\right) + \bar{\alpha}T, \tag{4.16}$$

$$\varepsilon_\theta = \frac{1}{E}\left(\sigma_\theta - \mu\sigma_\phi\right) + \bar{\alpha}T, \tag{4.17}$$

$$U = (\bar{R}/C)\left(N_\theta - \mu N_\phi + N_T\right), \tag{4.18}$$

$$W = \int_\phi \left[(\bar{Z}'/C)\left(N_\phi - \mu N_\theta + N_T\right) - \bar{R}'\beta\right] d\phi, \tag{4.19}$$

where: (see Figure 3)

N_ϕ , N_θ = meridional and circumferential stress resultants

Q = shear stress resultant

M_ϕ , M_θ = meridional and circumferential couple resultants

σ_ϕ , σ_θ = meridional and circumferential stress as in function of distance, ζ, from middle surface.

ε_ϕ, ε_θ = meridional and circumferential strain corresponding to σ_ϕ , σ_θ , and $\bar{\alpha}T$.

In the present application, only single layered shells at uniform temperatures are considered. Hence, all temperature terms vanish from the equations, the middle surface is the geometrical middle surface (i.e., $\zeta = \pm h/2$ to extreme fibers), and

$$C = E\,h, \quad D = \frac{E\,h^3}{12\left(1-\mu^2\right)} \tag{4.20}$$

The band to shell compatibility condition is an analytical expression equating the displacements of the band and shell underlying the band at all pressures. Shear strength between band STRATA normal to the shell surface is assumed to be zero. This assumption decrees that gross motions of the band and shell are compatible. The approach of this analysis is to equate

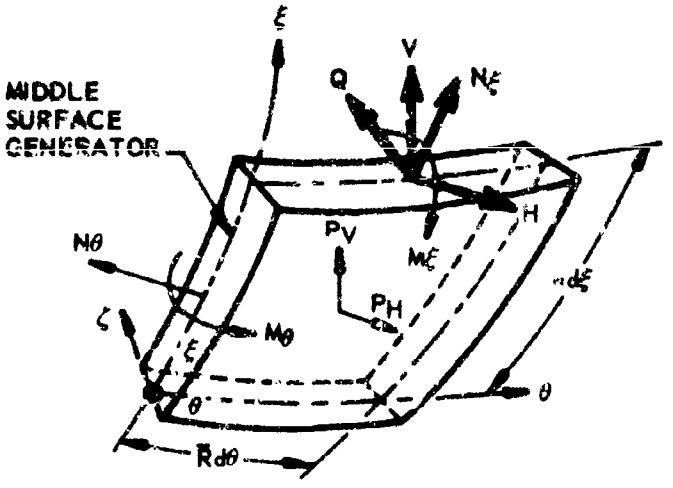

FIGURE 3 SHELL ELEMENT STRESSES

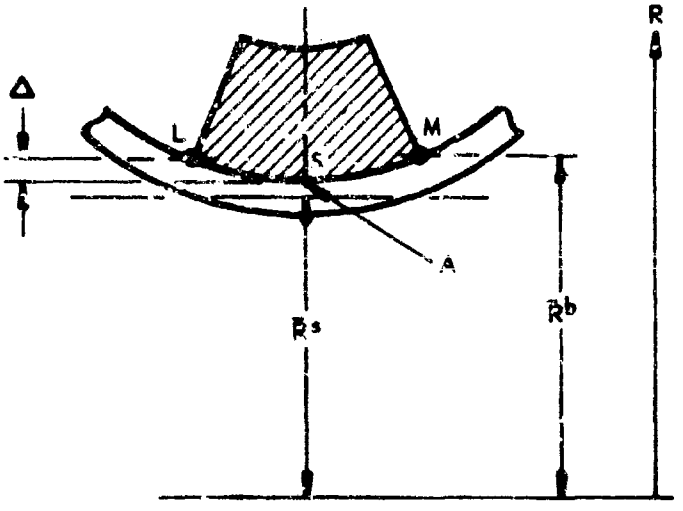

FIGURE 4 NODAL BAND GEOMETRY

the incremental radial displacements of the band to those of the middle surface of the shell, at the low point, A, of the node (Figure 4). Letting $\bar{R}^b$ and $\bar{R}^s$ denotes the radial positions of points in the band and shell middle surface adjacent to point A. The compatibility condition is:

$$\bar{R}^s = \bar{R}^b \tag{4.21}$$

Where (δ) denotes the variation due to a variation (δ_p) in the margin load of the uniform internal shell pressure (P). Writing $\bar{R}^s = R^s + U^s$, $R^b = R_o^b + U^b$, where R_o denotes the undeformed configuration and U the displacements, we see that (4.21) is equivalent to:

$$\delta U^s = \delta U^b \tag{4.22}$$

But since

$$U^s \cong \frac{\varepsilon^{AS}}{R_o^s}, \quad U^b \cong \frac{\varepsilon^{Ab}}{R_o^b}, \quad R_o^b \cong R_o^s \tag{4.23}$$

One can express the compatibility relation in terms of the circumferential shell and band strains ε_θ^{AS}, ε_θ^{Ab} at point A, as

$$\delta\varepsilon_\theta^{Ab} = \delta\varepsilon_\theta^{AS} \tag{4.24}$$

or simply

$$\varepsilon_\theta^{Ab} - \varepsilon_\theta^{AS} = \varepsilon_o \tag{4.25}$$

where (ε_o) is a prestrain; that is, (ε_o) is independent of the shell pressure (P). Obviously, both Equation (4.24) and (4.25) must hold for any value of pressure up to failure.

In general, the interaction of the band and shell can be replaced by a rotationally symmetric distribution of normal stress, f_ζ (ζ) and shearing stress f_η (ζ). However, since the compatibility relation (4.25) equates only radial displacements at a single point, only the resultants, N and T of these stress distributions are determinate:

$$N = \int_S f_\zeta(\zeta)\, d\zeta, \quad T = \int_S f_\eta(\zeta)\, d\zeta \tag{4.26}$$

The shear stress resultant, T, arises from a tendency of the band to slide out of the node. The condition can be neutralized (i.e., one can set T = 0) by designing the band node interface such that the extremities of the band (L, M of Figure) are at equal distances from the axis of the shell.

This was adopted as one of the design criteria.

The normal stress resultant, N, represents the constraint of the band against radial displacements of the shell and may be regarded as a function of the internal shell pressure (P). It follows that for small variations, δp, one can write

$$\delta\varepsilon_{\theta}^{AS} = \frac{\partial \varepsilon_{\theta}^{AS}}{\partial N}\frac{\partial N}{\partial P}\delta P + \frac{\partial \varepsilon_{\theta}^{AS}}{\partial P}\delta P, \quad \delta\varepsilon_{\theta}^{Ab} = \frac{\partial \varepsilon_{\theta}^{Ab}}{\partial N}\frac{\partial N}{\partial P}\delta P \tag{4.27}$$

Hence, from equality Equation (4.24), band shell compatibility implies

$$\frac{\partial N}{\partial P} = \frac{\partial \varepsilon_{\theta}^{AS}}{\partial P} \div \left(\frac{\partial \varepsilon_{\theta}^{Ab}}{\partial N} - \frac{\partial \varepsilon_{\theta}^{AS}}{\partial N}\right) \tag{4.28}$$

If the problem in linear in a range $P_1 \leq P \leq P_2$, then the influence coefficients

$$\frac{\partial \varepsilon_{\theta}^{Ab}}{\partial N} = \varepsilon_{\theta N}^{Ab}, \quad \frac{\partial \varepsilon_{\theta}^{AS}}{\partial N} = \varepsilon_{\theta N}^{Ab} \tag{4.29}$$

depend only on the normal stress distribution, $f_{\xi}(\xi)$, and the coefficient

$$\frac{\partial \varepsilon_{\theta}^{AS}}{\partial P} = \varepsilon_{\theta P}^{AS}$$

is a constant. In the present analysis, it is assumed that the normal stress, $f_{\xi}(\xi)$, is uniformly distributed across the band-node interface.

$$f_{\xi}(\xi) = f = \text{const.} \tag{4.30}$$

This assumption is implemented by adopting as a design criteria the band shape illustrated in Figure 4.

With this last assumption, one can write Equation (4.28) in the form

$$\frac{df}{dP} = \varepsilon_{\theta P}^{AS} \div \left(\varepsilon_{\theta f}^{Ab} - \varepsilon_{\theta F}^{AS}\right) \tag{4.31}$$

where $\varepsilon_{\theta r}^{Ab} = \frac{\partial \varepsilon_{\theta}^{Ab}}{\partial r}$, $\varepsilon_{\theta r}^{AB} = \frac{\partial \varepsilon_{\theta}^{AB}}{\partial r}$, are constants. Therefore, the band shell compatibility relation in the linear case can be written as

$$f(P) - f(P_A) = \left[\varepsilon_{\theta P}^{AB} / (\varepsilon_{\theta r}^{Ab} - \varepsilon_{\theta r}^{AB})\right] (P - P_A) \qquad (4.32)$$

This is the form of the equation of compatibility that is used in this analysis.

APPENDIX IV

CONFIGURATION WITHOUT BAND AMPLIFICATION FACTORS

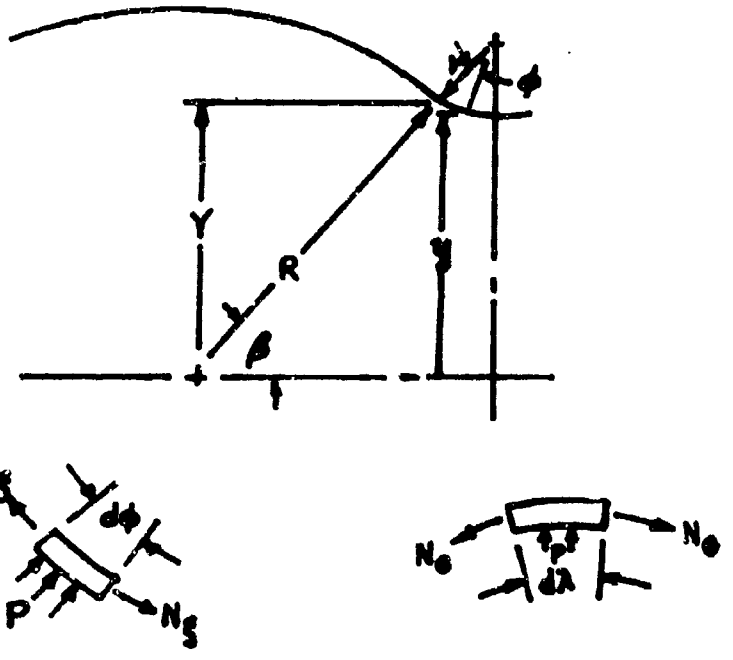

Setting the element in equilibrium and summing forces in a radial (+ R) direction yields:

$$P \frac{Y}{\cos \phi} \quad (d\lambda) \quad (r d\phi)$$

$$+ 2 N_\zeta \quad (\sin \frac{d\phi}{2}) \; (\frac{Y}{\cos \phi} \, d\lambda) \; (1)$$

$$- 2 N_\theta \; (\sin \frac{d\lambda}{2}) \; (r d\phi) \; (1) = 0$$

$$Pry + N_\zeta \, y - N_\theta r \cos \phi = 0$$

$$(1) \quad Pry = N_\theta r \cos \phi - N_\zeta \, y$$

Also, the shell resists a horizontal force equal to the pressure times the cross sectional area.

$$P\pi y^2 = N_\phi \cos\phi \; 2\pi y$$

$$(2) \quad N = \frac{yP}{2\cos\phi}$$

Substituting this value of N_ϕ into (1) yields

$$Pry = N_\theta r \cos\phi - \frac{Py}{2\cos\phi}\, y$$

$$P\,ry = N_\theta r \cos\phi - \frac{Py^2}{2\cos\phi}$$

$$P\left(ry + \frac{y^2}{2\cos\phi}\right) = N_\theta r \cos\phi$$

$$Py\left(r + \frac{y}{2\cos\phi}\right) = N_\theta r \cos\phi$$

$$N_\theta = P\,\frac{y\left(r + \frac{y}{2\cos\phi}\right)}{r\cos\phi}$$

$$(3) \quad N_\theta = \frac{Py}{\cos\phi}\left(1 + \frac{y}{2r\cos\phi}\right)$$

The stress in the shell if membrane conditions existed would be $(ft) = \frac{PR}{2}$. Using this membrane stress equation to normalize the stresses that exist, the amplification for the meridian stress A, becomes

$$(4) \quad A_\phi = \frac{N_\phi}{ft} = \frac{yP}{\frac{PR}{2}\cos^2\phi} = \frac{y}{R\cos\phi}$$

But $y = (R + r)\sin\phi - r\cos\phi$

Therefore

$$A_\xi = \frac{(R + r)\sin\beta - r\cos\phi}{R\cos\beta}$$

$$A_\xi = \frac{(R + r)}{R}\frac{\sin\beta}{\cos\phi} - r/R$$

$$= \frac{R}{R} + r/R \quad \frac{\sin\beta}{\cos\phi} - \frac{r}{R}$$

$$= (1 + r/R)\ \frac{\sin\beta}{\cos\phi} - r/R$$

But $\sin\beta = Y/R$

$$A_\xi = (1\ \ r/R)\ \frac{Y/R}{\cos\phi} - r/R$$

And

$$A_\xi = (1 + r/R)\ (Y/R)\ \left(\frac{1}{\cos\phi}\right) - r/R \tag{5}$$

Similarly, the circumferential amplification factor becomes:

$$A_\theta = \frac{N_\theta}{ft} = \frac{Py}{\cos\phi}\ \frac{\left(1 + \frac{y}{2r\cos\phi}\right)}{\frac{PR}{2}} = \frac{2y}{R\cos\phi}\left(1 + \frac{y}{2r\cos\phi}\right)$$

$$A_\theta = \frac{y}{R}\ \left(\frac{1}{\cos\phi}\right)\ \left(2 + \frac{y}{r\cos\phi}\right)$$

$$A_\theta = A_\xi\left[2 + (y/r)\ (R/R)\ \left(\frac{1}{\cos\phi}\right)\right]$$

$$A_\theta = A_\xi\left[2 + (r/R)^{-1}A_\xi\right] \tag{6}$$

APPENDIX V

PHASE II MANUFACTURING PLAN

1. INTRODUCTION AND SCOPE

Phase II of the Segmented Sphere Pressure Vessel (SSPV) Study will consist of a combined fabrication and quality certification effort consisting of performance of the following general tasks.

a. Fabrication of such tools as are required to support fabrication of detail configurations not previously attempted and modification of existing tooling based on knowledge gained during the Phase I - Engineering Development portion of the subject program.

b. Fabrication of one each of three specific classes of pressure vessels, as represented by the detailed drawings of the Appendix, will be performed in accordance with the detail specifications of the engineering design as contained therein.

c. Maintainance of control over the quality of the manufactured hardware by the use of in-process inspection and final acceptance test procedures, and maintainance of permanent records certifying that this hardware meets the requirements of the detailed engineering specification.

2. MANUFACTURING PROGRAM SUMMARY

Manufacture of the three classes of segmented sphere pressure vessels, as described in the Appendix to this document, will be accomplished as summarized by Figure 1.

The Manufacturing Department will perform all detail fabrication, weld subassembly, and final assembly operations with the exception of the explosive forming and chem-milling operations.

The chem-milling operation on the domes, segments, and interconnect rings will be performed as a vendor operation. The explosive forming operation, after the blank has been placed into the explosive die and properly set up, will be performed by the MSD-T Rocket Propulsion and Pyrotechnics Test Laboratory.

The Quality Control Department will be responsible for and perform receiving inspections on all incoming materials; in-process dimensional, X-ray, and florescent penetrant inspections; and final inspections prior to delivery. In addition, Quality Control will verify performance to specification requirements of all processing and will witness and verify adequacy of testing for final acceptance of the pressure vessels.

3. TOOLING REQUIREMENTS

The following is a detailed description of the tooling which will be used to accomplish the requirements of this plan.

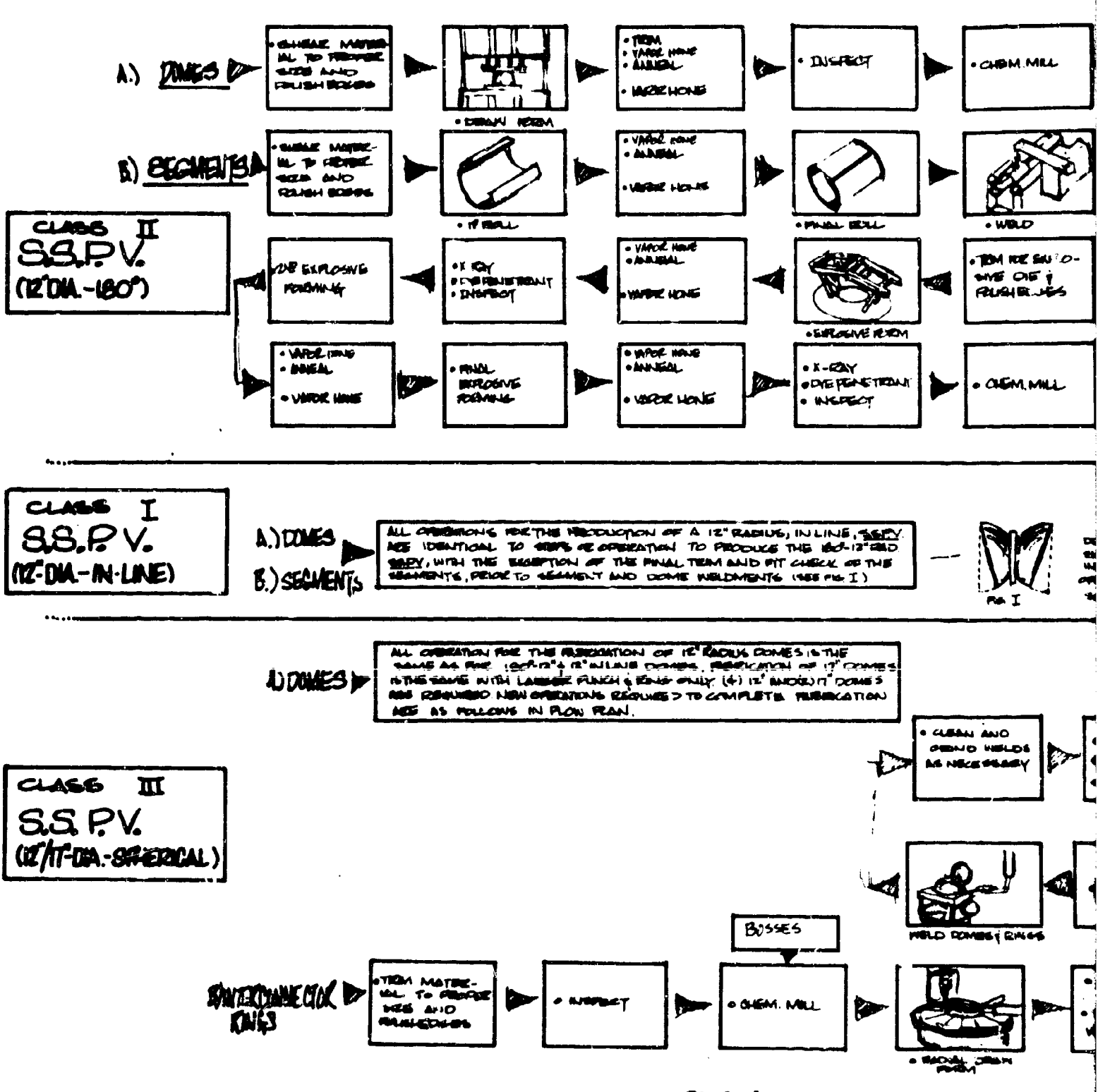

FIGURE 1. PRODUCTI

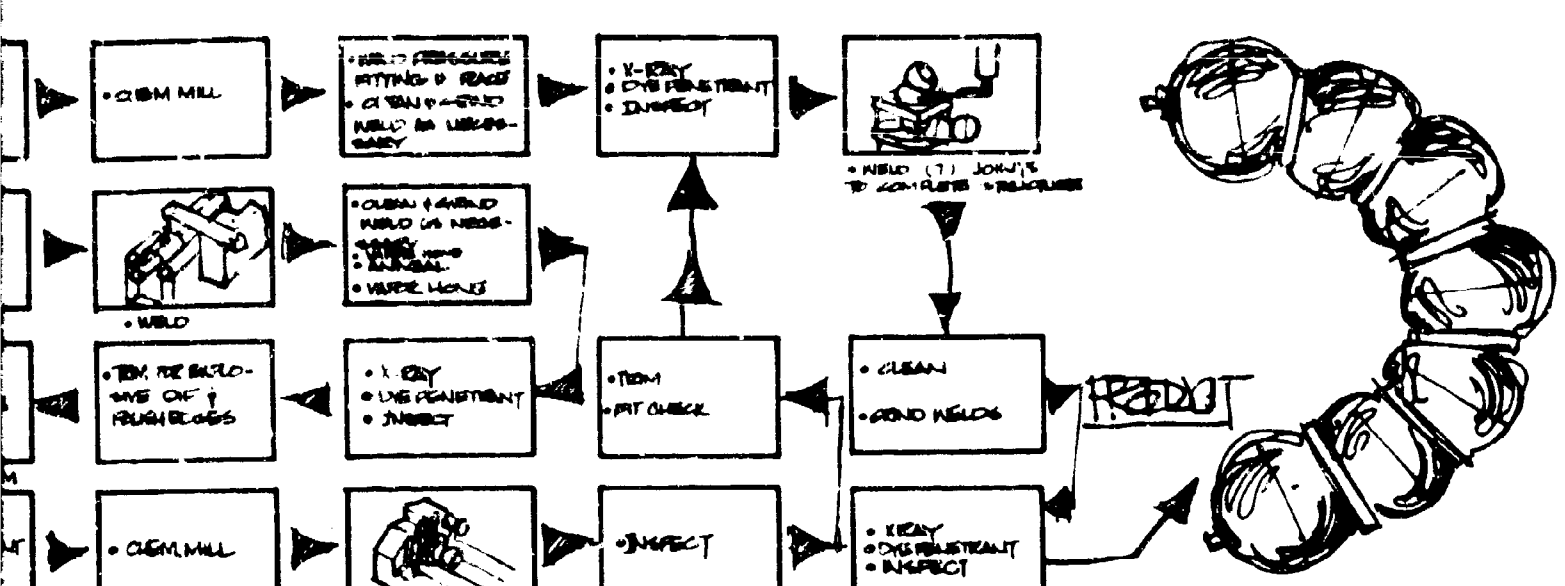

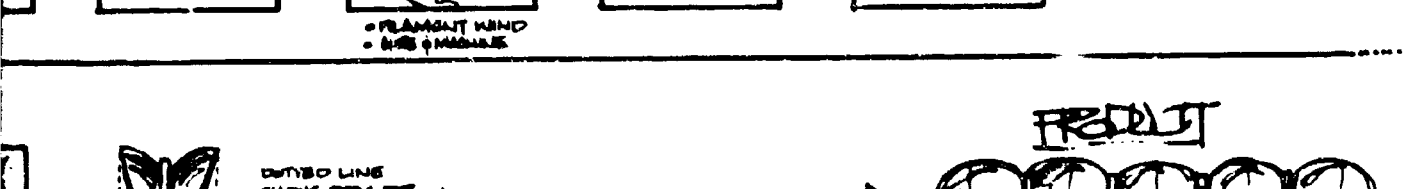

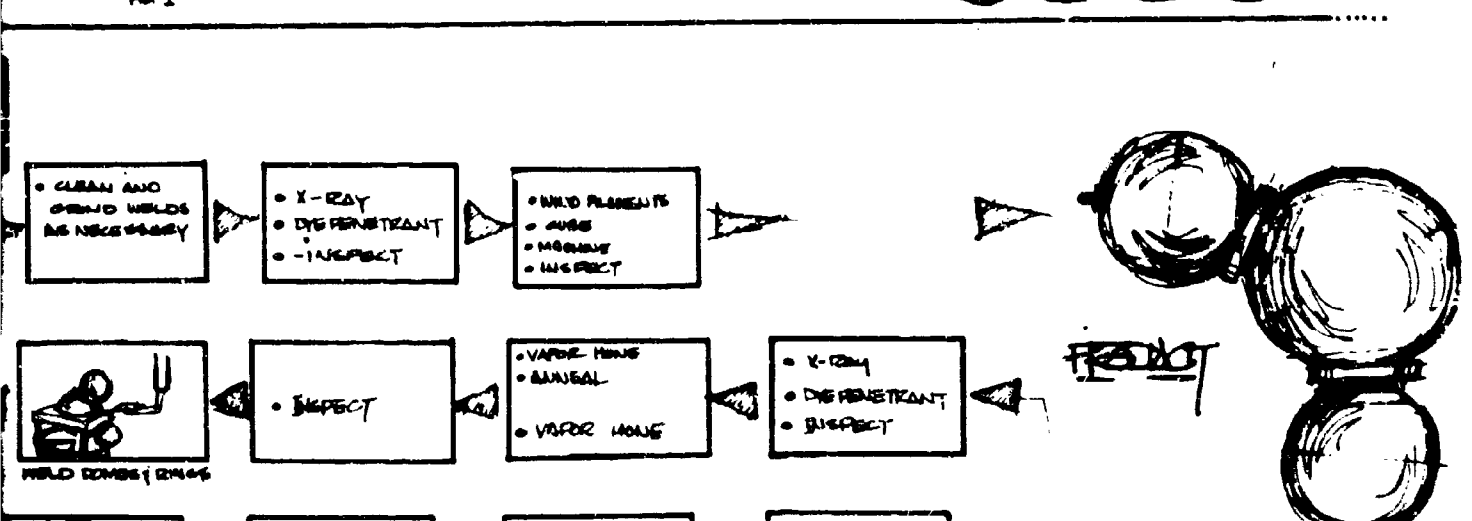

PRODUCTION FLOW PLAN

2

a. Explosive Form Die for 12 Inch Cylindrical Segments

This explosive form die is the tool for forming the 12" diameter "hourglass" shaped cylindrical segment which is the primary module of the segmented sphere concept as developed under this program to date. It consists of a steel split die which is configured internally to the final external dimensions of the desired module. The split die is externally tapered to mate with an internally tapered steel cylinder which retains the split die during the explosive operation. A set of end plates which bolt to the steel cylinder are used to apply a compressive loading on the seam-welded cylindrical part blank in order to relieve the biaxial strain condition which is produced within the part when the explosive charge is detonated.

b. Hemispherical Dome Draw Form Dies

Two former hemispherical cold draw form dies of 12 and 17 inch diameters, modified for use on this program, will be used in a Danley 500 ton triple action press for forming the hemispherical dome details. These dies consist of a male form punch, a draw ring, and a bolster for obtaining the necessary draw pressures. The 12 inch die was modified twice during Phase I; once for conversion to hot forming and the second time for accommodating three 3/16 inch thick steel cover plates over the titanium sheet for the purpose of reducing the effective diameter of the draw ring during early stages of the draw. The 17 inch die, used during Phase I for cold forming 17-7 steel, will be modified for hot form usage on titanium during Phase II.

c. Weld Joining Tooling

The tooling used in the welding operations consists of copper chill bars, cooling blankets for protection of the filament wound nodal bands, and restraining plates for supporting the parts on the positioner during circumferential welding. This tooling is adequate for performance of the various welding operations, but is uncontrolled and of the "shop aid" type (not production rate quality).

d. Interconnect Band Stretch Form Die

A steel one-piece die will be used for forming the interconnect band for the Class III pressure vessel. This die will be used on a Hufford Stretch Form machine.

e. Nodal Band Mold Fixture

This tool is comprised of two steel fences which constrain the nodal band filaments to the desired configuration during the winding process. These fences are each made in four 180° segments which are bolted together in a staggered fashion and restrained in position by studs which tie to an external frame which in turn supports the shell in place on the

lathe. A rubber gasket is placed beneath each fence to prevent resin and filaments from flowing beneath the fence. Silicone spray treatment of the fence prevents the resin from adhering during the cure process.

4. MANUFACTURING OPERATIONS

The following presents detailed descriptions of individual manufacturing operations which will be performed in satisfying the requirements of this plan. These operations are approximately identical for each individual pressure vessel configuration. Where a significant difference exists in the manner in which a given operation is performed on individual vessel configurations, specific note of this circumstance is taken.

The sequence of these operations as they are performed on individual detail parts and assemblies is shown pictorially by Figure 1 preceding.

a. Shearing Operation

The titanium sheet material from which the pressure vessels are to be formed will be rough cut to the necessary blank size on a Cincinnati shear. This operation will produce rectangular blanks for forming the explosively formed cylinder blanks, circular blanks of 30 and 20 inch diameter for the 17 and 12 inch diameter draw formed hemispherical domes, and the small rectangular blanks for the stretch formed interconnect band segments.

b. Draw Forming

The draw forming operation for fabrication of the 17 and 12 inch diameter hemispherical domes will be performed on a Danley Triple Action Press of 500 tons capacity. The hemispheres will be hot formed using the form dies as described under "Tooling Requirements." Prior to placement in the draw die, the titanium blanks and three-3/16 inch steel plates equivalent in diameter to the titanium blanks will be heated to 1000°F in a portable oven located adjacent to the press. The purpose of the steel plates is to inhibit the formation of buckles in the hemispheres during the forming operation by acting as staging dies for the draw ring. Using torches, the punch will be heated to 1050-1100°F and the draw ring to 1250-1300°F prior to commencing the operation. The three steel plates will be placed on top of the titanium blank in the die and the press will be placed on top of the titanium blank in the die and the press will be stroked in intervals of 1/3 and 1/2 the stroke distance required to completely form the dome with one steel plate being removed at the end of each stroke interval. The third steel plate will remain with the titanium through the third and final stroke.

c. Roll Forming

This operation is for forming the titanium cylindrical blank for the explosively formed module and will be performed on a Farnham open end

roll in three stages [illegible] to obtain the necessary pre-form of the rectangular sheet for starting in the roll. The sheet will be pre-rolled to a slightly larger diameter than is required. Subsequent to an annealing process, the detail will be finish rolled to the required diameter. Still later, after the part has been welded into a complete cylinder, a third rolling operation will be performed for the purpose of straightening the part.

d. Welding

Tungsten Inert Gas (TIG) welding is typically used for joining of the titanium details. Hand welding will be performed in joining the interconnect band details and installation of the fitting bosses in the completed pressure shell assemblies and automatic TIG welds for all other joints. The longitudinal weld which is used to close the cylindrical blank for the explosively formed module will be performed on the Welduction Automatic TIG Welder. Copper bar heat sinks will be placed adjacent to the weld area in order to reduce the heat affected area in the parent material.

Circumferential welds will be performed on the Sciaky Automatic Positioner TIG Welder. A constant flow inert gas purge will be used internal to the shells on all of the latter type of welds. This flow will be regulated in order to prevent weld blowout, incomplete penetration, or internal contamination of the weld. Trailing shields will provide a flow of inert gas to the external portion of these welds in order to protect the weld from contamination until the weld has had sufficient opportunity to cool. Copper chill bars will, in this case also, be placed adjacent to the weld for reduction of the parent metal heat affected zone.

Inspection of the fitup of the parts to be welded will be made and the welding operation allowed to proceed only when parts mate within tolerance.

e. Cleaning and Grinding

Cleaning operations will be performed prior to heat treat, welding, and florescent penetrant inspection operations. Grinding operations will be performed for the purpose of fitting up details prior to weld joining and for cleaning up welds prior to X-ray inspection or weld repair. This operation will be performed using a hand grinder and visual observation of the work piece.

f. Annealing and Vapor Honing

In order to relieve induced stresses, the formation of which is inherent in the forming operations, annealing of the titanium details and assemblies will be performed as intermediate steps throughout the explosive forming process on the 12 inch diameter cylindrical module and subsequent to all other forming operations. Annealing will be performed in a retort continuously inert gas purged to a minus 80°F (or better) dew

point reading. The inert gas atmosphere is necessary to avoid contamination of the material during the heat treat process. Vapor honeing will be performed on all titanium parts prior to heat treatment operation in order to reduce the contaminate level in the retort and subsequent to heat treatments to remove heat treat scale and residue prior to florescent penetrant inspections.

g. X-Ray Inspection

X-ray of details and assemblies will be performed for the purpose of detecting cracks in the material or welds after forming operations and porosity, cracks, and inclusions in welds after welding operations. This is the primary non-destructive means of ascertaining quality of manufacture of welded details and assemblies. A secondary means which will be used for determining whether or not surface cracks exist in or about a weld is the florescent penetrant (Zyglo) inspection technique. This technique will always be used prior to X-ray of a part and the results of both techniques applied to evaluation of the part for acceptance or rework.

h. Inspection

Inspection operations of a general nature will also be performed to ensure acceptable quality hardware for delivery and test.

Incoming raw materials will all undergo an inspection upon receipt. Shipments of titanium sheet and bar stock will be checked to ensure that vendor documentation certifying the chemical and physical properties of the material accompanied its shipment. Samples of the material will be taken and subjected to physical properties tests as a check against the vendor's conformance to the specification, and visual and dimensional inspection will be performed.

Proof pressure tests in accordance with engineering requirements will be performed on all completed pressure vessels to ensure structural deficiencies resulting from improper manufacture do not exist and that the vessel is of acceptable quality. A final end item inspection will be performed on each test article, before and after proof test, consisting of visual inspection to verify compliance of the hardware with final assembly drawing dimensional tolerances, finishes, etc.

i. Trim

The trimming operation is typically a machining operation in which an unfinished detail part having been formed from a rough cut blank is cut to final dimensions. Trim operations for all parts will be performed on a Lodge and Shipley lathe with a 9 inch swing. Primary dimensional control to be exercised in this operation will be with regard to diameter at the trim line. Detail parts will be trimmed to match adjoining parts.

j. Explosive Form

The 12 inch diameter cylindrical module for Classes I and II pressure vessels will be explosively formed from a 11.17 inch diameter cylindrical blank using the explosive form die described in paragraph 3.a. The blank will be placed in the die, the end closure plates installed, and the bolts securing these plates torqued (100 ft. lbs. for initial firing, 60 for subsequent shots) to obtain the required preload on the blank. A vacuum will be applied between the cylinder blank and the wall of the forming die, the explosive charge placed in the die, and the entire unit submerged in the water of the explosive form tank. The cylinder will be expanded to drawing dimensions in three successive shots with the cylinder being removed from the die, re-annealed, and inspected between each shot.

k. Stretch Form

The interconnecting band segment details will be hot stretch formed on a Hufford Stretch Form machine using the modified die as described in paragraph 3.d. Heat for this forming operation will be applied to the part by use of a welding resistor secured to each end of the stretch form blank. Temperature control will be accomplished by use of a thermocouple placed on the blank.

l. Wind Filament

The fiberglass nodal band will be filament wound on the 12 inch diameter titanium cylindrical shells using a Lodge and Shipley lathe with a 9 inch swing and an electromagnetic clutch filament tensioning device. The nodal band fence, described previously, will be used to constrain the filaments to drawing configuration during winding and cure. The nodal bands on the Class III pressure vessel will be wound without constraining tooling and will be machined to engineering configuration subsequent to the cure operation. This latter band will be wound in two stages with a cure cycle between each stage. The purpose of this is to avoid accumulation of wet filament in sufficient amount to collapse the pressure shell. Winding of the nodal bands on the Class III vessel will be performed on an open bed lathe using the same tensioning device as previously described.

m. Cure and Machine

Nodal bands will be cured in an oven at 350°F after winding. The constraining fence used for winding the 12 inch diameter cylindrical modules will be left in place throughout the cure cycle. After cure, a relief radius will be machined in the outer periphery of the band on the 12 inch diameter modules and the bands on the Class III vessel will be machined to configuration on all exposed sides. This machining operation will be performed on the respective lathes on which the filaments were wound.

n. Chemical Milling

The titanium pressure shell for each class of pressure vessel will be etched chemically to a lesser thickness leaving a band for the fusion weld joints. This operation is performed to bring the pressure vessels up to maximum efficiency for the particular detail design configuration being developed. The chemical milling process will be a vendor operation. The selected vendor will mask and etch to meet the requirements of the engineering specifications.

APPENDIX VI

PHASE III DEVELOPMENT TEST PLAN

1. INTRODUCTION AND SCOPE

The Phase III Testing portion of the SSPV Study as defined herein is an effort to perform pressure testing on two classes of segmented sphere pressure vessels, secure engineering data by instrumentation of the test articles, evaluate the data obtained from these tests, and revise the SSPV design criteria generated in Phase I of the SSPV Study Program in accordance with this data (if such revision is necessary).

2. DETAILED PLAN

Classes I and III segmented sphere pressure vessels will be subjected to pressure tests, the results of these tests reduced and evaluated, and the SSPV Design Criteria, developed during Phase I of this program, revised in accordance with the data obtained from these tests.

a. Test Article Definition

The test articles will consist of one each of a Class I and III pressure vessel manufactured in accordance with the engineering specifications and the Phase II Manufacturing Plan. These test articles will have been subjected to Quality Control acceptance procedures in accordance with the specifications and will be certified as acceptable quality hardware.

b. Test Instrumentation

The test articles will be instrumented with electrical strain gauges in order to obtain engineering information for performance evaluation. Approximately six strain gauges will be placed on each test article. Two gauges will be placed on each article near the nodal band area in order to verify nominal computed strains for these areas. The remaining gauges will be placed on or near locations which appear critical (have high probability for initial failure) on the basis of observations and measurements made in the in-process inspections during manufacture.

c. General Test Procedures

Detailed test procedures will be prepared in the form of a Test Request by SSPV Project personnel for execution in the MSD-T Rocket Propulsion and Pyrotechnics Test Laboratory. These procedures will specify in greater detail the manner in which the following requirements are to be accomplished.

(1) The test vessels, minus hydraulic attachment fittings, will be weighed and the weights recorded. These dry, empty weights will be the basis for establishment of an efficiency index for each of the two vessel designs.

(2) Volumetric measurement of the test vessels will be made by weighing the vessel filled with the hydraulic pressurizing fluid. Hydraulic fluid specific gravity determination will be made at the same temperature at which the weight measurement was taken and conversion of the net fluid weight to volume will be accomplished.

(3) Both test vessels will be pressurized hydrostatically using an aircraft type hydraulic fluid. Pressure loading will be applied in ten percent increments of predicted burst pressure. The vessels will be pressurized until failure occurs.

(4) Strain gauge readings will be obtained at each increment of loading to failure.

d. Test Data and Reporting

A test report will be prepared by the testing facility to illustrate the test methods and to document the test data. This report will include the strain gauge information and photographs which depict the test vessels before and after test. Closeup photographs of the failure area will be provided and the failure mode sequence will be specified based on visual observation and the strain gauge information.

e. Test Data Evaluation

Test results will be evaluated to resolve differences between predicted and actual measurements. Pressure vessel efficiency will be calculated for each class based on weights, volumes, and strength measurements made in the described procedure.

The design criteria prepared during Phase I of this program will be revised to incorporate the results of this evaluation of test data if differences which exist between actual and predicted performance are not reconciliable and such revision is warranted.

REFERENCES

1. INVESTIGATION OF A SEGMENTED SPHERE CONCEPT FOR A LIGHT WEIGHT PRESSURE VESSEL, J. W. Farrell, Ling Temco Report 00.294, July 61.

2. SEGMENTED SPHERE CONTAINERS, American Rocket Society Reprint 2428-62, J. W. Farrell, C. E. Howle, 1962.

3. MATERIALS IN A MULTIAXIAL STRESS FIELD, LTV Report No. TRD-TDR-63-4094, Nov., 63.

4. THE PETS CODE, L. A. Ney, ACF Industries, Inc., Albuquerque, New Mexico, Report No. ACF-SA-719, May 10, 1965.

5. A DIGITAL COMPUTER METHOD FOR DESIGN AND ANALYSIS OF AXISYMMETRIC THIN SHELLS SUBJECTED TO PRESSURE AND THERMAL EVNIRONMENTS, J. W. Neudecker, The University of California, Los Alamos Scientific Laboratory, Los Alamos, New Mexico, Report No. LAMS-3083, Nov 17, 1964.

6. A NUMERICAL ANALYSIS OF THE EQUATIONS OF THIN SHELLS OF REVOLUTION, Radkowsik, Davis, and Boldni, ARS Paper 1580-60, January, 1962.

7. ON THE THEORY OF THIN ELASTIC SHELLS, E. Reissner, Reissner Anniversary Volume, J. W. Edwards Co., Ann Arbor Michigan, 1949, p. 232.

8. STRESS ANALYSIS OF AXISYMMETRICALLY LOADED THIN SHELLS OF REVOLUTION BY NUMERICAL INTEGRATION, P. H. Estes, Jr., Report No. ACF-SA-3307, Albuquerque Division, ACF Industries, Inc., May 31, 1962.

UNCLASSIFIED
Security Classification

DOCUMENT CONTROL DATA - R&D

(Security classification of title, body of abstract and indexing annotation must be entered when the overall report is classified)

1 ORIGINATING ACTIVITY (Corporate author)
Missiles and Space Division - Texas
LTV Aerospace Corporation
Dallas, Texas 75222

2a REPORT SECURITY CLASSIFICATION
Unclassified

2b GROUP
N/A

3 REPORT TITLE
STUDY AND EVALUATION OF SEGMENTED SPHERE PRESSURE VESSELS -
PHASE I TECHNICAL REPORT

4 DESCRIPTIVE NOTES (Type of report and inclusive dates)
Phase I Final Report

5 AUTHOR(S) (Last name, first name, initial)
Farrell, J. W.

6 REPORT DATE	7a TOTAL NO OF PAGES	7b NO OF REFS
November 1967	185	8

8a CONTRACT OR GRANT NO	9a ORIGINATOR'S REPORT NUMBER(S)
F04611-67-C-0040	AFRPL-TR-67-261
b PROJECT NO 3058	
c	9b OTHER REPORT NO(S) (Any other numbers that may be assigned this report)
d	MSD-T Report No. 00.980

10 AVAILABILITY/LIMITATION NOTICES
This document is subject to special export controls and each transmittal to foreign governments or foreign nationals may be made only with prior approval of AFRPL(RPPR/STINFO).

11 SUPPLEMENTARY NOTES	12 SPONSORING MILITARY ACTIVITY
	Air Force Rocket Propulsion Laboratory Edwards AFB, California 93523

13 ABSTRACT

Two methods of structurally analyzing segmented sphere pressure vessels were developed. The method referred to as "AMC," defines design features to provide a membrane stress state in any segmented sphere system. The second method adapts a digital computer routine "PETS" to solutions of the general stress-strain equations. The results of the more rigorous but cumbersome computer solutions served to validate the AMC method as a simple and accurate design procedure. Process development studies and fabrication trials succeeded in demonstrating good producibility for longitudinally symmetric and toroidal systems. However, manufacture of systems employing segments of mixed diameter was complicated by inability to [illegible] standard shell [illegible] scheme used in the constant diameter systems. Pressure tests on full scale vessels indicate actual stress-strain conditions are in conformance with membrane theory. A design criteria was developed by parametric exercises with mathematical models. This criteria shows effects and interactions of the many design variables. Dimensioning formulas are explained and demonstrated by example problems.

DD FORM 1 JAN 64 1473

UNCLASSIFIED
Security Classification

14 KEY WORDS	LINK A		LINK B		LINK C	
	ROLE	WT	ROLE	WT	ROLE	WT

INSTRUCTIONS

1. ORIGINATING ACTIVITY: Enter the name and address of the contractor, subcontractor, grantee, Department of Defense activity or other organization (*corporate author*) issuing the report.

2a. REPORT SECURITY CLASSIFICATION: Enter the overall security classification of the report. Indicate whether "Restricted Data" is included. Marking is to be in accordance with appropriate security regulations.

2b. GROUP: Automatic downgrading is specified in DoD Directive 5200.10 and Armed Forces Industrial Manual. Enter the group number. Also, when applicable, show that optional markings have been used for Group 3 and Group 4 as authorized.

3. REPORT TITLE: Enter the complete report title in all capital letters. Titles in all cases should be unclassified. If a meaningful title cannot be selected without classification, show title classification in all capitals in parenthesis immediately following the title.

4. DESCRIPTIVE NOTES: If appropriate, enter the type of report, e.g., interim, progress, summary, annual, or final. Give the inclusive dates when a specific reporting period is covered.

5. AUTHOR(S): Enter the name(s) of author(s) as shown on or in the report. Enter last name, first name, middle initial. If military, show rank and branch of service. The name of the principal author is an absolute minimum requirement.

6. REPORT DATE: Enter the date of the report as day, month, year; or month, year. If more than one date appears on the report, use date of publication.

7a. TOTAL NUMBER OF PAGES: The total page count should follow normal pagination procedures, i.e., enter the number of pages containing information.

7b. NUMBER OF REFERENCES: Enter the total number of references cited in the report.

8a. CONTRACT OR GRANT NUMBER: If appropriate, enter the applicable number of the contract or grant under which the report was written.

8b, 8c, & 8d. PROJECT NUMBER: Enter the appropriate military department identification, such as project number, subproject number, system numbers, task number, etc.

9a. ORIGINATOR'S REPORT NUMBER(S): Enter the official report number by which the document will be identified and controlled by the originating activity. This number must be unique to this report.

9b. OTHER REPORT NUMBER(S): If the report has been assigned any other report numbers (*either by the originator or by the sponsor*), also enter this number(s).

10. AVAILABILITY/LIMITATION NOTICES: Enter any limitations on further dissemination of the report, other than those imposed by security classification, using standard statements such as:

(1) "Qualified requesters may obtain copies of this report from DDC."

(2) "Foreign announcement and dissemination of this report by DDC is not authorized."

(3) "U. S. Government agencies may obtain copies of this report directly from DDC. Other qualified DDC users shall request through _____."

(4) "U. S. military agencies may obtain copies of this report directly from DDC. Other qualified users shall request through _____."

(5) "All distribution of this report is controlled. Qualified DDC users shall request through _____."

If the report has been furnished to the Office of Technical Services, Department of Commerce, for sale to the public, indicate this fact and enter the price, if known.

11. SUPPLEMENTARY NOTES: Use for additional explanatory notes.

12. SPONSORING MILITARY ACTIVITY: Enter the name of the departmental project office or laboratory sponsoring (*paying for*) the research and development. Include address.

13. ABSTRACT: Enter an abstract giving a brief and factual summary of the document indicative of the report, even though it may also appear elsewhere in the body of the technical report. If additional space is required, a continuation sheet shall be attached.

It is highly desirable that the abstract of classified reports be unclassified. Each paragraph of the abstract shall end with an indication of the military security classification of the information in the paragraph, represented as (TS), (S), (C), or (U).

There is no limitation on the length of the abstract. However, the suggested length is from 150 to 225 words.

14. KEY WORDS: Key words are technically meaningful terms or short phrases that characterize a report and may be used as index entries for cataloging the report. Key words must be selected so that no security classification is required. Identifiers, such as equipment model designation, trade name, military project code name, geographic location, may be used as key words but will be followed by an indication of technical context. The assignment of links, roles, and weights is optional.